Roles of HSB-1 in Regulation of Heat Shock Factor Activity, Histone Levels, Mitochondrial Function and Longevity

by

Surojit Sural

A dissertation submitted in partial fulfillment
of the requirements for the degree of
Doctor of Philosophy
(Molecular and Integrative Physiology)
in the University of Michigan
2019

Doctoral Committee:

Associate Professor Ao-Lin Hsu, Co-Chair
Professor Scott Pletcher, Co-Chair
Associate Professor David Lombard
Professor Santiago Schnell
Professor Shawn Xu

Surojit Sural

ssural@umich.edu

ORCID iD: 0000-0002-0422-9799

© Surojit Sural 2019

DEDICATION

This dissertation is dedicated to my grandparents, my parents, my sister, my wife and her family, who have always encouraged me to pursue my dreams.

Thank you for making this journey so enjoyable.

ACKNOWLEDGEMENTS

First, I would like to thank my advisor Dr. Ao-Lin (Allen) Hsu for his support and guidance throughout the duration of this study. In addition, I sincerely acknowledge the contributions of my dissertation committee members, Dr. Scott Pletcher, Dr. David Lombard, Dr. Shawn Xu and Dr. Santiago Schnell, for providing advice and sharing their insights in my half-yearly committee meetings and beyond. In the Hsu Lab, I am most thankful to Carol Mousigian for her technical assistance in generating transgenic *C. elegans* strains, for preparing many reagents essential for my experiments and for performing large-scale life span screens. I acknowledge the help provided by Dr. Tzu-Chiao Lu in performing bioinformatic analysis of the RNA-Seq data described in Chapter 2, and for sharing his expertise in the interpretation of genome-wide sequencing data. I also sincerely thank Zhaoyu (Slash) Pan (4S Inc.) for his assistance in bioinformatic analysis of the MNase-Seq data included in Chapter 3. I am grateful to Dr. Chung-Yi Liang, Dr. Tsui-Ting (Jean) Ching, Weiqiao (Sara) Ding and Seung Ah Jung for contributing experimental data that are included in this dissertation. I am also thankful to previous Hsu Lab members, Dr. Wei-Chung (Daniel) Chiang, Dr. Eunju Kim, Dr. Xiaokun Yu and Chieh Chen, for their technical assistance. In addition, I am especially thankful to my lab colleague Dr. Eleni Gourgou for scientific discussions and for providing professional advice.

In the University of Michigan research community, I would like to thank the laboratories of Dr. David Lombard, Dr. Scott Pletcher, Dr. Rich Miller and Dr. Tristan Maerz, and the Orthopaedic Research Laboratories (ORL) for allowing me to use their research equipment. Among Lombard Lab members, I sincerely thank Dr. Surinder Kumar for his assistance in performing the Seahorse experiments included in this study, and Mary Skinner and Dr. William Giblin for their technical assistance in numerous other experiments. I thank Dr. Robert Lyons, Jeanne Geskes and Judith Opp from the University of Michigan DNA Sequencing Core, for their help in designing the high-throughput sequencing experiments reported in this study. Moreover, I am thankful to Dr. Rich Mc Eachin of the University of Michigan Bioinformatics Core for his assistance in submitting our RNA-Seq dataset to the NCBI Gene Expression Omnibus (GEO) database.

I am grateful to Dr. Steven Johnson (Brigham Young University) and Dr. Joel Meyer (Duke University) for sharing detailed protocols for micrococcal nuclease (MNase) digestion in *C. elegans* and a quantitative PCR-based DNA damage assay, respectively. I thank my scientific peers, especially Dr. Shweta Ramdas and Dr. Joseph Endicott, for providing feedback on my manuscripts. Most importantly, I am thankful to Dr. Mohita Tagore, for sharing her expertise in the field of epigenetics and for providing helpful comments on my research findings and writing. Finally, I would like to acknowledge the constant support and encouragement of my family through all the ups and downs of this project.

Many *C. elegans* strains used in this study were obtained from the laboratories of Dr. Andrew Dillin (University of California, Berkeley) and Dr. John Kim (Johns Hopkins), and from the *Caenorhabditis* Genetics Center (University of Minnesota), which is supported by the NIH Office of Research Infrastructure Programs (P40 OD010440). S.S. was supported by the Rackham Conference Travel Grant and the Department of Molecular and Integrative Physiology (MIP) Graduate Education Fund to present the findings of this study in four international meetings. This study was supported by grants from the National Institute of Aging, NIH and the Ministry of Science and Technology of Taiwan awarded to A-L. H.

TABLE OF CONTENTS

LIST OF FIGURES

LIST OF TABLES

LIST OF ABBREVIATIONS

AMPK	AMP-activated Protein Kinase
ChIP-qPCR	Chromatin Immunoprecipitation–Quantitative Polymerase Chain Reaction
DANPOS	Dynamic Analysis of Nucleosome Position and Occupancy by Sequencing
DAVID	Database for Annotation, Visualization and Integrated Discovery
DHIC	DDL-1-containing HSF-1 Inhibitory Complex
EMSA	Electrophoretic Mobility Shift Assay
ETC	Electron Transport Chain
FCCP	Carbonyl cyanide-4-(trifluoromethoxy)phenylhydrazone
FDR	False Discovery Rate
GO	Gene Ontology
HG	High-Growth medium
HSB-1	Heat Shock factor Binding protein 1
HSE	Heat Shock Element
HSF-1	Heat Shock Factor 1 (in *C. elegans*)
HSF1	Mammalian Heat Shock Factor 1
HSP	Heat Shock Protein

HSR	Heat Shock Response
IGF-1	Insulin-like Growth Factor 1
MNase	Micrococcal Nuclease
mtDNA	Mitochondrial DNA
NAD	Nicotinamide Adenine Dinucleotide
NGM	Nematode Growth Medium
NGS	Next Generation Sequencing
OASIS	Online Application for Survival Analysis
OCR	Oxygen Consumption Rate
PCA	Principal Component Analysis
PI3K	Phosphatidylinositol 3-Kinase
POLRMT	Mitochondrial RNA Polymerase
PTM	Post-Translational Modification
RNAi	Ribonucleic acid interference
ROS	Reactive Oxygen Species
RT-PCR	Reverse Transcription Polymerase Chain Reaction
SPTF-3	Specificity Protein Transcription Factor 3
TFAM	Mitochondrial Transcription Factor A
TOR	Target of Rapamycin
UPR^{mt}	Mitochondrial Unfolded Protein Response
UTR	Untranslated Region

ABSTRACT

Signaling pathways that are involved in stress resistance have often been implicated in the regulation of the rate of aging in normal physiological conditions. The evolutionarily conserved transcription factor heat shock factor 1 (HSF-1) provides protection to animals from a multitude of environmental stresses. In addition, overexpression of HSF-1 promotes longevity in the nematode worm *Caenorhabditis elegans* also in non-stressed conditions. Previous studies have shown that a negative regulator of HSF-1, termed as heat shock factor binding protein 1 (HSB-1), physically binds to HSF-1 and limits its transactivation potential. Genetic ablation of *hsb-1* induces a robust *hsf-1*-dependent life span extension in worms via mechanisms that are less understood. In this study, we show that ablation of *hsb-1* results in an altered transactivation status of the HSF-1 protein. In *hsb-1* null animals, HSF-1 shows increased binding to its genomic target sequences. However, the transcriptome of *hsb-1* null animals is largely distinct from that of HSF-1 overexpressing worms. While HSF-1 overexpression induces large-scale transcriptional upregulation in *C. elegans*, HSB-1 inhibition alters the expression of a much smaller number of genes, but still produces a similar life span extension as in HSF-1 overexpressing worms. Roughly half of the differentially regulated transcriptome in *hsb-1* null animals overlaps with that of worms overexpressing HSF-1, and these genes show a strongly correlated expression pattern in the two long-lived strains. Genes that are upregulated via both HSB-1 inhibition and

HSF-1 overexpression include many longevity-promoting transcriptional targets of the *C. elegans* FOXO homolog DAF-16. Overall, this suggests that HSB-1 acts as a selective regulator of HSF-1 transactivation potential and hence, inhibition of HSB-1 results in change in expression of a subset of HSF-1 target genes that are potentially involved in longevity determination in animals.

In addition to the characterization of transcriptional changes associated with HSB-1 inhibition in worms, we also performed an unbiased RNAi-based screen to identify genetic suppressors of HSB-1 associated longevity. We found that knockdown of several histone H4-coding genes can completely suppress the life span extension phenotype in *hsb-1* null animals. Worms lacking HSB-1 have elevated H4 protein levels in somatic tissues during development, while H4 overexpression in wild-type worms is sufficient to extend their life span. In *hsb-1* null animals, elevated H4 levels induce reduced MNase-accessibility of both nuclear chromatin and mitochondrial DNA (mtDNA). This results in an H4-dependent reduction in expression of mtDNA-encoded genes and lower respiratory capacity in *hsb-1* null worms, which leads to a mitochondrial unfolded protein response (UPR^{mt})-dependent life span extension. We further show that extranuclear histone H4 is present in mitochondria of intestinal tissue in *C. elegans*. This suggests a novel and unexpected role of histone H4 in regulating mitochondrial gene expression via directly modulating the accessibility of mtDNA. Moreover, our findings show interplay between three distinct cellular processes – stress resistance, chromatin dynamics and mitochondrial function – that were previously known to promote longevity in animals via seemingly independent mechanisms. In summary, this study has identified several novel HSF-1-mediated signaling interactions

in *C. elegans* that have significantly broadened our understanding of how HSB-1/HSF-1 pathway regulates organismal life span in normal physiological conditions. Our findings will potentially guide the design of targeted therapies to selectively modulate the function of HSF-1 in order to delay the progression of aging and age-related diseases in metazoans.

Chapter 1. Introduction

Aging and the regulation of longevity in animals

The world's population is aging. The global mean life expectancy at birth (in years) has increased from 53 in 1960 to 72 in 2016, and it is projected to surpass 82 by the end of the twenty-first century (United Nations Department of Economic and Social Affairs, 2017). As a result, the number of people over the age of 60 is growing steadily at a rate of approximately 3% every year. In 2017, the worldwide population aged 60 years and above was estimated to be 962 million. This number is expected to more than double to 2.1 billion by the year 2050 and more than triple to 3.1 billion by the year 2100 (United Nations Department of Economic and Social Affairs, 2017). This global increase in life expectancy can be attributed to commendable progress in medical research with regard to finding better cures to infectious diseases, and to the success of public health campaigns focused on vaccinations and improved household hygiene. However, this increase in life span of humans has not been accompanied by a corresponding increase in health span, i.e. the number of healthy years in one's lifetime. In the United States, more than half the population over the age of 65 suffer from two or more age-related chronic conditions that include cardiovascular disease, cancer, Alzheimer's disease, diabetes mellitus, kidney disorders etc. (Escoubas et al., 2017; Stroustrup, 2018). In 2016, these five non-communicable disease categories were among the ten leading

causes of death for people aged 65 and over in the United States and constituted more than half of all deaths in this age group (Heron, 2018).

The National Institute of Health spends billions of dollars every year to find cures for these age-related diseases so that the quality of health in the elderly can be improved. However, the high prevalence of multiple comorbidities in older individuals makes it difficult to increase health span by targeting only a few impact diseases. For example, finding a cure to cardiovascular diseases or all forms of cancer will merely add four years to human life span, as these individuals will still be susceptible to other competing causes of death due to old age (Mackenbach et al., 1999). The field of geroscience has tried to address this conundrum via searching for causes that lead to a simultaneous increase in vulnerability to multiple age-related diseases in older individuals.

Only in the past two decades, the biogerontology research community has reached consensus on aging being a genetically regulated process. Previously, aging was considered to be accumulation of molecular, cellular and organ damage due to metabolic ‘wear and tear’ that leads to an increased vulnerability to diseases (Weinert and Timiras, 2003). However, comparative studies have shown enormous diversity in the animal kingdom in terms of maximum life span (Cohen, 2018). The mayfly *Dolania americana* lives for less than an hour, and has the shortest known adult life span among insects (Welch, 1998). In contrast, the American lobster (*Homarus americanus*) lives for 100 years and is possibly the longest-lived arthropod (De Magalhães and Costa, 2009). In the order Rodentia, the house mouse (*Mus musculus*) has a maximum life span of

four years in captivity, while the evolutionarily related naked mole-rat (*Heterocephalus glaber*) lives for up to 32 years (Van Meter et al., 2015). Among vertebrates, the Greenland shark (*Somniosus microcephalus*) possibly has the longest life span of 500 years (Nielsen et al., 2016), while certain invertebrates such as hydra (*Hydra vulgaris*) and sea squirt (*Botryllus schlosseri*) are practically immortal (Martínez, 1998; Rinkevich, 2017).

Moreover, mortality curves have widely different shapes across the animal kingdom, suggesting lack of common evolutionary constraints that determine vulnerability to death in all organisms (Cohen, 2018; Jones et al., 2014). Intriguingly, mortality in the wild shows constant, increasing or decreasing trajectories across age in both short- and long-lived species (Jones et al., 2014). In laboratory conditions, numerous environmental, genetic and pharmacological interventions have been successful in extending the life span of model organisms ranging from the budding yeast (*Saccharomyces cerevisiae*) to mammals (Fontana et al., 2010). In this chapter, I will provide a brief overview of the signaling pathways and cellular processes that regulate longevity in animals across evolutionary taxa.

C. elegans as a model to study longevity regulation

Aging experiments are time-consuming and expensive to perform. This has led to the use of several short-lived invertebrate model organisms for discovery of evolutionarily conserved longevity-regulating pathways (Fontana et al., 2010). The most widely used invertebrate animals in laboratories include the fruit fly *Drosophila melanogaster* and the nematode worm *Caenorhabditis elegans*. Both models are genetically tractable,

possess all major tissue subtypes (except the skeletal system) and have relatively short life spans of 2–3 weeks for worms and 2–3 months for flies. However, worms require much lower maintenance effort in laboratory conditions and hence are very popular for large-scale screens. In addition, *C. elegans* strains can be stored frozen in liquid nitrogen for long periods of time and can be revived even up to a few decades later. Due to its transparent body, fluorescent-labeled proteins targeted to any subcellular compartment can be visualized in the live worm. Other major benefits of using *C. elegans* include its small size (~1 mm in length), free-living nature (non-parasitic), rapid life cycle (egg to adult in 3 days at 20°C), large brood size (up to 300 eggs per individual) and a fully-annotated genome. In laboratory conditions, they are normally grown on agar plates and fed with the bacterium *Escherichia coli*, though worms have also been shown to grow in various anexic media (Flavel et al., 2018).

C. elegans was the first multicellular organism to have its entire genome sequenced (The *C. elegans* Sequencing Consortium, 1998). Its genome size is ~100 million base pairs and encodes more than 20,000 protein-coding genes. In addition, the *C. elegans* genome contains at least 20,000 genes that encode functional non-coding RNA (ncRNA) transcripts, such as ribosomal RNA (rRNA), transfer RNA (tRNA), microRNA (miRNA), small nuclear RNA (snRNA), Piwi-interacting RNA (piRNA) etc. Depending on the particular bioinformatics approach used, roughly 60–80% of human genes are known to have orthologs in the *C. elegans* genome (Kaletta and Hengartner, 2006). In worms, depletion of gene function can be conveniently achieved via feeding them with bacteria that produce double-stranded RNA (dsRNA) corresponding to the gene of interest. Incidentally, *C. elegans* was the first multicellular organism in which a

single gene mutation was shown to significantly extend life span (Klass, 1983). Even though the life spans of worms and humans have a ~1,500-fold difference in magnitude, the age-associated increase in mortality shows a similar pattern in both species (Goto, 2015). In the subsequent sections, I will discuss different genetic pathways that have been shown to extend life span in multiple model organisms, with particular emphasis on discoveries made in *C. elegans*.

Signaling pathways involved in regulation of longevity in animals

The novel findings included in Chapters 2 and 3 of this dissertation primarily focus on the roles of the master stress regulator protein heat shock factor 1 (HSF-1) in regulation of longevity in *C. elegans*. In this section, I will provide a brief overview of various evolutionarily conserved aging-related signaling pathways, some of which interact with HSF-1 to induce their longevity-promoting effects. Modulation of several of these pathways via genetic or pharmacological approaches has been shown to be sufficient to extend life span in animals, indicating a direct role of these pathways in regulation of organismal longevity. In addition to these genetic mechanisms of life span regulation, dietary restriction is the most well-documented environmental manipulation that delays aging in organisms ranging from yeasts to primates (Fontana et al., 2010). This intervention primarily involves a reduction in food intake while avoiding starvation. Some of the signaling pathways discussed in this section are required for mediating the beneficial effects of dietary restriction on longevity of animals (Fontana and Partridge, 2015).

Insulin/IGF-1-like signaling pathway

The insulin/insulin-like growth factor 1 (IGF-1)-like signaling pathway is evolutionarily conserved from worms to humans. While mammals have different receptors for insulin and IGF-1 ligands, *C. elegans* and *Drosophila* have one primitive ortholog each that acts as the sole receptor in this pathway. Binding of insulin-like ligands to this receptor elicits the activation of phosphatidylinositol 3-kinase (PI3K), which stimulates the production of phosphatidylinositol (3,4,5)-trisphosphate (PIP3). PIP3 binds to the serine/ threonine kinase Akt, also known as protein kinase B (PKB), and induces its activation. The activated Akt kinase phosphorylates the transcription factor FOXO and inactivates it, thus suppressing the expression of FOXO target genes in animals. The first evidence of the role of insulin/IGF-1-like signaling pathway in longevity determination was found in *C. elegans*. A hypomorphic mutation in the insulin/IGF-1-like receptor homolog *daf-2* gene doubles the life span of worms (Kenyon et al., 1993). Moreover, this life span extension can be completely suppressed via genetic ablation of *daf-16* (Kenyon et al., 1993), the sole FOXO homolog in *C. elegans*. The intestinal tissue has a major role in mediating the longevity effects of suppressed insulin/IGF-1-like signaling pathway in *C. elegans*, as reintroduction of DAF-16 in the intestine is sufficient to extend the life span of *daf-16(-); daf-2(-)* double mutant worms (Libina et al., 2003). In flies, mutations in *InR*, the sole insulin-like receptor in *Drosophila*, or *chico*, an insulin receptor substrate protein, induce robust life span extension (Clancy et al., 2001; Tatar et al., 2001). Moreover, loss of the insulin-like peptide ILP2 promotes longevity in flies (Grönke et al., 2010). Overexpression of FOXO in the adult fat body has also been shown to be sufficient to extend life span in both male and female flies (Giannakou et al., 2004;

Hwangbo et al., 2004). In mice, homozygous genetic ablation of the insulin-like growth factor 1 receptor gene *Igf1r* results in embryonic lethality, but heterozygous *Igfr1*$^{+/-}$ female mice are 33% longer-lived than their wild-type littermates (Holzenberger et al., 2003). Interestingly, though IGF-1 signaling is impaired in these animals, *Igfr1*$^{+/-}$ mice do not develop dwarfism and show no major abnormalities in energy metabolism, fertility or reproduction. Also, fat-specific insulin receptor knockout (FIRKO) mice show reduced fat mass and increased median life span in both sexes (Blüher et al., 2003). In addition to these findings, many other studies have also manipulated insulin/IGF-1-like signaling using multiple approaches to show the evolutionarily conserved role of this signaling pathway in longevity determination.

Reduced insulin/IGF-1-like signaling pathway has been shown to involve the transcription factor HSF-1 to mediate its longevity promoting effects in organisms. The long-lived phenotype of *daf-2* mutant animals can be completely suppressed via knockdown of *hsf-1* in worms (Hsu et al., 2003; Morley and Morimoto, 2004). On the other hand, life span extension associated with increased *hsf-1* expression in worms is dependent on the activity of DAF-16, the sole FOXO homolog in *C. elegans* (Hsu et al., 2003). DAF-16 and HSF-1 share numerous transcriptional targets that are known to have life span-regulating roles in worms (Hsu et al., 2003; Morley and Morimoto, 2004). Moreover, insulin/IGF-1-like signaling has been shown to promote the sequestration of HSF-1 in a multiprotein complex that inhibits its transcriptional activation potential (Chiang et al., 2012). Hence, other than DAF-16/FOXO, HSF-1 is one of the key transcription factors that mediates the longevity-promoting transcriptional profile in animals with reduced insulin/IGF-1-like signaling.

Target of rapamycin (TOR) signaling pathway

The TOR protein is a serine/threonine kinase that is activated in response to nutrient and energy availability. TOR is the target of the drug rapamycin that has been shown to promote longevity in multiple species (Bjedov et al., 2010; Harrison et al., 2009; Robida-Stubbs et al., 2012). TOR forms two distinct multiprotein complexes, known as TOR complex 1 (TORC1) and TOR complex 2 (TORC2). In response to energy and growth signals, TORC1 phosphorylates several well-characterized substrates to promote protein translation. TORC1-mediated phosphorylation activates the ribosomal protein S6 kinase (S6K), which is involved in translation initiation, while TORC1 inhibits the eukaryotic translation initiation factor 4E-binding protein (4E-BP), a translation inhibitor. Inhibition of TOR1 or the S6K homolog Sch9 extends both chronological and replicative life span in budding yeast (Fabrizio et al., 2001; Kaeberlein et al., 2005; Powers et al., 2006). In *C. elegans*, inhibition of the TOR pathway via RNAi-mediated knockdown of the TOR homolog *let-363* or genetic ablation of the raptor (regulatory associated protein of TOR) homolog *daf-15* induces a robust extension of life span (Jia et al., 2004; Vellai et al., 2003). In addition, reducing the levels of *rsks-1*, the homolog of S6K, is sufficient to promote longevity in worms (Hansen et al., 2007; Pan et al., 2007). In *Drosophila*, inhibition of TOR or S6K using genetic or pharmacological approaches results in increased life span (Bjedov et al., 2010; Kapahi et al., 2004). In addition, ubiquitous overexpression of an activated form of Thor, the *Drosophila* ortholog of 4E-BP, is sufficient to promote longevity in flies (Zid et al., 2009). Genetic ablation of the S6K-encoding gene *Rps6kb1* induces up to 19% increase in median life span of female mice (Selman et al., 2009). The *Rps6kb1*$^{-/-}$ mice have better immunity, bone density, motor

coordination and insulin sensitivity than their wild-type counterparts at old age. Moreover, multiple studies have shown that the beneficial effects of dietary restriction on longevity are mediated via inhibition of the TOR signaling pathway in yeast, worms, flies and mammals (Fontana et al., 2010). Interestingly, similar to insulin/IGF-1-like signaling, life span extension associated with inhibition of the TOR pathway is also mediated via activation of HSF-1, at least in *C. elegans*. Increased life span due to *rsks-1*/S6K mutation or rapamycin treatment is completely suppressed via inhibition of HSF-1 activity in worms (Seo et al., 2013). In addition, reduced TOR signaling is associated with elevated expression of several transcriptional targets of HSF-1, some of which directly contribute to the longevity phenotype of *rsks-1(-)* animals (Seo et al., 2013).

AMP-activated protein kinase (AMPK) signaling pathway

The evolutionarily conserved AMPK protein is activated in conditions when the ratio of AMP:ATP is high. Hence, this kinase acts as a sensor of cellular energy levels. AMP:ATP ratio increases with age in *C. elegans* and has been shown to be strongly correlated with life expectancy (Apfeld et al., 2004). Reduction in levels of the AMPK homolog AAK-2 shortens life span, while increased AMPK activity enhances stress resistance and promotes longevity in worms (Apfeld et al., 2004; Greer et al., 2007). In addition, life span extension induced via some, but not all, forms of dietary restriction is dependent on the activity of AAK-2 (Greer and Brunet, 2009). In *Drosophila*, genetic manipulations of the AMP synthesis pathway to increase AMP:ATP ratios induces an *AMPKα*-dependent life span extension in both males and females (Stenesen et al., 2013). Moreover, *AMPKα* overexpression in adult fat body or adult muscle tissue is sufficient to prolong life span of female flies (Stenesen et al., 2013). Though AMPK

signaling has been implicated in several age-associated processes (Burkewitz et al., 2016), the sufficiency of AMPK activation to promote longevity is yet to be conclusively demonstrated in mammals. Interestingly, AMPK and HSF1 have an antagonistic relationship in the context of cellular stress response. In mammalian cells, HSF1 activation during heat stress inhibits AMPK, while AMPK activation during metabolic stress suppresses the activity of HSF1 (Dai et al., 2015). Nonetheless, HSF1 and AMPK are not known of interact in the context of longevity regulation in animals.

Nicotinamide adenine dinucleotide (NAD^+)/Sirtuin pathway

Sirtuins are a class of enzymes that primarily act as nicotinamide adenine dinucleotide (NAD^+)-dependent deacetylases, in addition to their many other cellular functions. Overexpression of *SIR2* extends replicative life span in some wild-type strains of yeast (Kaeberlein et al., 1999). Moreover, increased gene dosage of *sir-2.1* and *Sir2* have also been shown to promote longevity in *C. elegans* and *Drosophila*, respectively (Rogina and Helfand, 2004; Tissenbaum and Guarente, 2001). Intriguingly, a later study indicated that the previously reported life span extension due to sirtuin overexpression in worms and flies was due to genetic background effects (Burnett et al., 2011). However, the sufficiency of increased sirtuin activity to promote longevity in invertebrate model organisms was reestablished in subsequent studies. Overexpression of *Sir2* only in the adult fat body, but not in other tissues, was shown to be sufficient for life span extension in both male and female flies (Banerjee et al., 2012). In addition, *sir-2.1* overexpressing worms were reported to be 25% longer-lived than isogenic controls (Mouchiroud et al., 2013). NAD^+ levels decline with age in worms and increasing NAD^+ levels via genetic or pharmacological approaches is sufficient to extend *C. elegans* life

span in a *sir-2.1*-dependent manner (Mouchiroud et al., 2013). Moreover, overexpression of *Naam*, a nicotinamidase involved in NAD^+ metabolism, promotes longevity in *Drosophila* in a *Sir2*-dependent manner (Balan et al., 2008).

In contrast to invertebrates, mammals have seven sirtuins, namely SIRT1–7. Brain-specific *Sirt1*-overexpressing (BRASTO) mice show an ~11% increase in median life span (~16% in females and ~9% in males) and have delayed onset of cancer-induced deaths (Satoh et al., 2013). In addition, ubiquitous overexpression of *Sirt6* prolongs the mean life span of male mice by ~10–15%, but has no significant effect on the life span of female mice (Kanfi et al., 2012). A subsequent study showed that supplementation of diet with the NAD^+ precursor nicotinamide riboside (NR) increases NAD^+ concentrations, improves mitochondrial function in muscle stem cells, and induces a slight, but significant, extension of mean life span in mice (Zhang et al., 2016). Interestingly, some of the beneficial effects of NR supplementation in mice were not observed after knocking out SIRT1 in muscle stem cells (Zhang et al., 2016). These findings collectively indicate an evolutionarily conserved role of the NAD^+/Sirtuin pathway in longevity regulation from yeast to mammals. In mammals, SIRT1 has been shown to deacetylate HSF1 at lysine 80 (K80) residue, which regulates the activation status of HSF1 during heat shock response (Westerheide et al., 2009). K80-acetylated HSF1 has reduced DNA binding activity, while SIRT1-mediated deacetylation of HSF1 maintains it in a DNA binding-competent state (Westerheide et al., 2009). Intriguingly, sirtuins are not known to regulate HSF1 activity in the context of life span regulation in animals.

Table 1. Orthologs of some genes involved in longevity regulation across species.

Protein encoded	Human (*Homo sapiens*)	Mouse (*Mus musculus*)	Fruit fly (*Drosophila melanogaster*)	Nematode worm (*Caenorhabditis elegans*)
Insulin-like growth factor 1 (IGF-1) receptor	*IGF1R*	*Igf1r*	*InR*	*daf-2*
Forkhead box O (FOXO) 3 transcription factor	*FOXO3*	*Foxo3*	*foxo*	*daf-16*
Mechanistic target of rapamycin (TOR) kinase	*MTOR*	*Mtor*	*Tor*	*let-363*
Ribosomal protein S6 kinase	*RPS6KB1*	*Rps6kb1*	*S6k*	*rsks-1*
AMP-activated protein kinase (AMPK) alpha 2 catalytic subunit	*PRKAA2*	*Prkaa2*	*AMPKα*	*aak-2*
Sirtuin	*SIRT1*	*Sirt1*	*Sir2*	*sir-2.1*
Beclin 1 or Autophagy-related gene (ATG) 6	*BECN1*	*Becn1*	*Atg6*	*bec-1*
Heat shock factor 1	*HSF1*	*Hsf1*	*Hsf*	*hsf-1*

Cellular processes that regulate longevity in animals

In addition to the signaling pathways described in the previous section, many other cellular processes have also been shown to regulate the rate of aging in organisms. Some of these processes act downstream of signaling pathways such as insulin/IGF-1-like signaling, TOR signaling, etc., while others act independently to promote longevity. Here, I will provide a brief summary of some of these cellular processes that have been shown to be evolutionarily conserved hallmarks of aging. For the sake of brevity, I will primarily focus on discoveries pertaining to life span extension in *C. elegans*, while also introducing some key findings from other species.

Stress resistance, proteostasis imbalance and aging

Organisms have evolved several mechanisms to counteract the disruption of protein homeostasis induced in the presence of various forms of environmental stresses. Interestingly, many of these cellular processes have also been shown to extend life span even in the absence of stress (Epel and Lithgow, 2014; Rodriguez et al., 2013). Low doses of stress have been shown to promote longevity in animals potentially via activating adaptive responses. For example, treating worms with low concentrations of the reactive oxygen species (ROS)-producing compound juglone results in a DAF-16 and SIR-2.1-dependent extension of life span in worms (Heidler et al., 2010). These worms show increased expression of stress response targets of DAF-16 such as the superoxide dismutase protein SOD-3 and the small heat shock protein HSP-16.2 (Heidler et al., 2010). Intriguingly, overexpression of the ROS-scavenging enzyme SOD-1 elevates protein oxidation in worms and induces life span extension that is partially dependent on DAF-16 and HSF-1 (Cabreiro et al., 2011). Oxidative stress in organisms has also been shown to activate the Jun N-terminal kinase (JNK) signaling pathway. Interestingly, activation of JNK signaling is sufficient to extend life span in *Drosophila* even in the absence of oxidative stress (Wang et al., 2003). Similarly, overexpression of *jnk-1* in normal physiological conditions promotes longevity in *C. elegans* (Oh et al., 2005).

Components of the hypoxia response pathway have also been shown to be involved in the regulation of longevity in worms. Stabilization of hypoxia-induced factor 1 (HIF-1) via depletion of its negative regulator von Hippel–Lindau tumor suppressor homolog VHL-1 improves resistance to protein aggregation disorders and extends life

span in *C. elegans* (Mehta et al., 2009). With regard to heat stress, increased activity of the heat shock response transcription factor *hsf-1* slows the age-related progression of protein aggregation diseases and extends life span in *C. elegans* via increasing expression of small heat shock proteins (HSPs) (Hsu et al., 2003; Morley and Morimoto, 2004). A later study showed that the improved thermotolerance and extension of life span in *hsf-1* overexpressing worms is due to increased activity of the troponin-like calcium-binding protein PAT-10 that preserves actin cytoskeletal integrity (Baird et al., 2014). Moreover, *hsf-1* is required for protection against age-associated proteotoxicity and increased longevity in worms subjected to food deprivation (Steinkraus et al., 2008). Introducing extra copies of HSF-1 target genes, such as *hsp-16* in *C. elegans* and *hsp70* in *Drosophila*, has been shown to be sufficient to extend the life span of these animals after a brief exposure to mild heat shock (Tatar et al., 1997; Walker and Lithgow, 2003). The role of heat shock factor in longevity regulation is described in detail later in this chapter.

Mitochondrial function and aging

Mild disruption to mitochondrial activity using genetic or pharmacological approaches has been shown to promote longevity in multiple model organisms. In *C. elegans*, a hypomorphic mutation in *isp-1*, a nuclear gene encoding a Rieske iron-sulfur protein of the mitochondrial electron transport chain (ETC) complex III, induces robust increase in life span of animals (Feng et al., 2001). Subsequently, two simultaneous studies showed that RNAi-mediated knockdown of several nuclear genes encoding components of ETC complexes I, III, IV and V result in inhibition of respiration and extension of life span in worms (Dillin et al., 2002; Lee et al., 2002). Importantly, the extent of

mitochondrial inhibition influences *C. elegans* longevity in a non-linear manner. Mild knockdown of respiratory genes has no effect on life span, moderate knockdown produces a dose-dependent life span extension, while life span is shortened after strong RNAi inhibition (Rea et al., 2007). Follow-up studies in *Drosophila* also confirmed that knockdown of components of ETC complexes I, III, IV and V promote longevity in flies (Copeland et al., 2009). In mice, heterozygous inactivation of *Mclk1* (also known as *Coq7*), a gene that encodes a mitochondrial hydroxylase involved in ubiquinone biogenesis, results in significant extension of life span in three different genetic backgrounds (Liu et al., 2005). Moreover, genetic ablation of *Surf1*, a gene encoding a mitochondrial inner membrane protein involved in ETC complex IV assembly, induces a robust increase in life span of both male and female mice (Dell'Agnello et al., 2007).

Interestingly, inhibition of mitochondrial function during animal development seems to be essential to achieve increased longevity, at least in worms (Dillin et al., 2002). Similarly, RNAi-mediated knockdown of genes encoding subunits of ETC complexes III, IV and V (but not of complex I) only during adulthood confers minimal longevity benefits in flies, compared to the robust life span extension induced via whole-life RNAi of the same genes (Copeland et al., 2009). Furthermore, tissue-specific knockdown experiments have demonstrated the cell non-autonomous effect of mitochondrial inhibition on longevity. Knockdown of ETC genes in neurons induces mitochondrial stress response in the intestinal tissue of worms via retrograde transport-mediated Wnt signaling (Durieux et al., 2011; Zhang et al., 2018). Similarly, knockdown of ETC complex I genes in neurons alone is sufficient to promote longevity in flies (Copeland et al., 2009). At least two independent stress response pathways are known

to be activated in response to mitochondrial stress to promote longevity in organisms. In *C. elegans*, inhibition of mitochondrial respiration results in increased ROS production in animals that leads to feedback regulation between two longevity-promoting transcription factors, HIF-1 and AMPK, to extend life span (Hwang et al., 2014; Lee et al., 2010). Also, RNAi-mediated knockdown of nuclear-encoded mitochondrial proteins result in a stoichiometric imbalance between nuclear- and mtDNA-encoded subunits of ETC respiratory complexes (Houtkooper et al., 2013). This induces activation of the mitochondrial unfolded protein response (UPR^{mt}) in animals to promote longevity (Durieux et al., 2011; Merkwirth et al., 2016). This evolutionarily conserved role of UPR^{mt} in the mitochondrial longevity pathway is well-documented in both worms and mice (Houtkooper et al., 2013; Merkwirth et al., 2016).

Initial studies indicated that the life span extension due to slightly impaired mitochondrial function is not mediated via HSF-1 activation (Hsu et al., 2003). However, a recent study has shown that several forms of mitochondrial stress induce an imbalance in the protein levels of core histones (Matilainen et al., 2017). This results in increased expression of HSF-1 transcriptional targets and a life span extension phenotype that is dependent on activity of ISW-1, a chromatin remodeling factor (Matilainen et al., 2017). Chapter 3 of this dissertation includes further evidence for the interaction between HSF-1, histones and mitochondria in the context of life span determination in *C. elegans*.

Autophagy and aging

Macroautophagy, broadly known as autophagy, is an evolutionarily conserved process involved in degradation of cytosolic components in the lysosomes so that cellular macromolecules can be recycled. The first interaction between autophagy and longevity was established in a *C. elegans* study that showed the requirement of the autophagy-associated gene *bec-1*, an ortholog of mammalian beclin 1, in insulin/IGF-1-like signaling-mediated life span extension (Melendez et al., 2003). In addition, the pro-longevity effects of dietary restriction, inhibition of the TOR pathway and impaired mitochondrial respiration in worms were also found to be dependent on BEC-1 activity (Hansen et al., 2008; Tóth et al., 2008). A recent study has shown that longevity associated with hormetic heat shock or HSF-1 overexpression in *C. elegans* is mediated via activation of the autophagic response (Kumsta et al., 2017). In flies, life span extension due to rapamycin treatment is dependent on the activity of ATG5, a protein required for formation of autophagosomes (Bjedov et al., 2010). Furthermore, administration of spermidine, a natural polyamine, upregulates several autophagy genes to promote longevity in yeast, worms and flies (Eisenberg et al., 2009). Subsequent studies have demonstrated that activation of the autophagy pathway via genetic manipulation is sufficient to extend life span in organisms. Neuronal upregulation of the autophagy-specific protein kinase Atg1 in *Drosophila* improves intestinal homeostasis in a cell non-autonomous manner and prolongs life span (Ulgherait et al., 2014). Ubiquitous overexpression of Atg5 in mice results in enhanced autophagy, improved resistance to age-induced obesity and a ~17% increase in median life span compared to wild-type littermates (Pyo et al., 2013). Moreover, a recent study

showed that increased basal autophagic flux induced via activation of beclin 1 in mice results in extension of median life span in both sexes (Fernández et al., 2018). Hence, activation of components of the autophagic response seems to confer longevity-promoting effects in multiple species.

Cellular senescence and aging

Cellular senescence involves a near permanent cell cycle arrest of previously replication-competent cells and coincides with many other phenotypic changes. Senescence can be induced due to multiple factors such as shortened telomeres, accumulation of DNA damage, aberrant activation of oncogenic signaling and epigenetic derepression of the *CDKN2A* locus containing $p16^{INK4a}$ and $p19^{ARF}$ genes (He and Sharpless, 2017). In mice, the number of senescent cells increases by greater than twofold with age in multiple tissues such as liver, spleen, skin and lungs (Wang et al., 2009). Though these findings suggest that accumulation of senescent cells might directly contribute to age-associated decline in organ function, it has also been proposed that cellular senescence is a protective measure to restrict the proliferative ability of damaged cells in order to prevent their oncogenic transformation. Intriguingly, several recent studies have shown that removal of senescent cells can promote longevity in mammals. Treatment of mice with ABT263, a senolytic drug that selectively kills senescent cells, rejuvenates the aged hematopoietic and muscle stem cells in old individuals (Chang et al., 2016). Another study showed that clearance of $p16^{INK4a}$-expressing senescent cells in mice extends their median life span by 24% (Baker et al., 2016). Transplanting less than a million senescent cells in young mice accelerates their

age-associated physiological decline and results in a ~fivefold higher risk of death than age-matched control mice (Xu et al., 2018). Moreover, biweekly injections of the senolytic cocktail of dasatinib plus quercetin starting at 24-27 months of age causes selective elimination of senescent cells in old mice and increases their post-treatment survival by 36% (Xu et al., 2018). These recent findings have established that cellular senescence is a prominent hallmark of aging, at least in mammals. Interestingly, depletion of HSF1 in human fibroblasts induces cellular senescence via activation of the p53-p21 tumor suppressor pathway (Oda et al., 2018). It remains to be determined whether age-associated decline in HSF1 function contributes to the increase in number of senescent cells in older individuals.

Role of heat shock factor in longevity regulation

The heat shock response (HSR) is an evolutionarily conserved mechanism in all eukaryotic organisms. The HSR pathway responds to disruption of protein homeostasis induced by multiple environmental stressors such as heat, oxidative damage, pathogenic infection and various form of proteotoxic insults (Morimoto, 2011). In response to accumulation of misfolded proteins in the cytoplasm, HSR triggers the activation of a family of transcription factors termed as heat shock factors (HSFs) (Åkerfelt et al., 2010; Anckar and Sistonen, 2011). While yeast, worms and flies have only one member of the HSF family (Table 1), vertebrates have four different genes that encode for HSF1–4 proteins (Takii and Fujimoto, 2016). Among these HSF family members, HSF1 is the primary transcription factor responsible for the physiological response to heat shock in mammals (McMillan et al., 1998). When subjected to heat

stress, the HSF1 protein undergoes oligomerization and acquires several post-translational modifications (Chiang et al., 2012; Guettouche et al., 2005; Sarge et al., 1993). The activated HSF1 protein translocates to the nucleus and binds to specific genomic sequences termed as heat shock elements (HSEs) (Chiang et al., 2012; GuhaThakurta et al., 2002; Sarge et al., 1993). This results in transcriptional upregulation of several stress response genes that contain HSE sequences in their promoter regions (GuhaThakurta et al., 2002). The most broadly studied HSF1 transcriptional targets that are activated during heat stress belong to the family of heat shock proteins (HSPs). HSPs include a network of chaperones that are classified into five major evolutionarily conserved subfamilies: Hsp100s, Hsp90s, Hsp70s, Hsp60s and small HSPs (Richter et al., 2010). Some of the primary functions of these HSPs during heat stress are to assist in the folding of nascent polypeptides, physically sequester denatured proteins and prevent the formation of toxic protein aggregates in the cytoplasm (Richter et al., 2010). Hence, HSF1-induced expression of HSPs restores the balance of protein homeostasis and protects against the detrimental effects of a variety of stressful conditions (Figure 1).

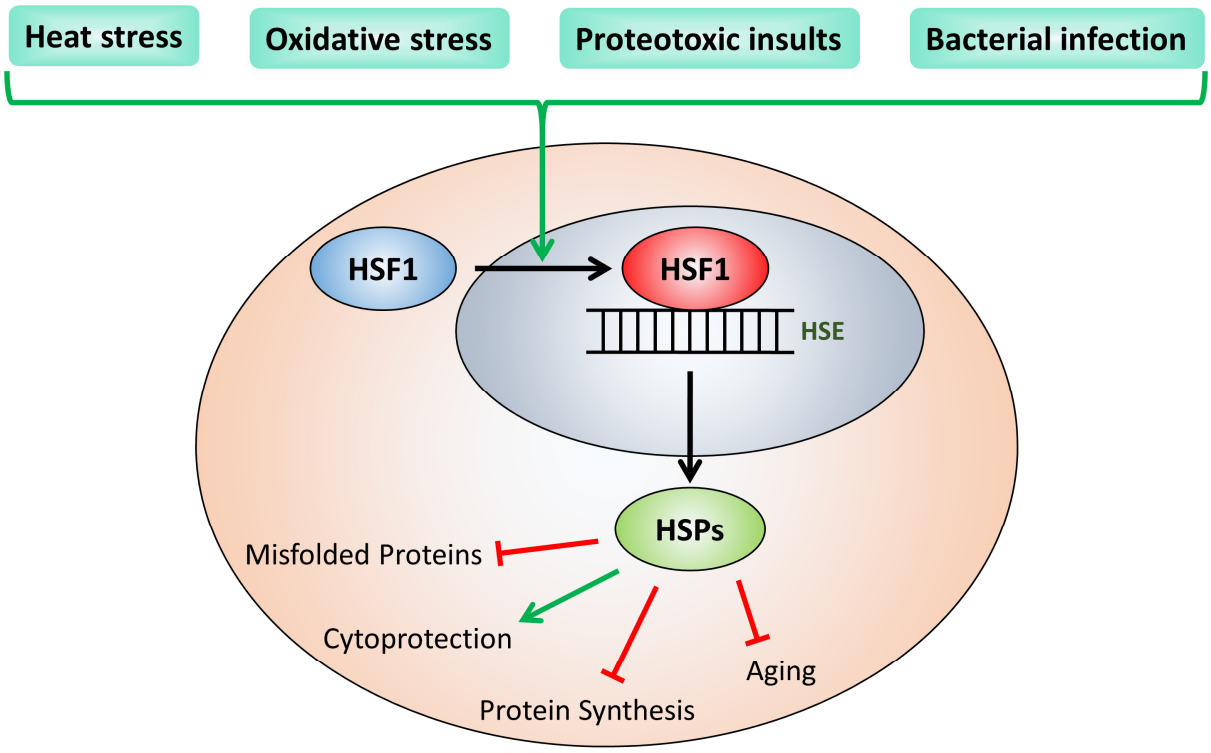

Figure 1. A schematic of the heat shock response (HSR) pathway.
In presence of multiple stress conditions, the transcription factor heat shock factor 1 (HSF1) is activated, translocates to the nucleus and binds to genomic sequences termed as heat shock elements (HSEs). This results in transcriptional activation of members of the heat shock protein (HSP) chaperone family. HSPs prevent the toxic aggregation of misfolded proteins, provide cytoprotection by chaperoning nascent polypeptides, and transiently block protein translation in presence of stressful conditions. Even in the absence of stress, activation of this pathway has been shown to delay aging and the progression of age-related diseases.

Even in the absence of environmental stress, HSF1 functions as a key regulator of longevity determination in organisms. In *C. elegans*, *hsf-1* has an essential role in mediating the life span extension associated via inhibition of the insulin/IGF-1-like signaling pathway and the target of rapamycin (TOR) signaling pathway (Hsu et al., 2003; Morley and Morimoto, 2004; Seo et al., 2013). Increased longevity associated with reduced function of the insulin/IGF-1-like receptor homolog DAF-2 in worms could be completely suppressed to wild-type life span via RNAi-mediated knockdown of *hsf-1* (Hsu et al., 2003; Morley and Morimoto, 2004). In addition, reducing HSF-1 activity also

suppresses the life span extension achieved via genetic inactivation of the worm S6K homolog *rsks-1* or via pharmacological treatment with rapamycin (Seo et al., 2013). In wild-type worms, inhibition of HSF-1 activity shortens life span, while increasing the gene dosage of *hsf-1* via overexpression is sufficient to promote longevity (Hsu et al., 2003; Morley and Morimoto, 2004). Moreover, elevated expression of stress-inducible targets of HSF-1 has been shown to extend life span in multiple organisms. Introducing extra copies of *hsp-16* in worms and of *hsp70* in flies is sufficient to increase longevity in these animals after a transient exposure to heat stress (Tatar et al., 1997; Walker and Lithgow, 2003). In mice, expression of an active form of HSF1 prolongs the median life span of the R6/2 Huntington disease model animals by ~14% (Fujimoto et al., 2005). On the other hand, the life span of HSF1 knockout mice is shortened by ~18% compared to their wild-type littermates after the brains of these animals were injected with a disease-causing prion (Steele et al., 2008). However, the HSF-1 target genes that mediate its longevity promoting effects in organisms still remain mostly undiscovered. Initial studies in *C. elegans* showed that increased longevity of *hsf-1* overexpressing worms could be partially suppressed by knockdown of small heat shock proteins (Hsu et al., 2003). The FOXO ortholog DAF-16 cooperates with HSF-1 to upregulate the expression of these small HSP genes in worms (Hsu et al., 2003). Interestingly, neural overexpression of HSF-1 induces expression of stress response genes in peripheral tissues of animals in a DAF-16-dependent manner (Douglas et al., 2015). However, a recent study showed that overexpression of a truncated form of the HSF-1 transcription factor in worms extends their life span, but it does not alter the stress-induced activation of HSPs (Baird et al., 2014). Furthermore, the increased life span of R6/2 Huntington disease model

mice was not due to increased expression of HSPs in the brain tissue (Fujimoto et al., 2005). Later evidence has suggested that a troponin-like calcium-binding protein PAT-10 has a prominent role in mediating life span extension in animals with increased HSF-1 activity (Baird et al., 2014). PAT-10 is a stress-induced transcription target of HSF-1 that is involved in maintaining integrity of the actin cytoskeleton during heat stress (Baird et al., 2014). This suggests that HSF-1-associated longevity is not solely due to increased expression of the HSP family of molecular chaperones, but it potentially also involves many other unidentified HSF-1 targets that influence additional facets of organismal physiology.

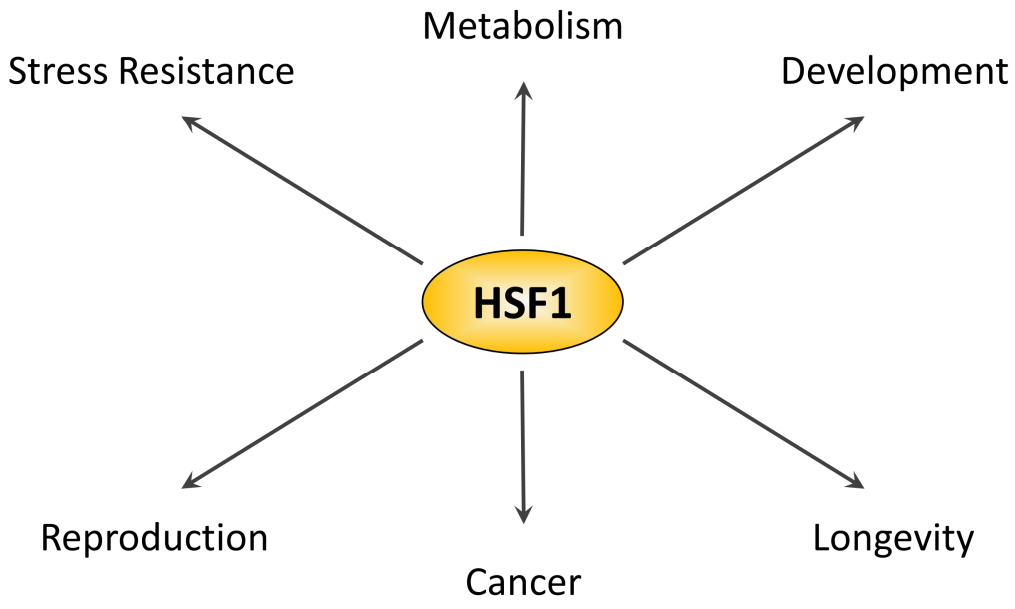

Figure 2. Different roles of the heat shock factor 1 protein in animals.
In addition to its well-characterized role in stress response, HSF1 also has important functions in multiple biological processes such as animal development, reproduction, metabolism, cancer and longevity regulation.

In addition to its roles in stress response and longevity regulation, HSF1 also has important functions in several other biological processes such as development, reproduction, metabolism and cancer (Åkerfelt et al., 2010; Gomez-Pastor et al., 2018; Li et al., 2017) (Figure 2). In *C. elegans*, HSF-1 regulates a gene network largely distinct from HSR during larval development via binding to a degenerate HSE sequence found in promoter regions of several genes (Li et al., 2016). This HSF-1-regulated developmental program requires binding of the E2F/DP transcriptional activator complex to a GC-rich motif upstream of the degenerate HSE sequence, thus promoting an HSF-1-induced activation of protein biogenesis and anabolic metabolism during early development (Li et al., 2016). Moreover, HSF-1 activates the E2 and E3 ligases of the ubiquitin proteasome system during development in *C. elegans* to induce linker cell-type death, a non-apoptotic cell death program that is also conserved in vertebrate development (Kinet et al., 2016). In *Drosophila*, HSF has essential roles in larval development and oogenesis, and surprisingly, these are not mediated via transcriptional activation of HSPs (Jedlicka et al., 1997). Homozygous *Hsf1*$^{-/-}$ mice exhibit high prenatal lethality and postnatal growth retardation, though basal expression of heat shock proteins is unaltered in these animals (Christians et al., 2000; Xiao et al., 1999). Moreover, altered HSF1 activity induces defective spermatogenesis and oogenesis in adult mice leading to infertility in both males and females (Metchat et al., 2009; Nakai et al., 2000). In the context of cellular metabolism, certain key metabolic regulators have been shown to post-translationally modify the HSF1 protein to modulate its transcriptional activation potential. SIRT1 deacetylates HSF1 to promote its DNA binding-competent active state (Westerheide et al., 2009), while the energy state-sensor

AMPK phosphorylates the Ser121 residue of HSF1 to inhibit its activation (Dai et al., 2015). Furthermore, mammalian HSF1 has a key role in promoting malignant progression of several forms of cancer. Inhibition of HSF1 suppresses carcinogen-, oncogene- or p53 mutation-induced tumor formation in mice, but without affecting intrinsic cellular growth rates (Dai et al., 2007). In human cancers, HSF1 drives a transcriptional program distinct from HSR that supports malignancy of highly metastatic forms of breast, colon and lung tumors (Mendillo et al., 2012). In summary, HSF1 function has been linked to several developmental, physiological and pathological processes in multicellular organisms, indicating that generic activation of HSF1 can potentially influence numerous biological pathways in addition to the ones being targeted.

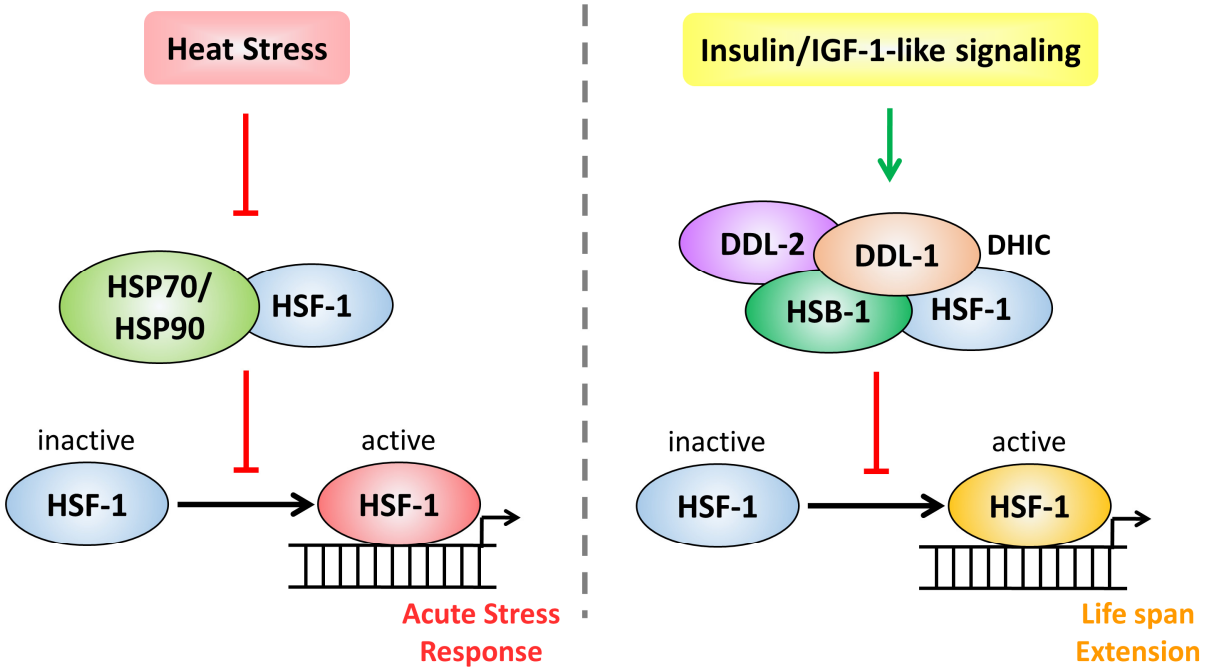

Figure 3. Mechanisms of negative regulation of HSF-1 activity.
Activity of the HSF-1 protein is regulated in different physiological contexts. In normal non-stressed physiological conditions, several large HSPs such as HSP70 and HSP90 physically bind to the HSF-1 protein to sequester it in the cytoplasm (*left*). In presence of thermal stress, this inhibition is reversed, HSF-1 protein is activated, and it induces the transcription of stress response genes. The insulin/IGF-1-like signaling pathway also regulates HSF-1 activity via

promoting the formation of the DDL-1-containing HSF-1 inhibitory complex (DHIC) (*right*). DHIC comprises of the DDL-1, DDL-2 and HSB-1 proteins that sequester HSF-1 in a multiprotein complex to inhibit its activation. Reduced insulin/IGF-1-like signaling or genetic inactivation of DHIC components result in activation of HSF-1 in normal physiological conditions that induces extension of organismal life span.

In normal physiological conditions, the activation status of the HSF1 transcription factor is regulated via its sequestration in several multiprotein complexes in a context-dependent manner. In the absence of proteotoxic stress, large multichaperone complexes physically bind to HSF1 and limit its transcriptional activation potential (Åkerfelt et al., 2010; Anckar and Sistonen, 2011; Gomez-Pastor et al., 2018). Hsp90, a large heat shock protein, sequesters HSF1 in an inactive monomeric state in unstressed cells (Zou et al., 1998). Moreover, the molecular chaperones Hsp70 and Hdj1 bind directly to the transactivation domain of HSF1 protein to prevent HSF1-induced transcriptional upregulation of stress response genes in non-stressed conditions (Shi et al., 1998). During heat-induced disruption of proteostasis , the large HSPs bind to the cytosolic pool of misfolded proteins, and this releases HSF1 for its role in mediating the stress-induced expression of protective molecular chaperones (Åkerfelt et al., 2010; Gomez-Pastor et al., 2018; Takaki and Nakai, 2016; Zou et al., 1998) (Figure 3). Hence, in the context of heat stress, HSF1 regulates its own activation status via a negative feedback loop that involves the binding and inactivation of HSF1 by its transcriptional targets. Furthermore, recent studies have demonstrated that TRiC/CCT, an ATP-dependent chaperonin complex involved in folding of cytosolic proteins, also physically binds to HSF1 and represses its activity in yeast, worms and mammalian cells (Guisbert et al., 2013; Neef et al., 2014). Interestingly, systemic knockdown of the TRiC/CCT chaperone complex selectively induces expression of HSF-1 target genes only in muscle cells of *C. elegans*, thus indicating presence of tissue-specific HSF-1 regulatory

mechanisms in multicellular organisms (Guisbert et al., 2013). Nonetheless, HSF1 is also bound by other proteins that are not components of the cellular chaperone machinery. A yeast two-hybrid protein interaction assay identified an evolutionarily conserved 76 amino acid protein, termed as heat shock factor binding protein 1 (HSBP1), that physically binds to the oligomerization domain of HSF1 and inhibits its transcriptional activation potential (Satyal et al., 1998). Subsequent studies revealed that HSB-1, the *C. elegans* homolog of HSBP1, sequesters HSF-1 in a multiprotein complex known as the DDL-1-containing HSF-1 inhibitory complex (DHIC) (Chiang et al., 2012). Interestingly, the formation of DHIC is not influenced by heat stress, but instead by the insulin/IGF-1-like signaling pathway that regulates the phosphorylation status of DDL-1 to promote sequestration of HSF-1 in DHIC (Figure 3). Inhibition of multiple DHIC components, such as HSB-1, DDL-1 and DDL-2, results in HSF-1 activation and an *hsf-1*-dependent extension of life span in *C. elegans* (Chiang et al., 2012). This indicates that a better understanding of the context-specific regulatory mechanisms of HSF-1 transactivation status is essential for the design of targeted strategies that can selectively promote the beneficial effects of HSF-1 in complex organisms (Figure 4).

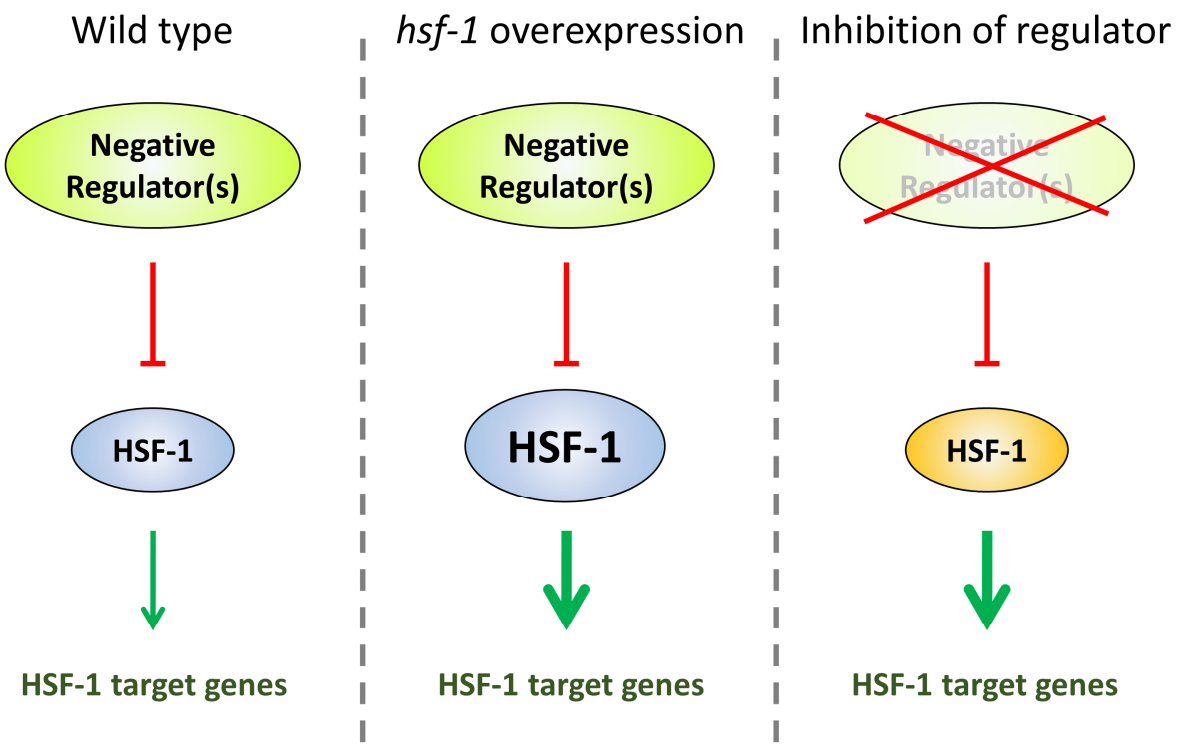

Figure 4. Approaches for non-specific versus specific activation of HSF-1 transcriptional target genes. In wild-type animals, several negative regulators bind to HSF-1 and limits its transactivation potential (*left*). Ectopically increasing the gene dosage of *hsf-1* results in altered expression of most genes that are transcriptional targets of HSF-1 (*middle*). These genes modulate several biological processes related to stress response, development, reproduction, longevity etc. HSF-1 activation can also be achieved via selective inhibition of its negative regulators (*right*). In the absence of negative regulators, HSF-1 acquires an altered transactivation potential (shown in orange). This potentially leads to a specific change in the HSF-1-regulated transcriptome, which can activate a small subset of HSF-1 target genes involved in a specific biological pathway.

Role of histones in longevity regulation

Most histones proteins share high-level of sequence similarity across species and are involved in the compaction of nuclear DNA. There are five subtypes of histones, namely H1, H2A, H2B, H3 and H4, and these subtypes have multiple variants with specialized functions (Henikoff and Smith, 2015). H2A, H2B, H3 and H4 are termed as core histones because they form the core of the nucleosome complex. Each nucleosome comprises a histone octamer of two H2A–H2B and two H3–H4 heterodimers around which ~147 bp of DNA wraps around 1.7 turns (Luger et al., 1997). Histone H1, on the

other hand, binds to the outside of the nucleosome core particle and its amino acid sequence is less conserved across species.

Post-translational modifications (PTMs) of the tails of core histone proteins influence epigenetic regulation of DNA by controlling processes such as transcription and chromatin compaction (Lawrence et al., 2016). Many of these epigenetic marks, especially the ones involving modifications of lysine (K) residues in the N-terminal tail regions of histones, have been shown to change during the process of aging in organisms ranging from yeast to humans (Benayoun et al., 2015). As a general trend, epigenetic marks involved in transcriptional repression mostly decline with age, while histone PTMs that promote gene expression are known to accumulate during organismal aging (Booth and Brunet, 2016; Sen et al., 2016) (Figure 5). For example, several repressive histone modifications such as H3K9 di- and trimethylation and H3K27 trimethylation decrease at the genome-wide level during aging in multiple organisms (Benayoun et al., 2015). In *C. elegans* somatic tissues, trimethylation of both H3K9 and H3K27 are reduced in old animals (Maures et al., 2011; Ni et al., 2012). Similarly, the proportion of total H3 protein that is dimethylated at K9 residue decreases during aging in male flies (Larson et al., 2012). Repressive marks such as H3K9 trimethylation are redistributed from heterochromatin to euchromatin regions with age in *Drosophila* and this induces transcriptional activation of numerous silenced genomic loci (Wood et al., 2010). Moreover, the global levels of H3K9 di- and trimethylation marks are reduced by ~30% during replicative aging in cultured human fibroblasts (O'Sullivan et al., 2010). On the other hand, histone PTMs such as H3K4 methylation that correspond to gene activation have been shown to accumulate with age. In the

prefrontal cortex of rhesus macaques, H3K4 dimethylation modification increases globally at promoters and enhancer-like regions during aging and this strongly correlates with more open and active chromatin (Han et al., 2012). However, these patterns are not consistent for all types of histone modifications across all organisms. A few repressive marks increase with age, certain activation marks decline with age, while some marks do not change at the global level, but instead show altered genomic loci-specific redistribution (Benayoun et al., 2015).

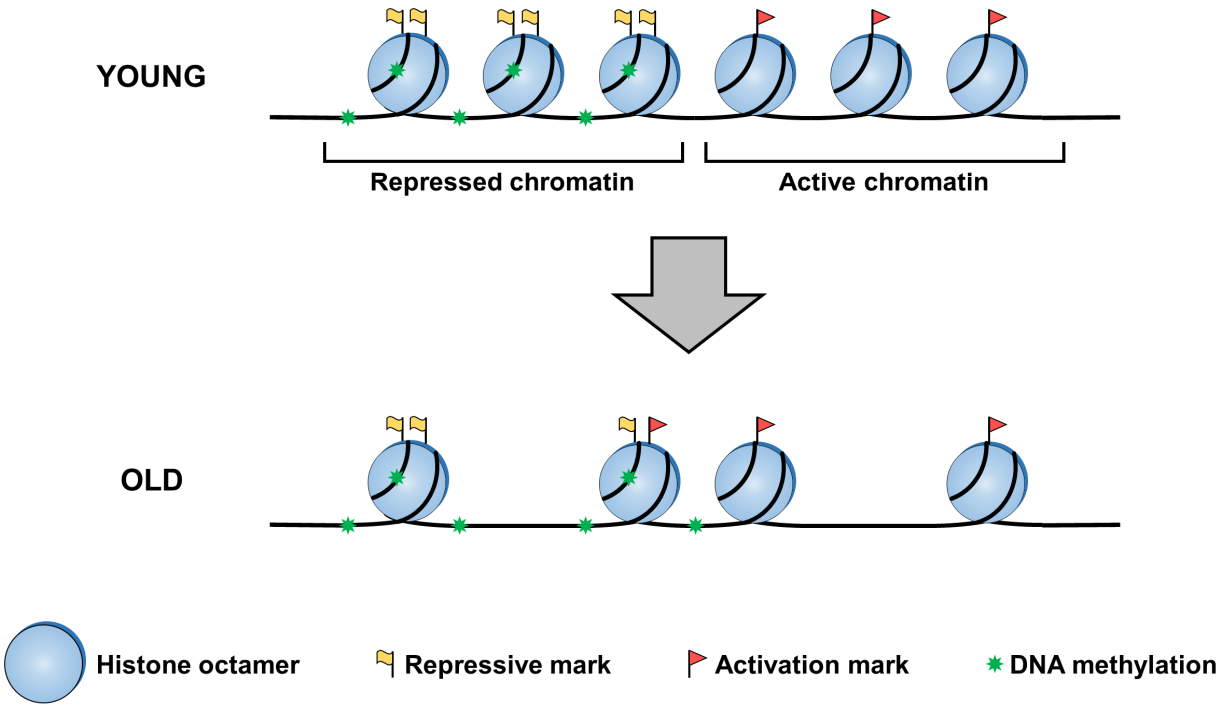

Figure 5. Changes in chromatin state during aging.
Epigenetic alterations during the process of aging include loss of histones, global reduction in repressive histone marks (such as H3K9 trimethylation), altered patterning of activating histone marks (such as H3K4 trimethylation) and DNA methylation.

Research in the past decade has shown that modulation of the activity of several histone-modifying enzymes is sufficient to promote longevity in multiple organisms. The activation mark H4K16 acetylation accumulates at subtelomeric regions in old yeast

cells (Dang et al., 2009). Overexpression of the H4K16 deacetylase *SIR2* or deletion of the H4K16 acetyltransferase *SAS2* is sufficient to extend replicative life span in yeast via modulation of H4K16 acetylation levels at subtelomeric loci (Dang et al., 2009). The H3K36 trimethylation mark is lost from certain genomic loci during replicative aging in yeast and this induces cryptic transcription of genes in old cells (Sen et al., 2015). Deletion of the H3K36 demethylase *RPH1* gene restores H3K36 trimethylation at these loci, suppresses cryptic transcription, and extends replicative life span in yeast (Sen et al., 2015). Interestingly, mitochondrial ROS-induced extension of chronological life span in yeast is achieved via inactivation of the H3K36 demethylase Rph1 specifically at subtelomeric heterochromatin regions (Schroeder et al., 2013). In *C. elegans*, the global somatic levels of H3K27 trimethylation decline with age (Maures et al., 2011). Two simultaneous studies showed that inhibition of UTX-1, an H3K27 trimethyl demethylase, increases the global levels of H3K27 trimethylation mark and extends the life span of worms by ~30% (Jin et al., 2011; Maures et al., 2011). Furthermore, genetic inactivation of the H3K4 trimethylation complex components ASH-2, WDR-5 or SET-2 induces transgenerational longevity in *C. elegans* (Greer et al., 2012). The life span extension in these animals with defective H3K4 trimethylation is dependent on the activity of RBR-2, an H3K4 trimethyl demethylase (Greer et al., 2012). In addition, deletion of *spr-5*, an H3K4 dimethyl demethylase, also induces a similar transgenerational longevity phenotype in worms (Greer et al., 2016). A recent study has shown that mild mitochondrial stress extends life span in *C. elegans* via increasing activity of two H3K27 demethylases, JMJD-1.2 and JMJD-3.1 (Merkwirth et al., 2016). Moreover, overexpression of *jmjd-1.2* or *jmjd-3.1* in worms is sufficient to prolong their life span via

activation of UPR^{mt} (Labbadia and Morimoto, 2015; Merkwirth et al., 2016). Interestingly, expression levels of the mammalian homologs of these H3K27 demethylases, *PHF8* and *JMJD3*, show strong correlation with murine life span in BXD inbred lines (Merkwirth et al., 2016). In addition to yeast and worms, the role of histone modifying enzymes in regulation of organismal life span has also been demonstrated in *Drosophila*. Male flies with a heterozygous mutation in *E(z)*, an H3K27 methyltransferase, show a ~35% reduction in global H3K27 trimethylation levels and these animals live ~33% longer than wild-type controls (Siebold et al., 2010). Furthermore, overexpression of *Su(var)3–9*, an H3K9 methyltransferase, promotes formation of heterochromatin and extends the median life span of female flies by 36% (Wood et al., 2016).

Several recent studies have indicated that in addition to histone modifications, the protein levels of histones also influence the rate of aging. During replicative aging in budding yeast, histone protein levels decline drastically resulting in a 50% reduction in nucleosome occupancy across the entire genome in old yeast cells (Feser et al., 2010; Hu et al., 2014). This induces global transcriptional activation of all yeast genes, especially the ones that are normally suppressed by nucleosome positioning over their promoter region (Hu et al., 2014). Furthermore, the loss of histones with age correlates with characteristics of increased genomic instability such as elevated levels of DNA strand breaks and large-scale chromosomal alterations (Hu et al., 2014). Similarly, an age-association reduction in protein levels of histone H3 has been reported in somatic tissues of *C. elegans* (Ni et al., 2012). A study performed in mice showed that quiescent muscle satellite cells in aged individuals have higher levels of the repressive mark

H3K27 trimethylation in the promoter region of histone genes and this correlates with reduced expression of histones with age (Liu et al., 2013). Moreover, a similar depletion of histones has also been observed during replicative aging of cultured human fibroblasts (O'Sullivan et al., 2010). Interestingly, increasing histone levels via inactivation of the histone information regulator (Hir) or co-overexpression of histone genes extends replicative life span in budding yeast (Feser et al., 2010). A recent study has shown that mild impairment of mitochondrial function in worms induces an increase in protein levels of several core histones (Matilainen et al., 2017). This results in an imbalance in histone levels that activates HSF-1 and ISW-1, a chromatin remodeling factor, to extend life span in worms (Matilainen et al., 2017). Prior to the findings from our study reported in Chapter 3 of this dissertation, supplementation of histones was not known to be sufficient to promote longevity in any multicellular organism. In summary, histone proteins are a major determinant of the rate of aging in multiple organisms. Alteration of histone levels and/or modulation of histone tail modifications can potentially be used as a strategy to extend life span in complex organisms.

Structure, function and regulation of the mitochondrial genome

Mitochondria supposedly originated over 1.5 billion years ago due to an endosymbiotic association of an α-proteobacterium with an ancestral eukaryotic cell (Dyall et al., 2004). During the course of eukaryotic evolution, hundreds of genes have translocated from the mitochondrial genome to the nuclear genome in all organisms (Timmis et al., 2004). Mitochondrial DNA (mtDNA) in *C. elegans* is similar to the human mitochondrial genome in terms of its size and gene content (Okimoto et al., 1992). Similar to

mammals, mtDNA in worms is inherited exclusively from the parent that contributes the egg. *C. elegans* mtDNA is a circular chromosome of ~13.8 kilobases, compared to the ~16.6 kilobases long circular mitochondrial genome in humans. The *C. elegans* mitochondrial genome encodes 36 genes that include: seven subunits of the mitochondrial electron transport chain (ETC) complex I (ND1, ND2, ND3, ND4, ND4L, ND5 and ND6), one subunit of complex III (cytochrome *b*), three subunits of complex IV (COI, COII and COIII), one subunit of complex V (ATP6), two mitochondrial rRNA genes (12S rRNA and 16S rRNA) and 22 mitochondrial tRNA genes (Figure 6). In comparison, the human mtDNA encodes 37 genes that include orthologs of all 36 genes encoded by the *C. elegans* mtDNA, and an additional subunit of complex V, ATP8. >90% of the mitochondrial genome has coding function; there are no introns and very few non-coding nucleotides between genes. The only sizable stretch of non-coding bases in the human and *C. elegans* mitochondrial genomes is termed as the displacement loop or D-loop, which contains the origin of replication of the heavy strand of mtDNA. In addition, promoters for transcription initiation are also located in the D-loop region of mtDNA in both worms and humans (Barshad et al., 2018).

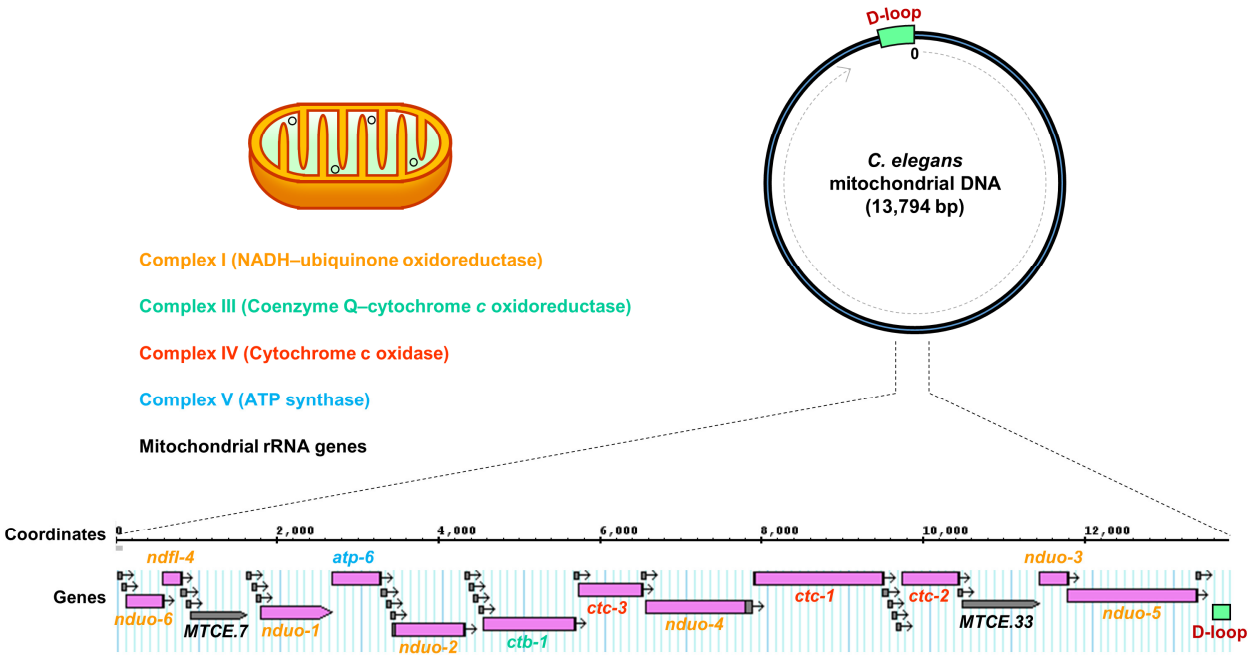

Figure 6. Structure of *C. elegans* mitochondrial DNA.
C. elegans mtDNA is a ~13.8 kb circular chromosome. The linearized form shows location of the different genes encoded by mtDNA. Genes encoding subunits of mitochondrial ETC complexes I, III, IV and V are labeled with different colors. The non-coding D-loop region is also shown. In total, mtDNA in *C. elegans* encodes twelve protein-coding genes, two mitochondrial rRNA genes, and 22 mitochondrial tRNA genes (unlabeled).

Several hundreds of nuclear-encoded proteins are required for replication, transcription and maintenance of the mitochondrial genome. Similar to the nuclear genome, mtDNA also exists in a packaged form termed as the mitochondrial nucleoid. However, unlike in nuclear chromatin, histone proteins are not conventionally known to participate in the packaging of mtDNA. The most abundant protein constituent of the mitochondrial nucleoprotein complexes is mitochondrial transcription factor A (TFAM) (Gilkerson et al., 2013; Lee and Han, 2017). Though initial studies identified TFAM as a mtDNA-specific transcription factor, recent evidence has indicated that TFAM also has an essential role in packaging of the mitochondrial genome (Kukat et al., 2015). TFAM has two high mobility group (HMG)-box domains that are involved in DNA binding. In *C. elegans*, the functional ortholog of TFAM is HMG-5, a mitochondrially-localized protein

that packages mtDNA via non-specifically coating it (Sumitani et al., 2011). In addition to TFAM, other major protein constituents of the mitochondrial nucleoid are mitochondrial single-stranded DNA-binding protein (mtSSB), mtDNA polymerase gamma (POLG), Twinkle helicase and the mitochondrial RNA polymerase (POLRMT) (Gilkerson et al., 2013; Lee and Han, 2017). POLRMT, along with two mitochondrial transcription factors, TFAM and TF2BM, constitute the three core proteins involved in mtDNA transcription. Other components of this transcription machinery include a transcription elongation factor (TEFM) and a transcription termination factor 1 (mTERF1). Interestingly, recent studies have shown the association of mtDNA with several regulators of nuclear gene expression. Proteins that were known to primarily associate with nuclear chromatin, such as cyclic AMP response element binding protein (CREB) and signal transducer and activator of transcription 3 (STAT3), have been shown to physically translocate to mitochondria and regulate mtDNA gene expression (Macias et al., 2014; Ryu et al., 2005). Moreover, DNase I footprinting studies have revealed numerous protein-DNA interaction sites in the mitochondrial genome that correspond to binding of CREB, STAT3 and many unidentified nuclear proteins (Mercer et al., 2011). Recent discoveries have further demonstrated that mtDNA has a chromatin-like organization that is altered during development and immune response, but it does not correlate with TFAM binding pattern (Blumberg et al., 2018; Marom et al., 2019). This indicates that our understanding of the higher order organization of the mitochondrial genome is far from complete, and it is much more structured *in vivo* than previously thought (Barshad et al., 2018). In Chapter 3 of this dissertation, we provide novel evidence showing that histone H4 binds to the mitochondrial genome in *C.*

elegans and regulates transcription of mtDNA-encoded genes. We further show how H4-dependent regulation of mitochondrial function plays a prominent role in mediating the pro-longevity effects of HSF-1 activation in worms.

Since somatic cells contain hundreds of copies of mtDNA, mutations in individual mtDNA molecules are not detrimental for the survival of an organism. However, if the proportion of mtDNAs with deleterious mutations becomes high due to clonal expansion in certain cells, this can result in mitochondrial dysfunction leading to several diseases affecting the nervous, cardiac and muscular systems (Larsson, 2010; Stewart and Chinnery, 2015). During aging in flies, mice and humans, mtDNA is known to accumulate mutations at a much higher rate than the nuclear genome (Bua et al., 2006; Khaidakov et al., 2003; Khrapko et al., 1997; Yui et al., 2003). To study the effect of mtDNA mutations on mammalian aging, several mouse models have been developed that accumulate mtDNA mutations faster than wild-type animals. mtDNA mutator mouse lines, which have a proofreading-deficient version of the mtDNA polymerase gamma (POLG), show accelerated aging and have a median life span of only 48–60 weeks (Kujoth et al., 2005; Trifunovic et al., 2004). These $Polg^{mut}/Polg^{mut}$ mice have a ~2,500-fold higher mtDNA mutation load compared to their wild-type littermates (Vermulst et al., 2007), and they show multiple age-related phenotypes at an early age, such as hair loss, curvature of the spine, loss of bone mass and reduced fertility (Kujoth et al., 2005; Trifunovic et al., 2004). Interestingly, the mtDNA mutation burden in the heterozygous $Polg^{+}/Polg^{mut}$ mice is ~500-fold higher than in their age-matched wild-type counterparts, but surprisingly, these animals have a normal life span (Vermulst et al., 2007). Nonetheless, not all animal models that have defective mitochondrial genome integrity

show premature aging. mtDNA deletor mice, which express a mutated form of the mitochondrial replicative helicase Twinkle, accumulate mtDNA deletions in multiple tissues (Tyynismaa et al., 2005). These mice show respiratory chain dysfunction in muscle tissue starting at one year of age. Surprisingly, this does have a detrimental effect on muscle strength, endurance capacity or life span in comparison to wild-type controls (Tyynismaa et al., 2005). Furthermore, a recent study showed that mtDNA mutations are not a major contributor to aging in *Drosophila*. Flies expressing a defective form of the mtDNA polymerase gamma accumulate high levels of mtDNA mutations. This results in impaired mitochondrial function, defective proliferation of intestinal stem cells and elevated sensitivity to mechanical and starvation stress (Kauppila et al., 2018). However, the life span of these flies is unaffected even at high levels of somatic mtDNA mutation. Interestingly, accumulation of mtDNA mutations blunts the ability of dietary restriction to promote longevity in flies (Kauppila et al., 2018). Hence, though maintenance of mitochondrial genome integrity has been shown to be essential for organismal survival, it is not clear whether mtDNA mutations that accumulate during normal aging contribute to the age-associated deterioration of organ function in animals.

Novel roles of HSB-1/HSF-1 signaling in regulation of organismal life span

Heat shock factor has been predominantly studied in the context of the evolutionarily conserved heat shock response (HSR) mechanism in eukaryotes (Anckar and Sistonen, 2011). However, recent evidence has suggested important roles of this transcription factor in other biological processes such as animal development, reproduction,

metabolism and disease progression (Åkerfelt et al., 2010; Gomez-Pastor et al., 2018; Li et al., 2017). As described previously in this chapter, increased activity of HSF-1 promotes longevity in *C. elegans* (Baird et al., 2014; Chiang et al., 2012; Douglas et al., 2015; Hsu et al., 2003; Morley and Morimoto, 2004), though the underlying mechanisms remain relatively less understood. In Chapter 2 of this dissertation, we compare the transcriptional profiles associated with HSF-1 activation achieved via increasing the gene dosage of *hsf-1* or inhibition of HSB-1, an evolutionarily conserved negative regulator of HSF-1 (Chiang et al., 2012; Satyal et al., 1998). We further show how both of these manipulations to increase HSF-1 function in worms result in activation of several longevity-promoting transcriptional targets of DAF-16/FOXO. In Chapter 3, we describe a previously unknown role of the HSB-1/HSF-1 signaling pathway in regulating histone levels and mitochondrial function. Animals with increased HSF-1 activity show elevated protein levels of histone H4, which translocates to mitochondria, binds to mtDNA and regulates expression of mtDNA-encoded genes. In summary, the novel findings included in this dissertation provide a holistic understanding of how the HSB-1/HSF-1 signaling pathway modulates numerous cellular processes to act as a key determinant of organismal longevity in non-stressed physiological conditions.

Chapter 2. HSB-1 inhibition and HSF-1 overexpression trigger overlapping transcriptional changes to promote longevity in *Caenorhabditis elegans* †

Abstract

Heat shock factor 1 (HSF-1) is a component of the heat shock response pathway that is induced by cytoplasmic proteotoxic stress. In addition to its role in stress response, HSF-1 also acts as a key regulator of the rate of organismal aging. Overexpression of HSF-1 promotes longevity in *C. elegans* via mechanisms that remain less understood. Moreover, genetic ablation of a negative regulator of HSF-1, termed as heat shock factor binding protein 1 (HSB-1), results in *hsf-1*-dependent life span extension in animals. Here we show that in the absence of HSB-1, HSF-1 acquires increased DNA binding activity to its genomic target sequence. Using RNA-Seq to compare the gene expression profiles of the *hsb-1* mutant and *hsf-1* overexpression strains, we found that while more than 1,500 transcripts show ≥1.5-fold upregulation due to HSF-1 overexpression, HSB-1 inhibition alters the expression of less than 500 genes in *C. elegans*. Roughly half of the differentially regulated transcripts in the *hsb-1* mutant have altered expression also in *hsf-1* overexpressing animals, with a strongly correlated fold-expression pattern between the two strains. In addition, genes that are upregulated via both HSB-1 inhibition and HSF-1 overexpression include numerous DAF-16 targets that

† Some of the findings from this chapter have been published in: Sural, S., Lu, T.-C., Jung, S.A., and Hsu, A.-L. (2019) HSB-1 inhibition and HSF-1 overexpression trigger overlapping transcriptional changes to promote longevity in *Caenorhabditis elegans*. G3: Genes, Genomes, Genetics *9*, 1679–1692.

have known functions in longevity regulation. We further show that the Sp1 family transcription factor SPTF-3 is required for life span extension and increased DNA binding activity of HSF-1 in *hsb-1* mutant animals. This study identifies how HSB-1 acts as a specific regulator of the transactivation potential of HSF-1 in non-stressed conditions, thus providing a detailed understanding of the role of HSB-1/HSF-1 signaling pathway in transcriptional regulation and longevity in *C. elegans*.

Introduction

Genes that are involved in stress response pathways have often been implicated in the regulation of organismal longevity in non-stressed conditions (Epel and Lithgow, 2014; Rodriguez et al., 2013). Comparative studies have shown that cellular resistance to stress is strongly correlated with maximum life span in biologically-related species (Harper et al., 2007, 2011; Kapahi et al., 1999). Heat shock response (HSR) is one such evolutionarily conserved pathway that is activated in response to various stress conditions such as heat, oxidative damage, proteotoxic insults and bacterial infections (Morimoto, 2011). In harsh environmental conditions, HSR triggers the activation of members of the heat shock factor (HSF) family of transcription factors in animals (Åkerfelt et al., 2010; Morimoto, 2011). In vertebrates, the HSF family has four members, namely HSF1–4, while yeast, *C. elegans* and *Drosophila* have a sole ortholog of HSF1 (Takii and Fujimoto, 2016). In the presence of stress stimuli, the HSF-1 protein acquires post-translational modifications (PTMs), undergoes oligomerization, translocates to the nucleus and shows increased binding to its target sequences in the genome termed as heat shock elements (HSE) (Chiang et al., 2012; Sarge et al., 1993).

Increased HSF-1 activity induces transcriptional upregulation of members of the heat shock protein (HSP) family, which function as molecular chaperones to assist in the folding of nascent polypeptides and prevent the toxic aggregation of misfolded cytosolic proteins (Richter et al., 2010). Hence, HSF-1-mediated transcriptional changes influence the survival of organisms in harsh environmental conditions via ameliorating the stress-induced loss of protein homeostasis (Hsu et al., 2003; McMillan et al., 1998).

HSF-1 has also been found to be a major determinant of organismal life span in non-stressed physiological conditions. *hsf-1* is required for life span extension associated with several longevity-regulating mechanisms, such as insulin/IGF-1-like signaling, target of rapamycin (TOR) signaling and food deprivation (Hsu et al., 2003; Morley and Morimoto, 2004; Seo et al., 2013; Steinkraus et al., 2008). In the nematode worm *C. elegans*, overexpression of *hsf-1* is sufficient to extend life span and slow the age-related progression of protein aggregation disorders, while RNAi-mediated knockdown of *hsf-1* has the opposite effects on these phenotypes (Hsu et al., 2003; Morley and Morimoto, 2004). In addition, increased expression of HSF-1 target genes has been shown to be sufficient for extension of life span in *C. elegans* and *Drosophila* in non-stressed conditions (Tatar et al., 1997; Walker and Lithgow, 2003). Initial studies reported that increased survival associated with *hsf-1* overexpression is at least partially due to transcriptional upregulation of small *hsp* genes (Hsu et al., 2003). However, a recent study showed that overexpression of a modified form of HSF-1 extended life span of animals without affecting their ability to trigger stress-induced activation of HSPs (Baird et al., 2014). Moreover, transgenic HSF-1 activation promotes survival in a neurodegenerative mouse model without inducing increased expression of HSPs in

brain tissue (Fujimoto et al., 2005). These findings suggest that life span extension associated with increased HSF-1 activity in animals is not solely due to upregulation of canonical HSR genes, but it presumably also involves transcriptional regulation of other unidentified HSF-1 targets. In addition to its role in HSR, HSF-1 has major functions in other biological processes such as development, reproduction, metabolism and cancer (Gomez-Pastor et al., 2018; Li et al., 2017). Hence, increasing the gene dosage of *hsf-1* might ectopically affect the expression of a large number of HSF-1 target genes that are not directly involved in regulation of longevity in animals.

In normal physiological conditions, the transactivation potential of HSF-1 is limited by several regulatory mechanisms that dictate the context-dependent activation status of the HSF-1 protein (Anckar and Sistonen, 2011; Gomez-Pastor et al., 2018). One such negative regulator of HSF-1 is the evolutionarily conserved heat shock factor binding protein 1 (HSB-1) (Morimoto, 1998). Direct interaction between the human homologs of HSB-1 and HSF-1 in a yeast two-hybrid screen suggested that binding of HSB-1 to the trimerization domain of HSF-1 can inhibit its transactivation potential *in vivo* (Satyal et al., 1998). In *C. elegans*, HSB-1 physically binds to HSF-1 to form an inhibitory multiprotein complex (Chiang et al., 2012; Satyal et al., 1998). Interestingly, the formation of this HSF-1-inhibitory complex is not affected by heat stress, but instead is promoted by insulin/IGF-1-like signaling (Chiang et al., 2012), an evolutionarily conserved longevity regulating pathway (Riera et al., 2016). Genetic ablation of *hsb-1* results in dissociation of HSF-1 from this inhibitory complex and induces a robust increase in life span of animals that is dependent on HSF-1 activity (Chiang et al., 2012). However, it remains elusive how the absence of HSB-1 alters the transactivation

potential of HSF-1, and thus promotes organismal longevity via potentially modifying the expression of certain HSF-1 target genes. We hypothesized that inhibition of HSB-1 influences a small subset of the HSF-1-regulated transcriptome that has a specific role in regulation of longevity in *C. elegans*. In contrast, increasing the gene dosage of *hsf-1* potentially induces transcriptional changes for a vast majority of HSF-1 target genes involved in varied biological processes. A previous study established that a sizeable proportion of the entire *C. elegans* transcriptome comprises HSR-independent downstream targets of HSF-1 (Brunquell et al., 2016). Interestingly, expression levels of most of the HSF-1-regulated genes identified in that study were not found to be significantly altered during normal aging in *C. elegans* (Brunquell et al., 2016; Budovskaya et al., 2008). This further indicates that studying the transcriptional changes associated with inhibition of HSB-1 can help in narrowing down the HSF-1 target genes that are essential for mediating the HSR-independent longevity-promoting effects of HSF-1. Though homologs of *C. elegans hsb-1* exist in genomes of all multicellular eukaryotes (Morimoto, 1998), the function of this gene in normal physiological conditions remains less explored in complex organisms (Dirks et al., 2010; Eroglu et al., 2014).

Here we show that in the absence of HSB-1 regulation, heat shock factor acquires an altered transactivation profile, which results in extensive changes to the *C. elegans* transcriptome. Genetic ablation of *hsb-1* induces increased *in vitro* DNA binding activity of the HSF-1 transcription factor similar to that observed in an HSF-1 overexpression strain, even though HSF-1 protein level is not elevated in the *hsb-1* mutant. Roughly 45% of the genes that are differentially expressed in the *hsb-1(-)* strain

also constitute a subset of the altered transcriptome in *hsf-1* overexpressing animals, but the global transcriptional changes associated with HSB-1 inhibition are distinct from that induced via overexpression of HSF-1. We further show that the subset of genes that are differentially expressed in both *hsb-1(-)* and *hsf-1* overexpressing animals have a strongly correlated expression pattern in the two strains. In addition, we have identified that the transcription factor SPTF-3 is required for life span extension and increased DNA binding activity of HSF-1 in *hsb-1(-)* animals. Overall, our findings collectively suggest that HSB-1 controls the expression of a small subset of the HSF-1-regulated transcriptome, which might be essential for mediating the longevity promoting effects of HSF-1 in normal physiological conditions.

Materials and Methods

C. elegans strains

All *C. elegans* strains used in this study were maintained at 20°C on nematode growth medium (NGM) plates seeded with *E. coli* OP50 strain using the standard method. Animals were maintained for at least three generations without starvation before they were used for experiments. The following strains were used in this study:

N2: Wild-type

EQ150: *hsb-1(cg116) IV* – CH116 outcrossed 4x to wild-type N2

CF1037: *daf-16(mu86) I*

EQ402: *daf-16(mu86) I; hsb-1(cg116) IV*

EQ140: *iqIs37*[pAH76(*hsf-1p::myc-hsf-1*) + pRF4(*rol-6p::rol-6(su1006)*)]

AGD710: *uthIs235*[(*sur-5p::hsf-1::unc-54* 3' UTR) + (*myo-2p::tdTomato::unc-54* 3' UTR)]

AGD836: *uthIs257*[(*rab-3p::hsf-1(CT):: unc-54* 3' UTR) + (*myo-2p::tdTomato::unc-54* 3' UTR)]

Wild-type (N2) and CH116 strains were obtained from *Caenorhabditis* Genetics Center (Saint Paul, MN). AGD710 and AGD836 strains were generous gifts from the laboratory of Andrew Dillin (UC Berkeley). All experiments in this study were performed using day 1 adult animals that were obtained after age-synchronization of unhatched eggs.

RNA interference analysis

RNAi clones were picked from Julie Ahringer's library and were confirmed by sequencing using the M13 forward primer (5'-TGTAAAACGACGGCCAGT-3'). *E. coli* HT115(DE3) strain bacteria transformed with either empty vector (L4440) or plasmid expressing double-stranded RNA for the gene of interest were grown in LB medium supplemented with 100 µg/mL carbenicillin at 37°C overnight. Bacterial cultures were then seeded on NGM plates containing 100 µg/mL carbenicillin and IPTG was added to the plates to a final concentration of 1 mM. Animals were subjected to RNAi by transferring unhatched eggs to NGM RNAi plates.

Life span analysis

Synchronized *C. elegans* eggs were picked and transferred to NGM plates seeded with *E. coli* OP50 or HT115(DE3) strain bacteria (for RNAi conditions) at 20°C. Worms were transferred to fresh plates with bacteria on day 1 of adulthood at a density of 12–14 worms per plate. Worms were subsequently transferred to fresh plates at least every

alternate day till they ceased producing progeny. Viability of worms was scored every 2–3 days. We scored animals as alive if they responded to gentle touch of a platinum pick. Worms that exploded, bagged, crawled off plates or were accidentally killed during the experiment were counted as unnatural deaths and hence were censored.

RNA isolation and quantitative RT-PCR

~2,000 age-synchronized young adults grown on NGM plates were collected in M9 buffer containing 0.01% Triton X-100 and were immediately washed three times with M9 buffer. TRIzol reagent (Thermo Fisher) was used to extract total RNA using the manufacturer's protocol and TURBO DNA-free kit (Themo Fisher) was used to perform DNase-treatment. cDNA was synthesized from 5 µg RNA with 0.5 µg of oligo$(dT)_{12-18}$ primer (Thermo Fisher) using SuperScript III reverse transcriptase (Thermo Fisher). Quantitative PCR was performed with Power SYBR Green PCR master mix (Thermo Fisher) and PCR primers listed in Table 5 using a CFX96 Real-Time PCR detection system (Bio-Rad). Primers were designed using the Primer3Plus online tool. Comparative Ct method was used to measure relative transcript levels while using the housekeeping gene *cdc-42* as an internal control for normalization (Hoogewijs et al., 2008). Normalization of transcript levels using another housekeeping gene *pmp-3* led to similar results (Hoogewijs et al., 2008; Zhang et al., 2012).

Immunoblot analysis

~10,000 age-synchronized young adults grown on HG plates were collected in M9 buffer containing 0.01% Triton X-100 and were immediately washed three times with M9 buffer. Pellets were suspended in three times the volume of 6x Sample Buffer (375 mM

Tris-Cl at pH 6.8, 12% SDS, 60% glycerol, 600 mM DTT, 0.06% Bromophenol Blue) diluted to 2X final concentration and were snap-frozen in liquid nitrogen for 30 sec. Samples were subsequently boiled for 10 min, vortexed for 15 sec, centrifuged at 16,000 x g for 30 min and subjected to SDS-PAGE on a SE 250 mini-vertical unit (GE Healthcare). Proteins were transferred to Immobilon-P PVDF membrane (Millipore Sigma) at 400 mA for 40 min on a Trans-blot SD semi-dry transfer cell (Bio-Rad) and the PVDF membrane was blocked in 5% non-fat dry milk-based blocking-grade blocker (Bio-Rad) for 1 hr at room temperature. Primary antibody incubation was performed for 12–16 hrs at 4°C using the following antibodies: HSF-1 – Abnova custom-made (1:1,000) lot no. F4271-3E11 and β-actin – Abcam ab8227 (1:10,000). The PVDF membrane was washed four times with TBS buffer containing 0.1% Tween 20 (TBS-T) for 5 min per wash, incubated with HRP-conjugated secondary antibody for 1 hr at room temperature and washed again four times with TBS-T buffer for 5 min per wash. Blots were developed using Immobilon Western Chemiluminescent HRP Substrate (Millipore Sigma) and visualized by autoradiography.

Preparation of worm nuclear extracts

~4,000 age-synchronized young adults grown on NGM plates were collected in M9 buffer containing 0.01% Triton X-100 and were immediately washed three times with M9 buffer. Samples were frozen in liquid nitrogen and thawed on ice for two freeze-thaw cycles. Pellets were resuspended in 10 times the volume of NPB buffer (15 mM HEPES-Na at pH 7.6, 10 mM KCl, 1.5 mM $MgCl_2$, 0.1 mM EDTA, 0.5 mM EGTA, 44 mM sucrose, 1 mM dithiothreitol, protease inhibitors, phosphatase inhibitors) containing 0.25% NP-40 and 0.1% Triton X-100. Animals were homogenized by 20 strokes of

pestle B of the Kontes Dounce tissue grinder. The homogenized samples were centrifuged at 4,000 x g for 5 min and the nuclear pellet was washed two times with NPB buffer containing 0.25% NP-40 and 0.1% Triton X-100. Nuclei were extracted in four times the volume of HEG buffer (20 mM HEPES-Na at pH 7.9, 0.5 mM EDTA, 10% glycerol, 420 mM NaCl, 1.5 mM $MgCl_2$, and protease inhibitors) at 4°C for 1 hr. The nuclear fraction was collected by centrifugation at 14,000 x g for 15 min. Protein concentrations were determined by Bradford assay.

Electrophoretic mobility shift assay

Binding of HSF-1 to its genomic target sequence was measured by Electrophoretic Mobility Shift Assay (EMSA) using a previously described protocol (Chiang et al., 2012). Briefly, 1 µg of nuclear extract was incubated for 20 min at room temperature in EMSA binding buffer (10 mM Tris-Cl at pH 7.5, 50 mM KCl, 1 mM DTT) supplemented with 50 ng/µL Poly (dI·dC) and 1 nM biotin-TEG-labeled oligonucleotide containing an HSE sequence. The biotin-TEG-labeled oligonucleotide was synthesized by annealing two complementary sequences (listed in Table 5) corresponding to an HSE from the promoter region of *hsp-16.1* gene. The DNA-bound nuclear extracts were resolved using native 3.5% polyacrylamide gel electrophoresis and were transferred to Immobilon-Ny+ charged nylon membrane (Millipore Sigma) at 400 mA for 1 hr on a Trans-blot SD semi-dry transfer cell (Bio-Rad). The HSF-1-HSE DNA complexes were visualized by autoradiography using LightShift Chemiluminescent EMSA kit (Thermo Fisher).

RNA-Seq library preparation

TRIzol reagent (Thermo Fisher) was used to extract total RNA from ~1,000 age-synchronized young adults of N2, EQ150 and EQ140 strains (three biological replicates per genotype) using the manufacturer's protocol and DNase-treatment was performed using TURBO DNA-free kit (Themo Fisher). mRNA was isolated from the DNase-treated total RNA using oligo(dT) and cDNA was synthesized by reverse transcription using TruSeq RNA Library Prep Kit v2 (Illumina). The samples were subsequently end-repaired, poly(A)-tailed, ligated to barcoded oligo adapters (Illumina) and PCR-amplified using Apollo 324 library preparation system (Wafergen Bio-systems) to prepare non-stranded poly(A)-based cDNA libraries with 120 bp insert size. All samples were multiplexed for 50 bp single-end sequencing on a HiSeq 2500 platform (Illumina).

RNA-Seq data analysis

Quality control and adaptor trimming of raw sequencing reads were performed using Trim Galore version 0.4.5 (available at https://github.com/FelixKrueger/TrimGalore) (Martin, 2011). Trimmed RNA-Seq reads were mapped to the *C. elegans* reference transcriptome (WS260 release) using STAR version 2.6.0c (Dobin et al., 2013). Subsequently, transcript abundance of each gene was measured using HTSeq version 0.9.1 (Anders et al., 2015). To identify genes that were differentially expressed relative to wild type, transcript counts were analyzed by DESeq2 version 1.20.0 (Love et al., 2014). Genes with read counts less than 10 reads were excluded for the DESeq2 analysis. In total, 15,787 genes were assayed for differential expression analysis between strains, using the following two criteria: false discovery rate (FDR)-adjusted *p* value < 0.05 and fold-change ≥ 1.5. For principal component analysis (PCA) and

pairwise distance analysis, counts with variance stabilizing transformation (VST) were used. Venn diagrams for differentially expressed genes were generated using Venn Diagram Plotter (Pacific Northwest National Laboratory; available at https://omics.pnl.gov/software/venn-diagram-plotter). For each genotype, the genes differentially expressed relative to wild-type were annotated with Gene Ontology (GO) terms from NCBI and the Database for Annotation, Visualization and Integrated Discovery (DAVID) was used to identify significantly enriched functional categories from the overrepresented GO terms (Huang et al., 2009). To determine the proportion of known longevity genes among the differentially expressed genes identified in this study, phenotype data for genes were accessed from https://www.wormbase.org. Specifically, a gene was classified as a longevity gene if it is annotated with one or more of these phenotype terms in Wormbase: 'shortened life span', 'extended life span' and 'life span variant'.

Statistical analysis

Kaplan-Meier survival analysis and Mantel-Cox log-rank test for life span experiments were performed using OASIS 2 (Han et al., 2016). GraphPad Prism 8 was used to perform statistical analyses and graphing. Hypergeometric tests were performed in R. Details of statistical tests used, number of biological replicates and *p* values for each experiment are included in the figure legends.

Data availability

Raw RNA-Seq reads for data reported in this chapter have been deposited at the NCBI Gene Expression Omnibus (GEO) under the accession number GSE119993.

Results

HSB-1 inhibition results in heat shock factor 1-dependent life span extension without increasing *hsf-1* expression

As reported previously (Chiang et al., 2012), we found that life span extension associated with genetic ablation of *hsb-1* in worms was completely dependent on HSF-1 activity (Figure 7A and Table 2). While worms with a loss-of-function *hsb-1* mutation showed a ~40% increase in mean life span relative to wild-type (N2) worms at 20°C, there was no significant difference in the life span of the two strains when the animals were subjected to *hsf-1* RNAi (Figure 7A and Table 2). Since HSF-1 has been previously implicated in the direct regulation of longevity in worms (Baird et al., 2014; Chiang et al., 2012; Douglas et al., 2015; Hsu et al., 2003; Morley and Morimoto, 2004), we investigated if life span extension in the *hsb-1(-)* strain shared genetic similarities with the longevity phenotype associated with increased HSF-1 activity. Previous studies have demonstrated that life span extension in *hsf-1* overexpressing worms is dependent on the activity of DAF-16, the sole *C. elegans* ortholog of the mammalian FOXO transcription factors (Douglas et al., 2015; Hsu et al., 2003). We found that genetic ablation of *hsb-1(-)* did not induce any significant increase in the life span of *daf-16(-)* animals (Figure 7B and Table 2). This indicates that similar to HSF-1 overexpression, HSB-1 inhibition also requires DAF-16 for its longevity-promoting effects. To elucidate whether inhibition of HSB-1 promotes longevity in animals via increasing *hsf-1* expression, we compared the transcript levels of *hsf-1* in N2, *hsb-1(-)* and a previously described long-lived *hsf-1* overexpression strain (Chiang et al., 2012). Surprisingly,

unlike in the *hsf-1* overexpression strain, the transcript levels of *hsf-1* were not significantly different in *hsb-1(-)* animals compared to wild-type (Figure 7C). Furthermore, while the protein level of HSF-1 was elevated by roughly 60% in the *hsf-1* overexpression strain, *hsb-1(-)* animals did not have increased HSF-1 protein level compared to wild-type (Figure 7D). This indicated that though HSB-1 inhibition has been shown to extend *C. elegans* life span in an HSF-1-dependent manner (Chiang et al., 2012), it does not involve an increase in expression of *hsf-1* in the long-lived *hsb-1(-)* strain.

HSF-1 acquires increased transactivation potential in the absence of HSB-1 regulation that is distinct from heat stress-induced HSF-1 activation

HSF-1 activation in the presence of heat stress does not involve transcriptional upregulation of *hsf-1* (Chiang et al., 2012), but instead necessitates several post-translational modifications to the HSF-1 protein (Anckar and Sistonen, 2011; Chiang et al., 2012; Gomez-Pastor et al., 2018). Since HSB-1 is known to bind to HSF-1 and form an inhibitory multiprotein complex (Chiang et al., 2012; Satyal et al., 1998), we speculated that the absence of HSB-1 might result in release of HSF-1 from this inhibitory complex and thus increase its transcriptional activation potential. Previous findings have shown that genetic ablation of *hsb-1* prevents the formation of this HSF-1-inhibitory complex (Chiang et al., 2012). We used EMSA to investigate if the DNA binding activity of HSF-1 to its genomic target sequence is altered in the absence of HSB-1 regulation. In nuclear extracts from wild-type animals subjected to heat stress, the *in vitro* binding activity of HSF-1 to its target HSE sequence increased by greater than twofold compared to that from non-stressed animals (Figure 8A), as shown

previously (Chiang et al., 2012). Interestingly, in non-stressed basal conditions, HSF-1 from nuclear extracts of both *hsb-1(-)* and *hsf-1* overexpressing animals showed ~80% increase in *in vitro* HSE binding activity compared to that in wild-type animals (Figure 8A). This suggests that even in non-stressed conditions, HSB-1 inhibition and HSF-1 overexpression can potentially promote increased HSF-1 binding to its genomic target sequences, similar to that observed during heat stress.

Next, we tested if HSB-1 inhibition and HSF-1 overexpression trigger HSF-1-mediated transcriptional changes in animals, as observed during heat stress. We measured transcript levels of two canonical HSF-1 target genes, *hsp-16.2* and *hsp-70*, that are upregulated during heat stress in *C. elegans* (Chiang et al., 2012; GuhaThakurta et al., 2002). The transcript levels of both *hsp-16.2* and *hsp-70* genes increased by several thousand-fold after animals were subjected to 90 min of heat shock at 37°C (Figures 8B and 8C). Intriguingly, both HSB-1 inhibition and HSF-1 overexpression resulted in a significant ~twofold increase in transcript levels of both these *hsp* genes relative to wild-type levels in non-stressed conditions (Figures 8B and 8C). These findings collectively indicate that though heat stress, HSB-1 inhibition and HSF-1 overexpression all induce an increase in the *in vitro* DNA binding activity of HSF-1 (Figure 8A), the latter two conditions have a widely distinct effect on the transcription profile of canonical HSR genes compared to that observed during heat stress (Figures 8B and 8C). Hence, the nature of HSF-1 activation resulting from overexpression of HSF-1 or inhibition of its negative regulator HSB-1 are possibly distinct from its broadly studied heat stress-induced activation (Gomez-Pastor et al., 2018; Li et al., 2017).

HSF-1 overexpression, but not HSB-1 inhibition, induces large-scale transcriptional upregulation in *C. elegans*

HSF-1 target genes that mediate its longevity-promoting effects in animals still remain largely unidentified. Since both HSB-1 inhibition and HSF-1 overexpression have been previously reported to induce life span extension via increasing the activity of the HSF-1 transcription factor (Chiang et al., 2012; Hsu et al., 2003; Morley and Morimoto, 2004), we speculated that these two manipulations might induce similar changes to the HSF-1-regulated transcriptome in *C. elegans*. For this comparison, we performed RNA-Seq to evaluate the gene expression profiles in N2, *hsb-1(-)* and *hsf-1* overexpression strains (Figure 9A). At the whole transcriptome level, within-group variation among the three biological replicates for each genotype was lesser than between-group variation across genotypes (Figures 9B and 9C). This indicates that both HSB-1 inhibition and HSF-1 overexpression induce highly reproducible gene expression changes in animals, at least when averaged over many individuals. Strikingly, the transcriptome-wide expression pattern in the *hsb-1(-)* strain was more similar to that of wild-type animals, rather than to the expression pattern in the *hsf-1* overexpression strain (Figure 9C).

Next, we generated MA plots and volcano plots to visualize genes for which the fold-change in expression relative to wild-type was statistically significant with an FDR-adjusted *p* value of less than 0.05 (Figures 10A–D). 954 transcripts were found to have a statistically significant difference in expression in *hsb-1(-)* animals (Figures 10A and 10C), while 5,144 transcripts had significantly different expression in the *hsf-1* overexpression strain (Figures 10B and 10D). The MA and volcano plots also indicated that HSF-1 overexpression induces large-scale transcriptional changes for a large

number of *C. elegans* genes (Figures 10B and 10D). In addition to the criterion of statistical significance, we set a threshold of at least 1.5-fold change in transcript levels relative to wild-type to identify gene expression changes that are potentially of biological relevance. Genes that were ≥1.5-fold (±0.585 on $\log_2$ scale) upregulated or downregulated with an FDR-adjusted *p* value of less than 0.05 were identified as being differentially expressed. With these two criteria, we found 1,662 genes to be differentially expressed in the *hsf-1* overexpression strain (Figure 11A). This was in agreement with previous studies showing thousands of genes as being potential transcriptional targets of HSF-1, even in non-stressed physiological conditions (Brunquell et al., 2016; Mendillo et al., 2012). More than 95% of these 1,662 genes had upregulated expression in *hsf-1* overexpressing animals, while the remaining less than 5% were downregulated (Figures 11B and 11C). In contrast, we found only 477 genes to be differentially expressed in the *hsb-1(-)* strain, though interestingly, roughly 45% of these overlapped with genes differentially expressed in the *hsf-1* overexpression strain (Figure 11A). In *hsb-1(-)* animals, the pattern of differential expression was slightly different than that in *hsf-1* overexpressing animals, with ~78% of genes being upregulated and remaining ~22% being downregulated (Figures 11B and 11C). In addition, more than 46% of genes that were upregulated in the *hsb-1(-)* strain also showed significant upregulation in the *hsf-1* overexpression strain, but this overlap was less than 18% for the downregulated genes (Figures 11B and 11C). These findings indicate a considerable overlap between the upregulated transcriptomes associated with HSB-1 inhibition and HSF-1 overexpression in *C. elegans*.

HSB-1 inhibition and HSF-1 overexpression induce differential expression of genes that represent overlapping biological processes

To identify the biological processes that are potentially affected by the altered transcriptome in *hsb-1(-)* and *hsf-1* overexpressing animals, we used pathway enrichment analysis using GO databases to determine functional categories associated with the genes that were differentially expressed in these two strains. Inhibition of HSB-1 and overexpression of HSF-1 affected expression of genes representing overlapping biological functions (Figures 12A and 12B). Some GO terms, such as pseudopodium (corresponding to genes involved in sperm motility), major sperm protein, PapD-like superfamily, acetylation and cell projection were represented by differentially expressed genes in both *hsb-1(-)* and *hsf-1* overexpression strains (Figures 12A and 12B). PapD-like superfamily in *C. elegans* constitutes major sperm proteins, which contain an immunoglobin-like domain structurally similar to PapD-like chaperones. Moreover, in the list of differentially expressed genes identified in our RNA-Seq comparison, the GO terms for acetylation and cell projection were primarily represented by multiple major sperm protein (*msp*) family genes that were found to be significantly upregulated in both *hsb-1(-)* and *hsf-1* overexpression strains. Previous studies performed in mice have indicated an essential role of *Hsf1* and *Hsf2* genes in spermatogenesis (Nakai et al., 2000; Wang et al., 2004). Mice expressing a constitutively active form of the HSF1 protein show altered expression of several genes involved in sperm production (Nakai et al., 2000). Since several differentially expressed genes in both *hsb-1(-)* and *hsf-1* overexpression strains in *C. elegans* represent multiple GO terms corresponding to sperm function (Figures 12A and 12B), we speculate that this is due to an evolutionarily

conserved role of the HSF-1 transcription factor in spermatogenesis (Abane and Mezger, 2010). Moreover, the GO term for cytoskeleton was enriched in the differentially expressed gene list for both *hsb-1(-)* and *hsf-1* overexpression strains (Figures 12A and 12B), which corroborates the recently discovered role of cytoskeletal components in HSF-1-induced longevity mechanisms (Baird et al., 2014). In addition, both of the long-lived strains showed elevated expression of several genes involved in the innate immune response (Figures 12A and 12B), a pathway that has been previously implicated in longevity regulation in *C. elegans* (Yunger et al., 2017). The gene encoding for the Toll/interleukin-1 receptor adaptor protein TIR-1, an essential component of the innate immune response in nematodes (Liberati et al., 2004), was found to be significantly upregulated in both *hsb-1(-)* and *hsf-1* overexpression strains. Interestingly, a recent study has shown a major role of *tir-1* in mediating the life span extension associated with activation of p38 MAPK pathway in *C. elegans* (Verma et al., 2018).

In contrast, certain functional categories were found to be unique to each genotype. Genes differentially expressed due to HSF-1 overexpression were associated with peroxisomal function (Figure 12B). The peroxisomal catalase gene *ctl-2* was significantly upregulated in *hsf-1* overexpressing animals, but not in the *hsb-1(-)* mutant. Previous studies have shown that *ctl-2* activity is required for the longevity induced via reduced insulin/IGF-1-like signaling in *C. elegans* (Murphy et al., 2003). On the other hand, genes differentially expressed due to HSB-1 inhibition were associated with TGF-β and Wnt signaling pathways (Figure 12A), processes that have been shown to have a direct role in longevity regulation in *C. elegans* (Lezzerini and Budovskaya, 2014; Shaw

et al., 2007). GO terms for these two pathways were enriched due to *hsb-1(-)*-specific upregulation of multiple members of the Skp1-related (*skr*) gene family. The *skr* genes encode components of the proteasomal E3 ubiquitin ligase complex and have a role in mediating life span extension in insulin/IGF-1-like signaling mutants (Ghazi et al., 2007). Overall, our pathway enrichment analyses suggested that HSB-1 inhibition and HSF-1 overexpression affect mostly overlapping but also certain unique biological processes in *C. elegans*.

DAF-16 targets that are upregulated via both HSB-1 inhibition and HSF-1 overexpression include numerous known longevity genes

Next, we compared the list of differentially expressed genes identified in this study with a previously reported dataset for transcriptional changes associated with insulin/IGF-1-like signaling in *C. elegans* (Tepper et al., 2013). Reduced activity of the insulin/IGF-1-like receptor DAF-2 is one of the first reported and most widely-studied longevity pathways in *C. elegans* (Kenyon et al., 1993). Life span extension in the loss-of-function *daf-2* mutant is mediated via increased activity of the FOXO transcription factor DAF-16 (Kenyon et al., 1993; Lin et al., 1997; Ogg et al., 1997). Interestingly, HSF-1 activity is also upregulated in the *daf-2* mutant (Chiang et al., 2012), and the longevity phenotype of this strain can be completely suppressed via knockdown of *hsf-1* (Hsu et al., 2003). Numerous studies have indicated cooperation between DAF-16 and HSF-1 to mediate life span extension in *C. elegans* (Cohen et al., 2006; Douglas et al., 2015; Hsu et al., 2003), though the nature of interaction between these two pro-longevity transcription factors remains largely unknown. Moreover, the longevity phenotype of *hsb-1(-)* animals could be completely suppressed via genetic ablation of *daf-16* (Figure 7B and Table 2).

Here, we compared the genes found to be differentially expressed via HSB-1 inhibition or HSF-1 overexpression in *C. elegans* with previously reported DAF-16 target genes that have altered expression in *daf-2* mutant animals (Tepper et al., 2013). DAF-16 targets are broadly classified into two categories: class I and class II. Class I DAF-16 targets are upregulated in the long-lived insulin/IGF-1-like signaling mutant *daf-2(-)* strain, while class II DAF-16 targets are downregulated in these animals (Tepper et al., 2013). Among the 1,784 genes found to be upregulated in either *hsb-1(-)* or *hsf-1* overexpression strains (Figure 11B), 293 genes, i.e., ~16.4% were class I DAF-16 targets (Figure 13A) (Tepper et al., 2013). On the other hand, among the 164 genes identified as downregulated in either *hsb-1(-)* or *hsf-1* overexpression strains (Figure 11C), 29 genes, i.e., ~17.7% were class II DAF-16 targets (Figure 13B) (Tepper et al., 2013). Interestingly, the proportion of class I DAF-16 targets in *hsf-1* overexpression-specific upregulated genes (256 out of 1,414 genes, i.e., ~18.1%) was significantly higher than that expected by chance ($p < 1.4 \times 10^{-19}$ in hypergeometric test) (Figure 13A). In addition, the proportion of class II DAF-16 targets in *hsb-1(-)*-specific downregulated genes (23 out of 88 genes, i.e., ~26.1%) was also significantly higher than that expected by chance alone ($p < 5.45 \times 10^{-5}$ in hypergeometric test) (Figure 13B). The number of DAF-16 target genes in the other categories (*hsf-1*-overexpression specific downregulated genes, *hsb-1(-)*-specific upregulated genes and genes upregulated or downregulated in both strains) were not found to be significantly higher than that expected by chance ($p > 0.05$ in hypergeometric tests) (Figures 13A and 13B).

In a parallel approach, we asked whether increased HSF-1 activity affected the expression of known longevity-regulating genes in *C. elegans*. For this comparison, we

tested whether the genes identified to be differentially expressed in our RNA-Seq analysis have been previously annotated with longevity-related phenotypes on Wormbase (https://www.wormbase. org). We found that among the 1,784 genes that were upregulated in *hsb-1(-)* or *hsf-1* overexpressing animals, 64 genes, i.e., ~3.6% have known longevity-regulating functions (Figure 13C). On the other hand, among the 164 genes that were downregulated via HSB-1 inhibition or HSF-1 overexpression, 6 genes, i.e., ~3.7% have known roles in life span regulation (Figure 13D). Next, we estimated the proportion of longevity-regulating genes among DAF-16 transcriptional targets that were found to be differentially expressed in our RNA-Seq analysis. Among the 293 class I DAF-16 targets identified in our study, 24 genes, i.e., ~8.2% have been previously implicated in life span regulation in *C. elegans* (Figures 13A and 13C), a proportion that was significantly higher than that expected by chance ($p < 2.8 \times 10^{-5}$ in hypergeometric test). However, this higher proportion of known longevity genes among DAF-16 transcriptional targets might be because in *C. elegans*, the longevity-promoting roles of insulin/IGF-1-like signaling have been more extensively characterized compared to other less-studied life span regulating pathways. To account for this potentially confounding factor, we performed this comparison only within gene lists that solely comprised of DAF-16 targets. We found that after accounting for the increased proportion of life span-regulating genes among DAF-16 transcriptional targets, the percentage of such longevity genes was not significantly higher in either *hsf-1* overexpression-specific or *hsb-1(-)*-specific upregulated genes ($p > 0.05$ in hypergeometric tests). In both these categories, only 6.25% of the class I DAF-16 targets had known life span-regulating functions in *C. elegans* (Figures 13A and 13C).

Interestingly, the proportion of longevity-related genes was much higher among class I DAF-16 targets that were upregulated in both *hsb-1(-)* mutant and *hsf-1* overexpressing animals (Figures 13A and 13C). 21 class I DAF-16 targets were found to be upregulated via both HSF-1 overexpression and HSB-1 inhibition (Figure 13A), and 7 out of these 21 genes (~33.3%) have known longevity-regulating functions (Figure 13C). This proportion was significantly higher than that expected by chance, even if the higher prevalence of longevity genes among DAF-16 targets was taken into consideration ($p < 0.001$ in hypergeometric test). In summary, we found that increased HSF-1 activity resulted in transcriptional upregulation of numerous DAF-16 target genes that have life span-regulatory functions in *C. elegans* (Figures 13A and 13C).

The class I DAF-16 targets that were upregulated via both HSB-1 inhibition and HSF-1 overexpression included *mtl-1*, *dod-3*, *dod-6*, *lys-7*, *asah-1* and *T20G5.8*, genes that are at least partially required for the life span extension phenotype in *daf-2* mutant animals (Murphy et al., 2003). However, not all longevity genes identified in our transcriptomic analysis were DAF-16 targets. For example, the FOXA transcription factor *pha-4* is upregulated in both *hsb-1(-)* and *hsf-1* overexpressing animals, but is not required for the long life span of *daf-2* mutant animals (Panowski et al., 2007). Instead, *pha-4* has been shown to have an essential role in dietary restriction-induced longevity in *C. elegans* (Panowski et al., 2007). This suggests that HSF-1 not only influences the expression of longevity-promoting genes that act downstream of insulin/IGF-1like signaling, but also of genes involved in other life span-regulating pathways. Surprisingly, none of the class II DAF-16 targets identified to be downregulated in *hsf-1* overexpressing or *hsb-1(-)* mutant animals have known longevity-related functions

(Figures 13B and 13D). This indicates that in the context of life span regulation, DAF-16 and HSF-1 might suppress gene expression in animals via potentially distinct mechanisms (Tepper et al., 2013).

Genes differentially expressed due to both HSB-1 inhibition and HSF-1 overexpression show a strongly correlated expression pattern

We speculated that genes that are differentially expressed in the same direction by both HSB-1 inhibition and HSF-1 overexpression might be contributing to their shared phenotype of HSF-1-associated life span extension in *C. elegans*. We visualized the fold-change in expression of the 214 genes that were differentially expressed in both *hsb-1(-)* and *hsf-1* overexpression strains relative to wild-type animals (Figures 11A and 14A). The heatmap showed that most of these genes have altered expression in the same direction with respect to the wild-type levels (Figure 14A; top hits are listed in Table 3). However, use of the same N2 control dataset for normalization could lead to a spurious correlation between the gene expression patterns in the two strains due to hidden covariates (Curran-Everett, 2013). Hence, to avoid false-positive (type I error) similarities in expression patterns of the two strains, we re-calculated the direction of change in gene expression in the *hsb-1(-)* and *hsf-1* overexpression strains by using two independent biological replicates of N2 for normalization. Using this method, we found that 191 out of the 214 genes were either significantly upregulated (172 genes) or significantly downregulated (19 genes) in both *hsb-1(-)* and *hsf-1* overexpression strains relative to wild-type (Figure 14B). In contrast, less than 11 percent (23 out of 214) of these genes were found to be differentially expressed in opposite directions, i.e., upregulated in one strain but downregulated in the other (Figure 14B). The proportion of

genes (89%) differentially expressed in the same direction in the two long-lived strains relative to wild-type was much higher than that expected by chance alone (chi-square value = 350.7, $p < 0.0001$), indicating the presence of common regulatory mechanisms for these genes in *hsb-1(-)* and *hsf-1* overexpressing animals.

On comparison of the fold-change in expression of the 214 genes that were differentially expressed in both *hsb-1(-)* and *hsf-1* overexpressing strains, we found a strongly correlated expression pattern even when two independent wild-type control datasets were used for normalization ($r = 0.7386$, $p < 0.0001$) (Figure 14C). As described previously (Figure 14B), more than 89 percent of the 214 differentially expressed genes were found in the first and third quadrants of the scatter plot for relative change in gene expression (Figure 14C). Finally, we used quantitative RT-PCR to validate the magnitude of change in gene expression determined from RNA-Seq (Figure 14D). Among the 24 genes tested using quantitative RT-PCR, we found that most of the genes showed similar fold-change in expression in *hsb-1(-)* animals relative to wild-type as observed in our RNA-Seq data (Figure 14D). For some genes such as *C08F1.10*, *clec-196* and *lfi-1*, the magnitude of fold-change in expression (relative to wild-type) measured using quantitative RT-PCR did not accurately represent the value determined from RNA-Seq (Figure 14D). This is possibly due to the difference in transcript-binding sites and amplification efficiencies of the primers used for quantitative RT-PCR validation. However, for 20 out of the 24 genes tested, the change in direction of gene expression in the *hsb-1(-)* strain was the same irrespective of whether RNA-Seq or quantitative RT-PCR was used to measure transcript abundance (Figure 14D).

Hence, our RNA-Seq analysis provides a fairly robust estimate of the transcriptome-wide changes in these long-lived *C. elegans* strains.

SPTF-3 is required for HSB-1-associated life span extension in worms

In a parallel approach to identify factors that are required for the longevity phenotype associated with HSB-1 inhibition, we performed an RNAi-based genetic screen for suppressors of life span extension in *hsb-1(-)* worms. Our goal was to identify genes, that when knocked down, resulted in reduced life span of the long-lived *hsb-1(-)* strain, without inducing a similar life span shortening effect in wild-type worms (Figure 15A). After screening RNAi clones corresponding to ~2, 700 genes (most of them located on chromosome I of *C. elegans*), we identified 11 RNAi clones that significantly shortened the mean life span of *hsb-1(-)* worms and produced a smaller (or no statistically significant) life span shortening effect in wild-type (N2) worms (Table 4). Among these 11 top hits from our genetic screen, the RNAi clone for *sptf-3* produced the maximum difference in life span suppression between *hsb-1(-)* and N2 worms (Table 4). Specificity Protein Transcription Factor 3 (SPTF-3) is a member of the evolutionarily conserved Sp1 family of proteins (Schaeper et al., 2010). In mammals, nine genes (Sp1–Sp9) encode Sp1-like transcription factors with DNA binding properties (Schaeper et al., 2010; Zhao and Meng, 2005). These proteins act synergistically with other transcription factors such as p53, p73, E2F-1, c-Jun and Smad family of proteins to regulate transcription of numerous downstream target genes (Wierstra, 2008). In vertebrates, the Sp1 family has been primarily studied in the context of its role in animal development (Zhao and Meng, 2005). In *C. elegans*, there are four members that encode prospective Sp family of transcription factors, namely *tlp-1*, *sptf-1*, *sptf-2* and

sptf-3. Among these genes, *sptf-3* has been shown to be involved in cell fate specification and programmed cell death during embryonic development (Hirose and Horvitz, 2013; Ulm et al., 2011). The SPTF-3 protein primarily localizes to the nuclei and is ubiquitously expressed in all tissues during the early larval stages in worms (Hirose and Horvitz, 2013). N-terminal of the 47 kDa SPTF-3 protein contains a glutamine (Q)-rich domain, while the C-terminus has three C2H2 zinc finger domains with DNA-binding properties, a characteristic of the Sp1 family of transcription factors (Figure 15B). Previous studies have focused on the functional requirement of *sptf-3* in the context of *C. elegans* development (Hirose and Horvitz, 2013; Ulm et al., 2011), but the role of this protein during adulthood and organismal aging remains less understood.

We observed that RNAi-mediated knockdown of *sptf-3* resulted in a 33% reduction in mean life span of *hsb-1(-)* animals, while the life span shortening effect of *sptf-3* RNAi was only 20% in wild-type worms (Figure 15C and Table 2). As a result, the extension of mean life span due to HSB-1 inhibition is suppressed from 40% in control RNAi to only 17% in *sptf-3* RNAi conditions (Figure 15C and Table 2). Furthermore, we found that knockdown of *sptf-3* also partially suppressed the life span extension associated with HSF-1 overexpression in worms (Figure 15D and Table 2). After subjecting to *sptf-3* RNAi, worms overexpressing *hsf-1* in all tissues or only in neuronal tissues were 10–17% longer lived than wild-type (N2) worms (Figure 15D and Table 2). In contrast, these *hsf-1* overexpression strains showed a 20–35% increase in mean life span relative to N2 worms in control RNAi conditions (Figure 15D and Table 2). These findings suggest that SPTF-3 is an important mediator of HSF-1-associated longevity in both *hsb-1(-)* and *hsf-1* overexpressing worms.

Since Sp1 family proteins are known to cooperate with other transcription factors to regulate gene expression (Wierstra, 2008), we speculated that knockdown of *sptf-3* might affect the increased DNA binding activity of HSF-1 in *hsb-1(-)* animals (Figure 8A). In nuclear extracts of *hsb-1(-)* worms that were subjected to *sptf-3* RNAi, HSF-1 showed a ~40% reduction in basal *in vitro* HSE binding activity in comparison to that from *hsb-1(-)* worms grown in control conditions (Figure 16A). However, *sptf-3* RNAi did not affect the heat stress-induced HSE binding activity of HSF-1 in these worms (Figure 16A). On comparing the transcript levels of two canonical HSF-1 target genes, *hsp-16.2* and *hsp-70*, we found that knockdown of *sptf-3* in *hsb-1(-)* animals did not have any significant effect on the expression level of these genes either in basal or in heat stressed conditions (Figures 16B and 16C). Together, these data show that SPTF-3 is required for the life span extension phenotype and for increased DNA binding activity of HSF-1 in *hsb-1(-)* worms (Figures 8A, 15C and 16A, and Table 2), but it is not required for the increased basal expression of *hsp-16.2* and *hsp-70* in these animals (Figures 8B, 8C, 16B and 16C). Hence, we conclude that though an increased basal expression of *hsp* genes is observed in the *hsb-1(-)* strain, this trait can be uncoupled from the longevity phenotype associated with inhibition of HSB-1 in *C. elegans*.

Discussion

Previous studies have established HSB-1 as an evolutionarily conserved negative regulator of HSF-1 that physically binds to the HSF-1 protein and sequesters it in an inhibitory complex (Chiang et al., 2012; Satyal et al., 1998). In this study, our findings collectively indicate that in the absence of HSB-1, transcriptional changes induced via

activation of the HSF-1 protein result in life span extension in animals (Figure 17). We report increased *in vitro* binding activity of HSF-1 to its genomic target sequence in both *hsb-1(-)* and *hsf-1* overexpression strains (Figure 8A), but interestingly, HSF-1 protein level is not elevated in *hsb-1(-)* animals (Figure 7D). The higher *in vitro* HSE binding induced via HSF-1 overexpression is presumably due to the elevated HSF-1 protein level in that strain (Figures 7B and 7C). However, the increased *in vitro* HSE binding phenotype observed in *hsb-1(-)* animals can possibly be a consequence of yet unknown factors such as increased nuclear localization of HSF-1, acquisition of PTMs that favor DNA binding, or a combination of both (Figure 17). This concurs with the diverse HSR-independent roles of the HSF-1 transcription factor in different biological contexts (Gomez-Pastor et al., 2018; Li et al., 2017). Here, we identified the HSF-1-regulated transcriptome that is relevant for the longevity-promoting effects of this transcription factor in *C. elegans*. Though life span extension has been previously achieved via overexpression of HSF-1 in *C. elegans* (Baird et al., 2014; Hsu et al., 2003; Morley and Morimoto, 2004), our findings suggest that the beneficial effects of HSF-1 activation upon longevity could also be achieved via modulating the expression of a limited number of its transcriptional targets (Figures 10A–D).

Our transcriptomic analyses show that a sizeable fraction of differentially expressed genes in the *hsb-1(-)* mutant and *hsf-1* overexpression strains have a strongly correlated expression pattern (Figures 14A and 14C), suggesting similar transcriptional regulation of a subset of HSF-1 target genes in both these strains. Incidentally, though the heat shock response genes *hsp-16.2* and *hsp-70* showed roughly twofold increase in expression compared to wild-type in both *hsb-1(-)* and *hsf-1*

overexpression strains in our quantitative RT-PCR experiments (Figures 8B and 8C), these *hsp* genes were not identified to be differentially expressed in our transcriptome-wide RNA-Seq comparison. We found that this was due to very low sequencing read counts for the *hsp* genes across all the samples. Quantitative RT-PCR data indicated that the expression levels of these *hsp* genes were ~10,000-fold lower than that of housekeeping genes in non-stressed conditions (data not shown). Hence, higher sequencing depth can potentially identify the difference in transcript levels of *C. elegans* genes that have extremely low basal expression in normal physiological conditions. Among the genes identified in our transcriptomic analysis, it remains to be determined which of those are causally linked to the life span extension phenotype in the *hsb-1(-)* mutant. It will be informative to estimate the extent to which inactivation of individual genes affects the life span of *hsb-1(-)* animals. However, the longevity phenotype associated with HSB-1 inhibition is most likely an additive effect of the contributions of numerous HSF-1 target genes identified in this study and might also involve epistatic interactions between those downstream targets. Moreover, it is possible that certain differentially expressed transcripts in the *hsb-1(-)* strain are regulated in an HSF-1-independent manner. Characterization of how HSF-1 genomic occupancy is altered in *hsb-1(-)* animals will help to identify loci that are directly under the control of HSB-1/HSF-1 pathway.

Nonetheless, our RNA-Seq analysis has identified several known longevity-promoting genes, such as *mtl-1*, *dod-3*, *lys-7* and *pha-4*, that are upregulated in the HSF-1-dependent long-lived strains (Figure 14C). Most of these longevity genes act downstream of the insulin/IGF-1-like signaling pathway in *C. elegans* (Murphy et al.,

2003; Tepper et al., 2013), while *pha-4* is involved in regulation of dietary restriction-induced macroautophagy (Hansen et al., 2008). In addition, our transcriptome-wide comparison also revealed increased expression of more than 1,500 *C. elegans* genes in *hsf-1* overexpressing animals (Figures 10B, 10D and 11B). Since the number of upregulated genes was comparatively much lower in the *hsb-1(-)* mutant strain (Figures 10A, 10C and 11B), we conclude that HSF-1-induced longevity can be achieved via altered expression of a much smaller subset of HSF-1 target genes. A recent transcriptome-wide study has reported that HSF-1 regulates the expression of more than 2,000 genes independently of the heat shock response in *C. elegans* (Brunquell et al., 2016). Many of these genes are involved in maintenance of nematode cuticle structure and other metabolic processes such as mitochondrial function, regulation of growth etc. Interestingly, roughly 90% of these HSF-1-regulated transcripts do not overlap with a gene expression dataset for aging-induced transcriptional changes in *C. elegans* (Brunquell et al., 2016). This further indicates that ectopic HSF-1 activation might inadvertently affect numerous biological pathways in addition to the ones involved in longevity regulation. Since mammalian HSF1 has been shown to support progression of highly malignant cancers (Dai et al., 2007; Mendillo et al., 2012), it is crucial to develop strategies that can selectively modulate the activity of this transcription factor to promote longevity in animals without producing undesired outcomes.

In an RNAi-based genetic screen, we identified the Sp1 family transcription factor SPTF-3 as a genetic suppressor of HSB-1-associated longevity in worms (Figure 15C, and Tables 2 and 4). Interestingly, SPTF-3 is required for the increased DNA binding activity of HSF-1 in *hsb-1* null animals (Figures 8A and 16A). Previous studies

performed in mammalian cells have shown cooperation between HSF1 and Sp1 transcription factors to co-regulate the expression of numerous target genes in different physiological conditions (Arora et al., 2017; Bevilacqua et al., 2000; Hamiel et al., 2009; Morgan, 1989; Singleton and Wischmeyer, 2008; Yang et al., 2014). It remains to be determined how depletion of SPTF-3 in *C. elegans* affects the genome-wide occupancy of HSF-1 in non-stressed animals. Moreover, transcriptomic analysis of *hsb-1(-)* mutant worms after knockdown of SPTF-3 will help in identifying the genes downstream of HSB-1/HSF-1 signaling that are co-regulated by this Sp1 family transcription factor. Since RNAi-mediated knockdown of *sptf-3* partially suppresses life span extension in both *hsb-1(-)* and *hsf-1* overexpressing animals (Figures 15C and 15D, and Table 2), it is possible that SPTF-3 cooperates with HSF-1 to regulate the expression of several longevity-promoting genes in *C. elegans*.

In summary, our study provides a better understanding of the function and regulation of heat shock factor in non-stressed physiological conditions. The findings from this study can potentially guide the design of targeted therapies to exploit the untapped potential of this evolutionarily conserved longevity-promoting factor in delaying age-associated physiological decline in complex organisms.

Figures

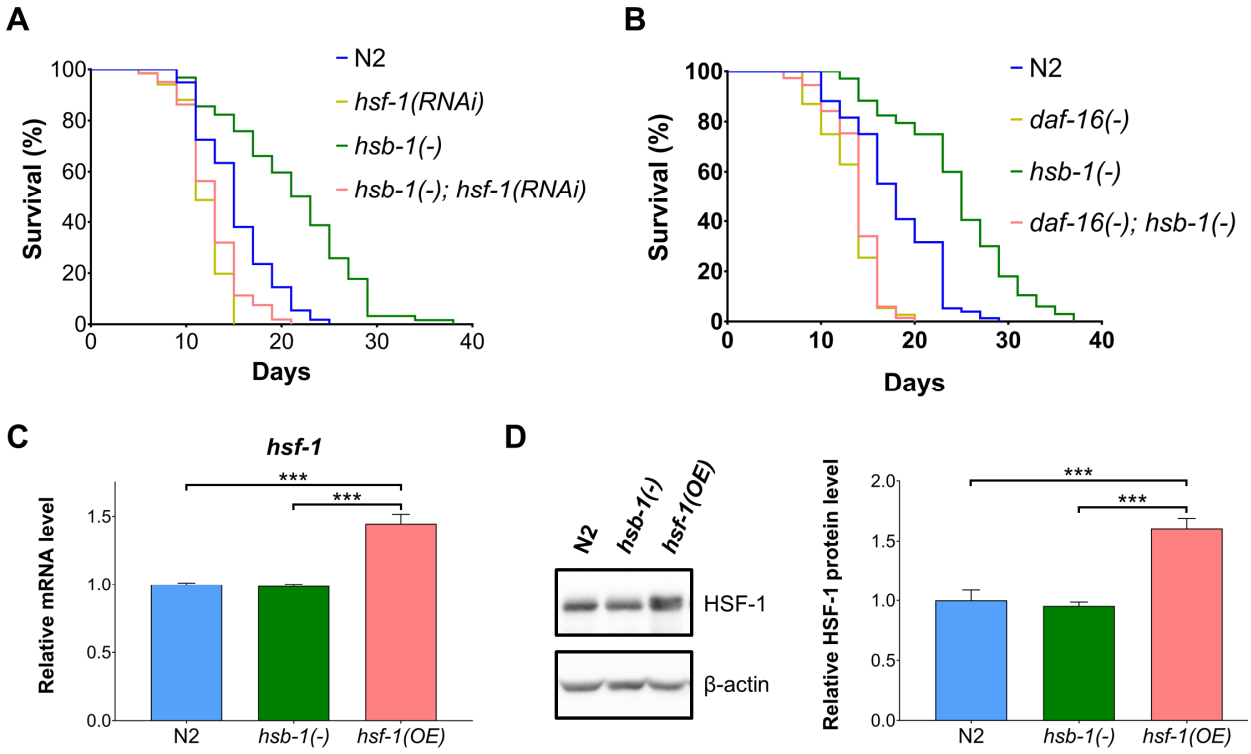

Figure 7. Life span extension in *hsb-1(-)* worms is *hsf-1*-dependent but does not involve an increase in HSF-1 levels.
(A) Life span analysis of wild-type (N2) and *hsb-1(-)* worms grown on control or *hsf-1* RNAi bacteria at 20°C. Statistical data are included in **Table 2**.
(B) Life span analysis of N2, *hsb-1(-)*, *daf-16(-)* and *daf-16(-); hsb-1(-)* worms at 20°C. Statistical data are included in **Table 2**.
(C) Relative transcript levels of *hsf-1* in N2, *hsb-1(-)* and *hsf-1* overexpression strains grown at 20°C. All values are reported in comparison to mean wild-type expression level in control conditions. Data represent mean ± SEM for ≥ 3 biological replicates. *** $p < 0.001$ in Tukey's multiple comparisons test performed after one-way ANOVA.
(D) Representative immunoblots for HSF-1 and β-actin proteins in N2, *hsb-1(-)* and *hsf-1* overexpression strains grown at 20°C (*left*). Densitometric quantification of HSF-1: β-actin ratio relative to wild-type levels (*right*). Data represent mean ± SEM for ≥ 3 biological replicates. *** $p < 0.001$ in Tukey's multiple comparisons test performed after one-way ANOVA.

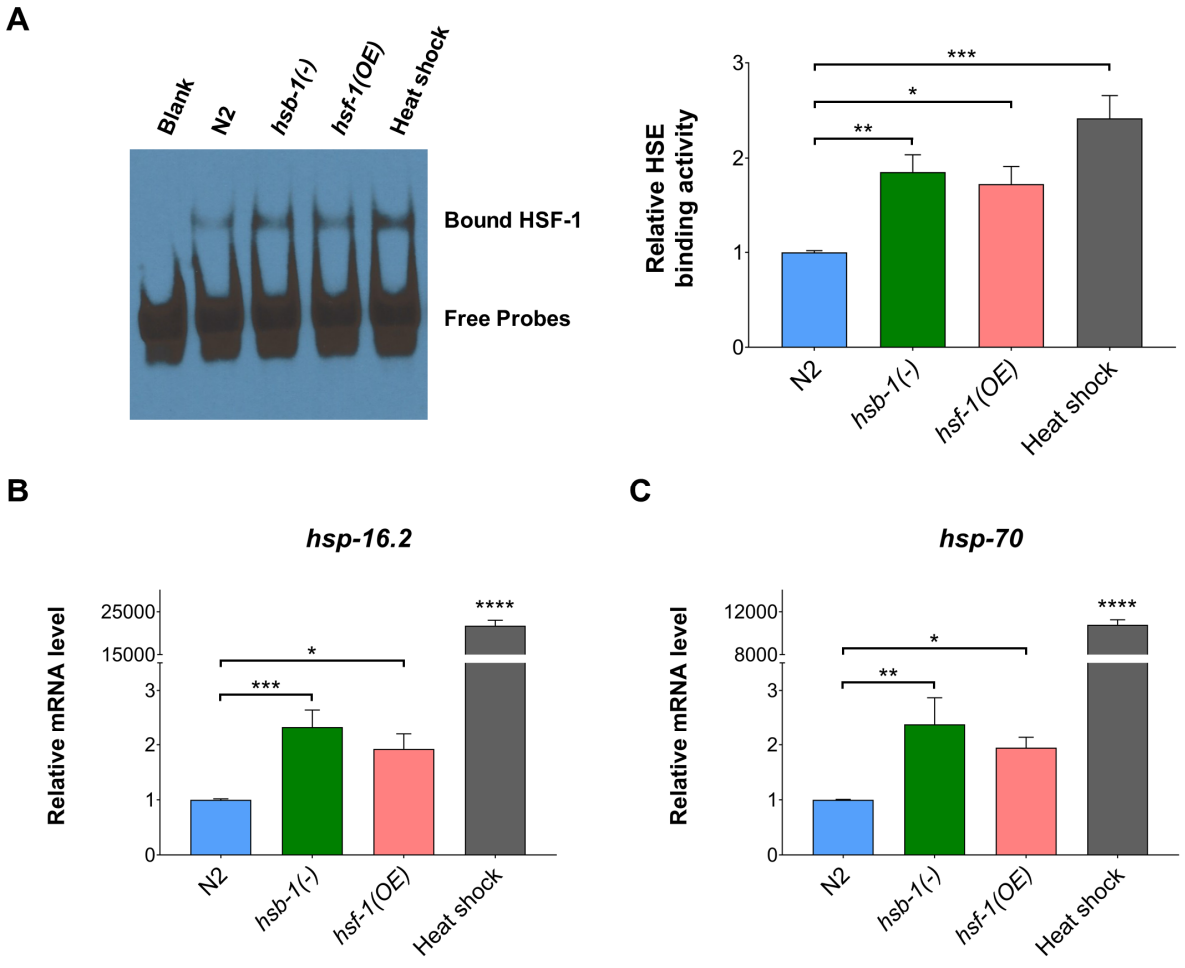

Figure 8. HSB-1 inhibition results in increased activity of HSF-1 that is distinct from heat stress-induced HSF-1 activation.
(A) Representative EMSA analysis for HSE binding activity of nuclear extracts from wild-type (N2), *hsb-1(-)* and *hsf-1* overexpression strains grown in non-stressed conditions at 20°C and N2 animals subjected to heat stress at 37°C for 90 min (*left*). Densitometric quantification of HSE binding activity relative to wild-type levels (*right*). Data represent mean ± SEM for ≥ 4 biological replicates. * $p < 0.05$, ** $p < 0.01$ and *** $p < 0.001$ in Tukey's multiple comparisons test performed after one-way ANOVA.
(B, C) Relative transcript levels of *hsp-16.2* and *hsp-70* in N2, *hsb-1(-)* and *hsf-1* overexpression strains grown in non-stressed conditions at 20°C and N2 animals subjected to heat stress at 37°C for 90 min. Data represent mean ± SEM for ≥ 3 biological replicates. * $p < 0.05$, ** $p < 0.01$ and *** $p < 0.001$ in Tukey's multiple comparisons test performed after one-way ANOVA. **** indicates $p < 0.0001$ compared to all other conditions in Tukey's multiple comparisons test.

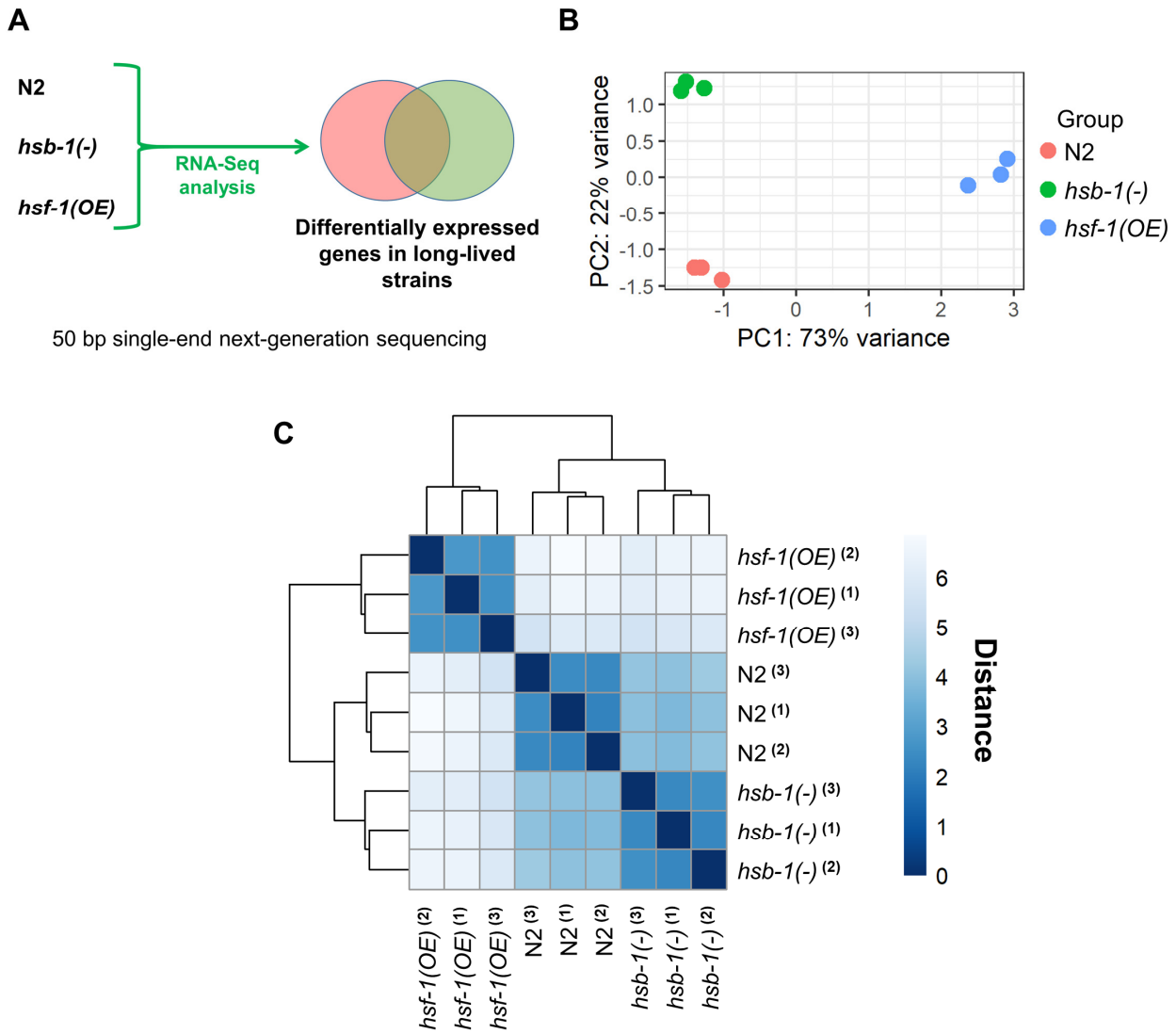

Figure 9. RNA-Seq analysis for comparison of the transcriptomes of *hsb-1(-)* and *hsf-1* overexpressing animals.
(A) Schematic of RNA-Seq study design for identifying differentially expressed genes in *hsb-1(-)* and *hsf-1* overexpression strains relative to wild-type (N2).
(B) Principal component analysis (PCA) plot showing variability between all biological replicates at the whole-transcriptome level.
(C) Pairwise distance heatmap showing similarities between biological replicates and genotypes based on transcriptome-wide expression pattern.

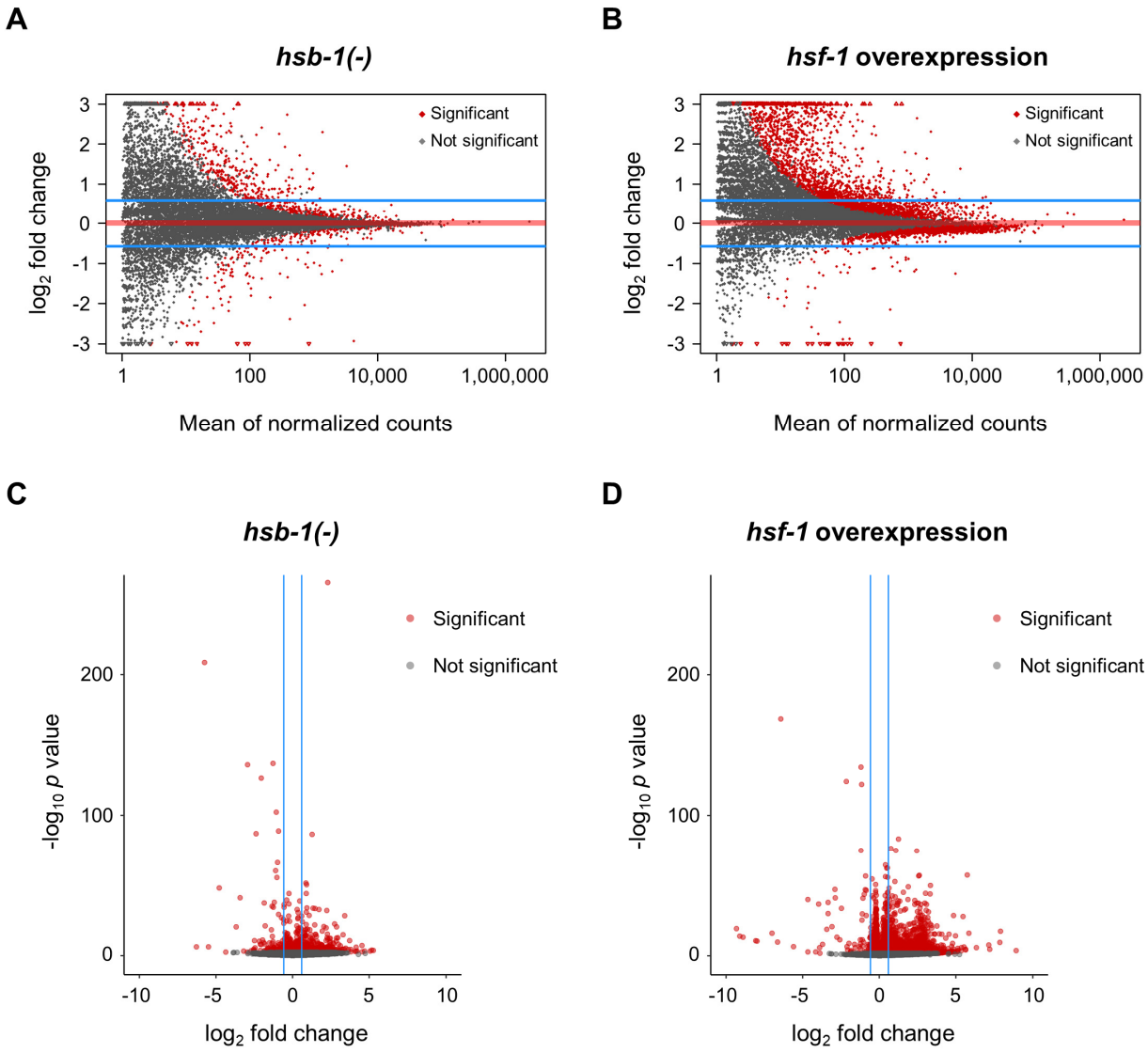

Figure 10. Global transcriptional profile indicates large-scale gene expression changes in *hsf-1* overexpressing animals.
(A, B) MA plots for all genes with significant (FDR-adjusted $p < 0.05$) or no significant change in expression in *hsb-1(-)* and *hsf-1* overexpression strains relative to wild-type (N2) arranged in order of mean expression level. Read counts for genes were normalized to the size factors determined from DESeq2. Horizontal blue lines encompass genes with less than 1.5-fold change in expression (±0.585 on $\log_2$ scale) relative to N2. Horizontal red line represents no change in expression.
(C, D) Volcano plots for all genes with statistically significant (FDR-adjusted $p < 0.05$) or no significant change in expression in *hsb-1(-)* and *hsf-1* overexpression strains relative to wild-type levels. Vertical blue lines encompass genes with less than 1.5-fold change in expression (±0.585 on $\log_2$ scale) relative to N2.

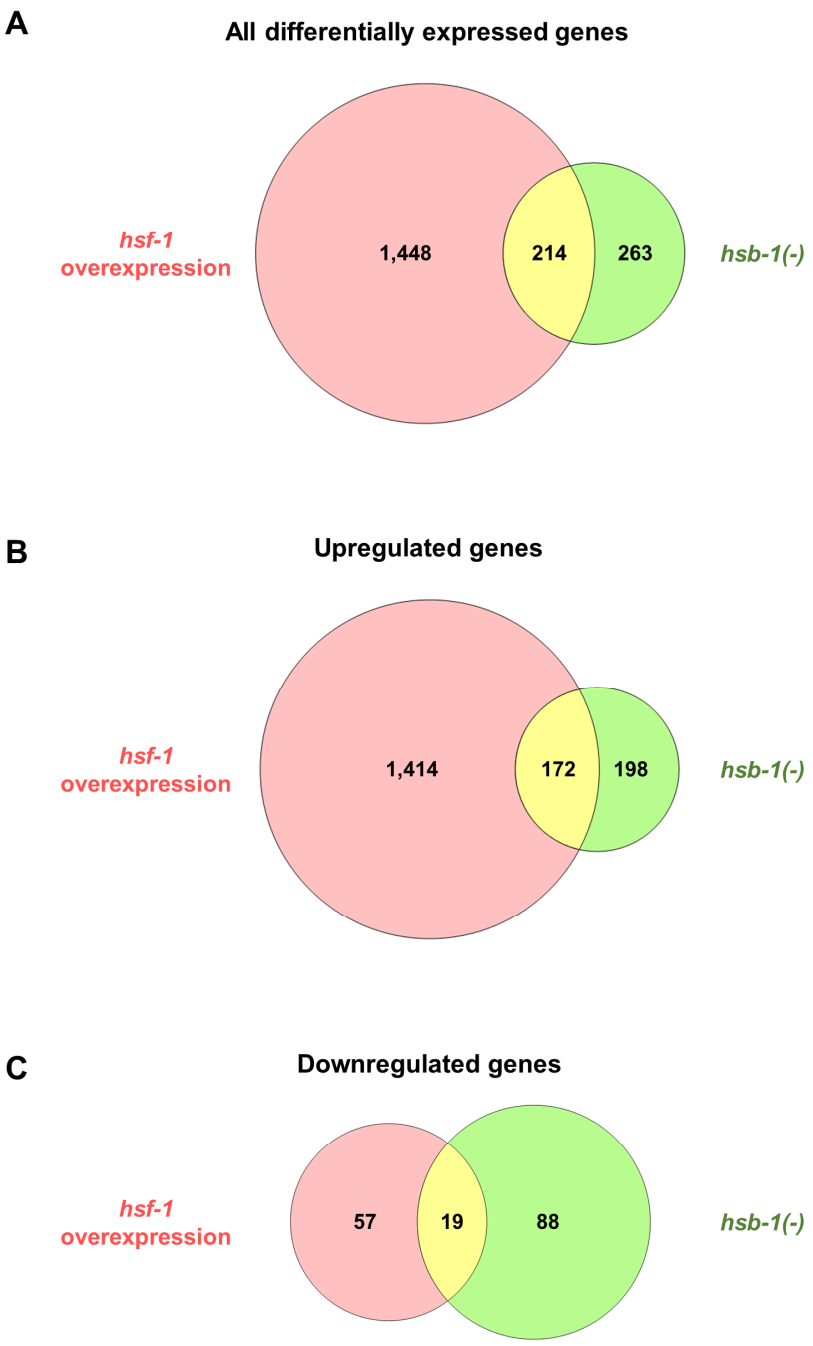

Figure 11. Venn diagrams for differentially expressed genes in *hsb-1(-)* and *hsf-1* overexpression strains. **(A–C)** Venn diagrams showing number of differentially expressed genes (fold-change ≥ 1.5) only in *hsb-1(-)* animals, only in *hsf-1* overexpressing animals or in both the strains relative to wild-type levels. **(B)** shows number of upregulated genes, **(C)** shows number of downregulated genes, while **(A)** shows number of genes in either of the two categories.

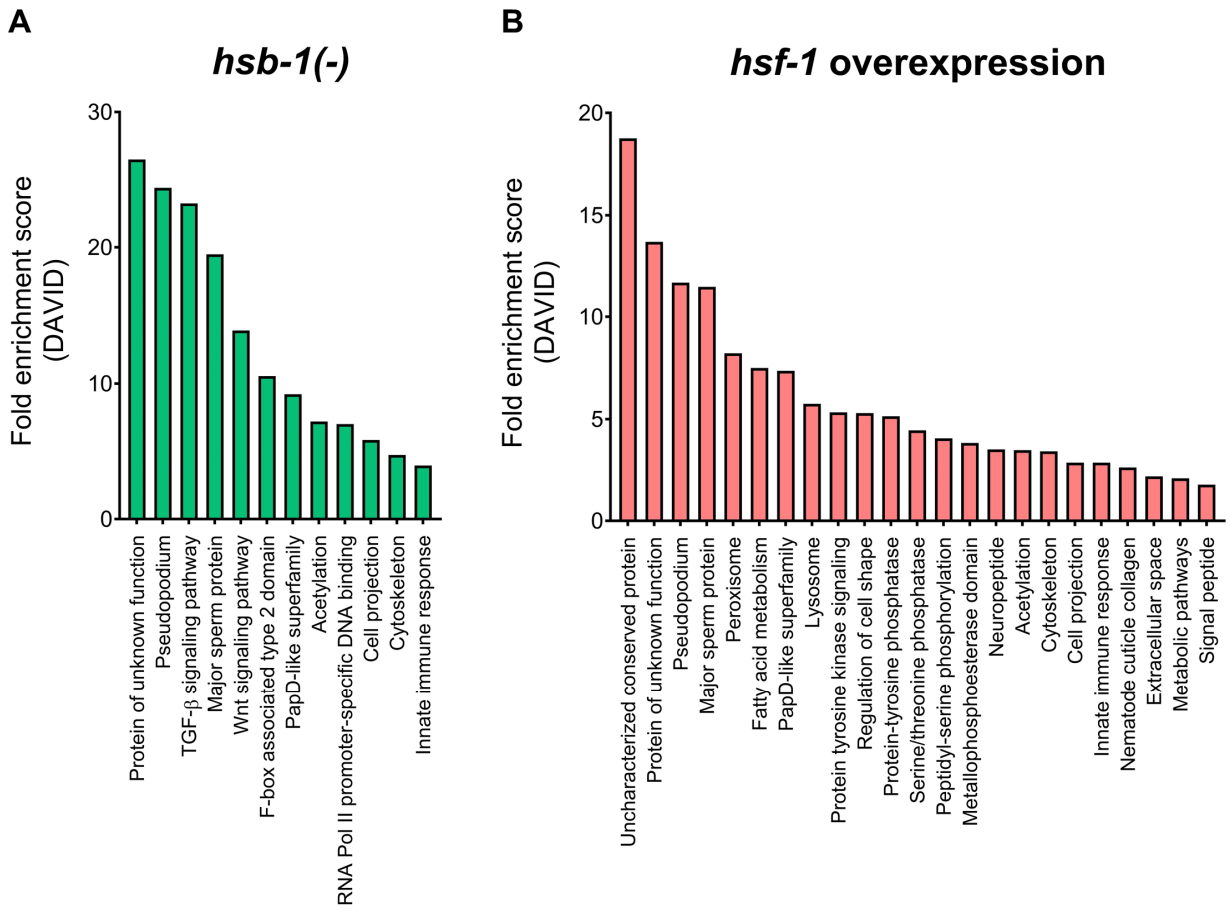

Figure 12. Gene ontology (GO) analysis of differentially expressed genes in *hsb-1(-)* and *hsf-1* overexpression strains.
(A, B) Functional enrichment analysis (DAVID) of differentially expressed genes in *hsb-1(-)* and *hsf-1* overexpression strains relative to wild-type. GO terms representing unique functional categories with FDR-adjusted $p < 0.05$ are shown.

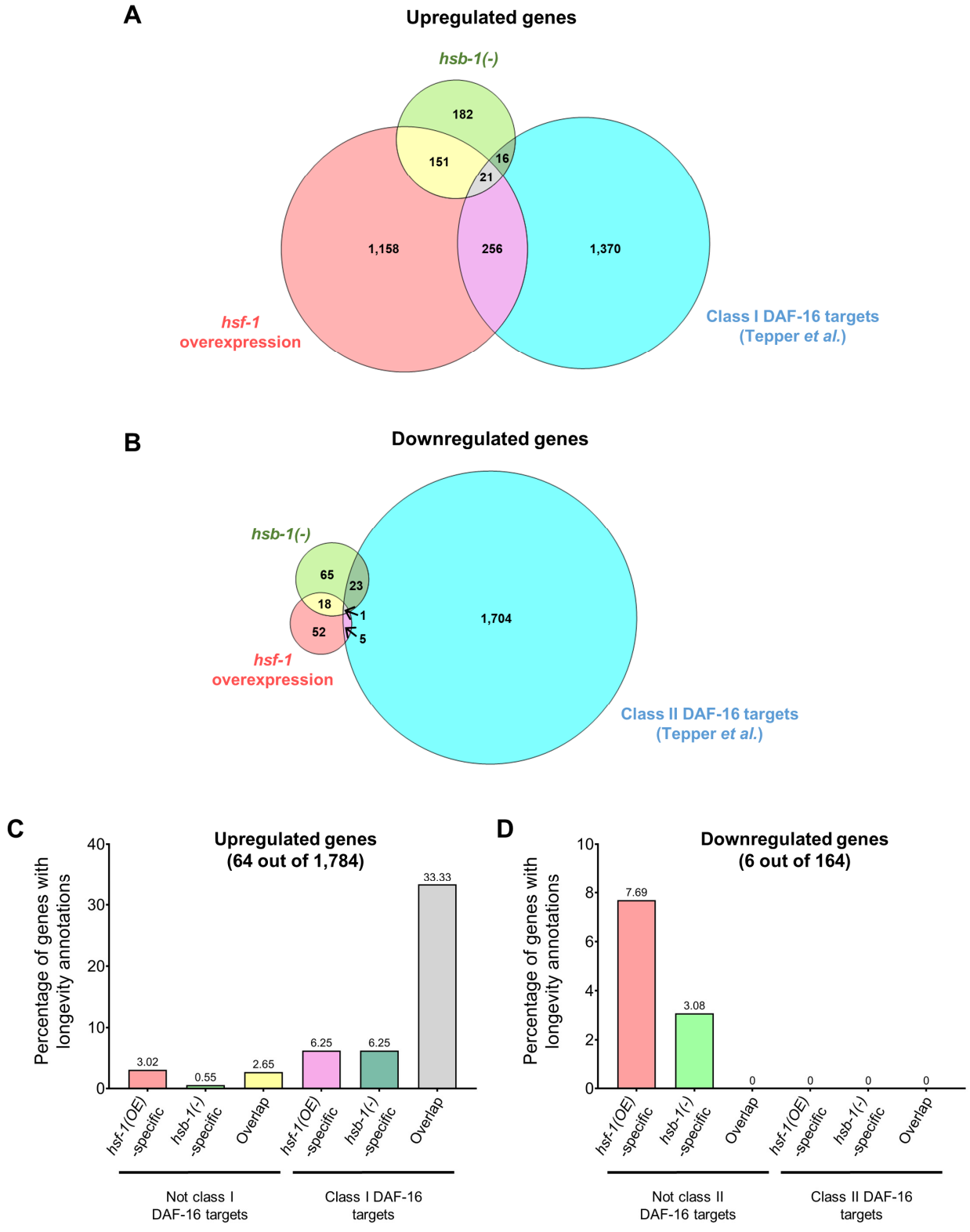

Figure 13. DAF-16 targets that are upregulated in both *hsb-1(-)* and *hsf-1* overexpression strains have a high proportion of known longevity genes.
(A) Venn diagram showing overlap of genes upregulated in *hsb-1(-)* and *hsf-1* overexpression strains with previously reported class I DAF-16 targets (Tepper et al., 2013).

(B) Venn diagram showing overlap of genes downregulated in *hsb-1(-)* and *hsf-1* overexpression strains with previously reported class II DAF-16 targets (Tepper et al., 2013).
(C, D) Percentage of genes with known longevity functions among upregulated genes (*total:* 64 out of 1,784) or downregulated genes (*total:* 6 out of 164) in *hsb-1(-)* and *hsf-1* overexpression strains.

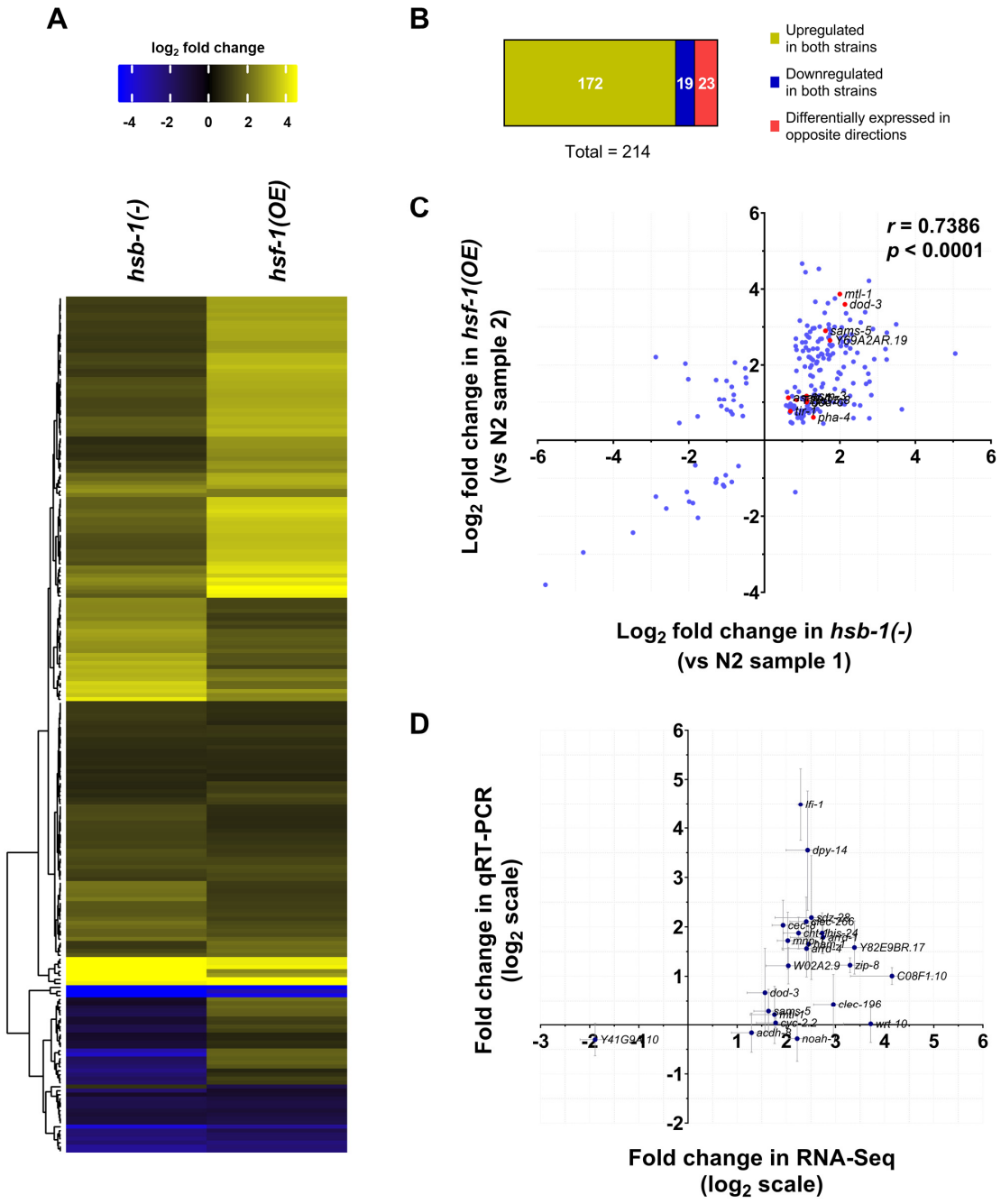

Figure 14. Correlation between expression pattern of genes that are differentially expressed in both *hsb-1(-)* and *hsf-1* overexpression strains.
(A) Heatmap for fold-change in expression of 214 genes that are differentially expressed (fold-change ≥ 1.5) in both *hsb-1(-)* and *hsf-1* overexpression strains relative to wild-type (N2). Genes (rows) are clustered based on similarity in expression pattern. Colors show magnitude of change in gene expression (*yellow*: high, *black*: no change, *blue*: low).
(B) Categorization of 214 genes shown in **(A)**. The three categories indicate genes that are upregulated in both *hsb-1(-)* and *hsf-1* overexpression strains, downregulated in both the strains or differentially expressed in opposite directions in the two strains.
(C) Correlation between fold-change in expression pattern of 214 genes shown in **(A)**. Fold-change in gene expression for *hsb-1(-)* and *hsf-1* overexpression strains were calculated using two independent replicates of the wild-type strain for normalization. Red dots represent known longevity-regulating genes in *C. elegans*.
(D) Fold-change in gene expression in *hsb-1(-)* animals relative to wild-type determined using RNA-Seq and

quantitative RT-PCR. Expression data are shown for 24 transcripts that were among the top hits from RNA-Seq analysis. Data represent mean ± SEM for three biological replicates.

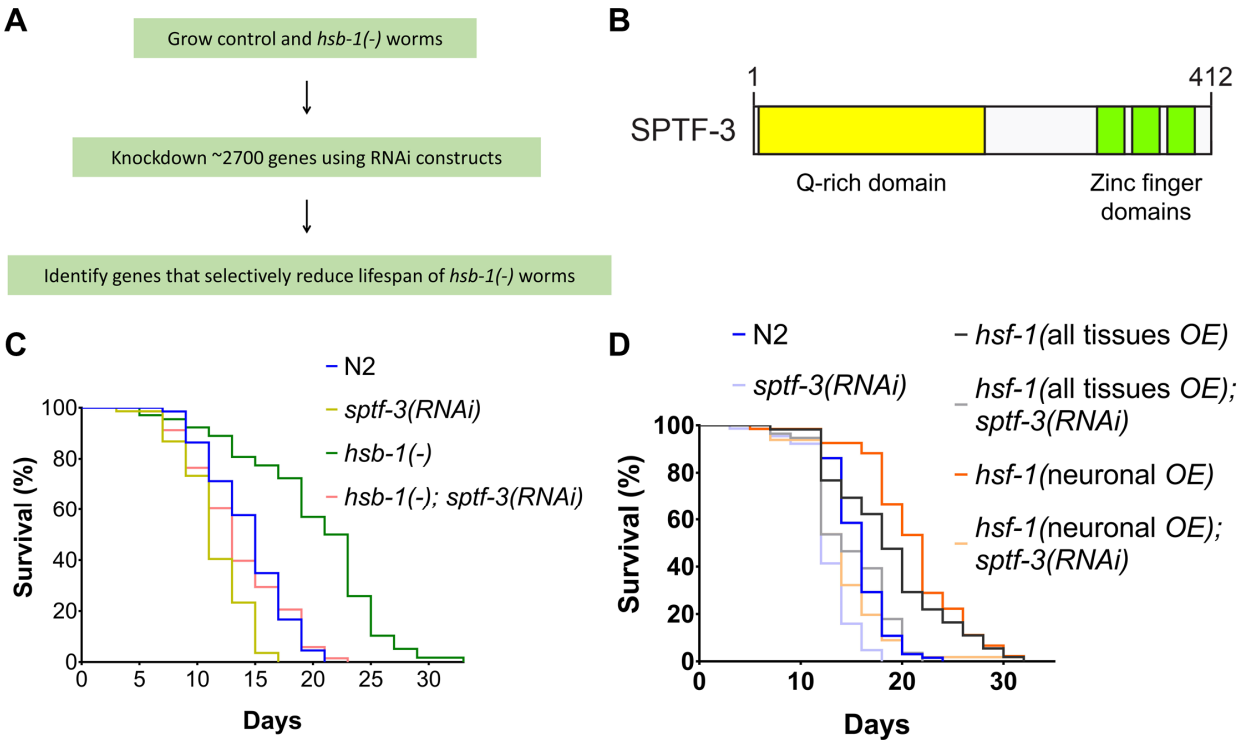

Figure 15. *sptf-3* is a genetic suppressor of *hsb-1(-)*-associated longevity.
(A) Schematic of the RNAi-based genetic screen used to identify suppressors of life span extension in *hsb-1(-)* worms. RNAi clones corresponding to ~2,700 *C. elegans* genes were screened for suppression of the *hsb-1(-)*-associated longevity phenotype.
(B) Functional domains of the SPTF-3 protein. N-terminus of the protein has a glutamine (Q)-rich domain, while the C-terminus has three zinc finger domains. Adapted from (Hirose and Horvitz, 2013).
(C) Life span analysis of wild-type (N2) and *hsb-1(-)* worms grown on control or *sptf-3* RNAi bacteria at 20°C. Statistical data and additional life span replicates are included in **Table 2**.
(D) Life span analysis of N2, *hsf-1* overexpression (all tissues) and *hsf-1* overexpression (neuronal) strains grown on control or *sptf-3* RNAi bacteria at 20°C. Statistical data are included in **Table 2**.

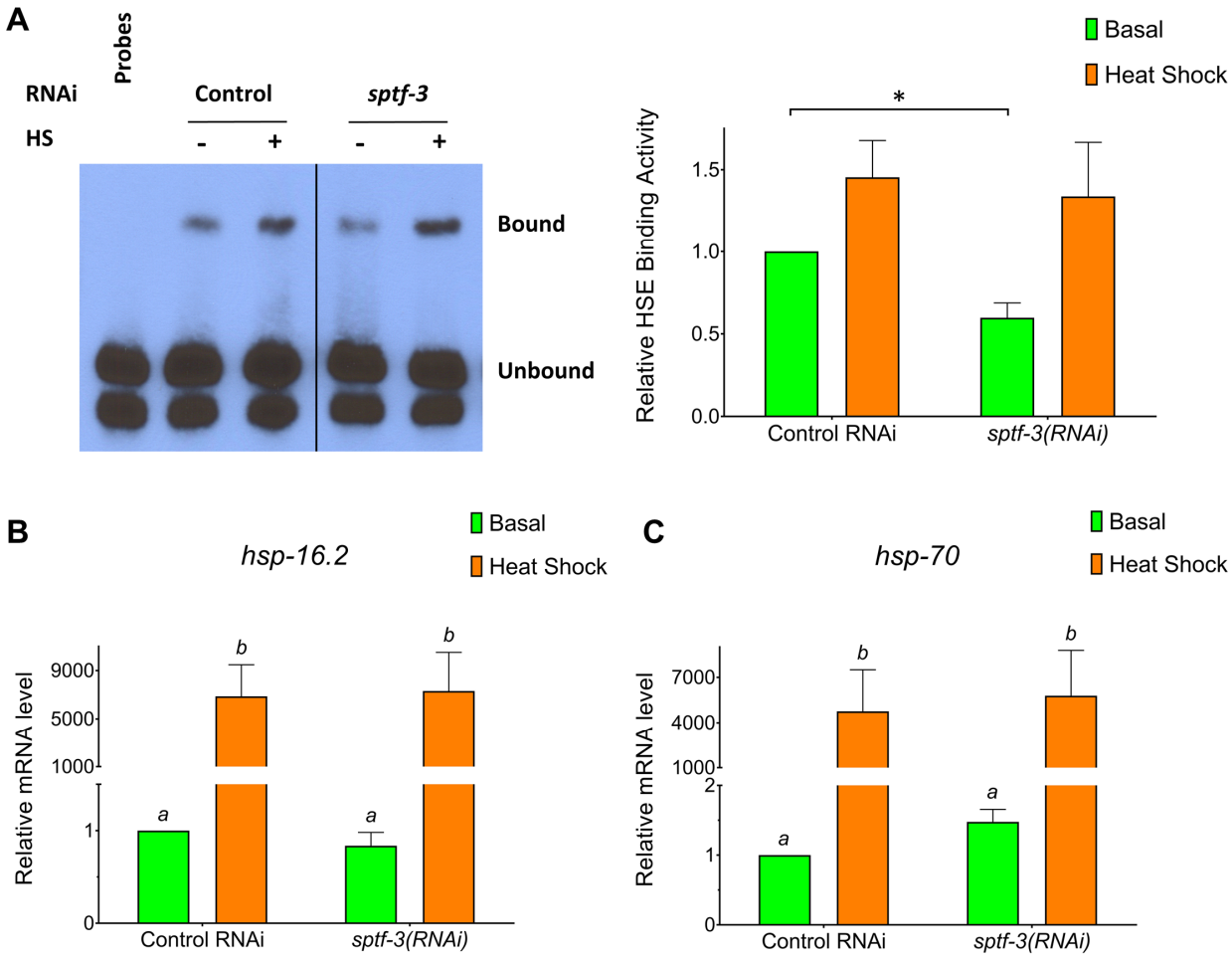

Figure 16. Inhibition of SPTF-3 suppresses DNA binding ability of HSF-1 but does not affect expression of *hsp* genes.

(A) Representative EMSA analysis for HSE binding activity of nuclear extracts from *hsb-1(-)* worms grown on control or *sptf-3* RNAi bacteria in non-stressed conditions at 20°C before or after heat shock at 37°C for 90 min (*left*). Black vertical line indicates lanes were cropped to show only data relevant to this experiment. Densitometric quantification of relative HSE binding activity relative to basal levels in control RNAi condition (*right*). Data represent mean ± SEM for ≥ 3 biological replicates. * indicates $p < 0.05$ in Fisher's least significant difference test performed after two-way ANOVA.

(B, C) Relative transcript levels of *hsp-16.2* and *hsp-70* genes in *hsb-1(-)* worms grown on control or *sptf-3* RNAi bacteria at 20°C in non-stressed conditions before or after heat shock at 37°C for 90 min. Data represent mean ± SEM for ≥ 4 biological replicates. Bars labeled with different letters are significantly different ($p < 0.05$) in Fisher's least significant difference test performed after two-way ANOVA.

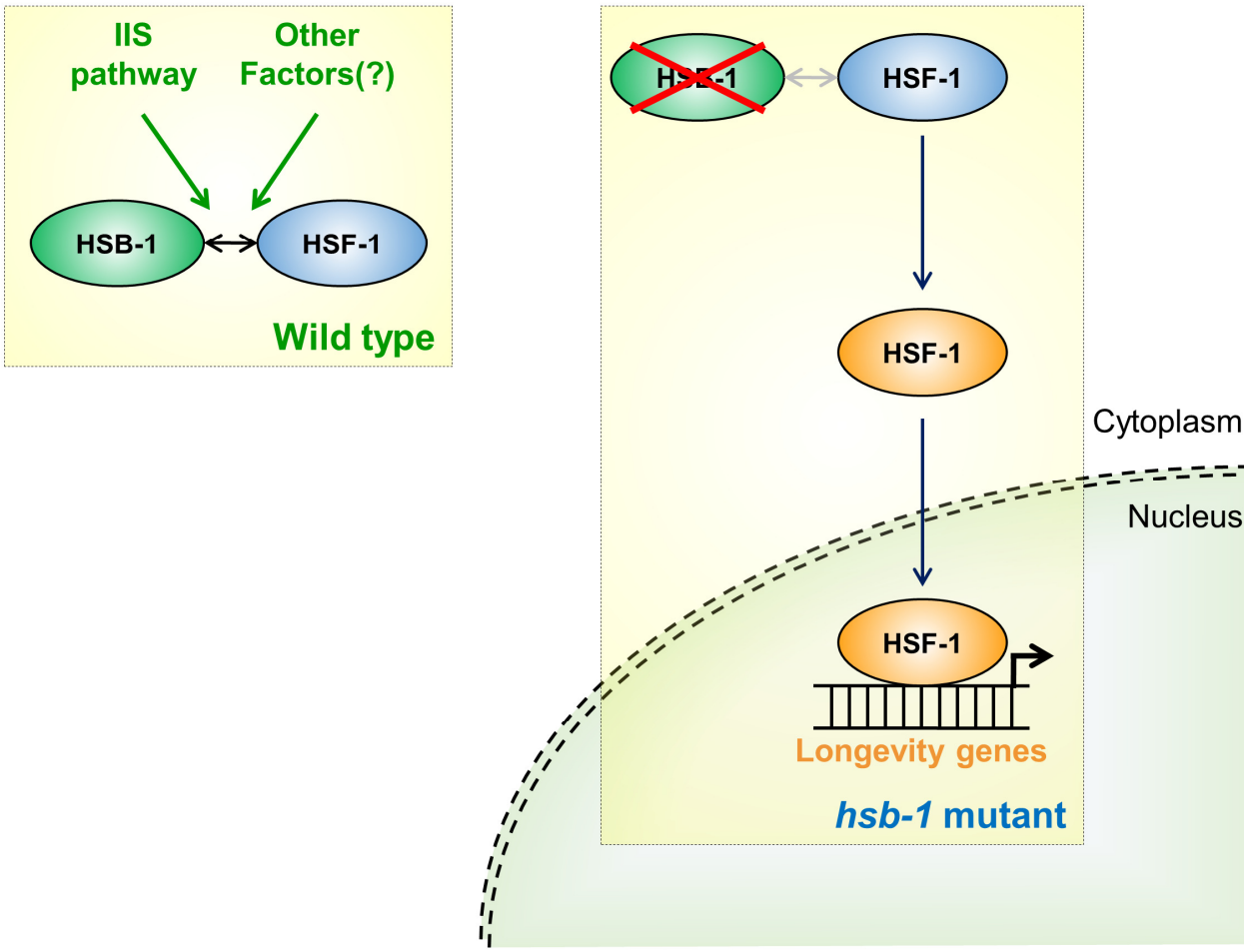

Figure 17. Model for longevity due to an HSF-1-induced altered transcriptional profile in the absence of HSB-1 regulation.
The proposed model indicates HSF-1-associated regulation of longevity in *hsb-1(-)* mutant animals. In wild-type animals, HSB-1 binds to HSF-1 and limits its transcriptional activation potential. As shown previously (Chiang et al., 2012), this binding is promoted by insulin/IGF-1-like signaling (IIS) pathway and potentially, also by other unknown factors. In the absence of HSB-1 regulation in *hsb-1(-)* mutant animals, HSF-1 protein is activated (blue to orange), translocates to the nucleus and promotes expression of its target genes. This HSF-1-induced change in the transcriptional profile results in increased life span of *hsb-1(-)* animals.

Tables

Table 2. Statistical data for life span experiments (Chapter 2).

Strain	Mean life span ± SEM (days)	75% dead (days)	n	*p* value	
N2; control (i)	15.49 ± 0.55	17	57/72	—	a
N2; *hsf-1(RNAi)* (i)	11.98 ± 0.27	15	66/72	< 0.0001[a]	b
hsb-1(cg116); control (i)	21.20 ± 0.84	27	62/72	< 0.0001[a]	c
hsb-1(cg116); hsf-1(RNAi) (i)	12.77 ± 0.41	15	55/72	0.0001[a], 0.0647[b], < 0.0001[c]	d
N2 (ii)	17.97 ± 0.55	23	76/84	—	a
daf-16(mu86) (i)	13.17 ± 0.34	16	75/84	< 0.0001[a]	b
hsb-1(cg116) (ii)	24.55 ± 0.75	29	67/84	< 0.0001[a]	c
daf-16(mu86); hsb-1(cg116) (i)	13.85 ± 0.32	18	68/84	< 0.0001[a], 0.2034[b], < 0.0001[c]	d
N2; control (iii)	15.71 ± 0.35	18	65/72	—	a
N2; *sptf-3(RNAi)* (i)	12.86 ± 0.30	16	63/72	< 0.0001[a]	b
hsb-1(cg116); control (iii)	22.36 ± 0.57	26	48/72	< 0.0001[a]	c
hsb-1(cg116); sptf-3(RNAi) (i)	17.83 ± 0.73	22	64/72	0.0028[a], < 0.0001[b], 0.0031[c]	d
*sur-5p::hsf-1(*all tissues *OE);* control (i)	18.75 ± 0.77	22	55/68	< 0.0001[a], 0.0129[c]	e
*sur-5p::hsf-1(*all tissues *OE); sptf-3(RNAi)* (i)	14.99 ± 0.50	18	56/64	0.8016[a], < 0.0001[b], < 0.0001[c], 0.0009[d], < 0.0001[e]	f
*rab-3p::hsf-1(*neuronal *OE);* control (i)	21.18 ± 0.70	24	46/72	< 0.0001[a], 0.3341[c], < 0.0001[e]	g
*rab-3p::hsf-1(*neuronal *OE); sptf-3(RNAi)* (i)	14.20 ± 0.52	16	58/72	0.0265[a], 0.0098[b], < 0.0001[c], 0.0002[d], < 0.0001[e], 0.1723[f], < 0.0001[g]	h
N2; control (iv)	14.40 ± 0.43	17	66/72	—	a
N2; *sptf-3(RNAi)* (ii)	11.50 ± 0.35	13	63/72	< 0.0001[a]	b
hsb-1(cg116); control (iv)	20.13 ± 0.76	25	59/72	< 0.0001[a]	c
hsb-1(cg116); sptf-3(RNAi) (ii)	13.47 ± 0.51	17	68/72	0.5212[a], 0.001[b], < 0.0001[c]	d

Adult 'mean life span ± SEM' in days. '75% dead' refers to 75th percentile, age at which surviving proportion of the population reaches 0.25. 'n' indicates number of observed deaths relative to total number of animals on day 1 of the experiment. The difference refers to animals that were censored at different time points due to bagging, exploding, crawling off plates or being accidentally killed. Statistical analysis was performed using Mantel-Cox log-rank test to obtain *p* values. Conditions for which life span analysis was performed more than once, their descriptions are followed by a Roman numeral in parentheses to identify independent biological replicates.

Table 3. Top RNA-Seq hits that are differentially expressed in both *hsb-1(-)* and *hsf-1* overexpression strains relative to wild-type.

Gene	Description	Log_2 fold-change in *hsb-1(-)*	Log_2 fold-change in *hsf-1* overexpression
F35E2.2	Contains F-box motif involved in protein-protein interactions	5.27	3.74
dct-9	DAF-16/FOXO controlled, germline tumor affecting	5.16	5.62
C08F1.11	Unknown function	5.05	3.73
Y41D4B.26	Unknown function	4.68	3.87
hch-1	Zinc-dependent metalloprotease; affects hatching and neuroblast migration	4.53	2.25
C08F1.10	Unknown function	4.15	2.55
Y54G2A.13	Unknown function	3.80	4.72
wrt-10	Hedgehog-like protein predicted to be involved in intercellular trafficking	3.72	2.28
fbxb-10	Contains F-box motif involved in protein-protein interactions	3.37	2.56
ceh-36	Homeodomain transcription factor expressed in the AWC and ASE chemosensory neurons	3.16	2.24
fbxb-35	Contains F-box motif involved in protein-protein interactions	2.94	2.14
F45C12.17	Unknown function	2.43	2.07
T28B8.4	Ortholog of human PSME4 (proteasome activator subunit 4)	2.35	3.81
lfi-1	Interacts with LIN-5, which is essential for proper spindle positioning and chromosome segregation	2.29	2.64
msp-19	Member of the major sperm protein family	2.23	3.60
K09C6.7	Ortholog of human TTBK1 (tau tubulin kinase 1)	2.12	3.26
W02A2.9	Unknown function	2.04	2.05
ssp-16	Sperm Specific protein family protein, class P	2.01	3.56
C17H12.5	Predicted to have protein tyrosine phosphatase activity	2.00	2.86
fbxa-192	Contains F-box motif involved in protein-protein interactions	-3.43	-2.47
fbxa-193	A predicted pseudogene	-4.79	-2.89
T20D4.7	Ortholog of human NXNL1 (nucleoredoxin-like 1) and NXNL2 (nucleoredoxin-like 2)	-5.50	-3.71
F40H7.12	Unknown function	-6.27	-5.61

Description of gene function is from www.wormbase.org. Genes with a statistically significant (FDR-adjusted $p < 0.05$) and ≥ fourfold (± 2.00 in $\log_2$ scale) increase or decrease in expression in both *hsb-1(-)* and *hsf-1* overexpression strains relative to wild-type (N2) are listed.

Table 4. Top hits identified in an RNAi-based genetic screen for suppressors of HSB-1-associated longevity.

RNAi Clone	Gene	Description	RNAi effect in wild-type [% of control]	RNAi effect in *hsb-1(-)* [% of control]	Δ (% mean life span suppression)
1 B4	*F53G12.9*	Human FAXC (Failed AXon Connections) protein ortholog	93.90*	83.44*	10.46
10 G2	*rege-1*	Human ZC3H (Zinc fingers CCCH-type) family ortholog	84.72*	73.76*	10.96
12 B3	*wdr-23*	CUL-4/DDB-1 ubiquitin ligase complex subunit that negatively regulates SKN-1	85.76*	78.73*	7.03
12 D4	*F58H10.1*	Unknown function	82.37*	70.63*	11.74
14 B6	*F43G9.12*	Predicted to have DNA binding and transcription factor activity	90.05*	79.23*	10.82
17 A9	*T23D8.3*	Human LTV1 ortholog that inhibits DHC-1 (Dynein Heavy Chain)	96.56	86.24*	10.32
17 A11	*his-67*	Histone H4 protein	84.36*	67.31*	17.05
18 D9	*pash-1*	Human DGCR8 ortholog involved in processing of primary miRNAs	89.74*	75.60*	14.14
20 H11	*ubc-12*	Ubiquitin-conjugating enzyme whose substrate is ubiquitin-like NED-8 protein	95.21	86.44*	8.77
22 E12	*clec-102*	C-type lectin with carbohydrate-binding properties	92.79	76.20*	16.59
24 C1	*sptf-3*	Zinc finger domain-containing member of the Sp1 family of transcription factors	87.36*	66.22*	21.14

'RNAi clone' location indicates plate and well information in Julie Ahringer's RNAi library. Description of gene function is from www.wormbase.org. 'RNAi effect' indicates mean life span of animals grown on RNAi bacteria calculated as a percentage of mean life span of animals grown on control bacteria for wild-type or *hsb-1(-)* genetic backgrounds. 'Δ (% mean life span suppression)' is the difference between percentage suppressions of mean life span due to RNAi in *hsb-1(-)* and wild-type genetic backgrounds. * indicates a significant ($p < 0.05$) effect of RNAi on mean life span determined using Mantel-Cox log-rank test.

Table 5. List of primer sequences used for EMSA and quantitative RT-PCR experiments (Chapter 2).

Target	Forward Primer (5' – 3')	Reverse Primer (5' – 3')
EMSA		
hsp-16.1 HSE	5'-biotin-TEG-labeled-AACCGTATCCTGCAGCCGTTTAGAATGTTCTAGAAGGTCCTAGATGCATT	5'-biotin-TEG-labeled-TTGAAATGAATGCATCTAGGACCTTCTAGAACATTCTAAACGGCTGCAGG
Quantitative RT-PCR		
cdc-42	GCGTTGACGCAGAAGGGACTG	CAAGGAAGACGTTCCTAGAGAATATTGCACTTC
pmp-3	GGAACTTAGAGTCAAGGGTCGCAG	GAACTGTATCGGCACCAAGGAAACTG
hsf-1	GGCTCAGCCGCAACAAGACTATTC	CTGATGTGGTTGAAGGTATTGATGAGATGGTTG
hsp-16.2	CTCCATCTGAGTCTTCTGAGATTGTTAACAATGATC	GGATTGATAGCGTACGACCATCCAAATTAATTTTC
hsp-70	CAATGGGAAGGACCTCAACTGCTC	GATAGTATCATCTTTTACTCCAGAAAGTACAGCTGC
C08F1.10	TGAAACGGTATTTGACGGCAG	TCATTTCTTTCGCCCAGCTG
Y82E9BR.17	GACAATGATCAAAAGCCACTTC	TAAATTATTTCAAACGACGACTCG
zip-8	TATGTCTATCGAACGAGAAGCATAC	ACGAAGTGGTTGCGGAGGTTCG
arrd-1	GACAGCCGACATTTAAGGTTAC	CGGCATAGATTTTTTTGACAGTTG
his-24	GGCCATCAAGCAGCTCAAG	GATGAGCATTGATCTGGATGACATT
dpy-14	GATGGAAGAGTTATTAATGTCAATGGAC	CTGATCCTGGAACTCCCTTTG
ham-1	CCTACCAAGAATAAGTACCCGAC	CATTCCGAACTAGACGAGAGTAG
sdz-28	CTGAAGAGTTTAAAGACGCATTGC	GCCATAACTACTTCTGGATCCATG
clec-266	CAACTAGACTCAACTGGCTCATC	AAAGAGCATGGCTGGAAGTATG
arrd-4	CGATTTCGTTGAAGGTTTCTGTTC	TTCGTTGATTGTTGAGGAGCTG
lfi-1	GAAGATTCGGGATCGGTGTAC	CGCACGAGAGATGGAATCG
cht-1	CGTTCTTTGTCTGAGCTCAAAATC	GTAGTGGTCACAGAACATCCAG
noah-1	CCACTTCAACAGGTAAATGAGC	TGACAGAGTTCAGGCAGATTG
W02A2.9	CTCTTCTTCTCCCACCAATTG	GGTATGAAGCCGAGAATTGTG
mnp-1	TCTGTGTTTAAGTTCATGGCTC	GCATTTCTCGGATTGCGTG
cec-8	GGAGAAGAGCTTGAGAACTGTC	CATCTTCAGACTCCTCAGAATCG
wrt-10	GGAAGTTACAACTACCCCAGCAC	GCTCTACGGATTCCAGTCGATTG
mtl-1	GGCTTGCAAGTGTGACTGCA	ACTGGCCTCCTCACAGCAG
dod-3	CGAATGAGCCGGTGTTCATGTG	GACAACAGCAATAAGGAGGACGTATC
clec-196	GAGGAGGAATTAGAATGGCTGTACGAG	GTTGGTGACGAGTAGAAGGCGATAC
acdh-8	TGCTTGTCAGATCTTCGGAGGTG	GTGCGACCAATGACCATACGTTG
sams-5	GATCATCAAAAATCTGGACTTGAAGAGAG	CTTGAGCTTACGAGCCTGCTC

cyc-2.2	CGGAACTAAGATGGTCTTCGCTG	TGGTTTCTTGGCAGCTTCCAC
Y41G9A.10	GGAATTCTGAACAGGGTGAAACGTG	CTCCAGGTTGTCCATAACCACTTG

Contributions

Figures 9–13 and 14A–C: Bioinformatic analysis of RNA-Seq data was performed by Dr. Tzu-Chiao Lu. The plots were generated from the analyzed data by the author.

Figure 14D: Quantitative RT-PCR measurements for some of the genes were performed by Seung Ah Jung.

Figure 15A: The RNAi-based genetic screen for identifying suppressors of HSB-1-associated longevity was performed by Carol Mousigian.

Chapter 3. HSB-1/HSF-1 pathway modulates histone H4 in mitochondria to control mtDNA transcription and longevity ‡

Abstract

Heat shock factor-1 (HSF-1) is a master regulator of stress responses across taxa. Overexpression of HSF-1 or genetic ablation of its conserved negative regulator, heat shock factor binding protein 1 (HSB-1), results in robust life span extension in *C. elegans*. Here we found that increased HSF-1 activity elevates histone H4 levels in somatic tissues during development, while knockdown of H4 completely suppresses HSF-1-mediated longevity. Moreover, overexpression of H4 is sufficient to extend life span. Ablation of HSB-1 induces an H4-dependent increase in MNase-protection of both nuclear chromatin as well as mitochondrial DNA (mtDNA), which consequently results in reduced transcription of mtDNA-encoded complex IV genes, decreased respiratory capacity and a mitochondrial unfolded protein response (UPR^{mt})-dependent life span extension in animals. Collectively, our findings unveil a novel role of HSB-1/HSF-1 signaling in modulation of mitochondrial function via mediating histone H4-dependent regulation of the mitochondrial genome, and concomitantly acting as a determinant of organismal longevity. This phenomenon signifies interplay between three distinct longevity regulators: stress response, chromatin dynamics and mitochondrial

‡ The findings from this chapter have been submitted for publication as: Sural et al. (2019). HSB-1/HSF-1 pathway modulates histone H4 in mitochondria to control mtDNA transcription and longevity.

function, and suggests a role of histones in locus-specific regulation of the mitochondrial genome. These findings provide unexpected insights into the holistic inter-pathway network that manifests life span extension in complex organisms.

Introduction

The rate of aging in multicellular organisms is determined by several evolutionarily conserved cellular and metabolic processes (López-Otín et al., 2013; Riera et al., 2016). Some recent studies have identified interconnectedness among these pathways in the context of longevity regulation (Chiang et al., 2012; Hwang et al., 2014; Matilainen et al., 2017; Merkwirth et al., 2016), but the hierarchy between these hallmarks of aging at the systemic level remains less understood. Maintenance of protein homeostasis constitutes one such hallmark that undergoes impairment during normal aging and in numerous age-associated diseases (Hipp et al., 2019). Misregulation in the function of chaperone complexes results in elevated misfolding and aggregation of proteins with age that is further exacerbated by metabolic and environmental stress (Powers et al., 2009). A major component of the protein homeostasis network in eukaryotes is the evolutionarily conserved heat shock response (HSR) pathway (Taylor and Dillin, 2011). HSR involves activation of members of the heat shock factor (HSF) family in response to a variety of environmental stresses such as heat, oxidative damage, proteotoxic insults and pathogenic infection (Gomez-Pastor et al., 2018; Morimoto, 2011). While mammals have four distinct heat shock factors (HSF1–4), invertebrates such as *C. elegans*, *Drosophila* and yeast possess only one ortholog of HSF1. In the presence of stress stimuli, HSF1 binds to its target elements in the genome to induce the

transcription of proteases and heat shock proteins (HSPs) (Gomez-Pastor et al., 2018). HSPs often function as molecular chaperones to assist in the folding of nascent polypeptides and to prevent the toxic aggregation of misfolded proteins, thus attenuating the loss of protein homeostasis induced during stress conditions (Richter et al., 2010).

HSF1 has also been shown to regulate longevity of animals in non-stressed physiological conditions. In the nematode worm *C. elegans*, overexpression of *hsf-1* extends life span and delays the onset of age-related neurodegenerative diseases, while inhibition of HSF-1 activity accelerates aging (Cohen et al., 2006; Hsu et al., 2003; Morley and Morimoto, 2004). In mammals, transgenic HSF1 activation has been shown to promote longevity in a neurodegenerative mouse model (Fujimoto et al., 2005), while knockout of HSF1 dramatically shortens life span in a murine model of prion disease (Steele et al., 2008). Initial studies suggested that life span extension associated with HSF-1 activation is at least partially due to increased expression of small HSPs (Hsu et al., 2003). A recent study showed that overexpression of a truncated form of HSF-1 extended life span in worms independent of its ability to mount stress-induced activation of HSPs (Baird et al., 2014). Incidentally, prolonged life span due to transgenic HSF1 activation in a neurodegenerative mouse model did not involve increased expression of HSPs in brain tissue (Fujimoto et al., 2005). These findings indicate that the longevity promoting effects of HSF1 are not solely attributable to chaperone induction, but possibly also involve other unidentified cellular processes. In fact, HSF1 has also been ascribed regulatory functions in several physiological processes other than stress

response, such as animal development, reproduction, metabolism and cancer (Gomez-Pastor et al., 2018; Li et al., 2017).

Under normal conditions, the transcriptional activity of HSF1 is inhibited by several regulatory mechanisms that collectively dictate context-dependent modulation of HSF-1 function (Gomez-Pastor et al., 2018). One such negative regulator of HSF-1 is the heat shock factor binding protein 1 (HSB-1), which physically binds to HSF-1 to form an inhibitory multiprotein complex (Chiang et al., 2012; Satyal et al., 1998). The formation of this HSF-1-inhibitory complex in *C. elegans* is not affected by heat stress, but instead is facilitated by the insulin/IGF-1-like signaling (Chiang et al., 2012), a pathway implicated in regulation of longevity in animals across evolutionary taxa (Riera et al., 2016). A loss-of-function mutation in the *hsb-1* gene results in dissociation of HSF-1 from this inhibitory complex and induces a robust *hsf-1*-dependent extension of life span in worms (Chiang et al., 2012). However, the underlying longevity promoting mechanisms of the HSB-1/HSF-1 signaling pathway still remain elusive.

In this study, we show that longevity achieved via HSF-1 activation by inhibiting HSB-1 is largely due to increase in the levels of histone H4 protein. Overexpression of H4 in wild-type animals phenocopies the longevity effect of *hsb-1* null mutation. We also show that elevated H4 levels in *hsb-1(-)* worms influence the global compaction of nuclear chromatin, and strikingly, also of mitochondrial DNA (mtDNA). We further elucidate how histone H4 modulates the expression of mitochondrially-encoded electron transport chain (ETC) complex IV subunits, and how this affects respiratory capacity in animals. Moreover, we provide evidence for the presence of histone H4 in mitochondria

and how this results in a mitochondrial unfolded protein response (UPR^{mt})-dependent life span extension in worms. Overall, this study connects HSB-1/HSF-1 signaling to changes in histone H4 levels and provides direct evidence for a novel role of histone H4 in the regulation of mitochondrial activity.

Materials and Methods

C. elegans strains

All strains were maintained at 20°C on nematode growth medium (NGM) plates seeded with *E. coli* OP50 strain using the standard method, unless otherwise stated. Animals were cultured for at least three generations in optimum conditions before they were used for experiments. The following strains were used in this study:

N2: wild-type

EQ450: *hsb-1(cg116) IV*; CH116 outcrossed 4x to wild-type N2

CF512: *rrf-3(b26) II; fem-1(hc17) IV*

EQ196: *rrf-3(b26) II; fem-1(hc17) IV; hsb-1(cg116) IV*

CF1903: *glp-1(e2144) III*

EQ431: *glp-1(e2144) III; hsb-1(cg116) IV*

AGD710: *uthIs235*[(*sur-5p::hsf-1::unc-54* 3' UTR) + (*myo-2p::tdTomato::unc-54* 3' UTR)]

CF1041: *daf-2(e1370) III*

MQ887: *isp-1(qm150) IV*

EQ435: *iqEx136*[(*sur-5p::his-67*) + (*sur-5p::his-50*) + (*sur-5p::his-37*) + (*rol-6p::rol-6(su1006)*)]

SS104: *glp-4(bn2) I*

EQ454: *glp-4(bn2) I; hsb-1(cg116) IV*

SJ4103: *zcIs14*[*myo-3p::*GFP(mitochondrial)]

SJ4143: *zcIs17*[*ges-1p::*GFP(mitochondrial)]

QK701: *rde-1(ne219) V; xkIs*[(*ges-1p::rde-1*) + (*myo-2p::rfp*)]

EQ1404: *hsb-1(cg116) IV; rde-1(ne219) V; xkIs*[(*ges-1p::rde-1*) + (*myo-2p::rfp*)]

EQ1426: *iqIs276*[(*ges-1p::tomm-20::mCherry*) + (*rol-6p::rol-6(su1006)*)]

Wild-type (N2), CH116, MQ887, SS104, SJ4103 and SJ4143 strains were obtained from *Caenorhabditis* Genetics Center (Saint Paul, MN). AGD710 and QK701 strains were generous gifts from the laboratories of Andrew Dillin (UC Berkeley) and John Kim (Johns Hopkins), respectively. CF1903, EQ431, SS104 and EQ454 strains, carrying temperature-sensitive *glp-1(e2144)* or *glp-4(bn2)* mutation, were maintained at 15°C. For generation of EQ435 strain, a plasmid DNA mix consisting of 80 ng/µL of pRF4(*rol-6p::rol-6(su1006)*) and 10 ng/µL each of pAH186(*sur-5p::his-67*), pAH187(*sur-5p::his-50*) and pAH188(*sur-5p::his-37*) was microinjected into the gonad of young adult N2 hermaphrodite animals. F1 progeny was picked on the basis of roller phenotype and individuals from F2 progeny were isolated to generate the EQ435 strain. *his-67*, *his-50* and *his-37* genes were selected for overexpression because each of these correspond to one of the three structural variants of *C. elegans* histone H4 genes, all coding for the identical H4 protein. The promoter region of the ubiquitously expressed *sur-5* gene was used for H4 overexpression. Microinjection of N2 worms with pRF4(*rol-6p::rol-6(su1006)*) alone did not affect the mean life span of wild-type animals when grown on OP50 or HT115(DE3) bacteria (data not shown). For generation of EQ1426 strain, a

plasmid DNA mix consisting of 80 ng/µL of pRF4(*rol-6p::rol-6(su1006)*) and 20 ng/µL of pAH785(*ges-1p::tomm-20::mCherry*) was microinjected to obtain F1 progeny with extrachromosomal arrays. Integrated lines were generated via UV irradiation followed by six generations of backcrossing to N2 worms. The mCherry signal was confirmed via fluorescence microscopy and immunoblot analysis. All experiments in this study were performed using day 1 adult worms that were obtained after transferring unhatched eggs to 25°C, unless otherwise stated.

RNA interference analysis

RNAi clones used in this study were picked from Julie Ahringer's library and were confirmed by sequencing using M13 forward primer (5'-TGTAAAACGACGGCCAGT-3'). HT115(DE3) *E. coli* bacteria transformed with either empty vector (L4440) or plasmid expressing double-stranded RNA for desired gene were grown in LB supplemented with 100 µg/mL carbenicillin at 37°C overnight. Bacterial cultures were seeded on NGM or high-growth (HG) plates containing 100 µg/mL carbenicillin. IPTG was added to the plates to a final concentration of 1 mM. Animals were subjected to RNAi by transferring unhatched eggs to RNAi plates at 25°C, unless otherwise stated. For RNAi only during adulthood, worms were transferred from L4440 plates to RNAi plates at late L4–young adult stage.

Life span analysis

Synchronized eggs were transferred by picking to NGM plates seeded with OP50 or HT115(DE3) bacteria (for RNAi conditions) at 25°C, unless otherwise stated. On day 1 of adulthood, worms were transferred to fresh plates with bacteria at a density of 12–15

worms per plate. Worms were subsequently transferred to new plates everyday till egg-laying continued. Viability of worms was scored every 1–2 days. Animals that were immobile and did not respond to gentle touch of a platinum pick were scored as dead. Worms that bagged, exploded, crawled off plates or were accidentally killed during the experiment were censored.

Genome-wide RNA interference screen

For the primary screen, ~50 synchronized *rrf-3(-); fem-1(-); hsb-1(-)* eggs were transferred to 25°C on NGM plates seeded with double stranded RNA-expressing HT115(DE3) bacteria (corresponding to 2,700 RNAi clones from Julie Ahringer's library) at a density of ~50 eggs per plate on three plates per RNAi condition. On day 14–17 of adulthood, the proportion of alive worms on RNAi plates was compared to that on plates in which worms were fed empty vector-transformed bacteria. RNAi clones for which the proportion of surviving worms was at least 25 percentage points lower than that observed in control bacteria-fed worms were selected for subsequent analyses. For the secondary screen, ~50 synchronized eggs for both *rrf-3(-); fem-1(-)* and *rrf-3(-); fem-1(-); hsb-1(-)* strains were transferred to 25°C on three plates per RNAi condition for clones that passed the criterion for primary screening. Proportion of alive worms on RNAi plates was estimated on days 12, 13 and 15 of adulthood. RNAi clones for which the proportion of surviving *rrf-3(-); fem-1(-)* worms was at most 10 percentage points lower than that observed in control bacteria-fed *rrf-3(-); fem-1(-)* worms were selected for the tertiary screen. The purpose of the secondary screening step was to eliminate RNAi clones that induce a similar life span shortening effect in both *hsb-1(WT)* and *hsb-1(-)* strains. For the final step of the screen, a comprehensive life span analysis was

performed with *rrf-3(-); fem-1(-)* and *rrf-3(-); fem-1(-); hsb-1(-)* worms at 25°C using RNAi clones that passed the criterion for secondary screening. RNAi clones for which the mean life span shortening effect in *rrf-3(-); fem-1(-); hsb-1(-)* worms was at least 10 percentage points greater than that observed in *rrf-3(-); fem-1(-)* worms were identified as suppressors of *hsb-1(-)*-associated life span extension.

Immunoblot analysis

~4000 age-synchronized young adult worms or ~20,000 age-synchronized L1 stage worms grown on NGM plates at 25°C were collected in M9 buffer containing 0.01% Triton X-100 and were washed three times with M9 buffer. Worms were suspended in 3 times the volume of 6x Sample Buffer (375 mM Tris-Cl at pH 6.8, 12% SDS, 60% glycerol, 600 mM DTT, 0.06% Bromophenol Blue) diluted to 2X final concentration and snap-frozen in liquid nitrogen for 30 sec. Samples were then boiled for 10 min, centrifuged at 16,000 x g for 1 min and subjected to SDS-PAGE using SE 250 mini-vertical unit (GE Healthcare). Proteins were transferred to Immobilon-P PVDF membrane (Millipore Sigma) at 400 mA for 40 min using Trans-blot SD semi-dry transfer cell (Bio-Rad) and membrane was blocked in 5% blocking-grade blocker (Bio-Rad) for 1 hr at room temperature. Primary antibody incubation was performed for 12 hr at 4°C using the following antibodies: Histone H4 – Millipore Sigma 05-858 (1:10,000); Histone H3 – Abcam ab1791 (1:10,000); Histone H2A – Abcam ab88770 (1:1,000); Histone H2B – Abcam ab1790 (1:10,000); β-actin – Abcam ab8227 (1:10,000); α-tubulin – Abcam ab52866 (1:10,000); γ-tubulin – Abcam ab50721 (1:2,000). Membrane was washed 4 times with TBS buffer containing 0.1% Tween 20 (TBS-T) for 5 min per wash, incubated with HRP-conjugated secondary antibody for 1 hr at room temperature and

washed again 4 times with TBS-T buffer for 5 min per wash. Blots were developed using SuperSignal West Pico Plus chemiluminescent substrate (Thermo Fisher) and visualized using ChemiDoc MP imaging system (Bio-Rad). Relative protein levels were quantitated using ImageJ densitometry.

RNA isolation and quantitative RT-PCR

~2,000 age-synchronized young adult worms or ~10,000 age-synchronized L1 stage worms grown on NGM plates at 25°C were collected in M9 buffer containing 0.01% Triton X-100 and were washed three times with M9 buffer. Total RNA was extracted with TRIzol reagent (Thermo Fisher) using the manufacturer's protocol and DNase-treatment was performed using TURBO DNA-free kit (Themo Fisher). cDNA was synthesized from 5 µg RNA with 6 µM random primer mix (New England Biolabs) using SuperScript III reverse transcriptase (Thermo Fisher). Real-time quantitative PCR was performed with Power SYBR Green PCR master mix (Thermo Fisher) and PCR primers (listed in Table 10) using CFX96 Real-Time PCR detection system (Bio-Rad). Primers were designed using the Primer3Plus online tool. Relative transcript levels were calculated using comparative Ct method and the housekeeping gene *cdc-42* was used as internal control for normalization (Hoogewijs et al., 2008), unless otherwise stated. For comparison of transcript levels across age groups, the gene *pmp-3* was used as internal control due to its stable expression pattern across different conditions (Hoogewijs et al., 2008; Zhang et al., 2012). For animals of the same age group, normalization of transcript levels using either *cdc-42* or *pmp-3* led to similar results. For comparison across strains, expression levels of mitochondrially-encoded genes were normalized to relative mitochondrial DNA copy number.

DNA damage assay

Age-synchronized young adult worms grown on NGM plates at 25°C were exposed to 254 nm wavelength UV radiation using UV Stratalinker 1800 (Stratagene). Worms were added to lysis buffer [1x standard *Taq* reaction buffer (New England Biolabs) containing 1 mg/mL proteinase K (Sigma-Aldrich)] in batches of 6 worms/60 µL buffer and were immediately frozen at -80°C for 15 min. Samples were incubated at 65°C for 1 hr, followed by at 95°C for 15 min and the purified DNA was stored at -80°C. DNA lesion frequency was calculated using a previously described quantitative PCR-based DNA damage assay protocol (Gonzalez-Hunt et al., 2016). The assay is based on the principle that DNA lesions block or inhibit the progression of DNA polymerases during PCR amplification of a large genomic fragment. Briefly, a 9.3 kb fragment of the *unc-2* gene was amplified from template DNA of UV-damaged worms using LongAmp hot start *Taq* 2x master mix (New England Biolabs) and PCR primers listed in Table 10. The PCR product was quantified using Quant-iT PicoGreen dsDNA assay kit (Thermo Fisher). To determine the starting amount of DNA for each condition, real-time quantitative PCR was performed for a 164 bp fragment of *W09C5.8* gene, as described previously, from template DNA of UV-damaged worms using PCR primers listed in Table 10. Relative amplification value for the long amplicon PCR product was quantified by normalization with starting amount of DNA determined from short amplicon PCR. Number of DNA lesions per 10 kb of DNA was estimated based on inhibition of PCR amplification of the large genomic fragment from UV-treated worms compared to amplification of non-damaged template DNA from control worms, assuming a Poisson distribution of UV-induced lesions.

Micrococcal nuclease (MNase) digestion

~50,000 age-synchronized young adult worms grown on HG plates at 25°C were collected in M9 buffer containing 0.01% Triton X-100. Worms were washed three times with M9 buffer and were resuspended in an equal volume of 2x Buffer A [30 mM HEPES-Na at pH 7.5, 680 mM sucrose, 120 mM KCl, 30 mM NaCl, 2 mM DTT, 1 mM spermidine (Sigma-Aldrich), 0.3 mM spermine tetrahydrochloride (Sigma-Aldrich), 50 mM sodium bisulphite]. Samples were frozen in liquid nitrogen and stored at -80°C. For MNase digestion, frozen worm pellets were grinded in liquid nitrogen in a mortar and pestle and $CaCl_2$ was added to a final concentration of 1 mM. Micrococcal nuclease (Sigma-Aldrich) was added to a final concentration of 0, 2.5 or 25 units/µL and digestion was performed at 16°C for 12 min. The digestion reaction was stopped by addition of an equal volume of worm lysis buffer (100 mM Tris-Cl at pH 8.5, 100 mM NaCl, 50 mM EDTA, 1% SDS). Proteinase K (Sigma-Aldrich) was added to a final concentration of 1 mg/mL and samples were incubated at 65°C for 45 min with intermittent vortexing. Samples were subjected to three sequential extraction steps using equal volumes of phenol, phenol: chloroform: isoamyl alcohol and chloroform with centrifugation at 13,000 x g for 5 min. One-tenth volume of 8 M ammonium acetate solution and 2x volume of ethanol were added to precipitate DNA and samples were centrifuged at 13,000 x g for 10 min. DNA pellets were washed with ethanol and resuspended in 1x TE buffer (10 mM Tris-Cl at pH 8.0, 1 mM EDTA). RNase A (Thermo Fisher) was added to a final concentration of 5 ng/µL and samples were incubated at 37°C for 2 hr. Subsequently, glycogen (Sigma-Aldrich) was added to a final concentration of 400 µg/mL followed by addition of 3x volume of DNA extraction buffer (1 M ammonium acetate, 10 mM EDTA,

0.2% SDS). Samples were then subjected to two sequential extraction steps using equal volumes of phenol: chloroform: isoamyl alcohol and chloroform with centrifugation at 13,000 x g for 6 min. DNA was precipitated by adding 2x volume of ethanol and incubation at -20°C for 1 hr, followed by centrifugation at 13,000 x g for 9 min. DNA pellets were resuspended in 1x TE buffer and subjected to electrophoresis on a 2% agarose gel to visualize the extent of MNase digestion. Concentration of mononucleosomal and dinucleosomal DNA fragments in the samples were quantified using a high sensitivity DNA analysis kit (Agilent Technologies) on a Bioanalyzer 2100 instrument (Agilent Technologies).

MNase sequencing and data analysis

C. elegans chromatin samples digested with 25 units/µL of MNase enzyme, as described previously, were used for library preparation (4 biological replicates per condition). For each sample, 20 ng DNA was end-repaired, adapter-ligated and PCR-amplified for 13 cycles using Apollo 324 library preparation system (Wafergen Bio-systems). All samples were multiplexed for 150 bp paired-end sequencing on two lanes of a HiSeq 4000 platform (Illumina). For bioinformatic analysis of raw sequencing data, low quality sequences and adapters were first trimmed using Trimmomatic tool (Bolger et al., 2014). FastQC (available at https://www.bioinformatics.babraham.ac.uk/projects/fastqc/) was then used for quality control of trimmed raw data. Next, Paired-End reAd mergeR (PEAR) was used to assemble read pairs (Zhang et al., 2014). Subsequently, Bowtie 2 was used to align sequencing reads to the *C. elegans* genomic dataset version WS254 (Langmead and Salzberg, 2012). Nucleosome dynamics was determined from aligned sequencing reads using the Dynamic Analysis of Nucleosome Position and

Occupancy by Sequencing version 2 (DANPOS2) tool (Chen et al., 2013). MNase-Seq data for specific genomic regions were visualized on Integrated Genome Browser (Freese et al., 2016).

Relative mitochondrial DNA copy number

Mitochondrial DNA content relative to nuclear DNA in worms was quantified using a previously described method (Gonzalez-Hunt et al., 2016). Briefly, age-synchronized young adult worms grown on NGM plates at 25°C were added to lysis buffer [1x standard *Taq* reaction buffer (New England Biolabs) containing 1 mg/mL proteinase K (Sigma-Aldrich)] in batches of 8 worms/60 µL buffer and were immediately frozen at -80°C for 15 min. Samples were incubated at 65°C for 1 hr, followed by at 95°C for 15 min. Mitochondrial and nuclear DNA content were estimated using real-time quantitative PCR, as described previously, with PCR primers listed in Table 10. Ratio of mitochondrial DNA: nuclear DNA copy number was calculated using comparative Ct method.

Mitochondrial oxygen consumption assays

Mitochondrial Oxygen Consumption Rate (OCR) was calculated using Seahorse XFe96 analyzer (Agilent Technologies) based on a previously described protocol (Koopman et al., 2016). Briefly, age-synchronized young adult worms grown on NGM plates at 25°C were collected in M9 buffer containing 0.01% Triton X-100. Worms were washed three times with M9 buffer and added to a 96 well plate at a density of 10–20 worms/well. Basal OCR measurement was performed 5 times, followed by measurement of maximal respiratory capacity for 9 times after addition of FCCP (10 µM; Sigma-Aldrich).

Subsequently, non-mitochondrial respiration was measured 4 times in presence of 40 mM sodium azide. Oxygen consumption rates per worm were determined after normalization to number of worms in each well. Basal mitochondrial OCR per worm and maximal mitochondrial respiratory capacity per worm were obtained from measured OCR values after subtraction of non-mitochondrial respiration rates. Spare respiratory capacity per worm was calculated as the difference between maximal mitochondrial respiratory capacity per worm and basal mitochondrial OCR per worm for each well.

Immunofluorescence and mitochondrial labeling

Fixation and immunostaining of worms were performed using a previously described protocol (Shakes et al., 2012). ~4,000 age-synchronized young adult worms grown on NGM plates at 25°C were harvested in M9 buffer containing 0.01% Triton X-100. Worms were washed three times with M9 buffer and if required, were incubated in 10 µM MitoTracker Orange CMTMRos solution (Thermo Fisher) for 1 hr at 25°C in the dark. Worms were then washed with ice-cold M9 buffer and fixed using a mixture of methanol, Bouin's fixative [1.2% (w/v) picric acid, 37% (w/v) formaldehyde and glacial acetic acid in 15:5:1 ratio] and β-mercaptoethanol (Sigma-Aldrich) in 50:50:1 ratio. Samples were frozen in liquid nitrogen and permeabilized by immediately thawing in a 25°C water bath for three freeze-thaw cycles. Worms were subsequently incubated on ice for 30 min, washed five times in BT buffer (50 mM H_3BO_3, 25 mM NaOH, 0.5% Triton X-100 at pH 9.5) for 5 min per wash and then washed 5 times in BT buffer containing 2% (v/v) β-mercaptoethanol for 1 hr per wash. Worms were then rinsed once with PBS buffer containing 0.1% Tween-20 and incubated in blocking solution (1% bovine serum albumin and 0.1% Tween-20 in PBS buffer) for 1 hr at room temperature.

For primary antibody incubation, worms were incubated with the following antibodies for 3 days at 4°C with gentle agitation: Alexa Fluor 488-conjugated H4 antibody – Abcam ab207387 (1:50); H4 – Abcam ab177840 (1:50); GFP – Abcam ab1218 (1:200). Subsequently, worms were washed six times in antibody wash buffer (0.1% bovine serum albumin in PBS buffer) for 5 min per wash at room temperature, and with a final wash for 2 hr at 4°C. For samples treated with unconjugated primary antibodies, secondary antibody incubation was performed for 1 day at 4°C with Alexa Fluor Plus 488-conjugated goat anti-mouse IgG or Alexa Fluor Plus 555-conjugated goat anti-rabbit IgG at 1:500 dilution. Worms were again washed six times in antibody wash buffer for 5 min per wash at room temperature, and then incubated in PBS containing 1 µg/mL 4′,6-Diamidine-2′-phenylindole dihydrochloride (DAPI) for 30 min at room temperature. Worms were mounted on a glass slide using Fluoroshield Mounting Medium (Abcam), and a coverslip was placed on top before imaging. Fluorescence imaging was performed on a Nikon A1 confocal microscope, equipped with diode-based laser system for 405, 488, 561 and 640 nm excitation, using NIS-Elements (Nikon) imaging software. Images were processed using the Fiji platform on ImageJ.

Mitochondrial isolation

Isolation of mitochondria was performed as described previously (Daniele et al., 2016; Jonassen et al., 2002). ~60,000 age-synchronized L4 stage worms grown on HG plates at 25°C were collected in M9 buffer containing 0.01% Triton X-100 and were washed three times with M9 buffer. The worms were then washed once with ice-cold mitochondria isolation buffer (10 mM HEPES-KOH at pH 7.5, 210 mM mannitol, 70 mM sucrose, 1 mM EDTA) with protease inhibitor cocktail (Roche), phosphatase inhibitors

(Roche) and 1 mM phenylmethylsulfonyl fluoride (PMSF; Sigma-Aldrich). The worm pellet was resuspended in 10 times the volume of mitochondria isolation buffer and transferred in a 7 mL Dounce tissue grinder (Kimble) placed on ice. The sample was homogenized with pestle A for 20 strokes and pestle B for 40 strokes on ice, and then centrifuged at 800 x g for 10 min to remove debris. The supernatant was carefully filtrated using a syringe filter with a pore size of 1.2 µm (Sartorius) to remove nuclei contamination. The filtrate was then centrifuged at 12,000 x g for 10 min to pellet total mitochondria. The mitochondrial pellet was gently washed for three times with mitochondria isolation buffer and resuspended in the same buffer.

Proteinase K protection assay

Freshly isolated mitochondria were digested with proteinase K as described previously (Chatterjee et al., 2016; Zhou et al., 2008). Briefly, the suspension of isolated mitochondria was first adjusted to a protein concentration at 1 µg/µL in mitochondria isolation buffer without protease inhibitors and was incubated with various concentrations of proteinase K (Invitrogen) for 15 min on ice. Proteinase K digestion was stopped with 20 mM PMSF (Sigma-Aldrich). Mitochondrial proteins were then subjected to SDS-PAGE followed by immunoblot analysis using the following antibodies: RFP – Rockland 600-401-379 (1:10,000); NDUFS3 – Abcam ab14711 (1:5,000); H3 – Abcam ab1791(1:10,000); H4 – Abcam ab7311(1:1,000).

Mitochondrial DNA chromatin immunoprecipitation and quantitative PCR

Chromatin immunoprecipitation (ChIP) of mtDNA was performed as described previously with the following modifications (Kucej et al., 2008; Mukhopadhyay et al.,

2008; Terzioglu et al., 2013). Freshly prepared suspensions of isolated mitochondria were cross-linked with 1% formaldehyde in mitochondria isolation buffer for 10 min at room temperature. This was followed by addition of 125 mM glycine for 10 min to quench the reaction. The mitochondria were then resuspended in 1X PBS containing 0.1% Triton X-100 and 1 mM $CaCl_2$ and digested with 4 units/µL of micrococcal nuclease (New England Biolabs) for 5 min at 37°C. The reaction was stopped by addition of 5 mM EDTA. The digested samples were then mixed with two times the volume of lysis buffer (25 mM HEPES-KOH at pH 7.5, 150 mM KCl, 10% glycerol, 5 mM $MgCl_2$, 0.5 mM EDTA, 1% Tween 20) with freshly added 1 mM PMSF and protease inhibitor cocktail (Roche). 10 µg of mitochondrial protein was saved as input, while 100 µg of mitochondrial protein was immunoprecipitated with 3 µg of H4 antibody (Abcam, ab7311) by shaking at 4°C overnight. 20 µL of magnetic protein A/G beads (Millipore) was added to the samples and incubated at 4°C for 2 hr to pull-down the DNA-protein complexes. Beads were washed once with lysis buffer, two times with lysis buffer containing 250 mM NaCl, two times with LiCl buffer (10 mM Tris-HCl at pH 8.0, 250 mM LiCl, 0.5% NP-40, 0.5% sodium deoxycholate, 1 mM EDTA) and two times with TE buffer (10 mM Tris at pH 8.0 and 1 mM EDTA). Beads were then incubated in elution buffer (250 mM NaCl, 1% SDS, 10 mM Tris-HCl at pH 8.0, 1 mM EDTA) at 65°C for overnight. Subsequently, the samples were treated with 50 µg of proteinase K at 55°C for 2 hr to digest proteins. Both input DNA and antibody-precipitated DNA were purified by Zymo DNA concentrator-5 kit (Zymo Research) and analyzed by real-time quantitative PCR using primers listed in Table 10. The PCR signal for each DNA region was normalized to the corresponding signal from input, and then divided by the signal

from a negative control region (mtDNA: 2,317–2,400) to determine the relative fold enrichment.

Statistical analysis

For life span experiments, Kaplan-Meier survival analysis and Mantel-Cox log-rank test were performed using OASIS 2 (Han et al., 2016). Statistical analysis of MNase-Seq data was performed using 'Stat' function of DANPOS2 tool (Chen et al., 2013), as described in the method details. Kolmogorov-Smirnov tests for comparison between genome-wide frequency distributions of nucleosomal parameters were performed in R. All other statistical analyses and graphing were performed using GraphPad Prism 8 for Windows. Details of statistical tests used, number of biological replicates and *p* values for each experiment are included in figure legends.

Data availability

Raw MNase-Seq reads for data reported in this chapter have been deposited as NCBI Sequence Read Archive (SRA): SRP140908.

Results

Life span extension due to HSB-1/HSF-1 signaling is suppressed by knockdown of histone H4

To identify factors that are required for HSB-1 inhibition-induced life span extension, we performed a genome-wide RNAi screen in *C. elegans* for genetic suppressors of the longevity phenotype of *hsb-1* null worms. Our goal was to identify genes, that when knocked down, resulted in reduction of life span in the long-lived *hsb-1(-)* strain, without

inducing a similar life span shortening effect in wild-type animals. To avoid progeny contamination, we performed this genome-wide suppressor screen in the *rrf-3(-); fem-1(-)* genetic background that is sterile at 25°C. One of the suppressors identified from this screen was a histone H4-coding gene *his-67* (Figure 18A and Table 6). While *his-67* RNAi had minimal effect on the life span of wild-type (N2 strain) worms, it suppressed the longevity phenotype of the *hsb-1* null mutant (Figure 18A and Table 6). Worms, like mammals, have only one histone H4 isotype with no known protein variants (Henikoff and Smith, 2015). There are 16 genes in the *C. elegans* genome that encode for an identical H4 protein that differs from the human H4 at only a single amino acid (Pettitt et al., 2002). Since these H4 genes share ~90% identity at the nucleotide sequence level (Figure 18B), we hypothesized that in addition to *his-67*, knockdown of other H4 genes might also affect *hsb-1(-)*-associated longevity. Indeed, we found that knockdown of two other H4-coding genes, *his-5* and *his-38*, resulted in complete suppression of the longevity phenotype in *hsb-1(-)* worms (Figures 18C and 18D, and Table 6). Interestingly, this suppression of *hsb-1(-)*-associated longevity was significantly weaker when life span analysis was performed at 20°C, instead of at 25°C (Figure 18E and Table 6). This suggests that temperature plays an important role in determining the H4-dependence of HSB-1-associated longevity phenotype, similar to that observed for several other longevity mechanisms (Miller et al., 2017). We found that knockdown of all three genes, *his-67*, *his-5* and *his-38*, led to reduction in total H4 protein levels in both N2 and *hsb-1(-)* animals (Figures 18F and 18G). Interestingly, H4 RNAi often also resulted in slightly reduced levels of other core histone proteins (Figures 18F and 18G). This can be attributed to the cell's ability to actively regulate

protein levels of the four core histones (Singh et al., 2009), as these proteins must assemble in a stoichiometric proportion to form the histone heterooctomer in nucleosome complexes.

Among the three H4 genes that were identified as suppressors of HSB-1-associated longevity, RNAi of *his-38* resulted in the most consistent reduction of H4 levels in both N2 and *hsb-1(-)* strains, and hence it was used in our subsequent H4 knockdown experiments (Table 6). We tested whether knockdown of H4 also affected the life span of other well-characterized long-lived *C. elegans* strains. H4 RNAi completely suppressed life span extension due to overexpression of *hsf-1* (Figure 19A and Table 6) (Baird et al., 2014). This indicates that histone H4 has a major role in mediating the longevity-promoting effects of increased HSF-1 activity achieved via either of the two approaches, *hsf-1* overexpression or HSB-1 inhibition (Figures 18D and 19A, and Table 6). H4 RNAi had no effect on longevity associated with reduced insulin/IGF-1-like signaling in *daf-2(-)* worms (Figure 19B and Table 6) (Kenyon et al., 1993) or via loss of germline in *glp-1(-)* worms (Figure 19C and Table 6) (Arantes-Oliveira et al., 2002). Interestingly, life span extension due to impaired mitochondrial function in *isp-1(-)* worms was completely suppressed by knockdown of H4 (Figure 19D and Table 6), even though longevity of this strain is known to be independent of HSF-1 activity (Feng et al., 2001; Hsu et al., 2003). This suggests a potential role of histones in longevity mechanisms associated with mitochondrial inhibition.

HSB-1-associated life span extension is due to elevated histone H4 levels in somatic tissues during development

A previous study has shown that co-overexpression of histones H3 and H4 extends replicative life span in yeast (Feser et al., 2010). We thus asked if increased histone levels in *hsb-1(-)* animals is the cause of their dependence on H4 for longevity. We observed that levels of H4, but not other core histones, were significantly higher in *hsb-1(-)* worms compared to wild-type during early adulthood (Figure 20A). To test if an increase in H4 protein level can directly contribute to life span extension in worms, we generated a strain with elevated H4 expression (Figure 20B). In *C. elegans*, H4 genes exist in three different structural variants: genes that have no UTRs or introns (*his-50*, *his-1*, *his-10*, *his-14*, *his-26*, *his-28*, *his-46*, *his-56*), genes with UTRs but no introns (*his-67*, *his-18*, *his-38*, *his-60*, *his-31*, *his-5*, *his-64*), and one H4-coding gene that has UTRs and an intron (*his-37*). We selected one gene from each of these three categories (*his-67*, *his-37* and *his-50*) and co-overexpressed them in the wild-type strain (Figure 20B). We found that overexpression of H4 in wild-type animals is sufficient to extend their mean life span by up to 25%, and this could be suppressed by RNAi-mediated knockdown of H4 (Figure 20C and Table 6). Interestingly, ectopic H4 overexpression in animals resulted in increased protein levels of the other core histones as well (Figure 20D), possibly due to cellular mechanisms that tend to maintain core histone protein levels in a stoichiometric proportion (Singh et al., 2009).

Since transcription of histone genes in *C. elegans* predominantly occurs only in dividing cells (Keall et al., 2007), we tested whether H4 RNAi suppresses *hsb-1(-)*-associated longevity in the absence of germline, the only proliferative tissue in adult

worms. For these experiments, we used animals with a temperature-sensitive mutation in either *glp-1* or *glp-4* genes, which are essential for proliferation and maintenance of the germline tissue in *C. elegans* (Beanan and Strome, 1992; Kodoyianni et al., 1992). Interestingly, life span extension due to *hsb-1(-)* mutation in germline-deficient *glp-1(-)* or *glp-4(-)* worms was completely suppressed by knockdown of H4 (Figures 21A and 21B, and Table 6), suggesting that depletion of H4 in somatic tissues alone is sufficient to abolish HSB-1 inhibition-induced longevity. We further confirmed that somatic protein levels of histones H3 and H4 were significantly elevated in *hsb-1(-)* animals during development (Figure 21C), but their levels were not significantly different in somatic tissues of young adult worms (Figure 21D).

Several studies have suggested the role of histone post-translational modifications (PTMs) in aging, but only few have focused on the effects of change in histone protein levels (Booth and Brunet, 2016; Sen et al., 2016). Histone levels decline with age in yeast and murine muscle stem cells, and this results in increased genomic instability and global transcriptional deregulation (Hu et al., 2014; Liu et al., 2013). As previously reported for histone H3 (Ni et al., 2012), we found that protein levels of all core histones decline drastically with age in somatic tissues of worms (Figure 22A). Moreover, this was associated with an increase in susceptibility to UV-induced DNA damage with age (Figures 22B and 22C). Interestingly, HSB-1 inhibition provided partial resistance to DNA lesion formation at lower doses of UV (Figure 22D). We also observed that a transposon-like element called *C09B7.2*, which has been previously shown to accelerate aging in *C. elegans* (Hamilton et al., 2005), showed increased expression with age in somatic tissues of worms (Figure 22E), suggesting loss of

silencing of repetitive elements with age. This age-associated increase in somatic *C09B7.2* expression was partially rescued in *hsb-1(-)* animals (Figure 22E).

Surprisingly, the decline in histone protein levels with age in somatic tissues of worms was not alleviated by HSB-1 inhibition (Figure 22F). To confirm if elevated histone expression only during development contributes to longevity of *hsb-1(-)* worms, we performed H4 knockdown in animals after they attained adulthood. Consistent with the observation that somatic H4 levels were elevated only during early development in *hsb-1(-)* animals (Figure 21C), H4 RNAi started post-developmentally did not suppress *hsb-1(-)*-associated longevity in either N2 or germline-less *glp-1(-)* worms (Figures 23A and 23B, and Table 6). Together, our findings indicate that the HSB-1/HSF-1 pathway regulates longevity by altering somatic H4 levels mainly during development.

Increased MNase-protection of nuclear chromatin and mitochondrial DNA due to HSB-1 inhibition is H4-dependent

To understand how elevated levels of H4 protein might regulate the rate of aging in worms, we first tested whether global chromatin organization is altered in *hsb-1(-)* animals. To address this, we digested native *C. elegans* chromatin with micrococcal nuclease (MNase), an endonuclease that digests exposed DNA until it reaches a nucleosome or a strongly DNA-bound protein. We observed that *hsb-1(-)* chromatin constituted a higher amount of MNase-protected DNA, and this could be suppressed by H4 RNAi (Figure 24A). Moreover, MNase-digested chromatin from *hsb-1(-)* worms showed an H4-dependent significant increase in the ratio of dinucleosomal to mononucleosomal DNA fragments (Figures 24B–F). Increased proportion of

dinucleosomal fragments indicates lower MNase-accessibility to DNA, a property associated with higher compaction of chromatin (Deniz et al., 2016). To test whether altered nucleosome positioning in specific regions of the genome contributes to the higher level of chromatin compaction in *hsb-1(-)* animals, we performed next-generation sequencing (NGS) of MNase-digested chromatin. Analysis of global nucleosome occupancy revealed that frequency of sharp low-width peaks was slightly elevated in chromatin of *hsb-1(-)* worms (Figure 25A and Table 7). In addition, fuzziness (or delocalization) in nucleosome positioning and frequency of low-height peaks were marginally reduced in *hsb-1(-)* chromatin compared to wild-type (Figures 25C and 25E, and Table 7). Small-scale changes in these three parameters indicate slightly better positioning of individual nucleosomes and a modest increase in sharpness of nucleosome peaks in *hsb-1(-)* worms, effects that were suppressed by knockdown of H4 (Figures 25B, 25D and 25F, and Table 7) (Chen et al., 2013).

We observed that nucleosome organization in most of the genome was unaffected in *hsb-1(-)* animals (Figure 26). Surprisingly, the region that showed the most significant increase in MNase-protection due to HSB-1 inhibition was the entire stretch of mitochondrial DNA (mtDNA) (Figure 27A and Table 8). Moreover, the increased MNase-protection of several mtDNA loci in *hsb-1(-)* animals was diminished after knockdown of histone H4 (Figure 27A and Table 9). Increased number of MNase-Seq reads from mtDNA of *hsb-1(-)* worms can be attributed to two possible contributors: (i) change in accessibility of mtDNA that protects it from endonuclease digestion, or (ii) an increased copy number of mtDNA per cell in *hsb-1(-)* animals. We found that mtDNA copy number relative to nuclear DNA was not significantly different between *hsb-1(-)*

and wild-type worms (Figure 27B), indicating that the higher number of MNase-Seq reads was not due to increase in mtDNA content per cell in *hsb-1(-)* animals. mtDNA is predicted to be non-specifically coated by the mitochondrial transcription factor A (TFAM)-like HMG-5 nucleoid protein (Sumitani et al., 2011), but we observed 'chromatin-like' peaks interspersed along the stretch of mtDNA (Figure 27A). The most prominent difference in peak height between *hsb-1(-)* and wild-type mtDNA was observed at the NADH-ubiquinone oxidoreductase subunit 4 (*nduo-4*) gene region, and this difference was partially suppressed when H4 is knocked down by RNAi (Figure 27A, shown with orange arrow). This indicates that the increased MNase-protection of the *nduo-4* gene region on mtDNA of *hsb-1(-)* worms is dependent on the levels of histone H4.

HSB-1 inhibition leads to H4-dependent decrease in expression of mtDNA-encoded genes, reduced respiratory capacity and UPR^{mt}-mediated longevity

Next, we analyzed whether the altered MNase-protection of mtDNA due to HSB-1 inhibition affected the expression of mitochondrially-encoded genes. We observed that transcript levels of five mitochondrially-encoded genes were significantly reduced in *hsb-1(-)* animals (Figure 28A), while expression of others was slightly attenuated. Interestingly, the significant reduction in expression of these five genes due to HSB-1 inhibition was suppressed when the *hsb-1(-)* worms were subjected to knockdown of H4 (Figures 28B and 28C). Under normal conditions, the expression levels of three of these five genes, *ctc-3*, *ctc-1* and *ctc-2*, were reduced by greater than 30% compared to wild-type levels in *hsb-1(-)* animals (Figure 28A). Intriguingly, these three genes are located adjacent to the MNase-Seq peak in mtDNA that was most amenable to both HSB-1

inhibition and H4 knockdown (Figure 27A, shown with orange arrow). The three *ctc* genes encode three large subunits that form the catalytic core of complex IV (i.e. cytochrome *c* oxidase) of mitochondrial electron transport chain (ETC). The function of ETC complex IV is to transfer protons across the inner mitochondrial membrane concomitant with conversion of molecular oxygen to water. It has been previously demonstrated that knockdown of nuclear genome-encoded mitochondrial ETC components in worms during development is sufficient to reduce their rate of respiration and extend life span during adulthood (Dillin et al., 2002). We tested whether reduced expression of mtDNA-encoded ETC complex IV components in *hsb-1(-)* worms affected their oxygen consumption rate (OCR). We found that maximal respiratory capacity was significantly reduced after HSB-1 inhibition, while basal mitochondrial OCR was not affected in *hsb-1(-)* animals compared to the wild-type level (Figures 29A, 29B and 29D). In addition, spare respiratory capacity (defined as the difference between maximal and basal OCR) of *hsb-1(-)* worms was comparable to that of animals subjected to direct mitochondrial inhibition via knockdown of *cyc-1*, a nuclear genome-encoded component of ETC complex III (Figure 29C). In contrast, the basal, maximal and spare respiratory capacities of *hsb-1(-)* worms were not significantly different from the corresponding wild-type levels after RNAi-mediated knockdown of H4 in these animals (Figures 29E–H). We further tested if increasing histone H4 expression in worms can directly affect their mitochondrial activity similar to that observed in *hsb-1(-)* animals. On comparing mitochondrial respiration rates in wild-type and long-lived H4 overexpressing animals (Figures 20B and 20C), we found that overexpression of H4 significantly reduced all three mitochondrial OCR parameters (basal, maximal and spare respiratory

capacities) compared to the corresponding wild-type levels (Figures 30A–C and 29D). Moreover, the reduced mitochondrial respiratory capacity in H4 overexpressing worms was not due to reduced mtDNA copy number in these animals (Figure 30D). This signifies that increased H4 level in worms is sufficient to phenocopy the effects of HSB-1 inhibition on mitochondrial function.

Since HSB-1 inhibition resulted in reduced expression of mtDNA-encoded ETC complex IV genes (Figure 28A), we speculated that this might involve activation of the same longevity pathways in *hsb-1(-)* worms that are required for increased life span achieved via direct inhibition of mitochondrial activity. Longevity phenotypes associated with reduced function of two nuclear genome-encoded mitochondrial ETC components, *isp-1* (complex III) and *cco-1* (complex IV), are both dependent on the activity of UBL-5, a ubiquitin-like protein involved in activation of the mitochondrial unfolded protein response (UPR^{mt}) in worms (Durieux et al., 2011; Houtkooper et al., 2013; Merkwirth et al., 2016). We found that RNAi-mediated knockdown of *ubl-5* had no effect on longevity of wild-type worms, but it significantly shortened the mean life span of *hsb-1(-)* animals by ~15% (Figure 31A and Table 6), suggesting that longevity mechanisms associated with HSB-1 inhibition potentially involve components of the UPR^{mt}. Moreover, we found that *ubl-5* knockdown also significantly suppressed the life span extension phenotype in H4 overexpressing worms (Figure 31B and Table 6). This indicates that UPR signaling in the mitochondria has a crucial role in mediating the longevity-promoting effects associated with increased histone H4 levels in worms. We further showed that HSB-1 inhibition induces a modest but significant increase in expression of *hsp-6*, a mitochondrial HSP70 chaperone that is upregulated in presence of mitochondrial stress

(Figure 31C) (Yoneda et al., 2004). However, the mRNA levels of other UPR^{mt} targets, *hsp-60* and *timm-23*, were unaltered in *hsb-1(-)* worms compared to wild-type levels (Figure 31C) (Bennett et al., 2014). These findings collectively suggest that reduced expression of mtDNA-encoded ETC genes in *hsb-1(-)* worms results in transcriptional upregulation of a subset of UPR^{mt} targets and thus produces an UPR^{mt}-dependent life span extension in these animals.

H4 binds to mtDNA and is present in the mitochondria of intestinal tissue in worms

Since knockdown of H4 suppressed both the mitochondrial phenotypes of decreased MNase-accessibility of mtDNA (Figure 27A) and reduced mtDNA-encoded gene expression in *hsb-1(-)* worms (Figures 28B and 28C), we asked if histone H4 protein physically translocates to mitochondria in these animals to regulate the function of this organelle. We found H4 to be primarily localized in the nuclei of most tissues of *hsb-1(-)* worms, with the exception of intestinal tissue, where H4 immunostaining revealed extranuclear foci that overlapped with mitochondria (Figures 32A–C). To further validate the mitochondrial localization of histone H4, we performed H4 immunofluorescence studies with *C. elegans* strains that express mitochondrially-localized GFP in specific tissues. H4 immunostaining clearly showed that extranuclear H4 foci co-localized with mitochondrial GFP in the intestine (Figure 33A), but not in the muscle cells of worms (Figure 33B). A previous study has shown that the intestine has a major role in mediating the longevity-promoting effects of increased HSF-1 activity in worms (Douglas et al., 2015). In addition, the *C. elegans* intestine is also the target tissue for life span extension induced via mitochondrial inhibition (Durieux et al., 2011; Zhang et

al., 2018). Based on these evidences and our H4 immunostaining data (Figures 32A and 33A), we speculated that increased H4 levels might promote longevity via acting in the intestinal tissue of *hsb-1(-)* worms. To address this, we knocked down histone H4 only in the intestine and tested its effect on the longevity phenotype associated with HSB-1 inhibition. We performed this experiment in an *rde-1*-deficient genetic background in which RDE-1 function was restored only in the intestinal tissue of worms (Figure 33C). The RDE-1 protein is a member of the Argonaute/PIWI family and is an essential component of the cellular RNAi machinery in *C. elegans*. Hence, restoring RDE-1 activity in *rde-1* mutant worms using a tissue-specific promoter allows for knockdown of a gene of interest in a particular tissue of these animals (Qadota et al., 2007). We found that RNAi-mediated knockdown of H4 in the intestine of *hsb-1(-)* worms is sufficient to completely suppress life span extension in these animals (Figure 33C and Table 6). This finding, together with our H4 co-localization data, indicates that H4-dependent inhibition of mitochondrial activity in the intestinal tissue might be a major contributor to the longevity phenotype associated with HSB-1 inhibition.

To obtain more conclusive evidence for the localization of histone H4 in mitochondria, we isolated intact mitochondria from worms and subjected the mitochondrial proteins to immunoblot analysis. Interestingly, we detected both histones H3 and H4 in isolated mitochondrial preparations (Figure 34A). A few studies involving mass spectrometry have previously detected core histones in mitochondria of mammalian cells (Choi et al., 2011; Johnson et al., 2007). However, since histones are among the most abundant cellular proteins, it is difficult to predict solely on the basis of biochemical fractionation whether histones were present inside the mitochondria or as

impurities of the fractionation method. To address this, we treated suspensions of intact *C. elegans* mitochondria with increasing concentrations of proteinase K, a membrane-impermeable protease. In this assay, as the concentration of proteinase K is increased gradually, it sequentially digests proteins that are present as extramitochondrial impurities, followed by outer mitochondrial membrane proteins, while inner mitochondrial membrane proteins are digested only at very high protease concentrations (Zhou et al., 2008). We observed that the proteinase K protection of both H3 and H4 histones was intermediate to that of the outer mitochondrial membrane protein TOMM-20 and of the inner mitochondrial membrane protein NUO-2 (homolog of mammalian NDUFS3) (Figure 34A). This indicates that histones H3 and H4 were not present as extramitochondrial impurities, but instead were enclosed within the *C. elegans* mitochondria. Next, we tested whether animals with elevated histone H4 levels also have increased levels of H4 in their mitochondria. For this experiment, we used the long-lived H4 overexpression strain as these animals showed a robust increase in total H4 protein levels in whole worm lysates (Figures 20C and 20D). We found that the level of histone H4 in mitochondria of H4 overexpressing animals was noticeably higher than that in wild-type worms (Figure 34B). This suggests that an increase in total H4 protein levels can result in higher amounts of mitochondrially-localized H4 in animals. Finally, we used chromatin immunoprecipitation (ChIP) to compare the binding of H4 to different regions of mtDNA in wild-type and *hsb-1(-)* animals. Five regions of mtDNA showed a significant ~twofold higher binding to H4 compared to the background binding observed for other mtDNA regions tested (Figure 34C). Interestingly, these five regions corresponded to mtDNA-encoded genes that have reduced expression in *hsb-1(-)*

animals (Figure 28A). One of these regions, corresponding to the *ctc-2* gene, showed a significant ~40% higher H4-binding in *hsb-1(-)* worms compared to wild-type (Figure 34C). Though the other four mtDNA regions associated with reduced gene expression did not show a difference in H4-binding across the two genotypes (Figures 28A and 34C), it is plausible that unidentified H4-interacting proteins might collectively determine the overall accessibility of these mtDNA loci in *hsb-1(-)* animals. Together, these results provide strong evidence for the presence of histone H4 in mitochondria and suggest a potential relationship between binding of H4 to mtDNA and regulation of gene expression from the mitochondrial genome.

Discussion

HSB-1 is a conserved negative regulator of HSF-1 that limits its ability to promote organismal longevity in normal physiological conditions (Chiang et al., 2012; Satyal et al., 1998). Our findings indicate that the life span extending effects of HSB-1 inhibition are mediated via increase in histone H4 level that results in altered global compaction of both nuclear and mitochondrial genomes, and consequently inhibiting mitochondrial activity (Figure 36). This study unravels an unexpected role of HSB-1/HSF-1 signaling in regulating levels of the core histone protein H4 and its previously undiscovered functions in modulating the transcription of mitochondrial genome-encoded genes. A recent study has shown that a mild disruption of mitochondrial activity in worms induces an imbalance in the levels of core histone proteins (Matilainen et al., 2017). This leads to elevated protein levels of some, but not all, core histones, increased transcription of HSF-1 target genes and extension of life span that is dependent on a chromatin

remodeling protein, ISW-1 (Matilainen et al., 2017). In agreement with these findings, our data also support the requirement of histone H4 in mediating the longevity-promoting effects of impaired mitochondrial function (Figure 19D). This provides evidence for a bidirectional crosstalk between the nuclear and mitochondrial genomes that is mediated via HSF-1 activation and increased histone protein levels. Though previous studies have unraveled mechanisms of how stress signals originating from the mitochondria can affect the expression of nuclear-encoded genes (Houtkooper et al., 2013; Matilainen et al., 2017; Merkwirth et al., 2016), our study provides novel evidence for how signals originating from the nucleus can affect gene expression from the mitochondrial genome in the context of longevity regulation.

Even though loss of histones has been identified as a conserved epigenetic hallmark of aging (Sen et al., 2016), increasing histone levels has rarely been used as a strategy to slow the rate of aging in multicellular organisms. Prior to this study, the only evidence of this was from budding yeast in which replenishment of histones by overexpression delays replicative senescence via counteracting the age-associated decline in histone levels (Feser et al., 2010; Hu et al., 2014). During replicative aging, lack of sufficient histone proteins to properly package newly-synthesized DNA leads to chromosomal instability and dramatic changes in gene expression in old yeast cells (Hu et al., 2014). Here, we show that H4 overexpression extends life span of *C. elegans*, a multicellular organism comprising non-dividing somatic cells, via a potentially distinct mechanism. Increase in H4 levels by activating HSF-1 does not significantly mitigate the age-associated decline in levels of core histones in somatic tissues of worms (Figure 22F), but instead mediates its longevity-promoting effects primarily during development

(Figures 21A, 21B, 21D and 23A). However, the mechanism through which HSB-1/HSF-1 signaling increases histone H4 levels in worms remains elusive. A recent study has shown that prolonged heat stress in *C. elegans* results in transcriptional upregulation of core histones and other genes involved in nucleosome assembly (Jovic et al., 2017). Nonetheless, our results indicate that the higher H4 protein level in *hsb-1(-)* worms is not due to elevated transcription of H4 genes during development or adulthood (Figures 35A and 35B). Further studies are needed to elucidate the HSB-1-associated mechanisms that regulate protein levels of H4 in animals.

Our findings show that knockdown of H4 suppresses the longevity phenotypes associated with HSF-1 activation and mitochondrial inhibition in *C. elegans* (Figures 18A, 18C, 18D, 19A and 19D), while overexpression of H4 extends life span of wild-type worms (Figure 20C). In addition, depletion of H4 suppresses the higher global compaction of nuclear chromatin in *hsb-1(-)* animals (Figures 25A–F). These findings collectively indicate that change in levels of a core histone can alter genome-wide chromatin organization and organismal life span. Though there are 16 H4-coding genes in *C. elegans*, RNAi directed against a single member of the H4 family can reduce the total protein levels of H4 in worms (Figure 18F). This is possibly due to ~90% nucleotide sequence identity between the members of the H4 gene family in *C. elegans* that all code for the identical amino acid sequence (Figure 18B). Interestingly, knockdown of H4 reduces the protein levels of other core histones as well (Figures 18F and 18G), while overexpression of H4 increases the protein levels of H3, H2A and H2B (Figures 20B and 20D). This raises the possibility that change in levels of other core histones might also be partially responsible for the phenotypes observed in animals with altered H4

protein levels. We found that directly targeting other core histones results in partial or no suppression of longevity associated with HSB-1 inhibition in worms (Figures 35C–E and Table 6). However, the biological effects solely attributable to change in protein levels of a single core histone cannot be conclusively determined by approaches involving RNAi-mediated knockdown or ectopic overexpression. This is because, as stated previously, altering the levels of any one core histone seemingly almost always affects the levels of other core histones to some extent (Figures 18F, 18G and 20D) (Matilainen et al., 2017), potentially due to the presence of cellular homeostasis mechanisms (Singh et al., 2009). Hence, it is possible that many of the biological effects due to H4 RNAi or overexpression might be due to change in levels of multiple core histones, and not only of H4. Nonetheless, as the triggering factor for the change in levels of the other histones was either knockdown or overexpression of H4 (Figures 18F, 18G and 20D), we can conclude that all the observed effects are either direct or indirect biological consequences of change in histone H4 levels. Follow-up studies are needed to develop tools that can induce major changes in the levels of one core histone protein without affecting the levels of other nucleosome constituents.

Another intriguing observation from our findings is the role of histone H4 in influencing gene expression from the mitochondrial genome. Across the animal kingdom, packaging of mitochondrial nucleoids is achieved via coating of mtDNA with TFAM, the most abundant protein constituent of the mitochondrial nucleoid complex (Gilkerson et al., 2013; Lee and Han, 2017). However, recent studies involving DNase I footprinting and ATAC-Seq have detected a potential chromatin-like organization of mtDNA that is labile to change in physiological conditions, but does not correlate with

TFAM binding pattern (Blumberg et al., 2018; Marom et al., 2019). Numerous protein-protected sites of mtDNA have been attributed to binding of primarily nuclear-localized transcription factors that have also been detected within mitochondria, and several other unidentified proteins that potentially regulate transcription of the mitochondrial genome (Barshad et al., 2018; Mercer et al., 2011). Prior to our study showing the presence of histone H4 in mitochondria of *C. elegans* (Figures 32A, 33A and 34A), a few studies have detected core histone proteins in mitochondria of mammalian tissues using mass spectrometry analysis (Choi et al., 2011; Johnson et al., 2007), though its physiological relevance was unknown. Moreover, *in vitro* binding studies have predicted an affinity of histone proteins for the conserved D-loop region of mtDNA (Choi et al., 2011). Intriguingly, our results showed that knockdown of H4 induces a significant decline in the MNase-protection of the D-loop region of mtDNA in *hsb-1(-)* animals (Figure 27A, shown with cyan arrow). These evidences indicate that during the course of eukaryotic evolution, the mitochondrial genome has partially acquired chromatin-like features for context-dependent and/or locus-specific regulation of mitochondrial gene expression. Presence of H4 in *C. elegans* mitochondria and its binding to specific sites of the mitochondrial genome suggest an extranuclear role of mitochondrially-translocated H4 in the *in vivo* packaging of mtDNA-nucleoid complexes (Figures 34A–C). Though H4 shows similar binding to mtDNA in wild-type and *hsb-1(-)* animals at all but one mtDNA regions tested (Figure 34C), it is presumable that the altered gene expression of multiple mtDNA-encoded genes in *hsb-1(-)* animals might be due to additional binding partners of H4 that determine the overall accessibility of the mitochondrial genome (Figures 27A and 28A–C). Since other core histones such as H3 have also been

detected in mitochondria of multiple species (Figure 34A) (Choi et al., 2011; Johnson et al., 2007), it remains elusive whether mitochondrial histones form nucleosomes and/or multiprotein complexes with other mitochondrially-localized proteins in order to bind mtDNA and regulate its transcription. Overall, our findings provide novel insights into the dynamic structure and expression pattern of the *C. elegans* mitochondrial genome and how these are amenable to longevity signals of the HSF-1/HSB-1 pathway.

Stress response, chromatin alterations and mitochondrial function were traditionally considered to regulate longevity as three distinct hallmarks of aging (López-Otín et al., 2013; Riera et al., 2016). This study establishes novel connections between these distinct cellular pathways, thus contributing to an integrated understanding of how they collectively manifest the regulation of organismal life span.

Figures

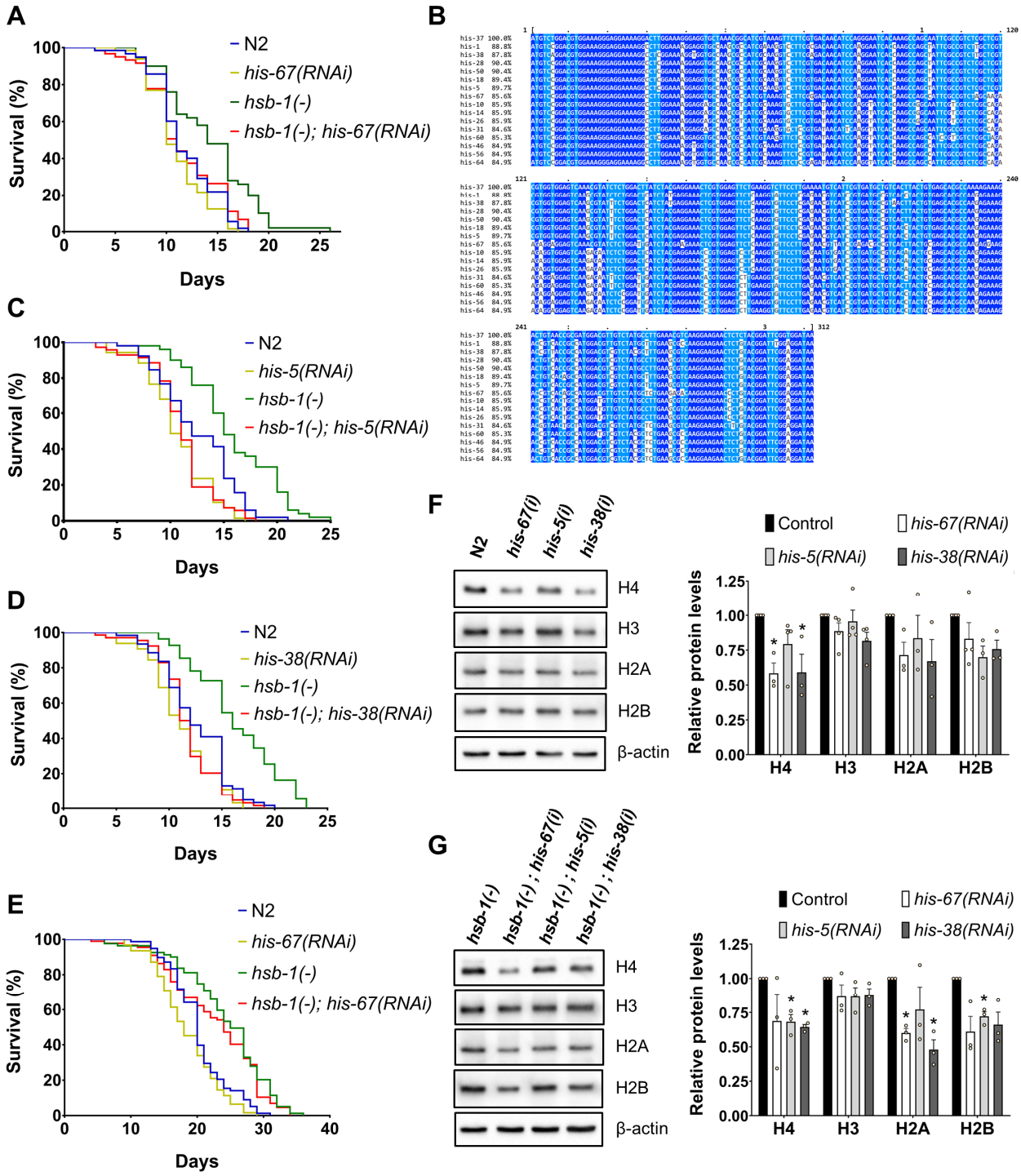

Figure 18. HSB-1-associated life span extension is suppressed by knockdown of histone H4.
(A) Life span analysis of wild-type (N2) and *hsb-1(-)* worms grown on control or *his-67* RNAi bacteria at 25°C. Statistical data are included in **Table 6**.
(B) Similarity between coding sequences of all 16 H4-coding genes in the *C. elegans* genome. Colored bases indicate sequence identity among genes (dark blue: purines, light blue: pyrimidines). Multiple sequence alignment was performed on Clustal Omega (https://www.ebi.ac.uk/Tools/msa/clustalo).

(C, D) Life span analysis of N2 and *hsb-1(-)* worms grown on control, *his-5* or *his-38* RNAi bacteria at 25°C. Statistical data and additional life span replicates are included in **Table 6**.
(E) Life span analysis of N2 and *hsb-1(-)* worms grown on control or *his-67* RNAi bacteria at 20°C. Statistical data and additional life span replicates are included in **Table 6**.
(F, G) Representative immunoblots for core histones in N2 and *hsb-1(-)* worms grown on control, *his-67*, *his-5* or *his-38* RNAi bacteria at 25°C (*left*). Densitometric quantification of histone: β-actin ratio relative to control RNAi condition (*right*). Mean ± SEM for ≥ 3 biological replicates. * $p < 0.05$ compared to corresponding control RNAi in two-tailed *t*-test.

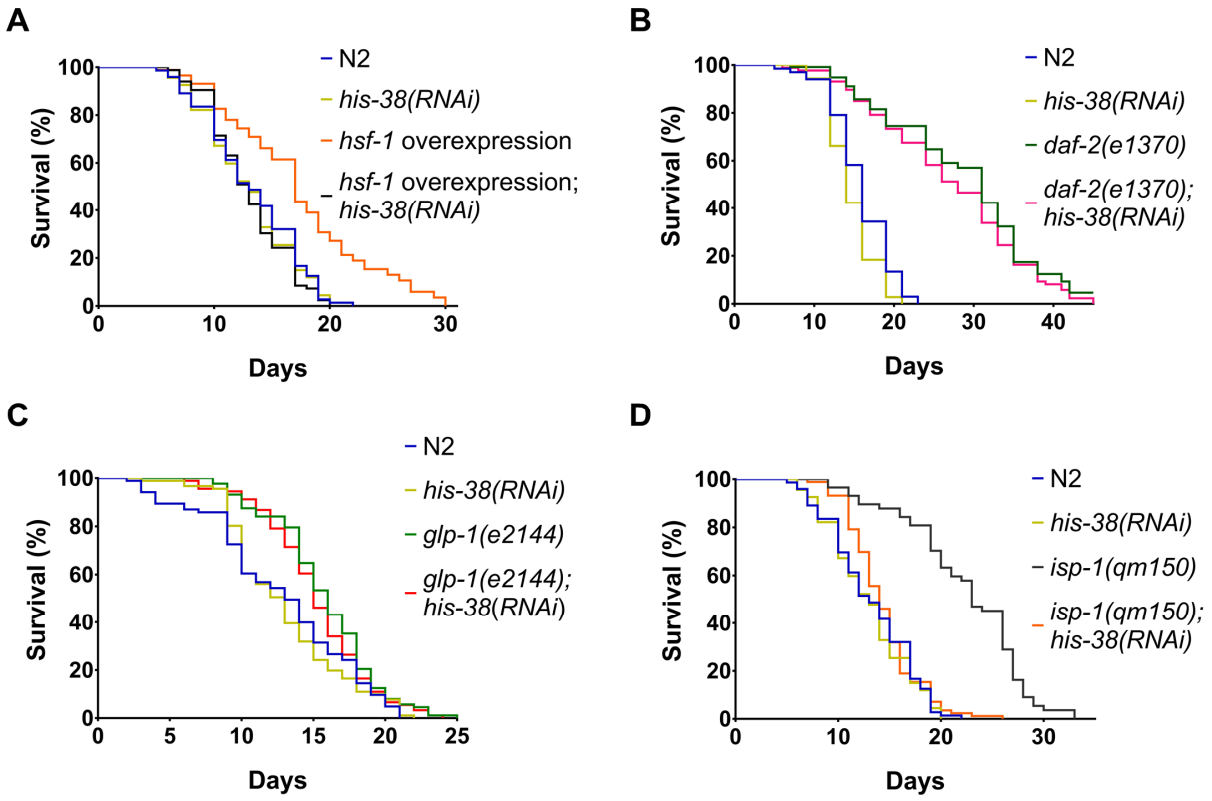

Figure 19. Life span extension achieved via *hsf-1* overexpression or mitochondrial inhibition is suppressed by knockdown of histone H4.
(A–D) Life span analysis of wild-type (N2), *hsf-1* overexpression strain, *daf-2(e1370)*, *glp-1(e2144)* and *isp-1(qm150)* worms grown on control or *his-38* RNAi bacteria at 25°C. Statistical data and additional life span replicates are included in **Table 6**.

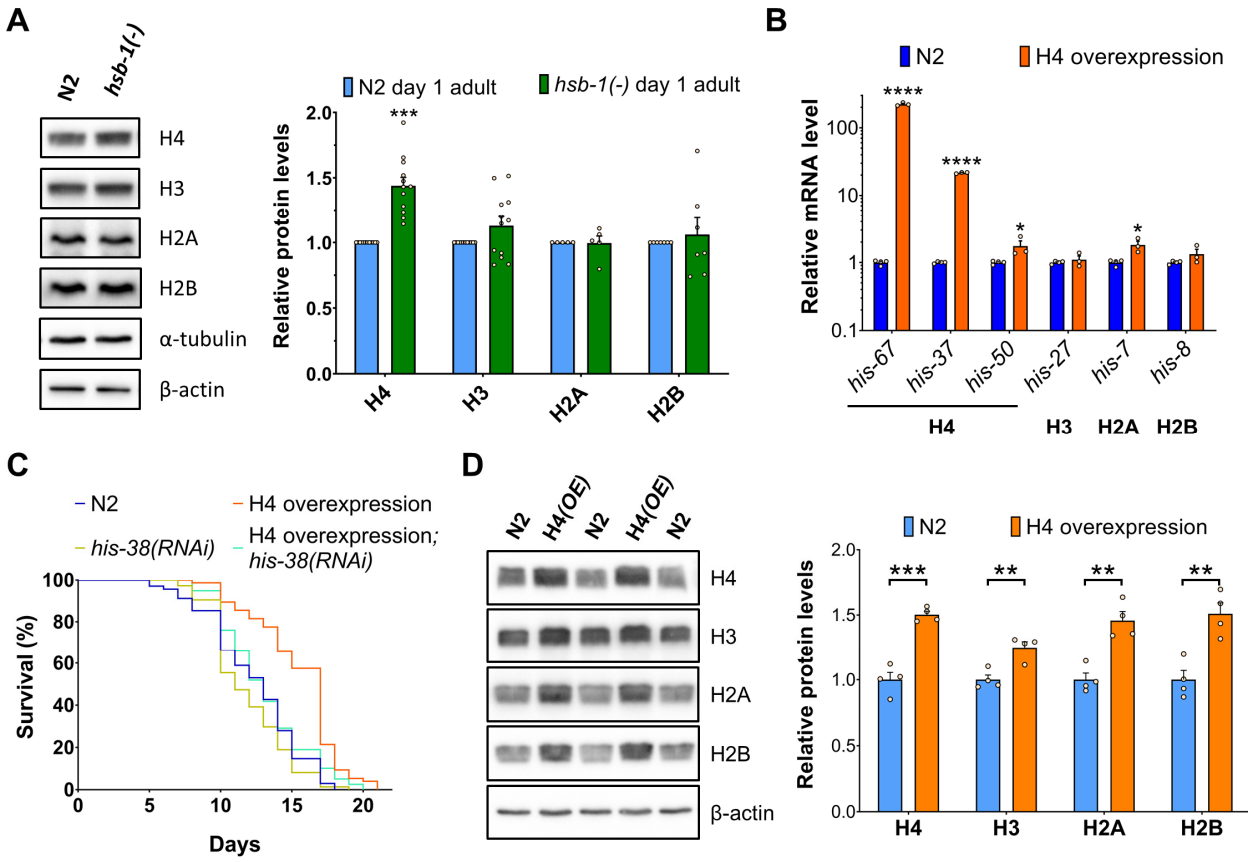

Figure 20. HSB-1 inhibition results in increased H4 protein level, which is sufficient for life span extension in worms.
(A) Representative immunoblots for core histones in day 1 adult wild-type (N2) and *hsb-1(-)* worms grown at 25°C (*left*). Densitometric quantification of histone: β-actin ratio relative to wild-type (*right*). Mean ± SEM for ≥ 5 biological replicates. *** $p < 0.001$ compared to corresponding wild-type protein levels in two-tailed *t*-test.
(B) Relative transcript levels of core histone genes in N2 and H4 overexpression strain grown at 25°C. Mean ± SEM for ≥ 3 biological replicates. * $p < 0.05$, **** $p < 0.0001$ compared to corresponding wild-type transcript levels in two-tailed *t*-test.
(C) Life span analysis of N2 and H4 overexpression strain grown on control or *his-38* RNAi bacteria at 25°C. Statistical data and additional life span replicates are included in **Table 6**.
(D) Representative immunoblots for core histones in N2 and H4 overexpression strain grown at 25°C (*left*). Densitometric quantification of histone: β-actin ratio relative to N2 worms (*right*). Mean ± SEM for four biological replicates. ** $p < 0.01$, *** $p < 0.001$ compared to corresponding wild-type transcript levels in two-tailed *t*-test.

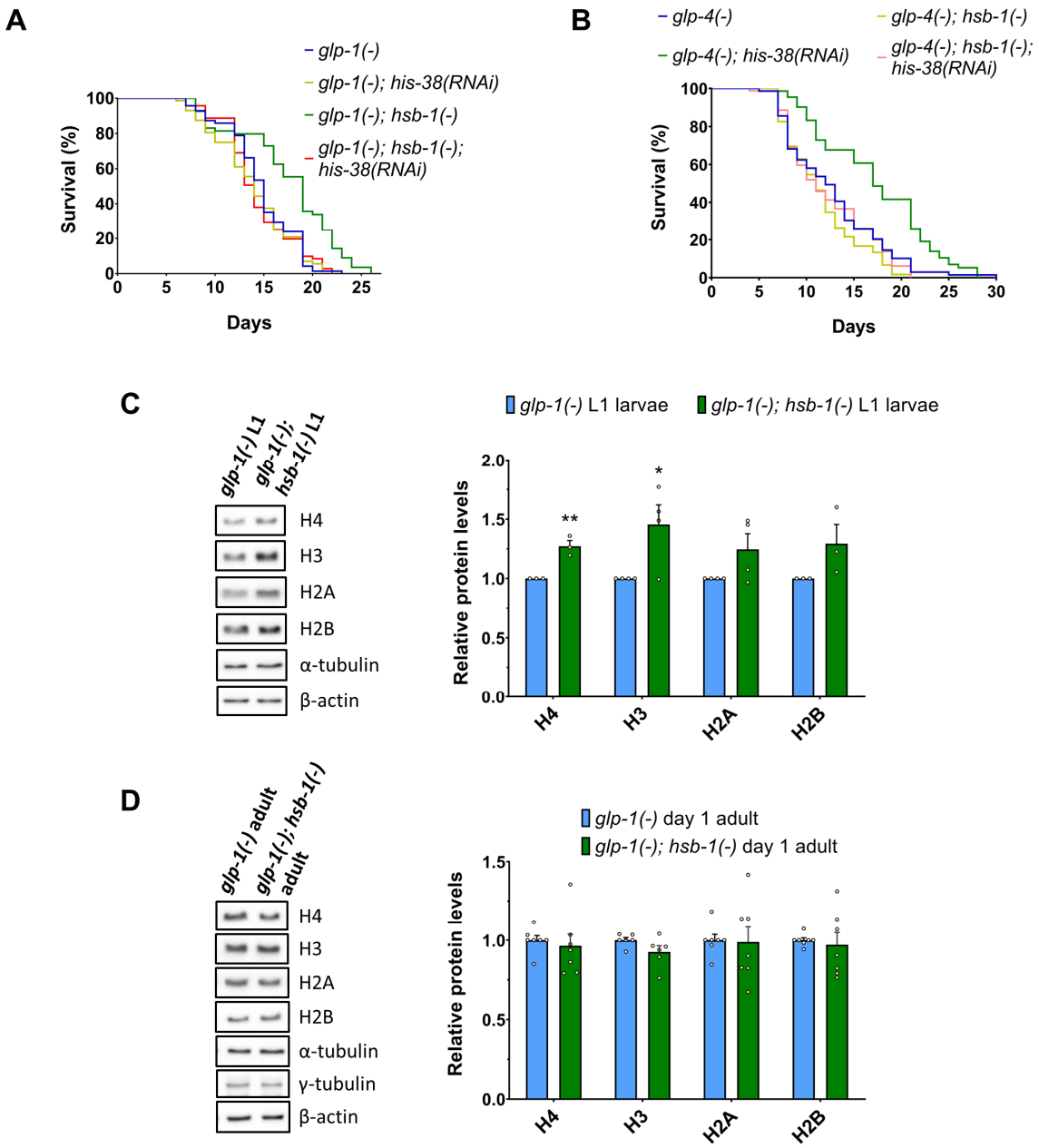

Figure 21. HSB-1 inhibition results in elevated somatic H4 protein levels during development, but not during adulthood.
(A) Life span analysis of *glp-1(-)* and *glp-1(-); hsb-1(-)* worms grown on control or *his-38* RNAi bacteria at 25°C. Statistical data and additional life span replicates are included in **Table 6**.
(B) Life span analysis of *glp-4(-)* and *glp-4(-); hsb-1(-)* worms grown on control or *his-38* RNAi bacteria at 25°C. Statistical data and additional life span replicates are included in **Table 6**.
(C) Representative immunoblots for core histones in *glp-1(-)* and *glp-1(-); hsb-1(-)* L1 larval worms grown at 25°C (*left*). Densitometric quantification of histone: β-actin ratio relative to *glp-1(-)* worms (*right*). Mean ± SEM for ≥ 3 biological replicates. * $p < 0.05$, ** $p < 0.01$ compared to corresponding *glp-1(-)* protein levels in two-tailed *t*-test.
(D) Representative immunoblots for core histones in day 1 adult *glp-1(-)* and *glp-1(-); hsb-1(-)* worms grown at 25°C (*left*). Densitometric quantification of histone: β-actin ratio relative to *glp-1(-)* worms (*right*). Mean ± SEM for ≥ 6 biological replicates.

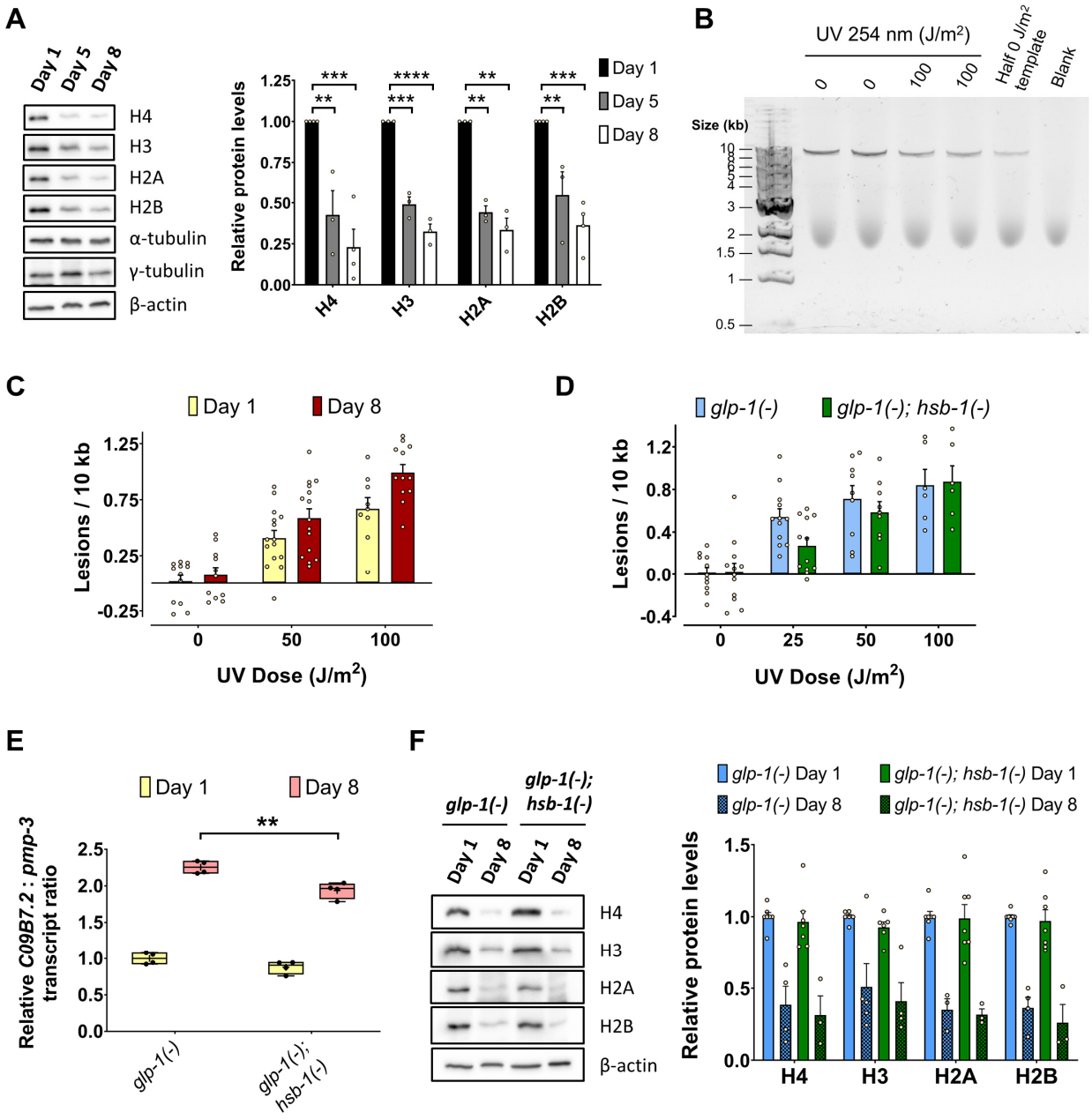

Figure 22. Histone levels decline with age in somatic tissues of worms resulting in genomic instability.
(A) Representative immunoblots for core histones in day 1, day 5 and day 8 old *glp-1(-)* worms grown at 25°C (*left*). Densitometric quantification of histone: β-actin ratio relative to day 1 worms (*right*). Mean ± SEM for ≥ 3 biological replicates. ** $p < 0.01$, *** $p < 0.001$, **** $p < 0.0001$ in Tukey's multiple comparisons test performed after one-way ANOVA.
(B) Representative agarose gel electrophoresis for 9.3 kb fragment of the *unc-2* gene amplified from genomic DNA of *glp-1(-)* worms that were exposed to 0 or 100 J/m^2 UV irradiation on day 1 of adulthood. 'Half 0 J/m^2 template': PCR with half the amount of template DNA as for the 0 J/m^2 reaction to confirm the quantitative nature of PCR amplification. 'Blank': PCR with no template DNA.
(C) UV-induced DNA lesions in day 1 and day 8 old *glp-1(-)* worms grown at 25°C. Mean ± SEM for ≥ 9 biological replicates, each of $n = 6$ worms. UV: $p < 0.0001$, age: $p < 0.01$ in two-way ANOVA.
(D) UV-induced DNA lesions in day 1 old *glp-1(-)* and *glp-1(-); hsb-1(-)* worms grown at 25°C. Mean ± SEM for ≥ 6 biological replicates, each of $n = 6$ worms. UV: $p < 0.02$, genotype: $p < 0.05$ in two-way ANOVA for intermediate doses.

(E) Relative *C09B7.2* transcript levels in day 1 and day 8 old *glp-1(-)* and *glp-1(-); hsb-1(-)* worms grown at 25°C. Central line, box limits, '+' and whiskers indicate median, interquartile range, mean and data range, respectively, for four biological replicates. Age: $p < 0.0001$, genotype: $p < 0.001$, interaction: $p = 0.05$ in two-way ANOVA. ** $p < 0.01$ in Sidak's multiple comparisons test.
(F) Representative immunoblots for core histones in day 1 and day 8 old *glp-1(-)* and *glp-1(-); hsb-1(-)* worms grown at 25°C (left). Densitometric quantification of histone: β-actin ratio relative to day 1 *glp-1(-)* worms (right). Mean ± SEM for ≥ 3 biological replicates. Age: $p < 0.0001$, genotype or interaction: no significant effect for all core histones in two-way ANOVA.

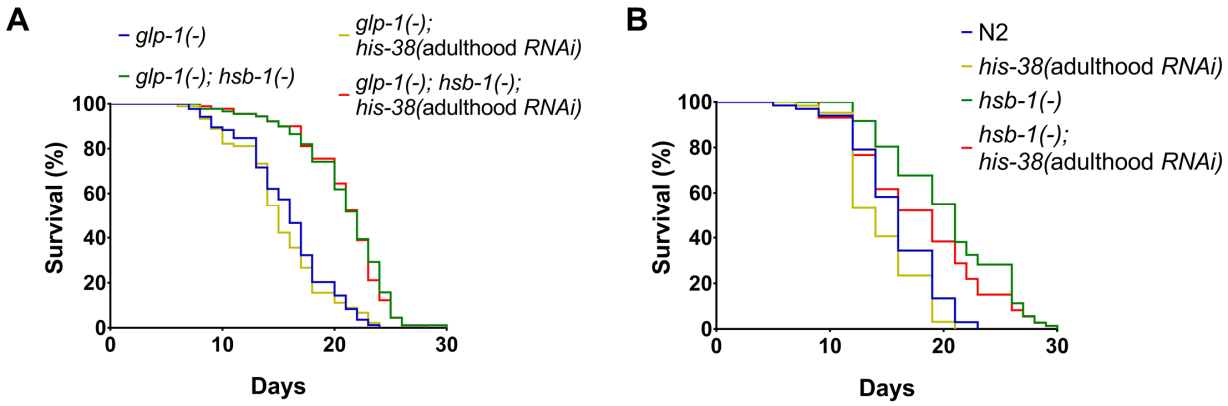

Figure 23. H4 RNAi only during adulthood does not suppress life span extension associated with HSB-1 inhibition.
(A) Life span analysis of *glp-1(-)* and *glp-1(-); hsb-1(-)* worms subjected to control or *his-38* RNAi only during adulthood at 25°C. Statistical data and additional life span replicates are included in **Table 6**.
(B) Life span analysis of wild-type (N2) and *hsb-1(-)* worms subjected to control or *his-38* RNAi only during adulthood at 25°C. Statistical data and additional life span replicates are included in **Table 6**.

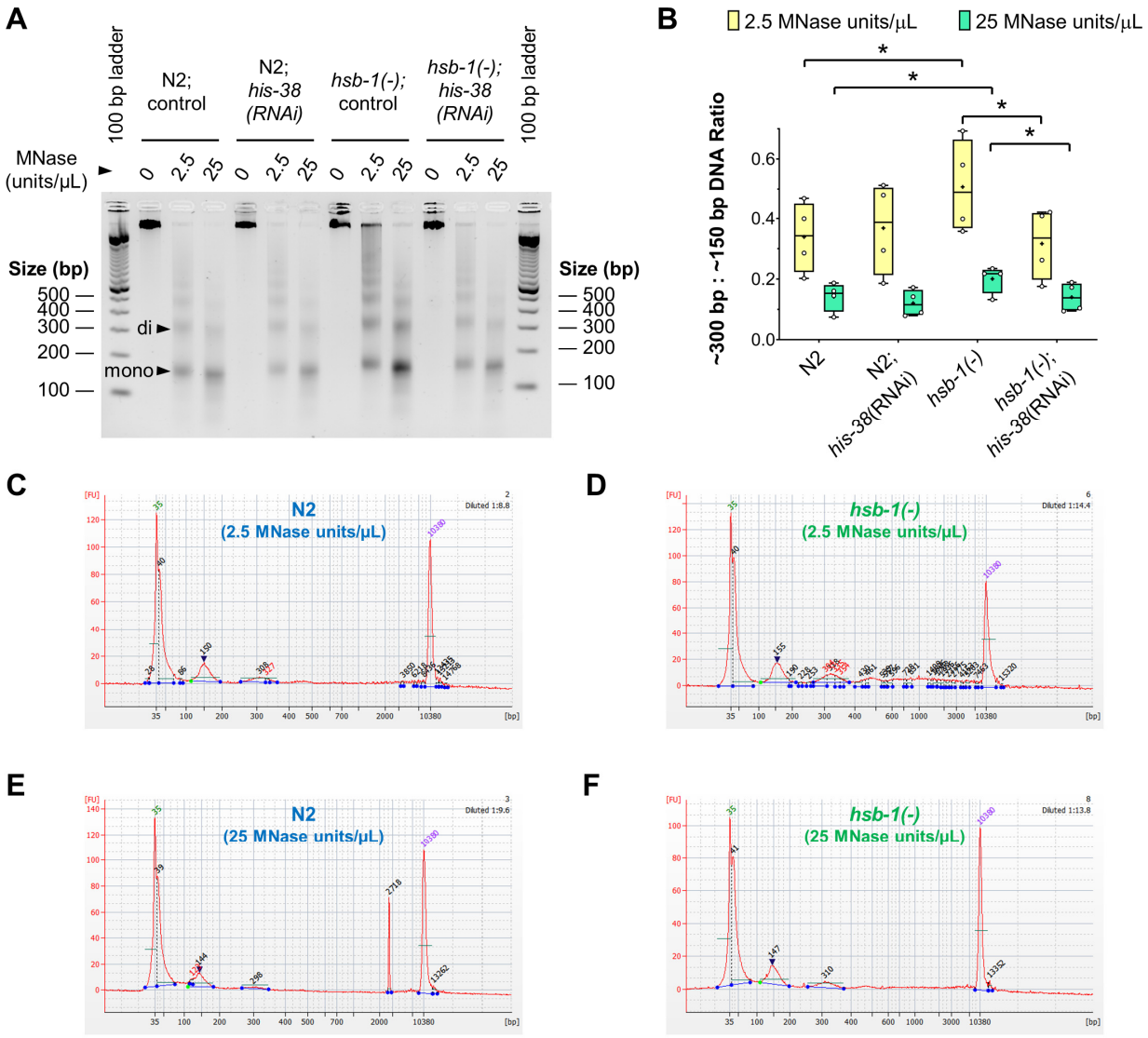

Figure 24. Higher chromatin compaction in *hsb-1(-)* worms is H4-dependent.
(A) Representative agarose gel electrophoresis for MNase-digested native chromatin of wild-type (N2) and *hsb-1(-)* worms grown on control or *his-38* RNAi bacteria at 25°C. Arrowheads on the gel indicate mononucleosomal (~150 bp) and dinucleosomal DNA (~300 bp) bands.
(B) Ratio of dinucleosomal: mononucleosomal DNA, quantified using Bioanalyzer 2100, in MNase-digested chromatin samples from N2 and *hsb-1(-)* worms grown on control or *his-38* RNAi bacteria at 25°C. Central line, box limits, '+' and whiskers indicate median, interquartile range, mean and data range, respectively, for four biological replicates. * indicates $p < 0.05$ in Sidak's multiple comparison test performed after repeated measures two-way ANOVA.
(C–F) Bioanalyzer 2100 electropherograms for DNA fragment analysis of native chromatin that was extracted from N2 and *hsb-1(-)* worms grown at 25°C and was digested with 2.5 or 25 units/µL of MNase. Mononucleosomal (~150 bp) and dinucleosomal (~300 bp) peaks were present in all conditions. Two large peaks at the ends represent DNA molecular weight markers.

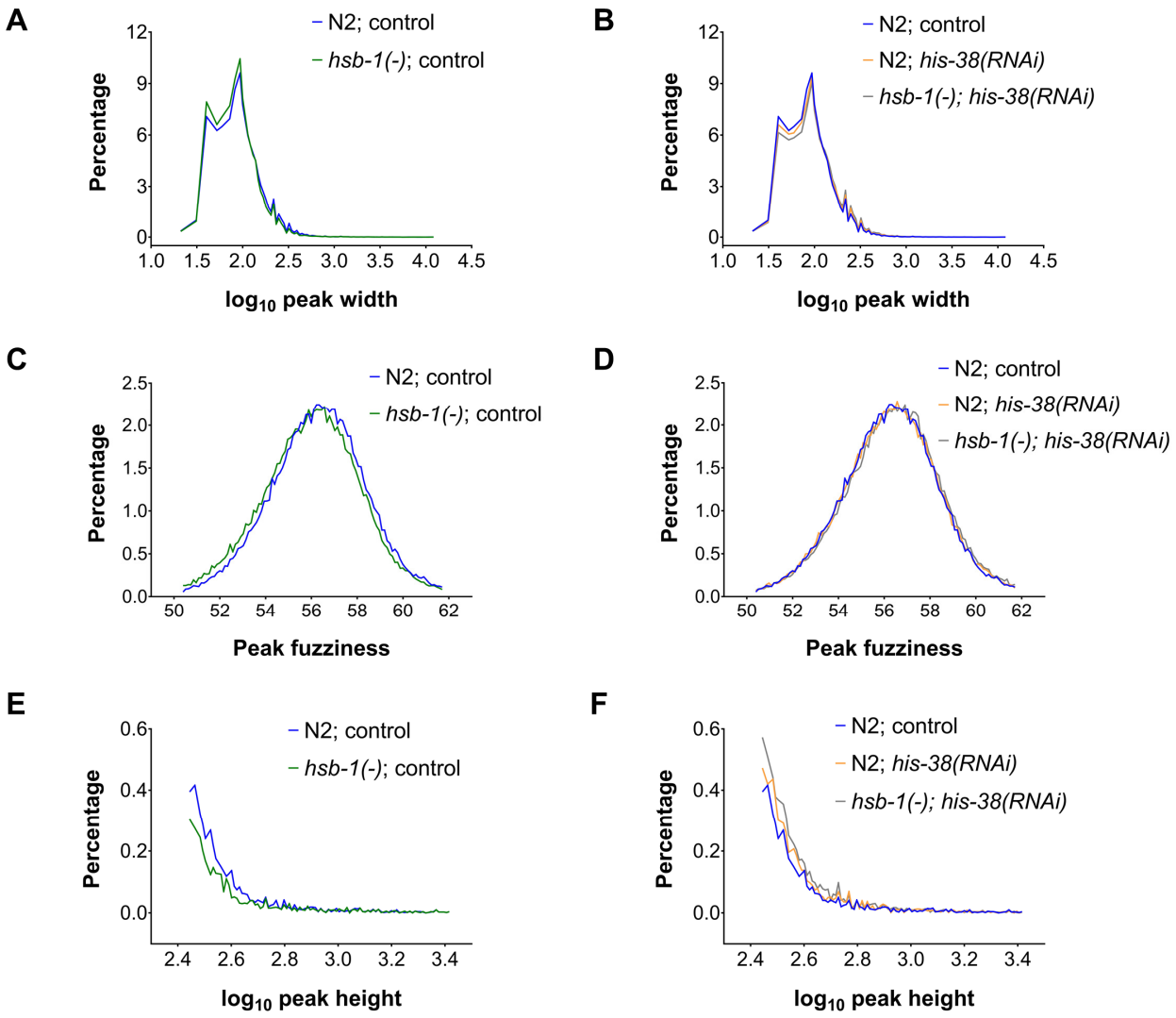

Figure 25. HSB-1 inhibition induces slightly better positioning of individual nucleosomes and a modest increase in sharpness of nucleosome peaks, which are both suppressed by H4 RNAi.
(A–F) Frequency distribution of nucleosome peak width, peak fuzziness and peak height in genome-wide sequencing data of MNase-digested chromatin from wild-type (N2) and *hsb-1(-)* worms grown on control or *his-38* RNAi bacteria at 25°C. Statistical data are included in **Table 7**.

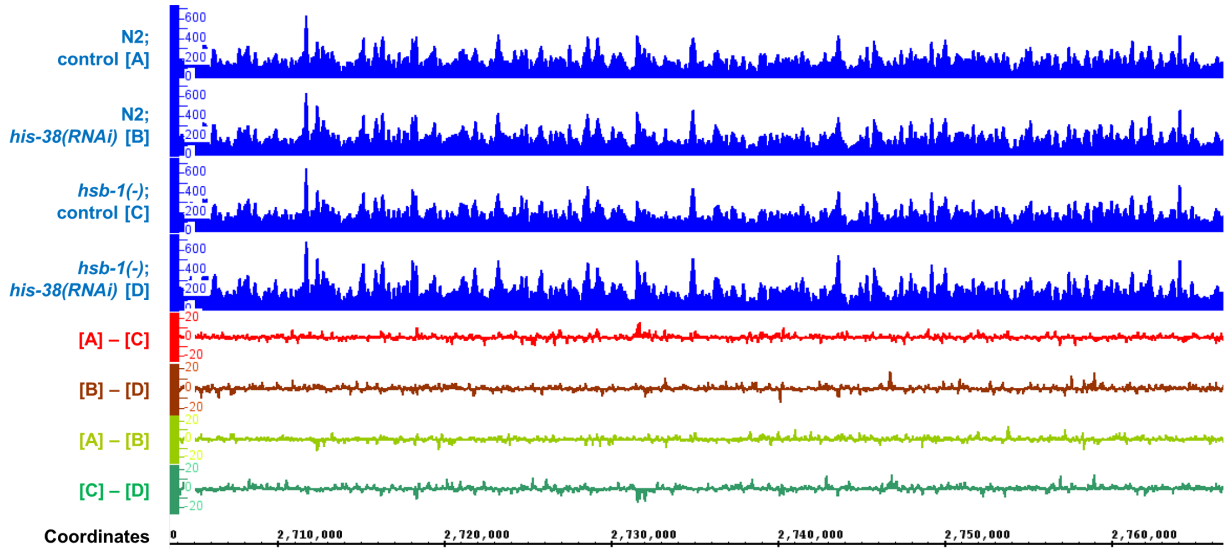

Figure 26. Chromatin compaction of most genomic regions is unaltered in *hsb-1(-)* worms.
MNase-Seq data for a representative genomic region in day 1 adult wild-type (N2) and *hsb-1(-)* worms grown on control or *his-38* RNAi bacteria at 25°C. Difference between groups, such as (A – B), indicates occupancy difference at each base pair between the two conditions. The region shown corresponds to genomic location X: 2,703,479 – 2,766,712 that spans *unc-2*, *igcm-3* and several ncRNA genes, a typical example of a genomic region at which MNase-accessibility is not significantly affected by either *hsb-1(-)* mutation or *his-38* RNAi.

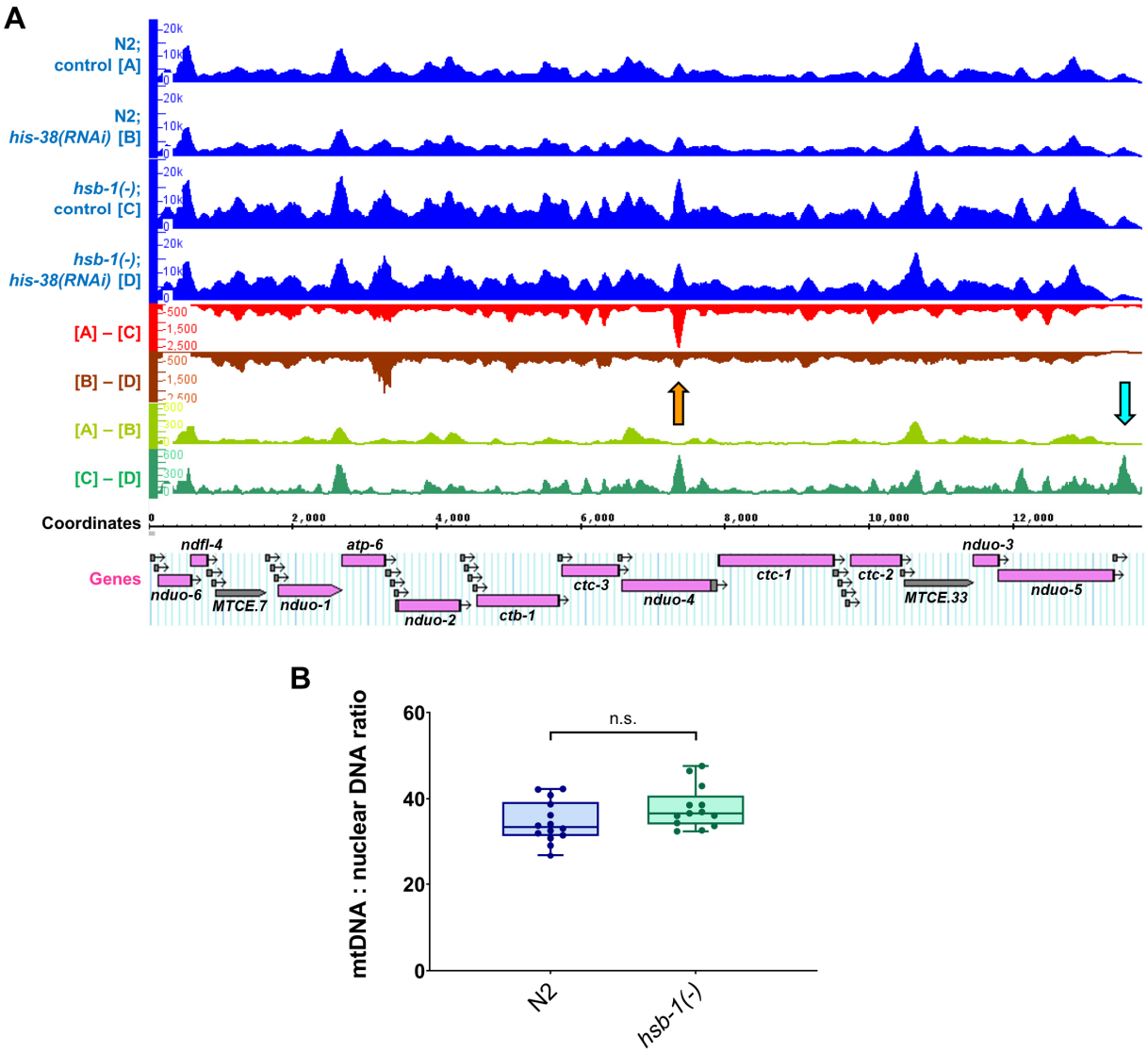

Figure 27. Mitochondrial DNA in *hsb-1(-)* worms shows higher MNase-protection.
(A) MNase-Seq data for entire ~13.8 kb stretch of *C. elegans* mitochondrial DNA from wild-type (N2) and *hsb-1(-)* worms grown on control or *his-38* RNAi bacteria at 25°C. Difference between groups, such as (A – B), indicates occupancy difference at each base pair. Orange and cyan arrows show the most prominent peak for (A – C) comparison and the location of mitochondrial D-loop region, respectively. Mitochondrially-encoded genes are shown. Labeled: Protein- and rRNA-coding genes; unlabeled: tRNA genes.
(B) Mitochondrial DNA copy number relative to nuclear DNA in N2 and *hsb-1(-)* worms grown at 25°C. Central line, box limits and whiskers indicate median, interquartile range and data range, respectively, for ≥ 13 biological replicates, each of $n = 8$ worms. $p = 0.09$ for comparison between the two genotypes in two-tailed *t*-test.

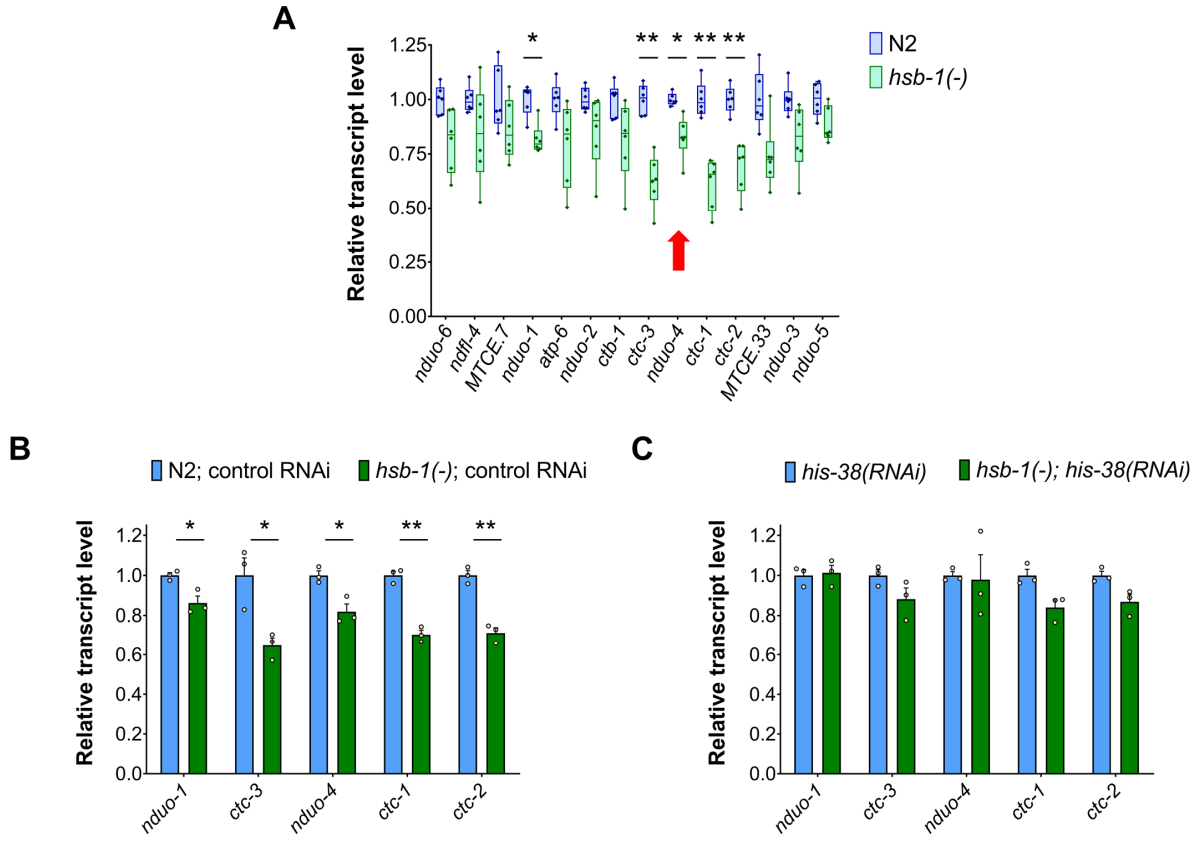

Figure 28. Reduced expression of mtDNA-encoded ETC complex IV genes in *hsb-1(-)* worms is H4-dependent.
(A) Relative transcript levels of mitochondrial rRNA (*MTCE.7* and *MTCE.33*) and protein-coding genes in wild-type (N2) and *hsb-1(-)* worms grown at 25°C. Central line, box limits and whiskers indicate median, interquartile range and data range, respectively, for six biological replicates. * $p < 0.05$, ** $p < 0.01$ in two-tailed *t*-test. Red arrow: Location of major H4-dependent peak in *hsb-1(-)* MNase-Seq data.
(B, C) Relative transcript levels of selected mitochondrial genes in wild-type (N2) and *hsb-1(-)* worms grown on either control or *his-38* RNAi bacteria at 25°C. Data represent mean ± SEM for three biological replicates. * $p < 0.05$, ** $p < 0.01$ in two-tailed *t*-test.

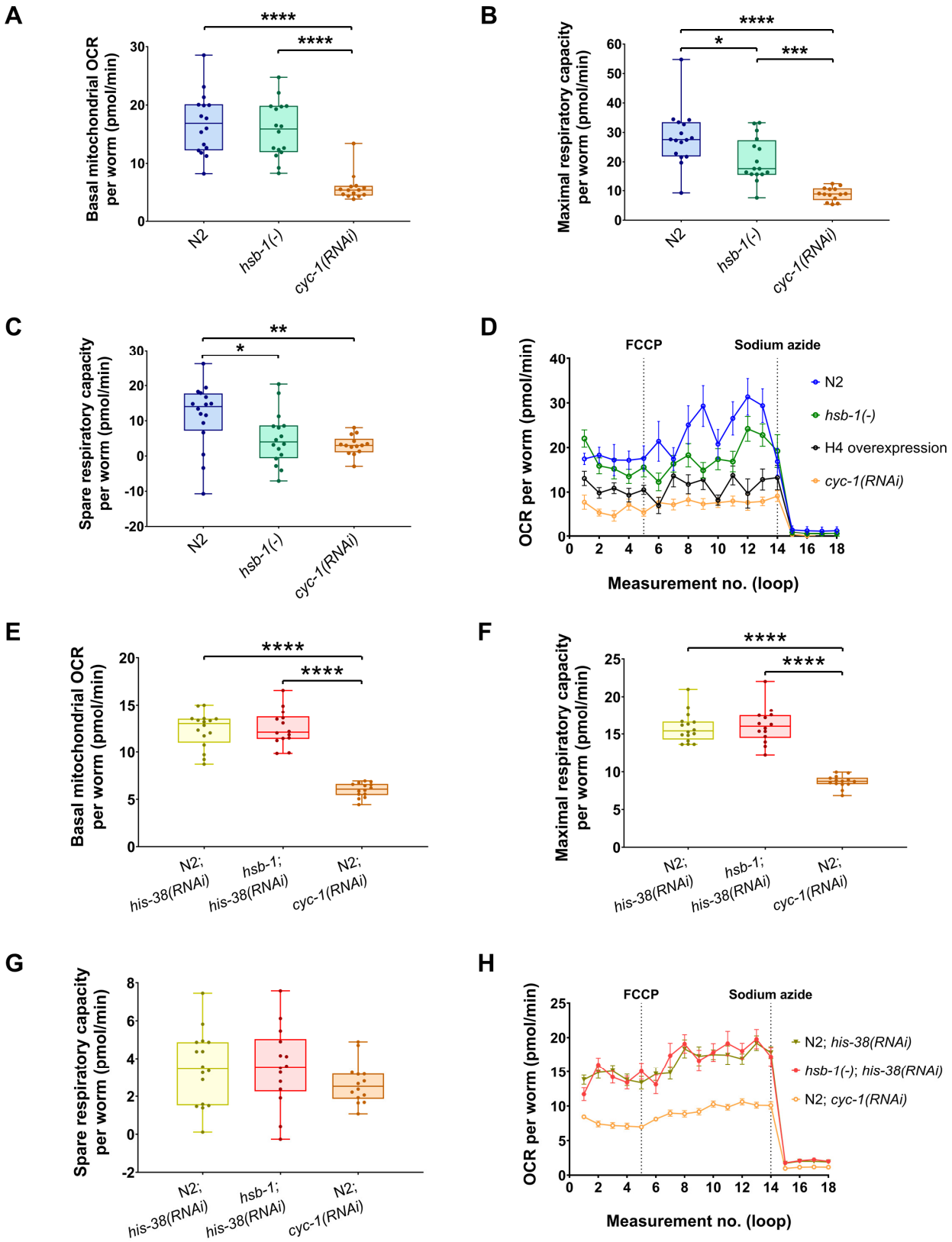

Figure 29. HSB-1 inhibition induces H4-dependent reduction in maximal and spare respiratory capacities in worms.

(A–C) Basal mitochondrial OCR, maximal respiratory capacity and spare respiratory capacity per worm in wild-type (N2), *hsb-1(-)* and N2; *cyc-1(RNAi)* worms grown at 25°C; corrected for non-mitochondrial oxygen consumption. Central line, box limits and whiskers indicate median, interquartile range and data range, respectively, for ≥ 14 biological replicates, each of n = 10–20 worms. * $p < 0.05$, ** $p < 0.01$, *** $p < 0.001$, **** $p < 0.0001$ in Tukey's multiple comparisons test performed after one-way ANOVA.
(D) Raw values for oxygen consumption rate (OCR) per worm in N2, *hsb-1(-)*, H4 overexpression strain and N2; *cyc-1(RNAi)* worms grown at 25°C. Mean ± SEM for ≥ 14 biological replicates, each of n = 10–20 worms. Measurement points (loops) 2–5 represent basal OCR. FCCP is a mitochondrial electron transport chain (ETC) accelerator that induces maximal uncontrolled OCR, while OCR measurements post-sodium azide injection correspond to non-mitochondrial respiration.
(E–G) Basal mitochondrial OCR, maximal respiratory capacity and spare respiratory capacity per worm in N2; *his-38(RNAi)*, *hsb-1(-); his-38(RNAi)* and N2; *cyc-1(RNAi)* worms grown at 25°C; corrected for non-mitochondrial oxygen consumption. Central line, box limits and whiskers indicate median, interquartile range and data range, respectively, for ≥ 14 biological replicates, each of n = 10–20 worms. **** $p < 0.0001$ in Tukey's multiple comparisons test performed after one-way ANOVA.
(H) Raw values for OCR per worm in N2; *his-38(RNAi)*, *hsb-1(-); his-38(RNAi)* and N2; *cyc-1(RNAi)* worms grown at 25°C. Mean ± SEM for ≥ 14 biological replicates, each of n = 10–20 worms. Measurement points (loops) 2–5 represent basal OCR. FCCP is a mitochondrial electron transport chain (ETC) accelerator that induces maximal uncontrolled OCR, while OCR measurements post-sodium azide injection correspond to non-mitochondrial respiration.

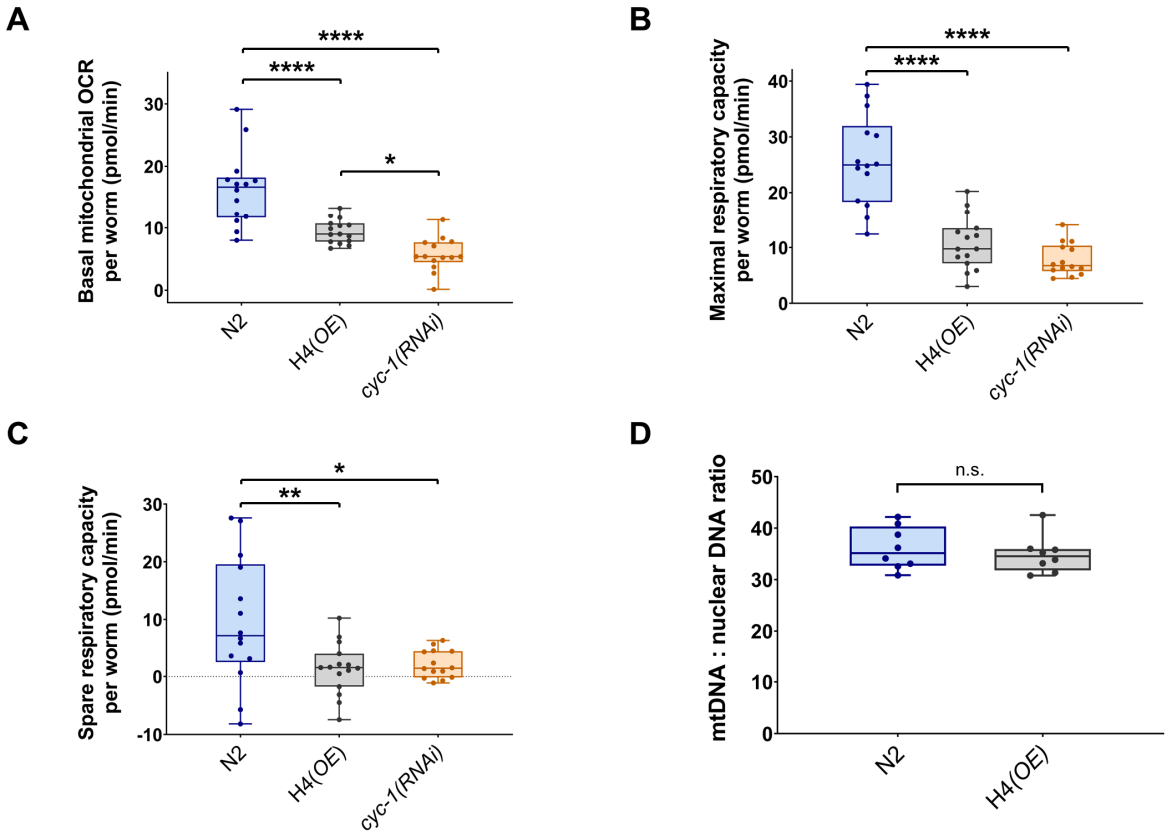

Figure 30. H4 overexpression results in lower respiratory capacity without affecting mtDNA copy number in worms.
(A–C) Basal mitochondrial OCR, maximal respiratory capacity and spare respiratory capacity per worm in wild-type (N2), H4 overexpression strain and N2; *cyc-1(RNAi)* worms grown at 25°C; corrected for non-mitochondrial oxygen consumption. Central line, box limits and whiskers indicate median, interquartile range and data range, respectively, for ≥ 14 biological replicates, each of n = 10–20 worms. * $p < 0.05$, ** $p < 0.01$, **** $p < 0.0001$ in Tukey's multiple comparisons test performed after one-way ANOVA.
(D) Mitochondrial DNA copy number relative to nuclear DNA in N2 and H4 overexpression strain grown at 25°C. Central line, box limits and whiskers indicate median, interquartile range and data range, respectively, for eight biological replicates, each of n = 8 worms. $p = 0.54$ for comparison between the two genotypes in two-tailed t-test.

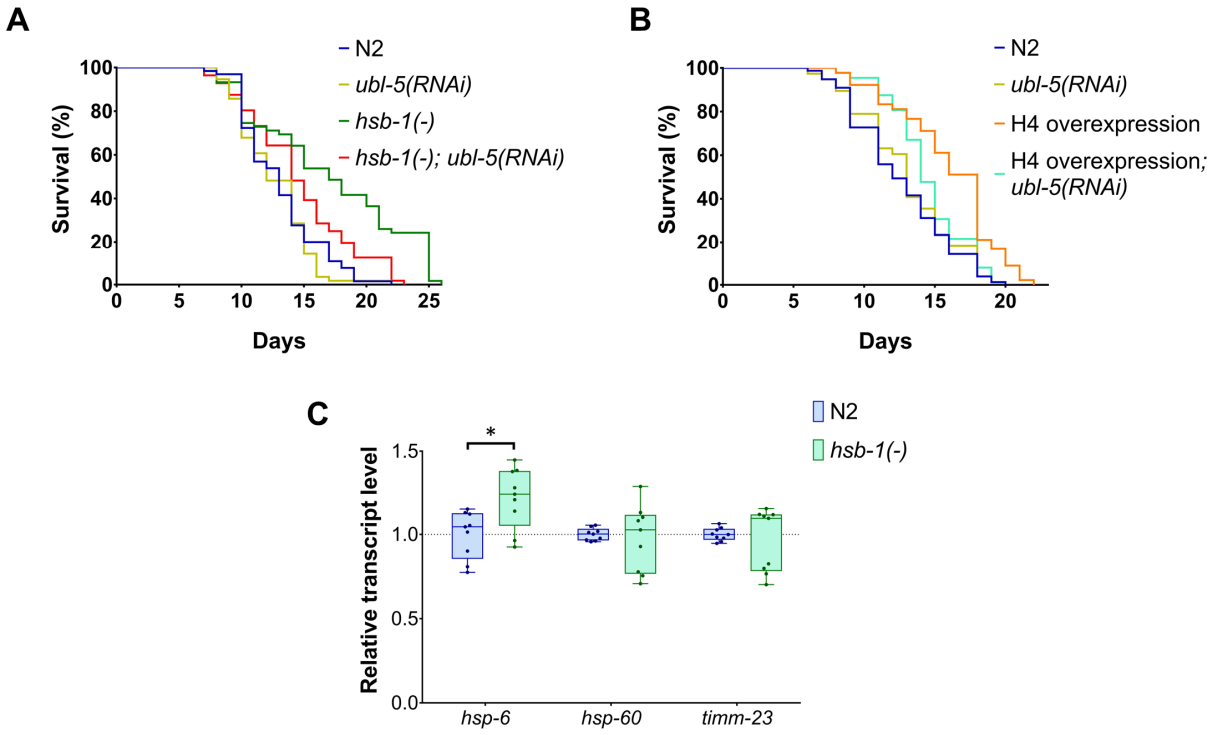

Figure 31. Inhibition of UPR^{mt} suppresses life span extension in *hsb-1(-)* and H4 overexpressing worms.
(A, B) Life span analysis of wild-type (N2), *hsb-1(-)* and H4 overexpressing worms grown on control or *ubl-5* RNAi bacteria at 25°C. Statistical data are included in **Table 6**.
(C) Relative transcript levels of UPR^{mt} genes in N2 and *hsb-1(-)* worms grown at 25°C. Central line, box limits and whiskers indicate median, interquartile range and data range, respectively, for nine biological replicates. * indicates $p < 0.05$ in two-tailed *t*-test.

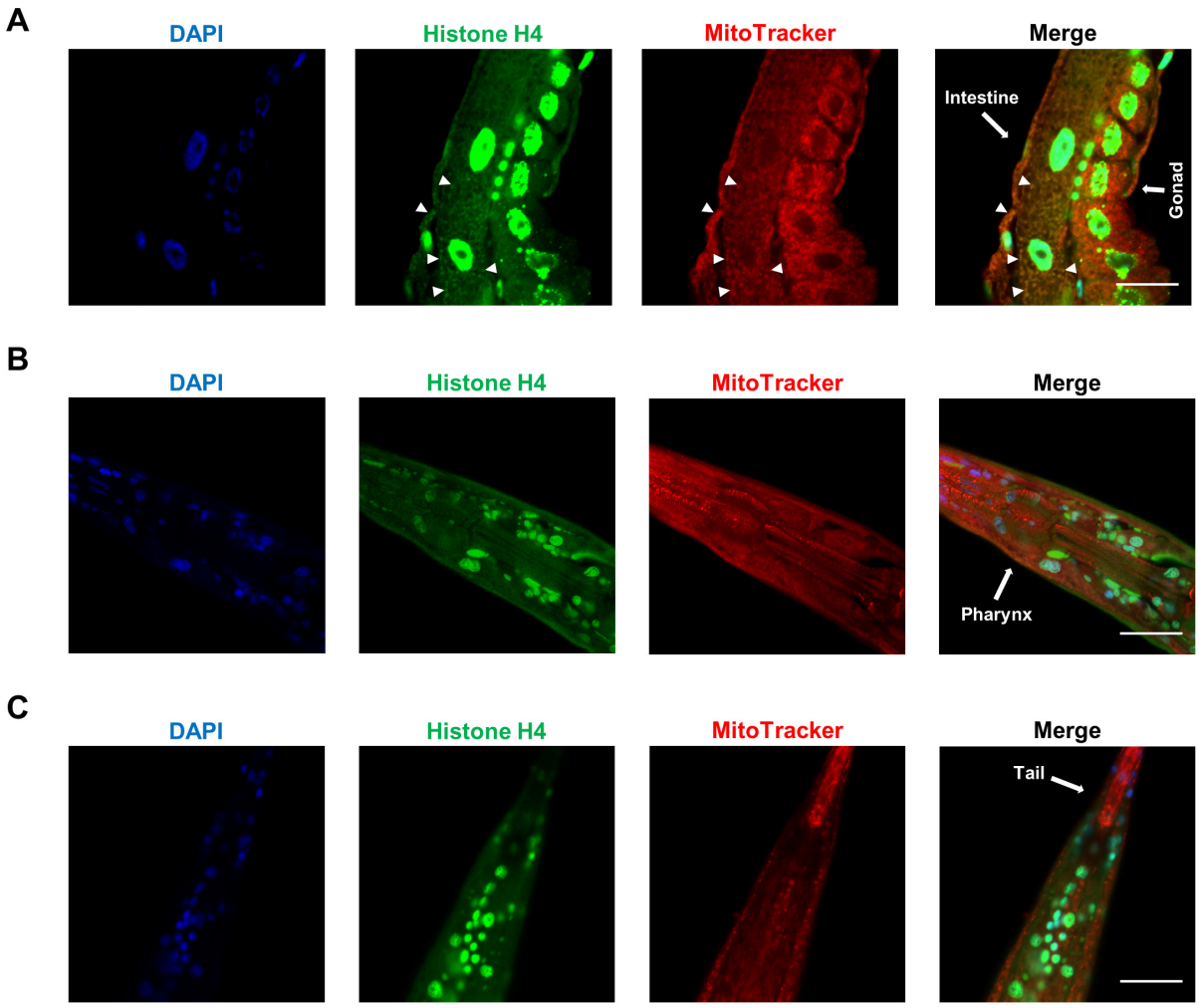

Figure 32. Extranuclear histone H4 foci co-localize with intestinal mitochondria.
(A–C) H4 immunofluorescence and labeling of mitochondria in different tissues of *hsb-1(-)* worms. White arrowheads show examples of co-localization of extranuclear histone foci with MitoTracker staining in intestine of worms. No obviously detectable co-localization of histone foci with MitoTracker staining was observed in other tissues. Scale bars represent 20 μM.

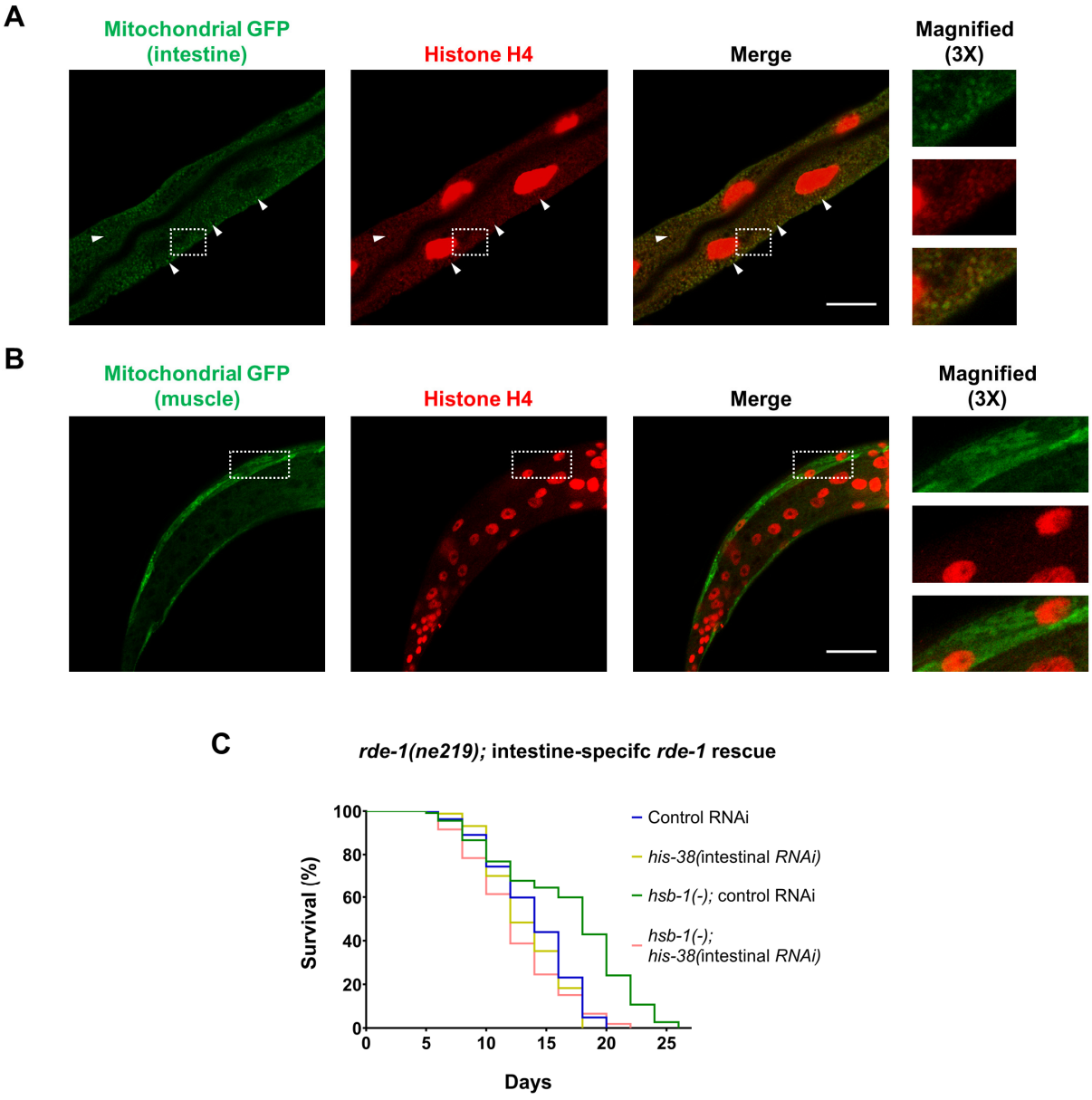

Figure 33. Extranuclear H4 foci co-localize with GFP expressed in intestinal, but not muscle, mitochondria.
(A, B) H4 immunofluorescence in worms expressing mitochondrially-localized GFP in intestinal tissue [*ges-1p::*GFP(mitochondrial)] or muscle tissue [*myo-3p::*GFP(mitochondrial)]. White arrowheads show examples of co-localization of extranuclear histone foci with intestinal mitochondria. Histone H4 immunostaining does not overlap with muscle mitochondria. Scale bars represent 20 µM. Regions outlined in white boxes are magnified (3X) and shown on the right.
(C) Life span analysis of *rde-1(-)* and *hsb-1(-); rde-1(-)* worms after intestine-specific rescue of *rde-1*. Worms were grown on control or *his-38* RNAi bacteria at 25°C. Statistical data and additional life span replicates are included in **Table 6**.

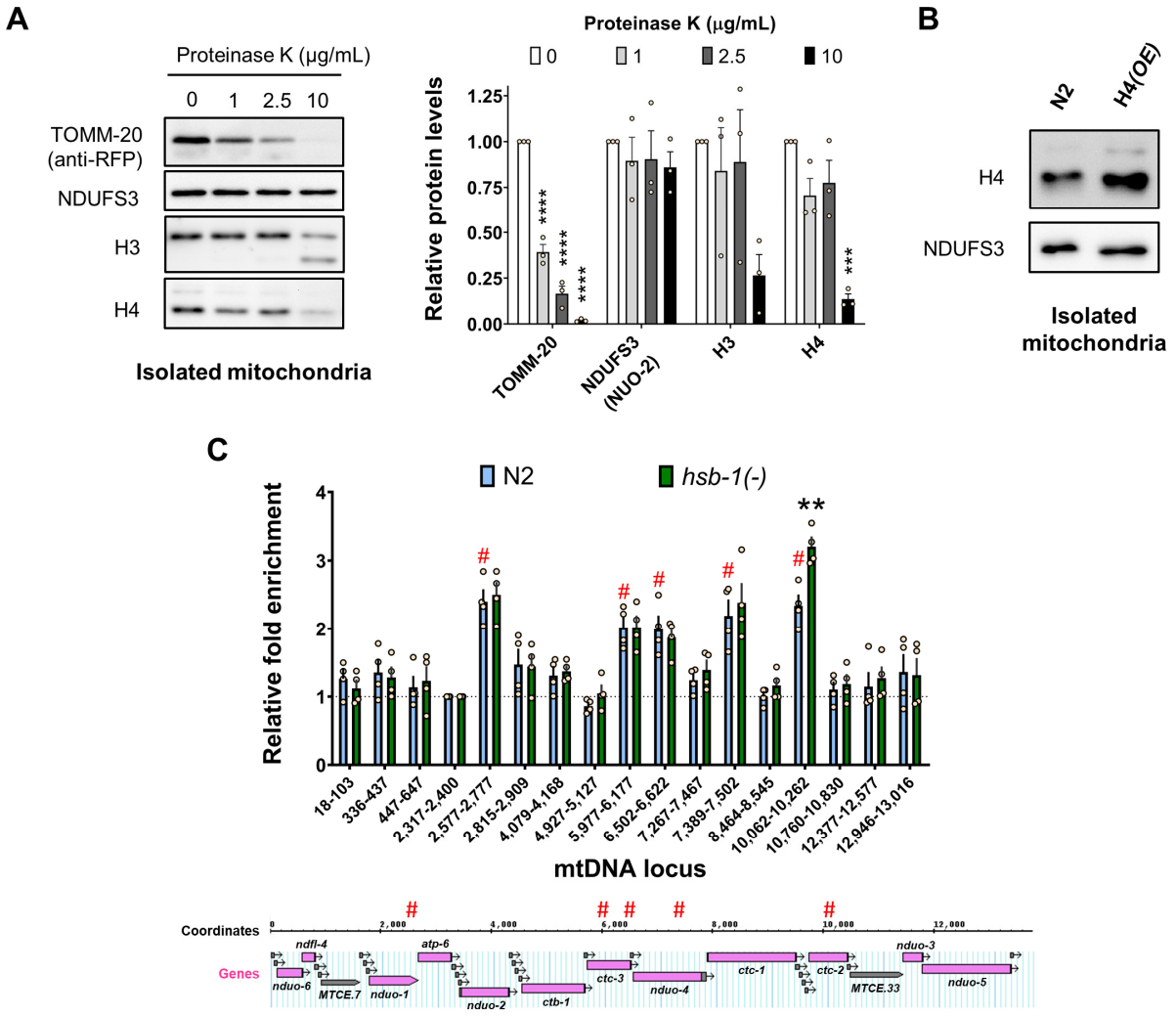

Figure 34. H4 is present inside mitochondria and binds to specific mtDNA loci.
(A) Representative immunoblots for outer mitochondrial membrane protein TOMM-20, inner mitochondrial membrane protein NUO-2 (NDUFS3 homolog) and histones H3 and H4 in mitochondria isolated from worms expressing RFP-tagged TOMM-20 protein. Isolated mitochondria were treated with indicated concentrations of proteinase K (*left*). Densitometric quantification of protein levels relative to control samples not subjected to proteinase K digestion (*right*). Mean ± SEM for three biological replicates. *** $p < 0.001$, **** $p < 0.0001$ compared to undigested control in Dunnett's multiple comparisons test performed after one-way ANOVA.
(B) Representative immunoblots for histone H4 and inner mitochondrial membrane protein NUO-2 (NDUFS3 homolog) in mitochondria isolated from wild-type (N2) and H4 overexpressing worms. Data are representative of two biological replicates.
(C) Relative fold enrichment for H4 chromatin immunoprecipitation-quantitative PCR (ChIP-qPCR) performed using isolated mitochondria from N2 and *hsb-1(-)* worms grown at 25°C. Values are reported relative to a control region that showed consistently low H4 binding across biological replicates (mtDNA: 2,317–2,400). Mean ± SEM for four biological replicates. # indicates loci that have significantly higher fold enrichment compared to the control region in both N2 and *hsb-1(-)* worms. ** indicates significantly higher fold enrichment in *hsb-1(-)* worms compared to wild-type. All significant differences correspond to $p < 0.01$ in Dunnett's multiple comparisons test performed after two-way ANOVA (*top*). Location of mitochondrially-encoded genes and H4 ChIP-qPCR peaks (marked with #) in the mitochondrial genome. Labeled: Protein- and rRNA-coding genes; unlabeled: tRNA genes (*bottom*).

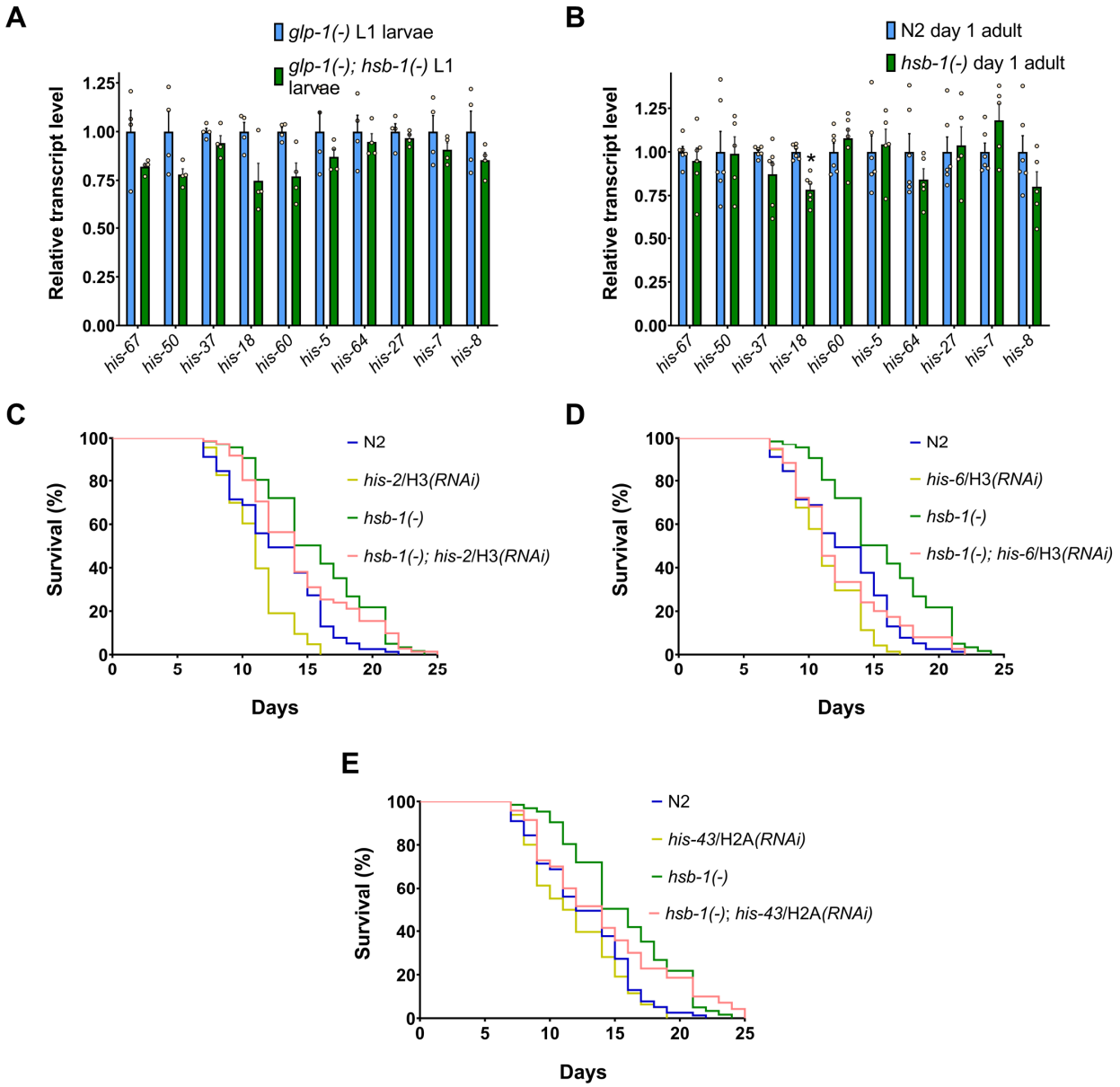

Figure 35. H4 transcript levels are not elevated in *hsb-1(-)* worms.
(A) Relative transcript levels of different core histone genes in *glp-1(-)* and *glp-1(-); hsb-1(-)* L1 larval worms grown at 25°C. Mean ± SEM for four biological replicates.
(B) Relative transcript levels of different core histone genes in day 1 adult wild-type (N2) and *hsb-1(-)* worms. Mean ± SEM for ≥ 5 biological replicates. * $p < 0.05$ compared to corresponding wild-type transcript levels in two-tailed *t*-test.
(C–E) Life span analysis of N2 and *hsb-1(-)* worms grown on control, *his-2*, *his-6* or *his-43* RNAi bacteria at 25°C. Statistical data are included in **Table 6**.

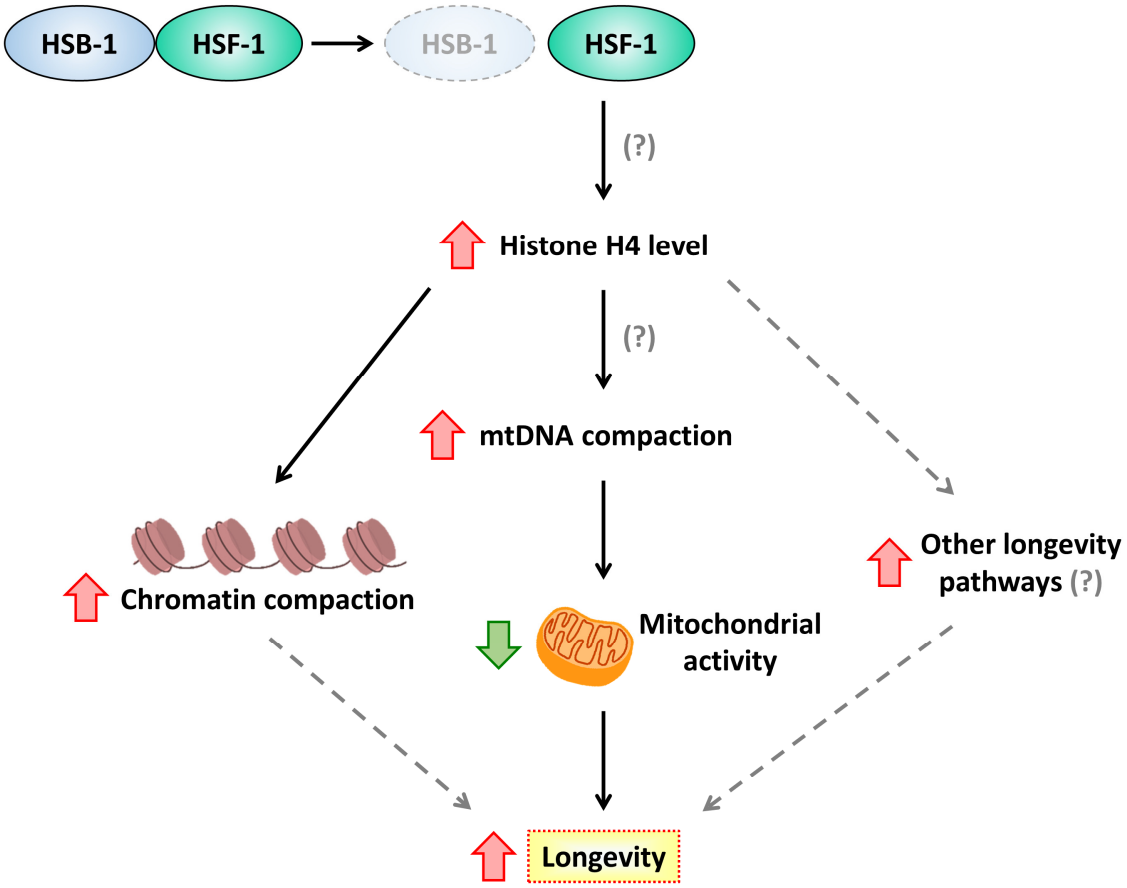

Figure 36. Model for longevity due to HSF-1-induced increase in histone H4 level that modulates mitochondrial function.
Proposed model of longevity associated with HSB-1 inhibition via increased H4 levels, mtDNA compaction and reduced mitochondrial activity. Dashed gray lines indicate other potential longevity pathways. (?) indicates unknown molecular mechanisms that need further investigation.

Tables

Table 6. Statistical data for life span experiments (Chapter 3).

Strain	Mean life span ± SEM (days)	75% dead (days)	n	*p* value	
Life span experiments at 25°C					
N2; control (i)	11.83 ± 0.41	14	55/72	—	a
N2; *his-67(RNAi)* (i)	11.05 ± 0.34	13	65/72	0.0956[a]	b
hsb-1(cg116); control (i)	14.26 ± 0.60	18	50/72	0.0001[a]	c
hsb-1(cg116); his-67(RNAi) (i)	11.64 ± 0.50	16	51/72	0.8419[a], 0.0964[b], 0.0005[c]	d
N2; control (ii)	12.59 ± 0.50	15	51/72	—	a
N2; *his-5(RNAi)* (i)	10.72 ± 0.36	12	68/72	0.0008[a]	b
hsb-1(cg116); control (ii)	15.88 ± 0.59	20	50/72	0.0001[a]	c
hsb-1(cg116); his-5(RNAi) (i)	11.07 ± 0.36	12	69/72	0.0101[a], 0.4150[b], < 0.0001[c]	d
N2; control (iii)	12.52 ± 0.42	15	61/72	—	a
N2; *his-38(RNAi)* (i)	11.13 ± 0.39	13	64/72	0.0146[a]	b
hsb-1(cg116); control (iii)	16.38 ± 0.54	20	55/72	< 0.0001[a]	c
hsb-1(cg116); his-38(RNAi) (i)	11.72 ± 0.35	13	64/72	0.0774[a], 0.4358[b], < 0.0001[c]	d
N2; control (iv)	11.78 ± 0.30	14	69/84	—	a
N2; *his-38(RNAi)* (ii)	11.87 ± 0.32	14	68/84	0.8386[a]	b
hsb-1(cg116); control (iv)	13.47 ± 0.42	16	69/84	0.0004[a]	c
hsb-1(cg116); his-38(RNAi) (ii)	10.20 ± 0.30	12	75/84	0.0004[a], 0.0005[b], < 0.0001[c]	d
N2; control (v)	13.44 ± 0.49	17	68/90	—	a
N2; *his-38(RNAi)* (iii)	13.05 ± 0.48	17	59/90	0.4376[a]	b
hsb-1(cg116); control (v)	17.56 ± 0.74	22	57/90	< 0.0001[a]	c
hsb-1(cg116); his-38(RNAi) (iii)	12.15 ± 0.44	14	66/90	0.0809[a], 0.2303[b], < 0.0001[c]	d
N2; control (vi)	13.22 ± 0.48	17	72/90	—	a
N2; *his-38(RNAi)* (iv)	12.95 ± 0.48	17	67/90	0.6626[a]	b
sur-5p::hsf-1(OE); control (i)	17.26 ± 0.65	21	85/90	< 0.0001[a]	c
sur-5p::hsf-1(OE); his-38(RNAi) (i)	12.99 ± 0.37	15	83/90	0.3456[a], 0.6651[b], < 0.0001[c]	d
N2; control (vii)	13.51 ± 0.49	16	65/90	—	a
N2; *his-38(RNAi)* (v)	11.14 ± 0.32	13	74/90	< 0.0001[a]	b
sur-5p::hsf-1(OE); control (ii)	19.99 ± 0.64	25	82/90	< 0.0001[a]	c
sur-5p::hsf-1(OE); his-38(RNAi) (ii)	14.85 ± 0.54	17	85/90	0.0542[a], < 0.0001[b], < 0.0001[c]	d
N2; control (vi)	13.22 ± 0.48	17	72/90	—	a

N2; *his-38(RNAi)* (iv)	12.95 ± 0.48	17	67/90	0.6626[a]	b
daf-2(e1370); control (i)*	31.51 ± 1.87	39	37/90	< 0.0001[a]	c
daf-2(e1370); his-38(RNAi) (i)*	30.04 ± 0.91	35	89/90	< 0.0001[a], < 0.0001[b], 0.2169[c]	d
N2; control (viii)	15.84 ± 0.45	19	67/90	—	a
N2; *his-38(RNAi)* (vi)	14.61 ± 0.34	16	71/90	0.0077[a]	b
daf-2(e1370); control (ii)*	28.64 ± 1.14	35	51/150	< 0.0001[a]	c
daf-2(e1370); his-38(RNAi) (ii)*	27.04 ± 1.00	33	86/90	< 0.0001[a], < 0.0001[b], 0.2205[c]	d
N2; control (ix)	12.36 ± 0.39	15	68/84	—	a
N2; *his-38(RNAi)* (vii)	11.88 ± 0.31	14	74/84	0.1942[a]	b
glp-1(e2144); control (i)	14.68 ± 0.42	17	71/72	< 0.0001[a]	c
glp-1(e2144); his-38(RNAi) (i)	13.88 ± 0.48	17	72/72	0.002[a], 0.0001[b], 0.5421[c]	d
N2; control (x)	12.75 ± 0.55	17	83/91	—	a
N2; *his-38(RNAi)* (viii)	12.95 ± 0.42	15	91/91	0.8499[a]	b
glp-1(e2144); control (ii)	15.76 ± 0.39	18	88/91	0.0025[a]	c
glp-1(e2144); his-38(RNAi) (ii)	15.24 ± 0.38	18	91/91	0.0202[a], 0.0015[b], 0.2934[c]	d
N2; control (vi)	13.22 ± 0.48	17	72/90	—	a
N2; *his-38(RNAi)* (iv)	12.95 ± 0.48	17	67/90	0.6626[a]	b
isp-1(qm150); control (i)	22.46 ± 0.77	27	56/90	< 0.0001[a]	c
isp-1(qm150); his-38(RNAi) (i)	14.35 ± 0.36	16	85/90	0.2856[a], 0.1004[b], < 0.0001[c]	d
N2; control (vii)	13.51 ± 0.49	16	65/90	—	a
N2; *his-38(RNAi)* (v)	11.14 ± 0.32	13	74/90	< 0.0001[a]	b
isp-1(qm150); control (ii)	23.15 ± 0.59	26	62/108	< 0.0001[a]	c
isp-1(qm150); his-38(RNAi) (ii)	14.54 ± 0.48	16	86/90	0.1713[a], < 0.0001[b], < 0.0001[c]	d
N2 (xi)	13.06 ± 0.39	15	70/84	—	a
hsb-1(cg116) (vii)	14.46 ± 0.49	18	66/84	0.0093[a]	b
sur-5p::his-67(OE); sur-5p::his-50(OE); sur-5p::his-37(OE) (i)	14.98 ± 0.53	19	69/84	0.0001[a], 0.4037[b]	c
N2; control (ix)	12.36 ± 0.39	15	68/84	—	a
N2; *his-38(RNAi)* (vii)	11.88 ± 0.31	14	74/84	0.1942[a]	b
sur-5p::his-67(OE); sur-5p::his-50(OE); sur-5p::his-37(OE); control (ii)	15.52 ± 0.34	17	75/84	< 0.0001[a]	c
sur-5p::his-67(OE); sur-5p::his-50(OE); sur-5p::his-37(OE); his-38(RNAi) (i)	13.10 ± 0.34	15	79/84	0.2235[a], 0.011[b], < 0.0001[c]	d
glp-1(e2144); control (i)	14.68 ± 0.42	17	71/72	—	a
glp-1(e2144); his-38(RNAi) (i)	13.88 ± 0.48	17	72/72	0.5421[a]	b
glp-1(e2144); hsb-1(cg116); control (i)	17.49 ± 0.65	22	58/72	< 0.0001[a]	c

glp-1(e2144); hsb-1(cg116); his-38(RNAi) (i)	14.35 ± 0.42	17	71/72	0.55[a], 0.6578[b], < 0.0001[c]	d
glp-1(e2144); control (iii)	15.77 ± 0.43	18	84/90	—	a
glp-1(e2144); his-38(RNAi) (iii)	14.62 ± 0.34	17	85/90	0.0032[a]	b
glp-1(e2144); hsb-1(cg116); control (ii)	20.83 ± 0.43	24	89/90	< 0.0001[a]	c
glp-1(e2144); hsb-1(cg116); his-38(RNAi) (ii)	16.10 ± 0.42	20	90/90	0.7401[a], 0.0013[b], < 0.0001[c]	d
glp-4(bn2); control (i)	12.23 ± 0.56	17	66/90	—	a
glp-4(bn2); his-38(RNAi) (i)	11.55 ± 0.48	14	63/90	0.22[a]	b
glp-4(bn2); hsb-1(cg116); control (i)	17.25 ± 0.76	22	58/90	< 0.0001[a]	c
glp-4(bn2); hsb-1(cg116); his-38(RNAi) (i)	12.72 ± 0.62	17	69/90	0.6043[a], 0.0898[b], < 0.0001[c]	d
glp-4(bn2); his-38(RNAi) (ii)	11.62 ± 0.42	14	66/90	—	a
glp-4(bn2); hsb-1(cg116); his-38(RNAi) (ii)	12.35 ± 0.51	17	65/90	0.20[a]	b
glp-1(e2144); control (i)	14.68 ± 0.42	17	71/72	—	a
glp-1(e2144); *his-38(*adulthood *RNAi)* (i)	15.60 ± 0.48	19	72/72	0.0581[a]	b
glp-1(e2144); hsb-1(cg116); control (i)	17.49 ± 0.65	22	58/72	< 0.0001[a]	c
*glp-1(e2144); hsb-1(cg116); his-38(*adulthood *RNAi)* (i)	17.14 ± 0.65	21	72/72	< 0.0001[a], 0.0018[b], 0.8655[c]	d
glp-1(e2144); control (iii)	15.77 ± 0.43	18	84/90	—	a
glp-1(e2144); *his-38(*adulthood *RNAi)* (ii)	15.17 ± 0.43	18	90/90	0.5274[a]	b
glp-1(e2144); hsb-1(cg116); control (ii)	20.83 ± 0.43	24	89/90	< 0.0001[a]	c
*glp-1(e2144); hsb-1(cg116); his-38(*adulthood *RNAi)* (ii)	20.80 ± 0.40	23	89/90	< 0.0001[a], < 0.0001[b], 0.6236[c]	d
N2; control (viii)	15.84 ± 0.45	19	67/90	—	a
N2; *his-38(*adulthood *RNAi)* (i)	14.47 ± 0.40	16	64/90	0.0126[a]	b
hsb-1(cg116); control (vi)	20.33 ± 0.60	26	71/90	< 0.0001[a]	c
*hsb-1(cg116); his-38(*adulthood *RNAi)* (i)	18.03 ± 0.65	22	73/90	0.0008[a], < 0.0001[b], 0.0594[c]	d
N2; control (ii)	12.59 ± 0.50	15	51/72	—	a
N2; *his-67(*adulthood *RNAi)* (i)	13.04 ± 0.39	15	54/72	0.7155[a]	b
hsb-1(cg116); control (ii)	15.88 ± 0.59	20	50/72	0.0001[a]	c
*hsb-1(cg116); his-67(*adulthood *RNAi)* (i)	14.58 ± 0.41	17	60/72	0.0165[a], 0.001[b], 0.0197[c]	d
N2; control (xii)	13.08 ± 0.39	15	65/90	—	a
N2; *ubl-5(RNAi)* (i)	12.61 ± 0.38	15	56/90	0.2935[a]	b
hsb-1(cg116); control (viii)	17.13 ± 0.78	22	58/100	< 0.0001[a]	c
hsb-1(cg116); ubl-5(RNAi) (i)	14.59 ± 0.57	18	56/90	0.012[a], 0.0012[b], 0.0009[c]	d
N2; control (xiii)	12.65 ± 0.39	15	77/100	—	a

N2; *ubl-5(RNAi)* (ii)	13.05 ± 0.40	15	76/100	0.5189[a]	b
sur-5p::his-67(OE); sur-5p::his-50(OE); sur-5p::his-37(OE); control (iii)	16.07 ± 0.38	18	90/100	< 0.0001[a]	c
sur-5p::his-67(OE); sur-5p::his-50(OE); sur-5p::his-37(OE); ubl-5(RNAi) (i)	14.55 ± 0.28	16	88/100	0.0065[a], 0.0378[b], < 0.0001[c]	d
rde-1(ne219); ges-1p::rde-1; control (i)	13.83 ± 0.40	16	82/96	—	a
rde-1(ne219); ges-1p::rde-1; his-38(RNAi) (i)	13.28 ± 0.35	16	82/97	0.1716[a]	b
hsb-1(cg116); rde-1(ne219); ges-1p::rde-1; control (i)	16.62 ± 0.53	20	112/119	< 0.0001[a]	c
hsb-1(cg116); rde-1(ne219); ges-1p::rde-1; his-38(RNAi) (i)	12.36 ± 0.39	14	106/120	0.0496[a], 0.3281[b], < 0.0001[c]	d
rde-1(ne219); ges-1p::rde-1; control (ii)	15.32 ± 0.42	18	59/72	—	a
rde-1(ne219); ges-1p::rde-1; his-38(RNAi) (ii)	14.43 ± 0.35	16	55/68	0.0458[a]	b
hsb-1(cg116); rde-1(ne219); ges-1p::rde-1; control (ii)	17.42 ± 0.83	21	42/72	0.0003[a]	c
hsb-1(cg116); rde-1(ne219); ges-1p::rde-1; his-38(RNAi) (ii)	14.46 ± 0.80	18	33/70	0.9176[a], 0.2844[b], 0.0033[c]	d
N2; control (xiv)	12.68 ± 0.42	16	77/90	—	a
N2; *his-2(RNAi)* (i)	11.00 ± 0.30	12	63/90	0.0002[a]	b
hsb-1(cg116); control (ix)	15.63 ± 0.53	19	60/90	< 0.0001[a]	c
hsb-1(cg116); his-2(RNAi) (i)	14.37 ± 0.51	17	71/90	0.0137[a], < 0.0001[b], 0.2527[c]	d
N2; control (xiv)	12.68 ± 0.42	16	77/90	—	a
N2; *his-6(RNAi)* (i)	11.21 ± 0.31	14	71/90	0.0004[a]	b
hsb-1(cg116); control (ix)	15.63 ± 0.53	19	60/90	< 0.0001[a]	c
hsb-1(cg116); his-6(RNAi) (i)	12.37 ± 0.45	14	75/90	0.8743[a], 0.0163[b], 0.0001[c]	d
N2; control (xiv)	12.68 ± 0.42	16	77/90	—	a
N2; *his-43(RNAi)* (i)	11.89 ± 0.40	15	79/90	0.2187[a]	b
hsb-1(cg116); control (ix)	15.63 ± 0.53	19	60/90	< 0.0001[a]	c
hsb-1(cg116); his-43(RNAi) (i)	14.15 ± 0.62	17	70/90	0.0121[a], 0.0006[b], 0.4155[c]	d
Life span experiments at 20°C					
N2; control (i)	15.36 ± 0.47	17	56/72	—	a
N2; *his-67(RNAi)* (i)	14.62 ± 0.35	17	65/84	0.0576[a]	b
hsb-1(cg116); control (i)	19.48 ± 0.69	24	72/84	< 0.0001[a]	c
hsb-1(cg116); his-67(RNAi) (i)	18.50 ± 0.42	22	78/84	< 0.0001[a], < 0.0001[b], 0.0035[c]	d
N2; control (ii)	20.26 ± 0.49	22	78/91	—	a
N2; *his-67(RNAi)* (ii)	18.44 ± 0.59	22	62/91	0.0443[a]	b

hsb-1(cg116); control (ii)	24.39 ± 0.72	29	79/91	< 0.0001[a]	c
hsb-1(cg116); his-67(RNAi) (ii)	22.72 ± 0.73	29	87/91	0.0001[a], < 0.0001[b], 0.2298[c]	d
N2; control (ii)	20.26 ± 0.49	22	78/91	—	a
N2; *his-38(RNAi)* (i)	16.48 ± 0.50	20	81/91	< 0.0001[a]	b
hsb-1(cg116); control (ii)	24.39 ± 0.72	29	79/91	< 0.0001[a]	c
hsb-1(cg116); his-38(RNAi) (i)	21.13 ± 0.70	27	79/91	0.0351[a], < 0.0001[b], 0.0002[c]	d

Adult 'mean life span ± SEM' in days. '75% dead' refers to 75th percentile, age at which surviving proportion of the population reaches 0.25. 'n' indicates number of observed deaths relative to total number of animals on day 1 of the experiment. The difference refers to animals that were censored at different time points due to bagging, exploding, crawling off plates or being accidentally killed. Statistical analysis was performed using Mantel-Cox log-rank test to obtain *p* values. Conditions for which life span analysis was performed more than once, their descriptions are followed by a Roman numeral in parentheses to identify independent biological replicates. * *daf-2(e1370)* animals, being dauer-constitutive at 25°C, were transferred from 20°C to 25°C on day 1 of adulthood.

Table 7. Statistical data for frequency distributions of genome-wide nucleosomal parameters determined from MNase-Seq analysis

Sample 1	Sample 2	Mean (sample 1)	Mean (sample 2)	SD (sample 1)	SD (sample 2)	*D* value	Bonferroni *p* value
Nucleosome peak width							
N2; control	N2; *his-38(i)*	136.30	142.22	303.56	304.11	0.0267	$< 1.4 \times 10^{-15}$
N2; control	*hsb-1(-);* control	136.30	128.54	303.56	299.39	0.0427	$< 1.4 \times 10^{-15}$
N2; control	*hsb-1(-); his-38(i)*	136.30	144.88	303.56	286.61	0.0528	$< 1.4 \times 10^{-15}$
N2; *his-38(i)*	*hsb-1(-);* control	142.22	128.54	304.11	299.39	0.0689	$< 1.4 \times 10^{-15}$
N2; *his-38(i)*	*hsb-1(-); his-38(i)*	142.22	144.88	304.11	286.61	0.0269	$< 1.4 \times 10^{-15}$
hsb-1(-); control	*hsb-1(-); his-38(i)*	128.54	144.88	299.39	286.61	0.0954	$< 1.4 \times 10^{-15}$
Nucleosome peak fuzziness							
N2; control	N2; *his-38(i)*	56.28	56.26	2.08	2.06	0.0069	0.27414
N2; control	*hsb-1(-);* control	56.28	56.01	2.08	2.11	0.0498	$< 1.4 \times 10^{-15}$
N2; control	*hsb-1(-); his-38(i)*	56.28	56.38	2.08	2.09	0.0215	$< 1.4 \times 10^{-15}$
N2; *his-38(i)*	*hsb-1(-);* control	56.26	56.01	2.06	2.11	0.0471	$< 1.4 \times 10^{-15}$
N2; *his-38(i)*	*hsb-1(-); his-38(i)*	56.26	56.38	2.06	2.09	0.0259	$< 1.4 \times 10^{-15}$
hsb-1(-); control	*hsb-1(-); his-38(i)*	56.01	56.38	2.11	2.09	0.0708	$< 1.4 \times 10^{-15}$
Nucleosome peak height							
N2; control	N2; *his-38(i)*	541.91	508.42	442.76	389.89	0.0294	0.27996
N2; control	*hsb-1(-);* control	541.91	587.17	442.76	487.94	0.0579	0.00013
N2; control	*hsb-1(-); his-38(i)*	541.91	503.10	442.76	387.76	0.0388	0.01165
N2; *his-38(i)*	*hsb-1(-);* control	508.42	587.17	389.89	487.94	0.0734	3.89×10^{-8}
N2; *his-38(i)*	*hsb-1(-); his-38(i)*	508.42	503.10	389.89	387.76	0.0156	1
hsb-1(-); control	*hsb-1(-); his-38(i)*	587.17	503.10	487.94	387.76	0.0845	1.63×10^{-11}

Statistical analysis was performed for comparison between genome-wide frequency distributions of nucleosome peak width, peak fuzziness and peak height across conditions. '*D* value' refers to *D* statistic determined from Kolmogorov-Smirnov test. *p* values are reported after Bonferroni's correction for multiple comparisons. '*his-38(i)*' indicates *his-38(RNAi)*.

Table 8. Genomic regions with large-scale changes in MNase-Seq signal intensity associated with HSB-1 inhibition.

Genomic location	Brief description of peak location	Occupancy difference
Gain of peak intensity in hsb-1(-) worms compared to N2 in control RNAi		
mtDNA: 40 – 13,790	Entire stretch of mitochondrial DNA	2,529.87
IV: 11,068,570 – 11,086,730	Contains pseudogene *Y5F2A.3*	1,972.07
I: 15,032,020 – 15,072,410	rRNA gene repeats and ncRNA genes near right arm telomere of chromosome I	1,280.87
V: 8,713,960 – 8,727,030	Region between genes *ZC178.2* and *glr-5*	617.03
Loss of peak intensity in hsb-1(-) worms compared to N2 in control RNAi		
I: 13,947,370 – 14,015,560	Includes genes *Y71A12B.18*, *Y71A12B.12* and four ncRNA genes	896.39
IV: 14,919,710 – 14,940,680	Possible background deletion close to *hsb-1(cg116)* deletion	689.88
IV: 12,557,590 – 12,594,200	*hsb-1(cg116)* deletion	607.49
IV: 3,567,570 – 3,629,160	Region between genes *unc-17* and *ZC416.2*	514.43
Gain of peak intensity in hsb-1(-) worms compared to N2 in his-38 RNAi		
mtDNA: 40 – 13,780	Entire stretch of mitochondrial DNA	2,126.29
IV: 11,068,560 – 11,086,710	Contains pseudogene *Y5F2A.3*	1,918.40
I: 15,031,930 – 15,072,410	rRNA gene repeats and ncRNA genes near right arm telomere of chromosome I	1,587.67
V: 8,713,970 – 8,720,440	Region between genes *ZC178.2* and *glr-5*	554.26
V: 18,695,560 – 18,792,030	Pseudogene-rich region on chromosome V	502.44
Loss of peak intensity in hsb-1(-) worms compared to N2 in his-38 RNAi		
IV: 14,919,770 – 14,939,020	Possible background deletion close to *hsb-1(cg116)* deletion	722.74
IV: 12,556,970 – 12,584,290	*hsb-1(cg116)* deletion	689.88
I: 13,946,630 – 14,015,560	Includes genes *Y71A12B.18*, *Y71A12B.12* and four ncRNA genes	566.36
IV: 3,626,530 – 3,629,160	Region between genes *unc-17* and *ZC416.2*	556.38

Occupancy difference was determined using Dregion function of DANPOS2. Genomic regions with occupancy difference values ≥ 500 are reported.

Table 9. Genomic regions with large-scale changes in MNase-Seq signal intensity associated with H4 RNAi.

Genomic location	Brief description of peak location	Occupancy difference
Loss of peak intensity in hsb-1(-) worms subjected to his-38 RNAi compared to control RNAi		
X: 15,788,520 – 15,838,140	Region between gene *Y7A5A.7* and pseudogene *Y7A5A.11*	725.67
mtDNA: 40 – 13,790	Entire stretch of mitochondrial DNA	609.78

Occupancy difference was determined using Dregion function of DANPOS2. Genomic regions with occupancy difference values ≥ 500 are reported. No region passed the threshold value of ≥ 500 for reduction in peak intensity after *his-38(RNAi)* in wild-type N2 strain. Also, no region showed an increase in peak intensity above the threshold value of ≥ 500 after *his-38(RNAi)* in either N2 or *hsb-1(-)* strain.

Table 10. List of primer sequences used for PCR experiments (Chapter 3).

PCR target	Forward Primer (5' – 3')	Reverse Primer (5' – 3')
Quantitative RT-PCR		
act-1	TGCCCCATCAACCATGAAGATCAAGA	GCCGGACTCGTCGTATTCTTGC
cdc-42	GCGTTGACGCAGAAGGGACTG	CAAGGAAGACGTTCCTAGAGAATATTGCA CTTC
pmp-3	GGAACTTAGAGTCAAGGGTCGCAG	GAACTGTATCGGCACCAAGGAAACTG
his-67	TCAATTGTCCTCCCGCTTC	CATTTATTGCAATCGGACTGTTTG
his-37	AAGGAAGAACTCTCTACGGATTC	TGAATTTCAAAGCGAGTGATCTG
his-50	GCCGTCACTTACTGTGAGCAC	CCGAATCCGTACAGAGTTCTTCCTTG
his-27	GCGTCTTGTTCGTGAGATCG	CTCGAAGAGTCCGACGAGGT
his-7	CTGCCCGTGACAACAAGAAG	GATGGTCACTCCAGCCAACA
his-8	CAACGACGTCTTCGAGCGTA	GGCAAGCTCTCCTGGAAGAA
C09B7.2	CAAGAGTTTTTGGAGCCATCG	CGTCGTGAGCTTGACGAATA
nduo-6	TTTGTTTTAGCTGTTTTAAGTAGGATTATTA GA	AAGAAAACCAAATATGTATTCTCATTGAA
ndfl-4	TGACAACGTTTAATTTTTATTCTAATTTCTT TAG	ACTACCATACCCAGGATTCTTGAAA
MTCE.7	TGATTTAAGAAACATTTGGCCTACAA	TTTGGGCAATTGATGGATGA
nduo-1	AGCGTCATTTATTGGGAAGAAGAC	AAGCTTGTGCTAATCCCATAAATGT
atp-6	TTGTCCTTGTGGAATGGTTGA	TTTCAAATATGTGTCTCCTGGTTTTC
nduo-2	AAAGCAGCAAGAGATATACCAGAATTT	TCAAAAGTGGAGCGGTGCTA
ctb-1	TGGTGTTACAGGGGCAACAT	TCACCGTGGCAATATAACCTAGA
ctc-3	CGGGATTTCACGGAATTCAT	GCAAATTCCAACCCCAGATG
nduo-4	AGGCACAGCGGGATTTTTAC	GCTGCTAAAGCCTTTGAATCTCTT
ctc-1	TTGGGATTTTCACGGGTGTT	TGCAAAATGTAGCGGGAAAA
ctc-2	CTGCTGATGTTATTCATGCTTGG	TGATTTGCTCCACAAATCTCTGA
MTCE.33	TTAAAGCTGGCTTCTGCCCTA	TTCATACTGGAACTCAATAAAAGCACA
nduo-3	AGTGTTTACGCTAGTTTTATTATTTGCTTT	CAAAACCACATTCAAACGCTCT
nduo-5	TTGGGCCTAGGGCTTAGGTT	CGTCCATCTTGTTGTCCAAATG
his-18	GAACTCTGTACGGATTCGGAG	CACATAAATTGGGATTTTTGAATTGTG
his-60	AGAACTCTGTACGGATTCGGAG	GATTTTGGATATTTGTGGCCCTAAAG
his-5	ACGCCAAGAGAAAGACTGTC	CGAGAGATAAAATTATCCTCCGAATC
his-64	CGTCGTCTACGCTCTGAAG	TATTTGGTTTGTATGAAAACAGGAAAG
hsp-6	AACAGATCGTTATCCAATCTTCTGG	CCTCGACGAGCTCCTTTCTC
hsp-60	AACTAAGGTGGTTCGCACAGC	CCAACTGCTTCTTCCTTTGGA
timm-23	GCGCTAGGACATATCGGATGG	TCCATGGTTTTCCGACCATT

DNA damage assay		
Long-amplicon	TGGCTGGAACGAACCGAACCAT	GGCGGTTGTGGAGTGTGGGAAG
Short-amplicon	GCCGACTGGAAGAACTTGTC	GCGGAGATCACCTTCCAGTA
Relative mitochondrial DNA copy number		
Mitochondrial template	AGCGTCATTTATTGGGAAGAAGAC	AAGCTTGTGCTAATCCCATAAATGT
Nuclear template	GCCGACTGGAAGAACTTGTC	GCGGAGATCACCTTCCAGTA
Chromatin immunoprecipitation–quantitative PCR		
mtDNA: 18–103	AAATATAGCATTTGGGTTGCTAAGA	ACCCCATCATTGTAAGTGATACA
mtDNA: 336–437	TTTGTTAAGAATGTTATATTTTTCTCC	AAAAACCTCTTAAACCTAAATATCTTC
mtDNA: 447–647	TTTTAAATTTTTCAGGTGCTTTACG	AGAAATTAGAATAAAAATTAAACGTTGTC
mtDNA: 2,317–2,400	TGAACTTAACCGGGCGCCAT	GCTACTCTGGCAAACTCCACATT
mtDNA: 2,577–2,777	TGTTTTTACGCAGTTATTTTT	AATACTCCTACTAACCTATTAAGAAA
mtDNA: 2,815–2,909	TTTTAACTTGTTGTTTTGGAGGTT	CACGCTACAGCAGCATAAACA
mtDNA: 4,079–4,168	TTGAGGGAAATTTTTAAATATGATAGA	TCAAAATCTAAATGCCAATACAGA
mtDNA: 4,927–5,127	TCCAATTTGAGGGCCAACTA	AATGTTGCCCCTGTAACACC
mtDNA: 5,977–6,177	CCAGTACACGAGTTGGGAGAG	TCTGTGATGTGCTCAAGTTACTG
mtDNA: 6,502–6,622	GCTTTGTTAGAATTTCTTTTTATCTCC	AAATAGTCCGCCTCATGAAAAA
mtDNA: 7,267–7,467	TGCTTATGCTAGCACACGGTTA	ACGCCTCCCAGATGTATGAT
mtDNA: 7,389–7,502	ATCATACATCTGGGAGGCGTA	AAGGTGGTACACCCCTATTTGA
mtDNA: 8,464–8,545	CGGTTTTAGCAGGGGCTATT	TTACCTCCAGTTCTTGGATCA
mtDNA: 10,062–10,262	CATGCTTGGGCATTAAATTCT	CACAAATCTCTGAACATTGACCA
mtDNA: 10,760–10,830	AGAACTTGAAGTCTTGATCAAATG	ATAGGGCAGAAGCCAGCTTTA
mtDNA: 12,377–12,577	AGGTGGTAGCCTTGAGGACACT	ACCTAAGCCCTAGGCCCAAAGTA
mtDNA: 12,947–13,016	TTTTAATCTTCTTAACATCCCAAGAC	AAATAAAAATACTAGAGGGCCAAAAA

Contributions

Figure 18A: *his-67* was originally identified as a suppressor of HSB-1-associated longevity in an RNAi-based genetic screen performed by Carol Mousigian.

Figures 25, 26 and 27A: Bioinformatic analysis of MNase-Seq data was performed by Zhaoyu Pan, 4S Inc. The plots were generated from the analyzed data by the author.

Figure 33C: Life span experiments for intestine-specific H4 RNAi were performed by Dr. Tsui-Ting Ching.

Figure 34: Biochemical and ChIP-qPCR studies using isolated mitochondria were performed by Dr. Chung-Yi Liang.

Chapter 4. Conclusions

HSF-1 acquires an altered transcriptional activation status in the absence of HSB-1 regulation

Heat shock factor 1 (HSF-1) is a multifunctional transcription factor that is at the nexus of numerous signaling pathways (Åkerfelt et al., 2010; Gomez-Pastor et al., 2018; Li et al., 2017; Vihervaara and Sistonen, 2014). Previous studies have shown that HSF-1 drives different transcriptional programs in organisms depending on the developmental, physiological or metabolic context (Douglas et al., 2015; GuhaThakurta et al., 2002; Jedlicka et al., 1997; Kim et al., 2016; Li et al., 2016; Mendillo et al., 2012; Metchat et al., 2009; Oda et al., 2018; Ooi and Prahlad, 2017). How the HSF-1 transcription factor acquires different roles depending on cellular needs remains less understood. It has been proposed that in the context of stress response, HSF-1 activity is regulated via sequestration of the HSF-1 protein by chaperone machineries (Takaki and Nakai, 2016). Large heat shock proteins (HSPs) such as HSP70 and HSP90, which are stress-induced transcriptional targets of HSF-1, physically bind to the HSF-1 protein and limit its transcriptional activation potential in non-stressed conditions (Shi et al., 1998; Zou et al., 1998). Hence, HSF-1 controls its own activation status via a negative feedback loop that involves the binding and inactivation of HSF1 by its transcriptional targets. In addition, the TRiC/CCT chaperonin complex, another component of the cellular chaperone machinery, has also been shown to physically sequester HSF-1 protein in an

inactivated state (Guisbert et al., 2013; Neef et al., 2014). In this study, we have investigated the role of heat shock factor binding protein 1 (HSB-1), a small 9 kDa protein that binds to the trimerization domain of HSF-1 and forms a multiprotein inhibitory complex termed as DDL-1-containing HSF-1 inhibitory complex (DHIC) (Chiang et al., 2012; Satyal et al., 1998). The binding of HSP90 to HSF-1 is reversed in the presence of stress stimuli, indicating that the large chaperone complexes regulate the HSF-1-induced transcription of stress response genes (Zou et al., 1998). In contrast, the amount of HSF-1 protein sequestered in the HSB-1-containing DHIC is not altered in the presence of heat stress (Chiang et al., 2012). This suggests that HSB-1 regulates HSF-1 activity in a context distinct from stress response. Since genetic ablation of HSB-1 induces an *hsf-1*-dependent life span extension in worms (Figure 7A and Table 2) (Chiang et al., 2012), we speculated that HSB-1 might be a selective regulator of HSF-1-induced activation of longevity-promoting genes in *C. elegans*.

Unlike the previously reported *hsf-1* overexpression models that extend *C. elegans* life span (Baird et al., 2014; Hsu et al., 2003; Morley and Morimoto, 2004), HSB-1 inhibition promotes longevity in worms without altering the mRNA or protein levels of HSF-1 (Figures 7C and 7D). Our EMSA analyses indicate that in *hsb-1(-)* animals, the endogenous HSF-1 protein acquires increased binding ability to its genomic target sequences, termed as heat shock elements (HSEs) (Figure 8A). However, it remains elusive how in the absence of HSB-1 regulation, HSF-1 acquires increased HSE-binding ability without involving an increase in HSF-1 protein levels, similar to that observed during heat stress (Figures 7D and 8A) (Chiang et al., 2012). Based on previous studies that have focused on the role of diverse post-translational

modifications (PTMs) that regulate the activation status of the HSF-1 protein (Anckar and Sistonen, 2011; Gomez-Pastor et al., 2018), it can be presumed that the increased DNA binding activity of HSF-1 in *hsb-1(-)* animals might be due to acquisition of a certain combination of PTMs. In presence of heat stress, the HSF-1 protein is hyperphosphorylated at several sites (Chiang et al., 2012; Guettouche et al., 2005), though phosphorylation can have either stimulatory or inhibitory effect on HSF-1 activity depending on the amino acid residues that are phosphorylated (Anckar and Sistonen, 2011; Gomez-Pastor et al., 2018). Interestingly, HSF-1 acquires PTMs even in the context of longevity regulation (Chiang et al., 2012), though the identity of these modifications is unknown. In *C. elegans*, inhibition of the insulin/IGF-1-like signaling pathway induces an *hsf-1*-dependent life span extension (Hsu et al., 2003; Morley and Morimoto, 2004). Moreover, in insulin/IGF-1-like signaling mutant *daf-2(-)* worms, the HSF-1 protein shows strong nuclear localization, acquisition of PTMs and increased DNA binding even in non-stressed conditions (Chiang et al., 2012). It remains to be determined if the PTMs acquired by the HSF-1 protein in *daf-2(-)* worms are identical to that in *hsb-1(-)* worms, since the longevity of both these strains is mediated via HSF-1 activation (Chiang et al., 2012). Identification of the HSF-1 amino acid residues that are modified in the context of longevity regulation will further our understanding of how site-specific modulators of the HSF-1 protein can be designed to extend organismal life span.

HSF-1 overexpression and HSB-1 inhibition induce overlapping transcriptional changes in *C. elegans*

Increasing the gene dosage of *hsf-1* is sufficient to extend life span in *C. elegans* (Hsu et al., 2003; Morley and Morimoto, 2004). The life span extension in *hsf-1* overexpressing animals was previously attributed to the increased expression of small HSPs that are direct transcriptional targets of HSF-1 (Hsu et al., 2003). However, recent evidences have suggested that overexpression of a truncated form of HSF-1 protein also extends life span in worms, but it does not alter the ability of these animals to mount stress-induced transcriptional activation of HSPs (Baird et al., 2014). In this study, we performed a comprehensive transcriptome-wide comparison of gene expression changes associated with increased HSF-1 activity in *C. elegans*. We used two parallel approaches to enhance HSF-1 activity, increase in the gene dosage of *hsf-1* and genetic ablation of *hsb-1*, both of which extend life span of worms in an *hsf-1*-dependent manner (Figure 7A and Table 2) (Chiang et al., 2012; Hsu et al., 2003). Overall, our transcriptome-level comparison using RNA-Seq showed broadly distinct global transcriptional profiles in the *hsb-1(-)* and *hsf-1* overexpression strains (Figures 10A–D). Overexpression of HSF-1 induced upregulation of more than 1,500 transcripts in *C. elegans* (Figure 11B). In contrast, genetic ablation of *hsb-1* affected the expression of a much smaller number of genes, while still producing a robust extension of organismal life span (Figures 7A and 11A, and Table 2). Importantly, roughly half of the differentially expressed transcriptome in *hsb-1(-)* animals overlapped with that in *hsf-1* overexpressing animals (Figure 11A). This indicates that HSB-1 potentially regulates a subset of HSF-1 target genes that are essential for life span determination in *C.*

elegans. We speculate that the 191 genes that are differentially expressed in the same direction in both *hsb-1(-)* and *hsf-1* overexpressing animals might be involved in HSF-1-dependent life span extension in these strains (Figures 14A–C). Further characterization of epistatic interactions is needed to identify the genes in this category that are required for the longevity phenotype of these strains. Moreover, the 263 genes that are differentially regulated in *hsb-1(-)* animals alone, but not in the *hsf-1* overexpression strain (Figure 11A), might also shed light on HSF-1-dependent or independent targets that are unique components of the HSB-1-associated longevity pathway in worms. Previous studies have identified thousands of genes that are direct or indirect transcriptional targets of heat shock factor in multiple organisms (Brunquell et al., 2016; Li et al., 2016; Mendillo et al., 2012). However, most of these genes are seemingly not involved in HSF-1-dependent regulation of longevity (Brunquell et al., 2016). Our study has identified how the modulation of a handful of HSF-1 targets via inhibition of HSB-1 can induce robust life span extension in animals without affecting the numerous other biological pathways that are regulated by HSF-1 (Figures 7A, 11A and 12A, and Table 2).

It will be interesting to determine if any specific DNA motifs are present in the promoter regions of genes that are differentially expressed in *hsb-1(-)* and/or *hsf-1* overexpressing worms. Previous studies have shown that the canonical HSE sequence repeats are present only in the promoter regions of HSF-1 target genes that are upregulated during heat stress in worms (GuhaThakurta et al., 2002). In contrast, there are numerous other genes that are direct transcriptional targets of HSF-1 in other physiological contexts, but their promoter architecture is distinct from that of stress

response targets of HSF-1. For example, not all genes that are upregulated by HSF-1 during cancer progression have HSE sequences in their promoter regions (Mendillo et al., 2012). In addition, HSF-1 cooperates with other transcription factors such as E2F in *C. elegans* for transcriptional regulation of genes during animal development (Li et al., 2016). These developmental targets of HSF-1 also do not have the consensus HSE in their promoter sequences, but instead contain a degenerate HSE adjacent to an E2F-binding motif (Li et al., 2016). It is possible that for the regulation of longevity-promoting genes, HSF-1 cooperates with other transcription factors to bind to DNA and drive the transcription of these genes. Previous studies have indicated possible association of HSF-1 with the worm FOXO-homolog DAF-16 to co-regulate the transcription of genes that are involved in longevity regulation (Hsu et al., 2003). Our study has also shown the requirement of DAF-16/FOXO for producing the longevity-promoting effects associated with HSB-1 inhibition in worms (Figure 7B and Table 2). We further show transcriptional activation of numerous DAF-16 targets with known longevity-related functions in both *hsb-1(-)* and *hsf-1* overexpressing animals (Figures 13A and 13C). It remains to be determined whether the two transcriptional factors, HSF-1 and DAF-16, co-occupy the promoter sequences of these genes to collectively regulate their expression. In addition, our RNAi-based genetic screen identified SPTF-3, a SP1 family transcription factor, as a suppressor of HSB-1-associated longevity in worms (Figure 15C and Table 2). It is possible that SPTF-3 and HSF-1 co-occupy certain regulatory genomic sequences that mediate gene expression changes associated with life span extension in the *hsb-1(-)* strain. Analysis of the transcriptome of SPTF-3-depleted *hsb-1(-)* animals will reveal

genes that are regulated by the HSB-1/HSF-1 pathway in an SPTF-3-dependent manner.

Histone H4 has an essential role in mediating the pro-longevity effects of HSF-1 activation and mitochondrial inhibition

Previous studies have identified change in histone levels as a hallmark of replicative aging in yeast and murine muscle stem cells (Feser et al., 2010; Hu et al., 2014; Liu et al., 2013). Given that histone proteins have extremely long half-lives *in vivo* and their primary role is in the compaction of nuclear chromatin (Commerford et al., 1982), it is apparent that depletion of histones will result in improper packaging of newly-synthesized DNA in dividing cells. Nonetheless, it is interesting that altering the levels of histone H4 protein also influences life span in *C. elegans*, an organism in which all the somatic tissues in the adult animal are post-mitotic. RNAi-mediated knockdown of histone H4 does not have a major effect on the life span of wild-type worms, but it completely suppresses the life span extension caused by HSB-1 inhibition, HSF-1 overexpression or mitochondrial inhibition (Figures 18A, 18C, 18D, 19A and 19D, and Table 6). As evident from our immunoblot analyses, the protein levels of other core histones also decline significantly when animals are subjected to H4 knockdown (Figures 18F and 18G). Hence, it is presumable that the effect of H4 RNAi on longevity of *hsb-1(-)* worms might be due to reduced levels of all core histones, and not just that of H4. However, the DNA sequences of the *C. elegans* genes encoding for histones H3, H2A and H2B show minimal similarity to that of the RNAi clones used to deplete H4-coding transcripts. Hence, it is unlikely that the H4 RNAi clones directly target the

expression of other histones. We speculate that the decrease in protein levels of the other core histones is most likely due to the cell's intrinsic response to reduction in levels of H4, as all the four core histone proteins need to be maintained in stoichiometric proportions (Singh et al., 2009). Hence, the effect of H4 RNAi on longevity of *hsb-1(-)* worms can still be attributed to a cellular response to H4 depletion in these animals, which comprises a compensatory decrease in the levels of H3, H2A and H2B proteins.

Our study does not establish a mechanistic understanding of why the longevity induced via mitochondrial inhibition in *isp-1(-)* animals is completely suppressed via depletion of H4 (Figure 19D and Table 6). Interestingly, a recent study has shown that inhibition of nuclear-encoded components of the mitochondrial electron transport chain (ETC) results in increased histone levels in worms (Matilainen et al., 2017). The study further showed that HSF-1 protein is activated in response to reduction in levels of nuclear-encoded mitochondrial ETC components (Matilainen et al., 2017). Mitochondrial ETC complexes are assembled using components encoded by both the mitochondrial and nuclear genomes. Any disruption to this stoichiometry can result in an imbalance of proteins that are required to assemble the ETC complexes. However, it is less understood how the gene expression of ETC components is coordinated across the nuclear and mitochondrial genomes to maintain the cellular levels of these proteins in the desired stoichiometric ratio. Based on our own results and the other recent findings (Matilainen et al., 2017), we hypothesize that HSF-1-induced increase in histone levels acts as a mediator between the mitochondrial and nuclear genomes during mitonuclear protein imbalance. Reduced expression of nuclear-encoded mitochondrial ETC components results in release of stress signals from the mitochondria (Durieux et al.,

2011; Merkwirth et al., 2016; Tian et al., 2016; Zhang et al., 2018). This potentially leads to HSF-1 activation and an increase in histone levels, as shown recently (Matilainen et al., 2017). Based on our own findings, we postulate that the excess H4 protein translocates to mitochondria, binds to mitochondrial DNA (mtDNA) and reduces expression of mtDNA-encoded ETC components. This results in reinstatement of the stoichiometric balance of ETC components synthesized by the nuclear and mitochondrial genomes and in the process, extends organismal life span due to the pro-longevity effects of the mitochondrial stress signals. Previous studies have indicated that mitonuclear protein imbalance is an evolutionarily conserved longevity mechanism across many species (Houtkooper et al., 2013). However, elaborate experimental design will be needed to validate this proposed model of nuclear-mitochondrial communication via HSF-1 signaling.

Increased H4 levels in somatic tissues during development is essential for HSB-1-associated longevity

Similar to replicative aging in yeast (Hu et al., 2014), protein levels of all core histones decline with age in somatic tissues of worms (Figure 22A). In *C.* elegans, this induces increased susceptibility to DNA damage and loss of silencing of repetitive genomic elements with age (Figures 22C and 22E). *hsb-1(-)* animals are partially protected from these age-associated detrimental effects of histone loss in worms (Figures 22D and 22E). We further show that HSB-1 inhibition induces increase in levels of histones H3 and H4 in somatic tissues, albeit only during the development (Figures 21C and 21D). Moreover, the direct role of increased histone levels in promoting longevity is supported

by the evidence that H4 overexpression is sufficient to extend the life span of wild-type worms (Figure 20C and Table 6). Surprisingly, the somatic H4 levels in *hsb-1(-)* animals are not significantly different from that in wild-type worms during adulthood (Figure 21D). Moreover, HSB-1 inhibition also does not extenuate the age-associated decline of somatic histone levels (Figure 22F). Hence, it is intriguing how elevated histone levels during development partially alleviates the detrimental effects of histone loss during adulthood. We speculate that the higher levels of histones during larval stages result in improved overall packaging of chromatin in *hsb-1(-)* animals. Even though the somatic histone levels are no longer elevated during adulthood in *hsb-1(-)* worms (Figure 21D), some residual effects of elevated histone levels during development are partially retained in the chromatin of adult *hsb-1(-)* animals. This leads to improved silencing of repetitive genomic elements and better protection from UV-induced DNA damage (Figures 22D and 22E). It will be interesting to determine how chromatin organization in the somatic tissues of adult *hsb-1(-)* worms differs from that in wild-type animals. This will help to ascertain the chromatin state induced via HSB-1 inhibition that preserves genomic integrity in somatic tissues of *C. elegans*.

We determined the accessibility of native chromatin to micrococcal nuclease (MNase) in wild-type and *hsb-1(-)* animals. Our results suggest that the chromatin in *hsb-1(-)* worms has reduced overall MNase-accessibility compared to that in wild-type worms, and this could be reversed via knockdown of histone H4 (Figures 24A–F). Moreover, individual nucleosomes have better positioning and generate sharper peaks in the chromatin of *hsb-1(-)* animals in an H4-dependent manner (Figures 25A–F and Table 7). However, only a small number of nuclear genomic loci show a large and

significant change in MNase-accessibility of chromatin in *hsb-1(-)* animals (Figure 26 and Table 8). Since the loss of integrity of repetitive elements in the genome has been identified as an epigenetic hallmark of aging (Booth and Brunet, 2016; O'Sullivan and Karlseder, 2012; Pal and Tyler, 2016; Sen et al., 2016), it will be interesting to determine if increased compaction of certain repetitive regions in the chromatin of *hsb-1(-)* worms contributes to their longevity phenotype. Surprisingly, H4 RNAi did not result in a large-scale decrease in MNase-protection of most of the genomic regions in worms (Figure 26 and Table 9). We speculate that our H4 knockdown strategy is not strong enough to counteract the constitutive transcription of histone genes during *C. elegans* development to the extent that it can massively alter genome-wide chromatin compaction at most loci (Keall et al., 2007). In addition, large-scale changes in the organization of nuclear chromatin during developmental stages might be detrimental for the survival of worms (Pettitt et al., 2002). Hence, we presume that the knockdown achieved via *his-38* RNAi in our study is not strong enough to cause major disruptions to the developmental and metabolic programs in *C. elegans*, but yet is sufficient to reverse the increased MNase-protection due to elevated histone levels in *hsb-1(-)* animals (Figures 24A, 24B and 25A–F). Follow-up studies are needed to investigate how increased chromatin compaction of specific regions in the genome induced via HSB-1 inhibition influences the expression of genes in and around those genomic loci. Furthermore, it will be interesting to determine if improved packaging of telomeres and rRNA gene repeats in *hsb-1(-)* animals is associated with improved stability of these repetitive genomic regions (Table 8).

H4 protein regulates mtDNA compaction, expression of mtDNA-encoded genes and mitochondrial function

One of the most intriguing observations in this study is the H4-dependent increase in MNase-protection of mtDNA in *hsb-1(-)* animals (Figure 27A and Table 8). To our knowledge, this is the first evidence of a core nucleosomal protein directly regulating the accessibility of the mitochondrial genome. Though mitochondrial transcription factor A (TFAM) is the major mtDNA packaging protein in the mitochondrial nucleoid complexes (Gilkerson et al., 2013; Kukat et al., 2015; Lee and Han, 2017), recent studies have also identified the presence of several predominantly nuclear-localized transcription factors and other regulatory proteins in the mitochondria (Barshad et al., 2018; Mercer et al., 2011). In the ENCODE project, the sequencing reads aligning to the mitochondrial genome have been traditionally 'blacklisted' (i.e. discarded prior to analysis) from MNase-Seq, DNase-Seq and ATAC-Seq datasets. Two recently published studies involving DNase I footprinting and ATAC-Seq have identified a potential 'chromatin-like' organization of the mitochondrial genome that is responsive to change in physiological conditions (Blumberg et al., 2018; Marom et al., 2019). This indicates that our knowledge of factors that regulate the dynamic structure of mitochondrial nucleoids remains far from complete. A previous study has shown *in vitro* binding of histones to the D-loop region of mtDNA (Choi et al., 2011). In this study, we have shown that H4 RNAi completely suppresses the increased MNase-protection of the D-loop region of mtDNA in *hsb-1(-)* animals (Figure 27A). Since D-loop is the only non-coding regulatory region in the mitochondrial genome (Figure 6), it will be interesting to determine how

accessibility of this region to different DNA-binding proteins affects the expression of mtDNA-encoded genes.

Interestingly, the most prominent H4-dependent mtDNA peak in our *hsb-1(-)* MNase-Seq data is associated with reduced transcription of genes encoded by that region of the mitochondrial genome (Figures 27A and 28A). In *hsb-1(-)* animals, we observe an increased MNase-protection of the mtDNA locus that encodes for the *nduo-4* gene (Figure 27A). The expression of three *ctc* genes neighboring this mtDNA region, *ctc-1*, *ctc-2* and *ctc-3*, is significantly reduced in *hsb-1(-)* worms in an H4-dependent manner (Figures 28A–C). This suggests a direct effect of mtDNA accessibility on gene expression from that locus of the mitochondrial genome, indicating presence of features similar to that in the nuclear chromatin (Hübner et al., 2013). The *ctc* genes encode the three key components of the catalytic core of complex IV (also known as cytochrome *c* oxidase) of mitochondrial ETC. Since complex IV catalyzes the conversion of molecular oxygen to water in the respiration process, we observe reduced maximal and spare respiratory capacities in *hsb-1(-)* animals (Figures 29B and 29C). However, basal mitochondrial oxygen consumption rate (OCR) is not affected in these animals (Figure 29A). We speculate that even though *ctc* gene expression is significantly reduced in *hsb-1(-)* worms (Figure 28A), the slightly diminished activity of ETC complex IV in these animals is sufficient to provide for the basal respiratory demands of the organism (Figure 29A). However, these weakened ETC complexes collectively fall short of the metabolic demand when the *hsb-1(-)* animals are pushed to their upper limit of respiratory capacity (Figures 29B and 29C). Interestingly, H4 overexpression in wild-type worms is sufficient to significantly suppress their basal OCR (Figure 30D). It

remains to be determined whether this phenotype is solely due to migration of the excess histones to mitochondria and inhibition of gene expression from mtDNA. Alternatively, it is possible that global transcriptional suppression due to excess packaging of the nuclear chromatin also indirectly contributes to the reduced respiration in the H4-overexpressing animals. In the future, we plan to generate stable *C. elegans* lines for H4 overexpression and study how the compaction of both the nuclear and mitochondrial genomes is affected in these animals.

We show that life span extension associated with HSB-1 inhibition and H4 overexpression is at least partially suppressed via knockdown of *ubl-5*, a ubiquitin-like protein required for activation of the mitochondrial unfolded protein response (UPR^{mt}) (Figures 31A and 31B, and Table 6). UPR^{mt} is a key mediator of life span extension achieved via inhibition of nuclear-encoded components of the mitochondrial ETC machinery (Durieux et al., 2011; Houtkooper et al., 2013; Merkwirth et al., 2016). This strongly suggests the convergence of H4-mediated longevity-promoting mechanisms in the *hsb-1(-)* animals to the well-studied mitochondrial longevity pathway in *C. elegans*. Recent studies have also provided evidence for crosstalk between mitochondrial perturbation and HSF-1 activation in worms (Labbadia et al., 2017; Matilainen et al., 2017). Interestingly, life span extension due to *hsf-1* overexpression was previously shown to not interact with the UPR^{mt}-dependent mitochondrial longevity pathway (Merkwirth et al., 2016). However, the experiments reported in this study were performed at a different environmental temperature compared to our study. While Merkwirth et al. performed their life span analyses at 20°C, the experiments reported in Chapter 3 of this dissertation were performed at 25°C. Multiple studies have shown that

depending on the environmental temperature, the same genetic manipulation can trigger different downstream signaling pathways to regulate organismal longevity (Horikawa et al., 2015; Miller et al., 2017; Zhang et al., 2015). It remains to be determined whether HSF-1 overexpression in worms induces activation of the UPR^{mt} pathway to promote longevity at 25°C. Moreover, unlike in worms subjected to inhibition of nuclear-encoded mitochondrial ETC components, HSB-1 inhibition in worms does not result in increased expression of all UPR^{mt} genes (Figure 31C). Nonetheless, there is lack of agreement in the field regarding genes that are transcriptionally upregulated by UPR^{mt} activation in *C. elegans*. While one study has shown a 1.5-fold to 2-fold increase in transcript levels of *hsp-6*, *hsp-60* and *timm-23* after RNAi-mediated knockdown of the nuclear genome-encoded ETC complex IV constituent *cco-1* in wild-type worms (Bennett et al., 2014), others have failed to detect any statistically significant change in expression of one or more of these genes in similar *cco-1(RNAi)* conditions (Matilainen et al., 2017; Merkwirth et al., 2016). Since it is relatively easier to manipulate the expression of nuclear genes via RNAi or mutagenesis screens, the stress signaling pathways activated in response to inhibition of nuclear-encoded mitochondrial ETC components are well characterized (Shpilka and Haynes, 2017). Developing tools that can modulate expression of mtDNA-encoded genes will shed new light on pathways that are activated in response to mitonuclear protein imbalance arising from anomalies in the mitochondrial genome.

Finally, we show the presence of histone H4 in the mitochondria of *C. elegans* using immunostaining and biochemical methods (Figures 32A, 33A and 34A). Histone H4 localizes to mitochondria in the worm intestine (Figures 32A and 33A), a tissue that

has a key role in mediating the longevity-promoting effects associated with HSF-1 activation and mitochondrial inhibition (Douglas et al., 2015; Durieux et al., 2011; Zhang et al., 2018). Moreover, tissue-specific knockdown of H4 in the intestine is sufficient to completely diminish the life span phenotype associated with HSB-1 inhibition (Figure 33C and Table 6). This can be attributed to two potential factors: (i) H4 protein level is elevated only in the intestinal tissue of *hsb-1(-)* animals and/or (ii) HSB-1 inhibition results in translocation of H4 to the mitochondria only in the intestine. Our biochemical analysis has confirmed that higher levels of total H4 protein results in increased levels of mitochondrially-localized H4 (Figure 34B). Further studies are needed to identify underlying mechanisms that regulate the context-dependent mitochondrial translocation of histones in animals. Using a proteinase K protection assay, we convincingly showed that histones H3 and H4 are enclosed within the mitochondria and are not present as impurities in our mitochondrial preparations (Figure 34A). In addition, we show the binding of histone H4 to several mtDNA loci in *C. elegans* using chromatin immunoprecipitation (Figure 34C). However, the binding pattern of H4 to mtDNA does not exactly correlate with the MNase-accessibility of the mitochondrial genome in these animals (Figures 27A and 34C). Hence, H4 is potentially one of the several uncharacterized mitochondrially-localized proteins that bind to mtDNA to regulate its accessibility *in vivo* (Barshad et al., 2018). Here we show that HSB-1 inhibition alters the binding of histone H4 to at least one mtDNA locus (Figure 34C). Future studies are needed to elucidate how H4 interacts with other proteins in the mitochondrial nucleoid to collectively regulate gene expression from the mitochondrial genome in a context-dependent manner.

Final remarks: Novel and intriguing roles of HSB-1/HSF-1 signaling pathway in longevity regulation

The transcription factor HSF-1 takes up different roles in animals depending on the physiological context (Åkerfelt et al., 2010; Gomez-Pastor et al., 2018; Li et al., 2017; Vihervaara and Sistonen, 2014). The role of HSF-1 in promoting organismal longevity was first suggested over a decade ago (Hsu et al., 2003; Morley and Morimoto, 2004). However, our knowledge of the role of HSF-1 in longevity regulation has so far been primarily restricted to its interactions with the insulin/IGF-1-like signaling pathway and the regulators of cytoskeletal integrity (Baird et al., 2014; Chiang et al., 2012; Douglas et al., 2015; Hsu et al., 2003; Morley and Morimoto, 2004). In Chapter 2, we have identified the transcriptome-level changes associated with HSF-1 overexpression and HSB-1 inhibition, two distinct genetic manipulations that promote HSF-1-induced longevity in *C. elegans*. Using the *hsb-1* null model, we show that life span extension in worms can be achieved via change in expression of a small subset of the entire HSF-1-regulated transcriptome. This indicates the possibility of selectively manipulating HSF1 function in mammals via inhibiting HSBP1, one of its evolutionarily conserved negative regulators, to improve the quality of health without introducing the detrimental effects of constitutive HSF-1 activation (Dai et al., 2007; Mendillo et al., 2012).

In Chapter 3, we show the interaction of HSB-1/HSF-1 signaling with the UPR^{mt}-associated mitochondrial longevity pathway via changes in levels of the core histone protein H4. Our findings suggest that increased HSF-1 activity in worms elevates the protein levels of histone H4, which can directly regulate gene expression from the

mitochondrial genome in worms. We further show that increase in levels of histone H4 is sufficient to alter mitochondrial function and thus promote longevity at the organismal level. This provides strong evidence for a previously undiscovered role of histone proteins other than their known function in compaction of the nuclear chromatin (Henikoff and Smith, 2015). In summary, our results show a novel mechanism of inter-organelle communication between the nuclear and mitochondrial genomes, and how it acts as a major determinant of organismal survival. Overall, the findings of this study will potentially guide the design of interventions that specifically target components of the HSB-1/HSF-1 signaling network to improve the quality of health in more complex metazoans.

References

Abane, R., and Mezger, V. (2010). Roles of heat shock factors in gametogenesis and development. FEBS J. *277*, 4150–4172.

Åkerfelt, M., Morimoto, R.I., and Sistonen, L. (2010). Heat shock factors: integrators of cell stress, development and lifespan. Nat. Rev. Mol. Cell Biol. *11*, 545–555.

Anckar, J., and Sistonen, L. (2011). Regulation of HSF1 function in the heat stress response: implications in aging and disease. Annu. Rev. Biochem. *80*, 1089–1115.

Anders, S., Pyl, P.T., and Huber, W. (2015). HTSeq–a Python framework to work with high-throughput sequencing data. Bioinformatics *31*, 166–169.

Apfeld, J., O'Connor, G., McDonagh, T., DiStefano, P.S., and Elixir, R.C. (2004). The AMP-activated protein kinase AAK-2 links energy levels and insulin-like signals to lifespan in *C. elegans*. Genes Dev. *18*, 3004–3009.

Arantes-Oliveira, N., Apfeld, J., Dillin, A., and Kenyon, C. (2002). Regulation of life-span by germ-line stem cells in *Caenorhabditis elegans*. Science *295*, 502–505.

Arora, N., Alsaied, O., Dauer, P., Majumder, K., Modi, S., Giri, B., Dudeja, V., Banerjee, S., Von Hoff, D., and Saluja, A. (2017). Downregulation of Sp1 by Minnelide leads to decrease in HSP70 and decrease in tumor burden of gastric cancer. PLoS One *12*, e0171827.

Baird, N.A., Douglas, P.M., Simic, M.S., Grant, A.R., Moresco, J.J., Wolff, S.C., Yates, J.R., Manning, G., and Dillin, A. (2014). HSF-1-mediated cytoskeletal integrity determines thermotolerance and life span. Science *346*, 360–363.

Baker, D.J., Childs, B.G., Durik, M., Wijers, M.E., Sieben, C.J., Zhong, J., A. Saltness, R., Jeganathan, K.B., Verzosa, G.C., Pezeshki, A., et al. (2016). Naturally occurring p16Ink4a-positive cells shorten healthy lifespan. Nature *530*, 184–189.

Balan, V., Miller, G.S., Kaplun, L., Balan, K., Chong, Z.Z., Li, F., Kaplun, A., VanBerkum, M.F.A., Arking, R., Freeman, D.C., et al. (2008). Life span extension and neuronal cell protection by *Drosophila* nicotinamidase. J. Biol. Chem. *283*, 27810–27819.

Banerjee, K.K., Ayyub, C., Ali, S.Z., Mandot, V., Prasad, N.G., and Kolthur-Seetharam, U. (2012). dSir2 in the Adult Fat Body, but Not in Muscles, Regulates Life Span in a Diet-Dependent Manner. Cell Rep. *2*, 1485–1491.

Barshad, G., Marom, S., Cohen, T., and Mishmar, D. (2018). Mitochondrial DNA Transcription and Its Regulation: An Evolutionary Perspective. Trends Genet. *34*, 682–692.

Beanan, M.J., and Strome, S. (1992). Characterization of a germ-line proliferation mutation in *C. elegans*. Development *116*, 755–766.

Benayoun, B. a., Pollina, E. a., and Brunet, A. (2015). Epigenetic regulation of ageing: linking environmental inputs to genomic stability. Nat. Rev. Mol. Cell Biol. *16*, 593–610.

Bennett, C.F., Vander Wende, H., Simko, M., Klum, S., Barfield, S., Choi, H., Pineda, V. V., and Kaeberlein, M. (2014). Activation of the mitochondrial unfolded protein response does not predict longevity in *Caenorhabditis elegans*. Nat. Commun. *5*, 3483.

Bevilacqua, A., Fiorenza, M.T., and Mangia, F. (2000). A developmentally regulated GAGA box-binding factor and Sp1 are required for transcription of the *hsp70.1* gene at the onset of mouse zygotic genome activation. Development *127*, 1541–1551.

Bjedov, I., Toivonen, J.M., Kerr, F., Slack, C., Jacobson, J., Foley, A., and Partridge, L. (2010). Mechanisms of Life Span Extension by Rapamycin in the Fruit Fly *Drosophila melanogaster*. Cell Metab. *11*, 35–46.

Blüher, M., Kahn, B.B., and Kahn, C.R. (2003). Extended Longevity in Mice Lacking the Insulin Receptor in Adipose Tissue. Science *299*, 572–574.

Blumberg, A., Danko, C.G., Kundaje, A., and Mishmar, D. (2018). A common pattern of DNase I footprinting throughout the human mtDNA unveils clues for a chromatin-like organization. Genome Res. *28*, 1158–1168.

Bolger, A.M., Lohse, M., and Usadel, B. (2014). Trimmomatic: A flexible trimmer for Illumina sequence data. Bioinformatics *30*, 2114–2120.

Booth, L.N., and Brunet, A. (2016). The aging epigenome. Mol. Cell *62*, 728–744.

Brunquell, J., Morris, S., Lu, Y., Cheng, F., and Westerheide, S.D. (2016). The genome-wide role of HSF-1 in the regulation of gene expression in *Caenorhabditis elegans*. BMC Genomics *17*, 559.

Bua, E., Johnson, J., Herbst, A., Delong, B., McKenzie, D., Salamat, S., and Aiken, J.M. (2006). Mitochondrial DNA–Deletion Mutations Accumulate Intracellularly to Detrimental Levels in Aged Human Skeletal Muscle Fibers. Am. J. Hum. Genet. *79*, 469–480.

Budovskaya, Y. V., Wu, K., Southworth, L.K., Jiang, M., Tedesco, P., Johnson, T.E., and Kim, S.K. (2008). An *elt-3*/*elt-5*/*elt-6* GATA Transcription Circuit Guides Aging in *C. elegans*. Cell *134*, 291–303.

Burkewitz, K., Weir, H.J.M., and Mair, W.B. (2016). AMPK as a Pro-longevity Target. In AMP-Activated Protein Kinase, M.D. Cordero, and B. Viollet, eds. (Cham, Switzerland:

Springer International Publishing), pp. 227–256.

Burnett, C., Valentini, S., Cabreiro, F., Goss, M., Somogyvári, M., Piper, M.D., Hoddinott, M., Sutphin, G.L., Leko, V., McElwee, J.J., et al. (2011). Absence of effects of Sir2 overexpression on lifespan in *C. elegans* and *Drosophila*. Nature *477*, 482–485.

Cabreiro, F., Ackerman, D., Doonan, R., Araiz, C., Back, P., Papp, D., Braeckman, B.P., and Gems, D. (2011). Increased life span from overexpression of superoxide dismutase in *Caenorhabditis elegans* is not caused by decreased oxidative damage. Free Radic. Biol. Med. *51*, 1575–1582.

Chang, J., Wang, Y., Shao, L., Laberge, R.-M., Demaria, M., Campisi, J., Janakiraman, K., Sharpless, N.E., Ding, S., Feng, W., et al. (2016). Clearance of senescent cells by ABT263 rejuvenates aged hematopoietic stem cells in mice. Nat. Med. *22*, 78–83.

Chatterjee, A., Seyfferth, J., Lucci, J., Gilsbach, R., Preissl, S., Böttinger, L., Mårtensson, C.U., Panhale, A., Stehle, T., Kretz, O., et al. (2016). MOF Acetyl Transferase Regulates Transcription and Respiration in Mitochondria. Cell *167*, 722–738.

Chen, K., Xi, Y., Pan, X., Li, Z., Kaestner, K., Tyler, J., Dent, S., He, X., and Li, W. (2013). DANPOS: Dynamic analysis of nucleosome position and occupancy by sequencing. Genome Res. *23*, 341–351.

Chiang, W.C., Ching, T.T., Lee, H.C., Mousigian, C., and Hsu, A.L. (2012). HSF-1 regulators DDL-1/2 link insulin-like signaling to heat-shock responses and modulation of longevity. Cell *148*, 322–334.

Choi, Y.-S., Hoon Jeong, J., Min, H., Jung, H., Hwang, D., Lee, S.-W., and Kim Pak, Y. (2011). Shot-gun proteomic analysis of mitochondrial D-loop DNA binding proteins: identification of mitochondrial histones. Mol. Biosyst. *7*, 1523–1536.

Christians, E., Davis, A.A., Thomas, S.D., and Benjamin, I.J. (2000). Maternal effect of Hsf1 on reproductive success. Nature *407*, 693–694.

Clancy, D.J., Gems, D., Harshman, L.G., Oldham, S., Stocker, H., Hafen, E., Leevers, S.J., and Partridge, L. (2001). Extension of Life-Span by Loss of CHICO, a Drosophila Insulin Receptor Substrate Protein. Science *292*, 104–106.

Cohen, A.A. (2018). Aging across the tree of life: The importance of a comparative perspective for the use of animal models in aging. Biochim. Biophys. Acta - Mol. Basis Dis. *1864*, 2680–2689.

Cohen, E., Bieschke, J., Perciavalle, R.M., Kelly, J.W., and Dillin, A. (2006). Opposing activities protect against age-onset proteotoxicity. Science *313*, 1604–1610.

Commerford, S.L., Carsten, A.L., and Cronkite, E.P. (1982). Histone turnover within nonproliferating cells. Proc. Natl. Acad. Sci. *79*, 1163–1165.

Copeland, J.M., Cho, J., Lo, T., Hur, J.H., Bahadorani, S., Arabyan, T., Rabie, J., Soh, J., and Walker, D.W. (2009). Extension of *Drosophila* Life Span by RNAi of the Mitochondrial Respiratory Chain. Curr. Biol. *19*, 1591–1598.

Curran-Everett, D. (2013). Explorations in statistics: the analysis of ratios and normalized data. Adv. Physiol. Educ. *37*, 213–219.

Dai, C., Whitesell, L., Rogers, A.B., and Lindquist, S. (2007). Heat Shock Factor 1 Is a Powerful Multifaceted Modifier of Carcinogenesis. Cell *130*, 1005–1018.

Dai, S., Tang, Z., Cao, J., Zhou, W., Li, H., Sampson, S., and Dai, C. (2015). Suppression of the HSF1-mediated proteotoxic stress response by the metabolic stress sensor AMPK. EMBO J. *34*, 275–293.

Dang, W., Steffen, K.K., Perry, R., Dorsey, J.A., Johnson, F.B., Shilatifard, A., Kaeberlein, M., Kennedy, B.K., and Berger, S.L. (2009). Histone H4 lysine 16 acetylation regulates cellular lifespan. Nature *459*, 802–807.

Daniele, J.R., Heydari, K., Arriaga, E.A., and Dillin, A. (2016). Identification and Characterization of Mitochondrial Subtypes in *Caenorhabditis elegans* via Analysis of Individual Mitochondria by Flow Cytometry. Anal. Chem. *88*, 6309–6316.

Dell'Agnello, C., Leo, S., Agostino, A., Szabadkai, G., Tiveron, C.C., Zulian, A.A., Prelle, A., Roubertoux, P., Rizzuto, R., and Zeviani, M. (2007). Increased longevity and refractoriness to Ca^{2+}-dependent neurodegeneration in Surf1 knockout mice. Hum. Mol. Genet. *16*, 431–444.

Deniz, Ö., Flores, O., Aldea, M., Soler-López, M., and Orozco, M. (2016). Nucleosome architecture throughout the cell cycle. Sci. Rep. *6*, 19729.

Dillin, A., Hsu, A.-L., Arantes-Oliveira, N., Lehrer-Graiwer, J., Hsin, H., Fraser, A.G., Kamath, R.S., Ahringer, J., and Kenyon, C. (2002). Rates of behavior and aging specified by mitochondrial function during development. Science *298*, 2398–2401.

Dirks, R.P., van Geel, R., Hensen, S.M.M., van Genesen, S.T., and Lubsen, N.H. (2010). Manipulating Heat Shock Factor-1 in *Xenopus* Tadpoles: Neuronal Tissues Are Refractory to Exogenous Expression. PLoS One *5*, e10158.

Dobin, A., Davis, C.A., Schlesinger, F., Drenkow, J., Zaleski, C., Jha, S., Batut, P., Chaisson, M., and Gingeras, T.R. (2013). STAR: ultrafast universal RNA-seq aligner. Bioinformatics *29*, 15–21.

Douglas, P.M., Baird, N.A., Simic, M.S., Uhlein, S., McCormick, M.A., Wolff, S.C., Kennedy, B.K., and Dillin, A. (2015). Heterotypic Signals from Neural HSF-1 Separate Thermotolerance from Longevity. Cell Rep. *12*, 1196–1204.

Durieux, J., Wolff, S., and Dillin, A. (2011). The cell-non-autonomous nature of electron transport chain-mediated longevity. Cell *144*, 79–91.

Dyall, S.D., Brown, M.T., and Johnson, P.J. (2004). Ancient Invasions: From Endosymbionts to Organelles. Science *304*, 253–257.

Eisenberg, T., Knauer, H., Schauer, A., Büttner, S., Ruckenstuhl, C., Carmona-Gutierrez, D., Ring, J., Schroeder, S., Magnes, C., Antonacci, L., et al. (2009). Induction of autophagy by spermidine promotes longevity. Nat. Cell Biol. *11*, 1305–1314.

Epel, E.S., and Lithgow, G.J. (2014). Stress Biology and Aging Mechanisms: Toward Understanding the Deep Connection Between Adaptation to Stress and Longevity. Journals Gerontol. Ser. A Biol. Sci. Med. Sci. *69*, S10–S16.

Eroglu, B., Min, J.-N., Zhang, Y., Szurek, E., Moskophidis, D., Eroglu, A., and Mivechi, N.F. (2014). An essential role for heat shock transcription factor binding protein 1 (HSBP1) during early embryonic development. Dev. Biol. *386*, 448–460.

Escoubas, C.C., Silva-García, C.G., and Mair, W.B. (2017). Deregulation of CRTCs in Aging and Age-Related Disease Risk. Trends Genet. *33*, 303–321.

Fabrizio, P., Pozza, F., Pletcher, S.D., Gendron, C.M., and Longo, V.D. (2001). Regulation of longevity and stress resistance by Sch9 in yeast. Science *292*, 288–290.

Feng, J., Bussière, F., and Hekimi, S. (2001). Mitochondrial electron transport is a key determinant of life span in *Caenorhabditis elegans*. Dev. Cell *1*, 633–644.

Fernández, Á.F., Sebti, S., Wei, Y., Zou, Z., Shi, M., McMillan, K.L., He, C., Ting, T., Liu, Y., Chiang, W.-C., et al. (2018). Disruption of the beclin 1–BCL2 autophagy regulatory complex promotes longevity in mice. Nature *558*, 136–140.

Feser, J., Truong, D., Das, C., Carson, J.J., Kieft, J., Harkness, T., and Tyler, J.K. (2010). Elevated histone expression promotes life span extension. Mol. Cell *39*, 724–735.

Flavel, M.R., Mechler, A., Shahmiri, M., Mathews, E.R., Franks, A.E., Chen, W., Zanker, D., Xian, B., Gao, S., Luo, J., et al. (2018). Growth of *Caenorhabditis elegans* in Defined Media Is Dependent on Presence of Particulate Matter. G3 Genes, Genomes, Genet. *8*, 567–575.

Fontana, L., and Partridge, L. (2015). Promoting health and longevity through diet: From model organisms to humans. Cell *161*, 106–118.

Fontana, L., Partridge, L., and Longo, V.D. (2010). Extending Healthy Life Span–From Yeast to Humans. Science *328*, 321–326.

Freese, N.H., Norris, D.C., and Loraine, A.E. (2016). Integrated genome browser: Visual analytics platform for genomics. Bioinformatics *32*, 2089–2095.

Fujimoto, M., Takaki, E., Hayashi, T., Kitaura, Y., Tanaka, Y., Inouye, S., and Nakai, A. (2005). Active HSF1 significantly suppresses polyglutamine aggregate formation in

cellular and mouse models. J. Biol. Chem. *280*, 34908–34916.

Ghazi, A., Henis-Korenblit, S., and Kenyon, C. (2007). Regulation of *Caenorhabditis elegans* lifespan by a proteasomal E3 ligase complex. Proc. Natl. Acad. Sci. *104*, 5947–5952.

Giannakou, M.E., Goss, M., Jünger, M.A., Hafen, E., Leevers, S.J., and Partridge, L. (2004). Long-lived Drosophila with over-expressed dFOXO in adult fat body. Science *305*, 361.

Gilkerson, R., Bravo, L., Garcia, I., Gaytan, N., Herrera, A., Maldonado, A., and Quintanilla, B. (2013). The mitochondrial nucleoid: integrating mitochondrial DNA into cellular homeostasis. Cold Spring Harb. Perspect. Biol. *5*, a011080.

Gomez-Pastor, R., Burchfiel, E.T., and Thiele, D.J. (2018). Regulation of heat shock transcription factors and their roles in physiology and disease. Nat. Rev. Mol. Cell Biol. *19*, 4–19.

Gonzalez-Hunt, C.P., Rooney, J.P., Ryde, I.T., Anbalagan, C., Joglekar, R., and Meyer, J.N. (2016). PCR-based analysis of mitochondrial DNA copy number, mitochondrial DNA damage, and nuclear DNA damage. In Current Protocols in Toxicology, (Hoboken, NJ, USA: John Wiley & Sons, Inc.), pp. 20.11.1-20.11.25.

Goto, S. (2015). The Biological Mechanisms of Aging: A Historical and Critical Overview. In Aging Mechanisms: Longevity, Metabolism, and Brain Aging, N. Mori, and I. Mook-Jung, eds. (Tokyo: Springer Japan), pp. 3–27.

Greer, E.L., and Brunet, A. (2009). Different dietary restriction regimens extend lifespan by both independent and overlapping genetic pathways in *C. elegans*. Aging Cell *8*, 113–127.

Greer, E.L., Dowlatshahi, D., Banko, M.R., Villen, J., Hoang, K., Blanchard, D., Gygi, S.P., and Brunet, A. (2007). An AMPK-FOXO Pathway Mediates Longevity Induced by a Novel Method of Dietary Restriction in *C. elegans*. Curr. Biol. *17*, 1646–1656.

Greer, E.L., Maures, T.J., Ucar, D., Hauswirth, A.G., Mancini, E., Lim, J.P., Benayoun, B.A., Shi, Y., and Brunet, A. (2012). Transgenerational Epigenetic Inheritance of Longevity in *C. elegans*. Nature *479*, 365–371.

Greer, E.L., Becker, B., Latza, C., Antebi, A., and Shi, Y. (2016). Mutation of *C. elegans* demethylase *spr-5* extends transgenerational longevity. Cell Res. *26*, 229–238.

Grönke, S., Clarke, D.-F., Broughton, S., Andrews, T.D., and Partridge, L. (2010). Molecular Evolution and Functional Characterization of *Drosophila* Insulin-Like Peptides. PLoS Genet. *6*, e1000857.

Guettouche, T., Boellmann, F., Lane, W.S., and Voellmy, R. (2005). Analysis of phosphorylation of human heat shock factor 1 in cells experiencing a stress. BMC

Biochem. *6*, 4.

GuhaThakurta, D., Palomar, L., Stormo, G.D., Tedesco, P., Johnson, T.E., Walker, D.W., Lithgow, G., Kim, S., and Link, C.D. (2002). Identification of a Novel cis-Regulatory Element Involved in the Heat Shock Response in *Caenorhabditis elegans* Using Microarray Gene Expression and Computational Methods. Genome Res. *12*, 701–712.

Guisbert, E., Czyz, D.M., Richter, K., McMullen, P.D., and Morimoto, R.I. (2013). Identification of a Tissue-Selective Heat Shock Response Regulatory Network. PLoS Genet. *9*, e1003466.

Hamiel, C.R., Pinto, S., Hau, A., and Wischmeyer, P.E. (2009). Glutamine enhances heat shock protein 70 expression via increased hexosamine biosynthetic pathway activity. Am. J. Physiol. Physiol. *297*, C1509–C1519.

Hamilton, B., Dong, Y., Shindo, M., Liu, W., Odell, I., Ruvkun, G., and Lee, S.S. (2005). A systematic RNAi screen for longevity genes in *C. elegans*. Genes Dev. *19*, 1544–1555.

Han, S.K., Lee, D., Lee, H., Kim, D., Son, H.G., Yang, J.-S., Lee, S.-J. V., and Kim, S. (2016). OASIS 2: online application for survival analysis 2 with features for the analysis of maximal lifespan and healthspan in aging research. Oncotarget *7*, 56147–56152.

Han, Y., Han, D., Yan, Z., Boyd-Kirkup, J.D., Green, C.D., Khaitovich, P., and Han, J.D.J. (2012). Stress-associated H3K4 methylation accumulates during postnatal development and aging of rhesus macaque brain. Aging Cell *11*, 1055–1064.

Hansen, M., Taubert, S., Crawford, D., Libina, N., Lee, S.-J., and Kenyon, C. (2007). Lifespan extension by conditions that inhibit translation in *Caenorhabditis elegans*. Aging Cell *6*, 95–110.

Hansen, M., Chandra, A., Mitic, L.L., Onken, B., Driscoll, M., and Kenyon, C. (2008). A Role for Autophagy in the Extension of Lifespan by Dietary Restriction in *C. elegans*. PLoS Genet. *4*, e24.

Harper, J.M., Salmon, A.B., Leiser, S.F., Galecki, A.T., and Miller, R.A. (2007). Skin-derived fibroblasts from long-lived species are resistant to some, but not all, lethal stresses and to the mitochondrial inhibitor rotenone. Aging Cell *6*, 1–13.

Harper, J.M., Wang, M., Galecki, A.T., Ro, J., Williams, J.B., and Miller, R.A. (2011). Fibroblasts from long-lived bird species are resistant to multiple forms of stress. J. Exp. Biol. *214*, 1902–1910.

Harrison, D.E., Strong, R., Sharp, Z.D., Nelson, J.F., Astle, C.M., Flurkey, K., Nadon, N.L., Wilkinson, J.E., Frenkel, K., Carter, C.S., et al. (2009). Rapamycin fed late in life extends lifespan in genetically heterogeneous mice. Nature *460*, 392–395.

He, S., and Sharpless, N.E. (2017). Senescence in Health and Disease. Cell *169*, 1000–1011.

Heidler, T., Hartwig, K., Daniel, H., and Wenzel, U. (2010). *Caenorhabditis elegans* lifespan extension caused by treatment with an orally active ROS-generator is dependent on DAF-16 and SIR-2.1. Biogerontology *11*, 183–195.

Henikoff, S., and Smith, M.M. (2015). Histone Variants and Epigenetics. Cold Spring Harb. Perspect. Biol. *7*, a019364.

Heron, M. (2018). Deaths: Leading Causes for 2016. Natl. Vital Stat. Reports *67*.

Hipp, M.S., Kasturi, P., and Hartl, F.U. (2019). The proteostasis network and its decline in ageing. Nat. Rev. Mol. Cell Biol.

Hirose, T., and Horvitz, H.R. (2013). An Sp1 transcription factor coordinates caspase-dependent and -independent apoptotic pathways. Nature *500*, 354–358.

Holzenberger, M., Dupont, J., Ducos, B., Leneuve, P., Géloën, A., Even, P.C., Cervera, P., and Le Bouc, Y. (2003). IGF-1 receptor regulates lifespan and resistance to oxidative stress in mice. Nature *421*, 182–187.

Hoogewijs, D., Houthoofd, K., Matthijssens, F., Vandesompele, J., and Vanfleteren, J.R. (2008). Selection and validation of a set of reliable reference genes for quantitative *sod* gene expression analysis in *C. elegans*. BMC Mol. Biol. *9*, 9.

Horikawa, M., Sural, S., Hsu, A.-L., and Antebi, A. (2015). Co-chaperone p23 Regulates *C. elegans* Lifespan in Response to Temperature. PLOS Genet. *11*, e1005023.

Houtkooper, R.H., Mouchiroud, L., Ryu, D., Moullan, N., Katsyuba, E., Knott, G., Williams, R.W., and Auwerx, J. (2013). Mitonuclear protein imbalance as a conserved longevity mechanism. Nature *497*, 451–457.

Hsu, A.L., Murphy, C.T., and Kenyon, C. (2003). Regulation of aging and age-related disease by DAF-16 and heat-shock factor. Science *300*, 1142–1145.

Hu, Z., Chen, K., Xia, Z., Chavez, M., Pal, S., Seol, J.H., Chen, C.C., Li, W., and Tyler, J.K. (2014). Nucleosome loss leads to global transcriptional up-regulation and genomic instability during yeast aging. Genes Dev. *28*, 396–408.

Huang, D.W., Sherman, B.T., and Lempicki, R.A. (2009). Systematic and integrative analysis of large gene lists using DAVID bioinformatics resources. Nat. Protoc. *4*, 44–57.

Hübner, M.R., Eckersley-Maslin, M.A., and Spector, D.L. (2013). Chromatin organization and transcriptional regulation. Curr. Opin. Genet. Dev. *23*, 89–95.

Hwang, A.B., Ryu, E.-A., Artan, M., Chang, H.-W., Kabir, M.H., Nam, H.-J., Lee, D.,

Yang, J.-S., Kim, S., Mair, W.B., et al. (2014). Feedback regulation via AMPK and HIF-1 mediates ROS-dependent longevity in *Caenorhabditis elegans*. Proc. Natl. Acad. Sci. *111*, E4458–E4467.

Hwangbo, D.S., Garsham, B., Tu, M.P., Palmer, M., and Tatar, M. (2004). *Drosophila* dFOXO controls lifespan and regulates insulin signalling in brain and fat body. Nature *429*, 562–566.

Jedlicka, P., Mortin, M. a, and Wu, C. (1997). Multiple functions of *Drosophila* heat shock transcription factor *in vivo*. EMBO J. *16*, 2452–2462.

Jia, K., Chen, D., and Riddle, D.L. (2004). The TOR pathway interacts with the insulin signaling pathway to regulate *C. elegans* larval development, metabolism and life span. Development *131*, 3897–3906.

Jin, C., Li, J., Green, C.D., Yu, X., Tang, X., Han, D., Xian, B., Wang, D., Huang, X., Cao, X., et al. (2011). Histone demethylase UTX-1 regulates *C. elegans* life span by targeting the insulin/IGF-1 signaling pathway. Cell Metab. *14*, 161–172.

Johnson, D.T., Harris, R.A., French, S., Blair, P. V, You, J., Bemis, K.G., Wang, M., and Balaban, R.S. (2007). Tissue heterogeneity of the mammalian mitochondrial proteome. Am J Physiol Cell Physiol *292*, 689–697.

Jonassen, T., Marbois, B.N., Faull, K.F., Clarke, C.F., and Larsen, P.L. (2002). Development and fertility in *Caenorhabditis elegans clk-1* mutants depend upon transport of dietary coenzyme Q_8 to mitochondria. J. Biol. Chem. *277*, 45020–45027.

Jones, O.R., Scheuerlein, A., Salguero-Gómez, R., Camarda, C.G., Schaible, R., Casper, B.B., Dahlgren, J.P., Ehrlén, J., García, M.B., Menges, E.S., et al. (2014). Diversity of ageing across the tree of life. Nature *505*, 169–173.

Jovic, K., Sterken, M.G., Grilli, J., Bevers, R.P.J., Rodriguez, M., Riksen, J.A.G., Allesina, S., Kammenga, J.E., and Snoek, L.B. (2017). Temporal dynamics of gene expression in heat-stressed *Caenorhabditis elegans*. PLoS One *12*, e0189445.

Kaeberlein, M., McVey, M., and Guarente, L. (1999). The *SIR2/3/4* complex and *SIR2* alone promote longevity in *Saccharomyces cerevisiae* by two different mechanisms. Genes Dev. *13*, 2570–2580.

Kaeberlein, M., Powers, R.W.P., Steffen, K.K., Westman, E.A., Hu, D., Dang, N., Kerr, E.O., Kirkland, K.T., Fields, S., and Kennedy, B.K. (2005). Regulation of Yeast Replicative Life Span by TOR and Sch9 in Response to Nutrients. Science *310*, 1193–1196.

Kaletta, T., and Hengartner, M.O. (2006). Finding function in novel targets: *C. elegans* as a model organism. Nat. Rev. Drug Discov. *5*, 387–399.

Kanfi, Y., Naiman, S., Amir, G., Peshti, V., Zinman, G., Nahum, L., Bar-Joseph, Z., and

Cohen, H.Y. (2012). The sirtuin SIRT6 regulates lifespan in male mice. Nature *483*, 218–221.

Kapahi, P., Boulton, M.E., and Kirkwood, T.B.. (1999). Positive correlation between mammalian life span and cellular resistance to stress. Free Radic. Biol. Med. *26*, 495–500.

Kapahi, P., Zid, B.M., Harper, T., Koslover, D., Sapin, V., and Benzer, S. (2004). Regulation of Lifespan in *Drosophila* by Modulation of Genes in the TOR Signaling Pathway. Curr. Biol. *14*, 885–890.

Kauppila, T.E.S., Bratic, A., Jensen, M.B., Baggio, F., Partridge, L., Jasper, H., Grönke, S., and Larsson, N.-G. (2018). Mutations of mitochondrial DNA are not major contributors to aging of fruit flies. Proc. Natl. Acad. Sci. 201721683.

Keall, R., Whitelaw, S., Pettitt, J., and Müller, B. (2007). Histone gene expression and histone mRNA 3' end structure in *Caenorhabditis elegans*. BMC Mol. Biol. *8*, 51.

Kenyon, C.J., Chang, J., Gensch, E., Rudner, A., and Tabtlang, R. (1993). A *C. elegans* mutant that lives twice as long a wild type. Nature *366*, 461–464.

Khaidakov, M., Heflich, R.H., Manjanatha, M.G., Myers, M.B., and Aidoo, A. (2003). Accumulation of point mutations in mitochondrial DNA of aging mice. Mutat. Res. Mol. Mech. Mutagen. *526*, 1–7.

Khrapko, K., Coller, H.A., Andre, P.C., Li, X.-C., Hanekamp, J.S., and Thilly, W.G. (1997). Mitochondrial mutational spectra in human cells and tissues. Proc. Natl. Acad. Sci. *94*, 13798–13803.

Kim, H.-E., Grant, A.R., Simic, M.S., Kohnz, R.A., Nomura, D.K., Durieux, J., Riera, C.E., Sanchez, M., Kapernick, E., Wolff, S., et al. (2016). Lipid Biosynthesis Coordinates a Mitochondrial-to-Cytosolic Stress Response. Cell *166*, 1539–1552.

Kinet, M.J., Malin, J.A., Abraham, M.C., Blum, E.S., Silverman, M.R., Lu, Y., and Shaham, S. (2016). HSF-1 activates the ubiquitin proteasome system to promote non-apoptotic developmental cell death in *C. elegans*. Elife *5*, e12821.

Klass, M.R. (1983). A method for the isolation of longevity mutants in the nematode *Caenorhabditis elegans* and initial results. Mech. Ageing Dev. *22*, 279–286.

Kodoyianni, V., Maine, E.M., and Kimble, J. (1992). Molecular basis of loss-of-function mutations in the *glp-1* gene of *Caenorhabditis elegans*. Mol. Biol. Cell *3*, 1199–1213.

Koopman, M., Michels, H., Dancy, B.M., Kamble, R., Mouchiroud, L., Auwerx, J., Nollen, E.A.A., and Houtkooper, R.H. (2016). A screening-based platform for the assessment of cellular respiration in *Caenorhabditis elegans*. Nat. Protoc. *11*, 1798–1816.

Kucej, M., Kucejova, B., Subramanian, R., Chen, X.J., and Butow, R.A. (2008). Mitochondrial nucleoids undergo remodeling in response to metabolic cues. J. Cell Sci. *121*, 1861–1868.

Kujoth, G.C., Hiona, A., Pugh, T.D., Someya, S., Panzer, K., Wohlgemuth, S.E., Hofer, T., Seo, A.Y., Sullivan, R., Jobling, W.A., et al. (2005). Mitochondrial DNA Mutations, Oxidative Stress, and Apoptosis in Mammalian Aging. Science *309*, 481–484.

Kukat, C., Davies, K.M., Wurm, C.A., Spåhr, H., Bonekamp, N.A., Kühl, I., Joos, F., Polosa, P.L., Park, C.B., Posse, V., et al. (2015). Cross-strand binding of TFAM to a single mtDNA molecule forms the mitochondrial nucleoid. Proc. Natl. Acad. Sci. *112*, 11288–11293.

Kumsta, C., Chang, J.T., Schmalz, J., and Hansen, M. (2017). Hormetic heat stress and HSF-1 induce autophagy to improve survival and proteostasis in *C. elegans*. Nat. Commun. *8*, 14337.

Labbadia, J., and Morimoto, R.I. (2015). Repression of the Heat Shock Response Is a Programmed Event at the Onset of Reproduction. Mol. Cell *59*, 639–650.

Labbadia, J., Brielmann, R.M., Neto, M.F., Lin, Y.-F., Haynes, C.M., and Morimoto, R.I. (2017). Mitochondrial stress restores the heat shock response and prevents proteostasis collapse during aging. Cell Rep. *21*, 1481–1494.

Langmead, B., and Salzberg, S.L. (2012). Fast gapped-read alignment with Bowtie 2. Nat. Methods *9*, 357–359.

Larson, K., Yan, S.-J., Tsurumi, A., Liu, J., Zhou, J., Gaur, K., Guo, D., Eickbush, T.H., and Li, W.X. (2012). Heterochromatin Formation Promotes Longevity and Represses Ribosomal RNA Synthesis. PLoS Genet. *8*, e1002473.

Larsson, N.-G. (2010). Somatic Mitochondrial DNA Mutations in Mammalian Aging. Annu. Rev. Biochem. *79*, 683–706.

Lawrence, M., Daujat, S., and Schneider, R. (2016). Lateral Thinking: How Histone Modifications Regulate Gene Expression. Trends Genet. *32*, 42–56.

Lee, S.R., and Han, J. (2017). Mitochondrial nucleoid: shield and switch of the mitochondrial genome. Oxid. Med. Cell. Longev. *2017*, 8060949.

Lee, S.J., Hwang, A.B., and Kenyon, C. (2010). Inhibition of respiration extends *C. elegans* life span via reactive oxygen species that increase HIF-1 activity. Curr. Biol. *20*, 2131–2136.

Lee, S.S., Lee, R.Y.N., Fraser, A.G., Kamath, R.S., Ahringer, J., and Ruvkun, G. (2002). A systematic RNAi screen identifies a critical role for mitochondria in *C. elegans* longevity. Nat. Genet. *33*, 40–48.

Lezzerini, M., and Budovskaya, Y. (2014). A dual role of the Wnt signaling pathway during aging in *Caenorhabditis elegans*. Aging Cell *13*, 8–18.

Li, J., Chauve, L., Phelps, G., Brielmann, R.M., and Morimoto, R.I. (2016). E2F coregulates an essential HSF developmental program that is distinct from the heat-shock response. Genes Dev. *30*, 2062–2075.

Li, J., Labbadia, J., and Morimoto, R.I. (2017). Rethinking HSF1 in stress, development, and organismal health. Trends Cell Biol. *27*, 895–905.

Liberati, N.T., Fitzgerald, K.A., Kim, D.H., Feinbaum, R., Golenbock, D.T., and Ausubel, F.M. (2004). Requirement for a conserved Toll/interleukin-1 resistance domain protein in the *Caenorhabditis elegans* immune response. Proc. Natl. Acad. Sci. *101*, 6593–6598.

Libina, N., Berman, J.R., and Kenyon, C. (2003). Tissue-Specific Activities of *C. elegans* DAF-16 in the Regulation of Lifespan. Cell *115*, 489–502.

Lin, K., Dorman, J.B., Rodan, A., and Kenyon, C. (1997). daf-16: An HNF-3/forkhead Family Member That Can Function to Double the Life-Span of *Caenorhabditis elegans*. Science *278*, 1319–1322.

Liu, L., Cheung, T.H., Charville, G.W., Hurgo, B.M.C., Leavitt, T., Shih, J., Brunet, A., and Rando, T.A. (2013). Chromatin modifications as determinants of muscle stem cell quiescence and chronological aging. Cell Rep. *4*, 189–204.

Liu, X., Jiang, N., Hughes, B., Bigras, E., Shoubridge, E., and Hekimi, S. (2005). Evolutionary conservation of the *clk-1*-dependent mechanism of longevity: Loss of *mclk1* increases cellular fitness and lifespan in mice. Genes Dev. *19*, 2424–2434.

López-Otín, C., Blasco, M.A., Partridge, L., Serrano, M., and Kroemer, G. (2013). The hallmarks of aging. Cell *153*, 1194–1217.

Love, M.I., Huber, W., and Anders, S. (2014). Moderated estimation of fold change and dispersion for RNA-seq data with DESeq2. Genome Biol. *15*, 550.

Luger, K., Mäder, A.W., Richmond, R.K., Sargent, D.F., and Richmond, T.J. (1997). Crystal structure of the nucleosome core particle at 2.8 Å resolution. Nature *389*, 251–260.

Macias, E., Rao, D., Carbajal, S., Kiguchi, K., and DiGiovanni, J. (2014). Stat3 Binds to mtDNA and Regulates Mitochondrial Gene Expression in Keratinocytes. J. Invest. Dermatol. *134*, 1971–1980.

Mackenbach, J.P., Kunst, A.E., Lautenbach, H., Oei, Y.B., and Bijlsma, F. (1999). Gains in life expectancy after elimination of major causes of death: revised estimates taking into account the effect of competing causes. J. Epidemiol. Community Heal. *53*, 32–37.

De Magalhães, J.P., and Costa, J. (2009). A database of vertebrate longevity records and their relation to other life-history traits. J. Evol. Biol. *22*, 1770–1774.

Marom, S., Blumberg, A., Kundaje, A., and Mishmar, D. (2019). mtDNA Chromatin-like Organization Is Gradually Established during Mammalian Embryogenesis. IScience *12*, 141–151.

Martin, M. (2011). Cutadapt removes adapter sequences from high-throughput sequencing reads. EMBnet.Journal *17*, 10–12.

Martínez, D.E. (1998). Mortality Patterns Suggest Lack of Senescence in Hydra. Exp. Gerontol. *33*, 217–225.

Matilainen, O., Sleiman, M.S.B., Quiros, P.M., Garcia, S.M.D.A., and Auwerx, J. (2017). The chromatin remodeling factor ISW-1 integrates organismal responses against nuclear and mitochondrial stress. Nat. Commun. *8*, 1818.

Maures, T.J., Greer, E.L., Hauswirth, A.G., and Brunet, A. (2011). The H3K27 demethylase UTX-1 regulates *C. elegans* lifespan in a germline-independent, insulin-dependent manner. Aging Cell *10*, 980–990.

McMillan, D.R., Xiao, X., Shao, L., Graves, K., and Benjamin, I.J. (1998). Targeted Disruption of Heat Shock Transcription Factor 1 Abolishes Thermotolerance and Protection against Heat-inducible Apoptosis. J. Biol. Chem. *273*, 7523–7528.

Mehta, R., Steinkraus, K.A., Sutphin, G.L., Ramos, F.J., Shamieh, L.S., Huh, A., Davis, C., Chandler-Brown, D., and Kaeberlein, M. (2009). Proteasomal Regulation of the Hypoxic Response Modulates Aging in C. elegans. Science *324*, 1196–1198.

Melendez, A., Tallóczy, Z., Seaman, M., Eskelinen, E.-L., Hall, D.H., and Levine, B. (2003). Autophagy Genes Are Essential for Dauer Development and Life-Span Extension in *C. elegans*. Science *301*, 1387–1391.

Mendillo, M.L., Santagata, S., Koeva, M., Bell, G.W., Hu, R., Tamimi, R.M., Fraenkel, E., Ince, T.A., Whitesell, L., and Lindquist, S. (2012). HSF1 Drives a Transcriptional Program Distinct from Heat Shock to Support Highly Malignant Human Cancers. Cell *150*, 549–562.

Mercer, T.R., Neph, S., Dinger, M.E., Crawford, J., Smith, M.A., Shearwood, A.M.J., Haugen, E., Bracken, C.P., Rackham, O., Stamatoyannopoulos, J.A., et al. (2011). The human mitochondrial transcriptome. Cell *146*, 645–658.

Merkwirth, C., Jovaisaite, V., Durieux, J., Matilainen, O., Jordan, S.D., Quiros, P.M., Steffen, K.K., Williams, E.G., Mouchiroud, L., Tronnes, S.U., et al. (2016). Two conserved histone demethylases regulate mitochondrial stress-induced longevity. Cell *165*, 1209–1223.

Metchat, A., Åkerfelt, M., Bierkamp, C., Delsinne, V., Sistonen, L., Alexandre, H., and

Christians, E.S. (2009). Mammalian Heat Shock Factor 1 Is Essential for Oocyte Meiosis and Directly Regulates Hsp90α Expression. J. Biol. Chem. *284*, 9521–9528.

Van Meter, M., Gorbunova, V., and Seluanov, A. (2015). Comparative Biology of Aging: Insights from Long-Lived Rodent Species. In Handbook of the Biology of Aging: Eighth Edition, M.R. Kaeberlein, and G.M. Martin, eds. (Elsevier Inc), pp. 305–324.

Miller, H., Fletcher, M., Primitivo, M., Leonard, A., Sutphin, G.L., Rintala, N., Kaeberlein, M., and Leiser, S.F. (2017). Genetic interaction with temperature is an important determinant of nematode longevity. Aging Cell *16*, 1425–1429.

Morgan, W.D. (1989). Transcription factor Sp1 binds to and activates a human *hsp70* gene promoter. Mol. Cell. Biol. *9*, 4099–4104.

Morimoto, R.I. (1998). Regulation of the heat shock transcriptional response: cross talk between a family of heat shock factors, molecular chaperones, and negative regulators. Genes Dev. *12*, 3788–3796.

Morimoto, R.I. (2011). The heat shock response: systems biology of proteotoxic stress in aging and disease. Cold Spring Harb. Symp. Quant. Biol. *76*, 91–99.

Morley, J.F., and Morimoto, R.I. (2004). Regulation of longevity in *Caenorhabditis elegans* by heat shock factor and molecular chaperones. Mol. Biol. Cell *15*, 657–664.

Mouchiroud, L., Houtkooper, R.H., Moullan, N., Katsyuba, E., Ryu, D., Cantó, C., Mottis, A., Jo, Y.-S., Viswanathan, M., Schoonjans, K., et al. (2013). The NAD^+/sirtuin pathway modulates longevity through activation of mitochondrial UPR and FOXO signaling. Cell *154*, 430–441.

Mukhopadhyay, A., Deplancke, B., Walhout, A.J.M., and Tissenbaum, H.A. (2008). Chromatin immunoprecipitation (ChIP) coupled to detection by quantitative real-time PCR to study transcription factor binding to DNA in *Caenorhabditis elegans*. Nat. Protoc. *3*, 698–709.

Murphy, C.T., McCarroll, S.A., Bargmann, C.I., Fraser, A., Kamath, R.S., Ahringer, J., Li, H., and Kenyon, C. (2003). Genes that act downstream of DAF-16 to influence the lifespan of *Caenorhabditis elegans*. Nature *424*, 277–283.

Nakai, A., Suzuki, M., and Tanabe, M. (2000). Arrest of spermatogenesis in mice expressing an active heat shock transcription factor 1. EMBO J. *19*, 1545–1554.

Neef, D.W., Jaeger, A.M., Gomez-Pastor, R., Willmund, F., Frydman, J., and Thiele, D.J. (2014). A Direct Regulatory Interaction between Chaperonin TRiC and Stress-Responsive Transcription Factor HSF1. Cell Rep. *9*, 955–966.

Ni, Z., Ebata, A., Alipanahiramandi, E., and Lee, S.S. (2012). Two SET domain containing genes link epigenetic changes and aging in *Caenorhabditis elegans*. Aging Cell *11*, 315–325.

Nielsen, J., Hedeholm, R.B., Heinemeier, J., Bushnell, P.G., Christiansen, J.S., Olsen, J., Ramsey, C.B., Brill, R.W., Simon, M., Steffensen, K.F., et al. (2016). Eye lens radiocarbon reveals centuries of longevity in the Greenland shark (*Somniosus microcephalus*). Science *353*, 702–704.

O'Sullivan, R.J., and Karlseder, J. (2012). The great unravelling: chromatin as a modulator of the aging process. Trends Biochem. Sci. *37*, 466–476.

O'Sullivan, R.J., Kubicek, S., Schreiber, S.L., and Karlseder, J. (2010). Reduced histone biosynthesis and chromatin changes arising from a damage signal at telomeres. Nat. Struct. Mol. Biol. *17*, 1218–1225.

Oda, T., Sekimoto, T., Kurashima, K., Fujimoto, M., Nakai, A., and Yamashita, T. (2018). Acute HSF1 depletion induces cellular senescence through the MDM2-p53-p21 pathway in human diploid fibroblasts. J. Cell Sci. *131*, jcs210724.

Ogg, S., Paradis, S., Gottlieb, S., Patterson, G.I., Lee, L., Tissenbaum, H.A., and Ruvkun, G. (1997). The Fork head transcription factor DAF-16 transduces insulin-like metabolic and longevity signals in *C. elegans*. Nature *389*, 994–999.

Oh, S.W., Mukhopadhyay, A., Svrzikapa, N., Jiang, F., Davis, R.J., and Tissenbaum, H.A. (2005). JNK regulates lifespan in *Caenorhabditis elegans* by modulating nuclear translocation of forkhead transcription factor/DAF-16. Proc. Natl. Acad. Sci. *102*, 4494–4499.

Okimoto, R., Macfarlane, J.L., Clary, D.O., and Wolstenholme, D.R. (1992). The mitochondrial genomes of two nematodes, *Caenorhabditis elegans* and *Ascaris suum*. Genetics *130*, 471–498.

Ooi, F.K., and Prahlad, V. (2017). Olfactory experience primes the heat shock transcription factor HSF-1 to enhance the expression of molecular chaperones in *C. elegans*. Sci. Signal. *10*, eaan4893.

Pal, S., and Tyler, J.K. (2016). Epigenetics and aging. Sci. Adv. *2*, e1600584–e1600584.

Pan, K.Z., Palter, J.E., Rogers, A.N., Olsen, A., Chen, D., Lithgow, G.J., and Kapahi, P. (2007). Inhibition of mRNA translation extends lifespan in *Caenorhabditis elegans*. Aging Cell *6*, 111–119.

Panowski, S.H., Wolff, S., Aguilaniu, H., Durieux, J., and Dillin, A. (2007). PHA-4/Foxa mediates diet-restriction-induced longevity of *C. elegans*. Nature *447*, 550–555.

Pettitt, J., Crombie, C., Schümperli, D., and Müller, B. (2002). The *Caenorhabditis elegans* histone hairpin-binding protein is required for core histone gene expression and is essential for embryonic and postembryonic cell division. J. Cell Sci. *115*, 857–866.

Powers, E.T., Morimoto, R.I., Dillin, A., Kelly, J.W., and Balch, W.E. (2009). Biological

and chemical approaches to diseases of proteostasis deficiency. Annu. Rev. Biochem. *78*, 959–991.

Powers, R.W., Kaeberlein, M., Caldwell, S.D., Kennedy, B.K., and Fields, S. (2006). Extension of chronological life span in yeast by decreased TOR pathway signaling. Genes Dev. *20*, 174–184.

Pyo, J.-O., Yoo, S.-M., Ahn, H.-H., Nah, J., Hong, S.-H., Kam, T.-I., Jung, S., and Jung, Y.-K. (2013). Overexpression of Atg5 in mice activates autophagy and extends lifespan. Nat. Commun. *4*, 2300.

Qadota, H., Inoue, M., Hikita, T., Köppen, M., Hardin, J.D., Amano, M., Moerman, D.G., and Kaibuchi, K. (2007). Establishment of a tissue-specific RNAi system in *C. elegans*. Gene *400*, 166–173.

Rea, S.L., Ventura, N., and Johnson, T.E. (2007). Relationship between mitochondrial electron transport chain dysfunction, development, and life extension in *Caenorhabditis elegans*. PLoS Biol. *5*, e259.

Richter, K., Haslbeck, M., and Buchner, J. (2010). The heat shock response: life on the verge of death. Mol. Cell *40*, 253–266.

Riera, C.E., Merkwirth, C., De Magalhaes Filho, C.D., and Dillin, A. (2016). Signaling networks determining life span. Annu. Rev. Biochem. *85*, 35–64.

Rinkevich, B. (2017). Senescence in Modular Animals: *Botryllid ascidians* as a Unique Ageing System. In The Evolution of Senescence in the Tree of Life, R.P. Shefferson, O.R. Jones, and R. Salguero-Gomez, eds. (Cambridge: Cambridge University Press), pp. 220–237.

Robida-Stubbs, S., Glover-Cutter, K., Lamming, D.W., Mizunuma, M., Narasimhan, S.D., Neumann-Haefelin, E., Sabatini, D.M., and Blackwell, T.K. (2012). TOR signaling and rapamycin influence longevity by regulating SKN-1/Nrf and DAF-16/FoxO. Cell Metab. *15*, 713–724.

Rodriguez, M., Snoek, L.B., De Bono, M., and Kammenga, J.E. (2013). Worms under stress: *C. elegans* stress response and its relevance to complex human disease and aging. Trends Genet. *29*, 367–374.

Rogina, B., and Helfand, S.L. (2004). Sir2 mediates longevity in the fly through a pathway related to calorie restriction. Proc. Natl. Acad. Sci. *101*, 15998–16003.

Ryu, H., Lee, J., Impey, S., Ratan, R.R., and Ferrante, R.J. (2005). Antioxidants modulate mitochondrial PKA and increase CREB binding to D-loop DNA of the mitochondrial genome in neurons. Proc. Natl. Acad. Sci. *102*, 13915–13920.

Sarge, K.D., Murphy, S.P., and Morimoto, R.I. (1993). Activation of heat shock gene transcription by heat shock factor 1 involves oligomerization, acquisition of DNA-binding

activity, and nuclear localization and can occur in the absence of stress. Mol. Cell. Biol. *13*, 1392–1407.

Satoh, A., Brace, C.S., Rensing, N., Cliften, P., Wozniak, D.F., Herzog, E.D., Yamada, K.A., and Imai, S.I. (2013). Sirt1 extends life span and delays aging in mice through the regulation of Nk2 Homeobox 1 in the DMH and LH. Cell Metab. *18*, 416–430.

Satyal, S.H., Chen, D., Fox, S.G., Kramer, J.M., and Morimoto, R.I. (1998). Negative regulation of the heat shock transcriptional response by HSBP1. Genes Dev. *12*, 1962–1974.

Schaeper, N.D., Prpic, N.-M., and Wimmer, E.A. (2010). A clustered set of three Sp-family genes is ancestral in the Metazoa: evidence from sequence analysis, protein domain structure, developmental expression patterns and chromosomal location. BMC Evol. Biol. *10*, 88.

Schroeder, E.A., Raimundo, N., and Shadel, G.S. (2013). Epigenetic silencing mediates mitochondria stress-induced longevity. Cell Metab. *17*, 954–964.

Selman, C., Tullet, J.M.A., Wieser, D., Irvine, E., Lingard, S.J., Choudhury, A.I., Claret, M., Al-Qassab, H., Carmignac, D., Ramadani, F., et al. (2009). Ribosomal Protein S6 Kinase 1 Signaling Regulates Mammalian Life Span. Science *326*, 140–144.

Sen, P., Dang, W., Donahue, G., Dai, J., Dorsey, J., Cao, X., Liu, W., Cao, K., Perry, R., Lee, J.Y., et al. (2015). H3K36 methylation promotes longevity by enhancing transcriptional fidelity. Genes Dev. *29*, 1362–1376.

Sen, P., Shah, P.P., Nativio, R., and Berger, S.L. (2016). Epigenetic Mechanisms of Longevity and Aging. Cell *166*, 822–839.

Seo, K., Choi, E., Lee, D., Jeong, D.-E., Jang, S.K., and Lee, S.-J. (2013). Heat shock factor 1 mediates the longevity conferred by inhibition of TOR and insulin/IGF-1 signaling pathways in *C. elegans*. Aging Cell *12*, 1073–1081.

Shakes, D.C., Miller, D.M., and Nonet, M.L. (2012). Immunofluorescence microscopy. Methods Cell Biol. *107*, 35–66.

Shaw, W.M., Luo, S., Landis, J., Ashraf, J., and Murphy, C.T. (2007). The *C. elegans* TGF-β Dauer Pathway Regulates Longevity via Insulin Signaling. Curr. Biol. *17*, 1635–1645.

Shi, Y., Mosser, D.D., and Morimoto, R.I. (1998). Molecular chaperones as HSF1-specific transcriptional repressors. Genes Dev. *12*, 654–666.

Shpilka, T., and Haynes, C.M. (2017). The mitochondrial UPR: mechanisms, physiological functions and implications in ageing. Nat. Rev. Mol. Cell Biol. *19*, 109–120.

Siebold, A.P., Banerjee, R., Tie, F., Kiss, D.L., Moskowitz, J., and Harte, P.J. (2010). Polycomb Repressive Complex 2 and Trithorax modulate *Drosophila* longevity and stress resistance. Proc. Natl. Acad. Sci. *107*, 169–174.

Singh, R.K., Kabbaj, M.-H.M., Paik, J., and Gunjan, A. (2009). Histone levels are regulated by phosphorylation and ubiquitylation-dependent proteolysis. Nat. Cell Biol. *11*, 925–933.

Singleton, K.D., and Wischmeyer, P.E. (2008). Glutamine Induces Heat Shock Protein Expression Via O-Glycosylation and Phosphorylation of HSF-1 and Sp1. J. Parenter. Enter. Nutr. *32*, 371–376.

Steele, A.D., Hutter, G., Jackson, W.S., Heppner, F.L., Borkowski, A.W., King, O.D., Raymond, G.J., Aguzzi, A., and Lindquist, S. (2008). Heat shock factor 1 regulates lifespan as distinct from disease onset in prion disease. Proc. Natl. Acad. Sci. *105*, 13626–13631.

Steinkraus, K.A., Smith, E.D., Davis, C., Carr, D., Pendergrass, W.R., Sutphin, G.L., Kennedy, B.K., and Kaeberlein, M. (2008). Dietary restriction suppresses proteotoxicity and enhances longevity by an *hsf-1*-dependent mechanism in *Caenorhabditis elegans*. Aging Cell *7*, 394–404.

Stenesen, D., Suh, J.M., Seo, J., Yu, K., Lee, K.S., Kim, J.S., Min, K.J., and Graff, J.M. (2013). Adenosine nucleotide biosynthesis and AMPK regulate adult life span and mediate the longevity benefit of caloric restriction in flies. Cell Metab. *17*, 101–112.

Stewart, J.B., and Chinnery, P.F. (2015). The dynamics of mitochondrial DNA heteroplasmy: implications for human health and disease. Nat. Rev. Genet. *16*, 530–542.

Stroustrup, N. (2018). Measuring and modeling interventions in aging. Curr. Opin. Cell Biol. *55*, 129–138.

Sumitani, M., Kasashima, K., Matsugi, J., and Endo, H. (2011). Biochemical properties of *Caenorhabditis elegans* HMG-5, a regulator of mitochondrial DNA. J. Biochem. *149*, 581–589.

Takaki, E., and Nakai, A. (2016). Regulation of HSF Activation and Repression. In Heat Shock Factor, A. Nakai, ed. (Tokyo: Springer Japan), pp. 51–72.

Takii, R., and Fujimoto, M. (2016). Structure and Function of the HSF Family Members. In Heat Shock Factor, A. Nakai, ed. (Tokyo: Springer Japan), pp. 31–50.

Tatar, M., Khazaeli, A.A., and Curtsinger, J.W. (1997). Chaperoning extended life. Nature *390*, 30.

Tatar, M., Kopelman, A., Epstein, D., Tu, M.P., Yin, C.M., and Garofalo, R.S. (2001). A mutant *Drosophila* insulin receptor homolog that extends life- span and impairs

neuroendocrine function. Science *292*, 107–110.

Taylor, R.C., and Dillin, A. (2011). Aging as an event of proteostasis collapse. Cold Spring Harb. Perspect. Biol. *3*, a004440.

Tepper, R.G., Ashraf, J., Kaletsky, R., Kleemann, G., Murphy, C.T., and Bussemaker, H.J. (2013). PQM-1 complements DAF-16 as a key transcriptional regulator of DAF-2-mediated development and longevity. Cell *154*, 676–690.

Terzioglu, M., Ruzzenente, B., Harmel, J., Mourier, A., Jemt, E., López, M.D., Kukat, C., Stewart, J.B., Wibom, R., Meharg, C., et al. (2013). MTERF1 Binds mtDNA to prevent transcriptional interference at the light-strand promoter but is dispensable for rRNA gene transcription regulation. Cell Metab. *17*, 618–626.

The *C. elegans* Sequencing Consortium (1998). Genome Sequence of the Nematode *C. elegans*: A Platform for Investigating Biology. Science *282*, 2012–2018.

Tian, Y., Garcia, G., Bian, Q., Steffen, K.K., Joe, L., Wolff, S., Meyer, B.J., and Dillin, A. (2016). Mitochondrial Stress Induces Chromatin Reorganization to Promote Longevity and UPR^{mt}. Cell *165*, 1197–1208.

Timmis, J.N., Ayliffe, M.A., Huang, C.Y., and Martin, W. (2004). Endosymbiotic gene transfer: organelle genomes forge eukaryotic chromosomes. Nat. Rev. Genet. *5*, 123–135.

Tissenbaum, H.A., and Guarente, L. (2001). Increased dosage of a *sir-2* gene extends lifespan in *Caenorhabditis elegans*. Nature *410*, 227–230.

Tóth, M.L., Sigmond, T., Borsos, É., Barna, J., Erdélyi, P., Takács-Vellai, K., Orosz, L., Kovács, A.L., Csikós, G., Sass, M., et al. (2008). Longevity pathways converge on autophagy genes to regulate life span in *Caenorhabditis elegans*. Autophagy *4*, 330–338.

Trifunovic, A., Wredenberg, A., Falkenberg, M., Spelbrink, J.N., Rovio, A.T., Bruder, C.E., Bohlooly-Y, M., Gidlöf, S., Oldfors, A., Wibom, R., et al. (2004). Premature ageing in mice expressing defective mitochondrial DNA polymerase. Nature *429*, 417–423.

Tyynismaa, H., Mjosund, K.P., Wanrooij, S., Lappalainen, I., Ylikallio, E., Jalanko, A., Spelbrink, J.N., Paetau, A., and Suomalainen, A. (2005). Mutant mitochondrial helicase Twinkle causes multiple mtDNA deletions and a late-onset mitochondrial disease in mice. Proc. Natl. Acad. Sci. *102*, 17687–17692.

Ulgherait, M., Rana, A., Rera, M., Graniel, J., and Walker, D.W. (2014). AMPK modulates tissue and organismal aging in a non-cell-autonomous manner. Cell Rep. *8*, 1767–1780.

Ulm, E.A., Sleiman, S.F., and Chamberlin, H.M. (2011). Developmental functions for the *Caenorhabditis elegans* Sp protein SPTF-3. Mech. Dev. *128*, 428–441.

United Nations Department of Economic and Social Affairs (2017). World Population Ageing 2017 - Highlights.

Vellai, T., Takacs-Vellai, K., Zhang, Y., Kovacs, A.L., Orosz, L., and Müller, F. (2003). Influence of TOR kinase on lifespan in *C. elegans*. Nature *426*, 620–620.

Verma, S., Jagtap, U., Goyala, A., and Mukhopadhyay, A. (2018). A novel gene-diet pair modulates *C. elegans* aging. PLOS Genet. *14*, e1007608.

Vermulst, M., Bielas, J.H., Kujoth, G.C., Ladiges, W.C., Rabinovitch, P.S., Prolla, T.A., and Loeb, L.A. (2007). Mitochondrial point mutations do not limit the natural lifespan of mice. Nat. Genet. *39*, 540–543.

Vihervaara, A., and Sistonen, L. (2014). HSF1 at a glance. J. Cell Sci. *127*, 261–266.

Walker, G.A., and Lithgow, G.J. (2003). Lifespan extension in *C. elegans* by a molecular chaperone dependent upon insulin-like signals. Aging Cell *2*, 131–139.

Wang, C., Jurk, D., Maddick, M., Nelson, G., Martin-ruiz, C., and Von Zglinicki, T. (2009). DNA damage response and cellular senescence in tissues of aging mice. Aging Cell *8*, 311–323.

Wang, G., Ying, Z., Jin, X., Tu, N., Zhang, Y., Phillips, M., Moskophidis, D., and Mivechi, N.F. (2004). Essential Requirement for Both *hsf1* and *hsf2* Transcriptional Activity in Spermatogenesis and Male Fertility. Genesis *38*, 66–80.

Wang, M.C., Bohmann, D., and Jasper, H. (2003). JNK signaling confers tolerance to oxidative stress and extends lifespan in *Drosophila*. Dev. Cell *5*, 811–816.

Weinert, B.T., and Timiras, P.S. (2003). Invited Review: Theories of aging. J. Appl. Physiol. *95*, 1706–1716.

Welch, C.H. (1998). Shortest Reproductive Life. In The University of Florida Book of Insect Records, pp. 92–93.

Westerheide, S.D., Anckar, J., Stevens, S.M., Sistonen, L., and Morimoto, R.I. (2009). Stress-Inducible Regulation of Heat Shock Factor 1 by the Deacetylase SIRT1. Science *323*, 1063–1066.

Wierstra, I. (2008). Sp1: Emerging roles—Beyond constitutive activation of TATA-less housekeeping genes. Biochem. Biophys. Res. Commun. *372*, 1–13.

Wood, J.G., Hillenmeyer, S., Lawrence, C., Chang, C., Hosier, S., Lightfoot, W., Mukherjee, E., Jiang, N., Schorl, C., Brodsky, A.S., et al. (2010). Chromatin remodeling in the aging genome of *Drosophila*. Aging Cell *9*, 971–978.

Wood, J.G., Jones, B.C., Jiang, N., Chang, C., Hosier, S., Wickremesinghe, P., Garcia, M., Hartnett, D.A., Burhenn, L., Neretti, N., et al. (2016). Chromatin-modifying genetic

interventions suppress age-associated transposable element activation and extend life span in *Drosophila*. Proc. Natl. Acad. Sci. *113*, 11277–11282.

Xiao, X., Zuo, X., Davis, A.A., Randy, M.D., Curry, B.B., Richardson, J.A., and Benjamin, I.J. (1999). HSF1 is required for extra-embryonic development, postnatal growth and protection during inflammatory responses in mice. EMBO J. *18*, 5943–5952.

Xu, M., Pirtskhalava, T., Farr, J.N., Weigand, B.M., Palmer, A.K., Weivoda, M.M., Inman, C.L., Ogrodnik, M.B., Hachfeld, C.M., Fraser, D.G., et al. (2018). Senolytics improve physical function and increase lifespan in old age. Nat. Med. *24*, 1246–1256.

Yang, X., Wang, J., Liu, S., and Yan, Q. (2014). HSF1 and Sp1 Regulate FUT4 Gene Expression and Cell Proliferation in Breast Cancer Cells. J. Cell. Biochem. *115*, 168–178.

Yoneda, T., Benedetti, C., Urano, F., Clark, S.G., Harding, H.P., and Ron, D. (2004). Compartment-specific perturbation of protein handling activates genes encoding mitochondrial chaperones. J. Cell Sci. *117*, 4055–4066.

Yui, R., Ohno, Y., and Matsuura, E.T. (2003). Accumulation of deleted mitochondrial DNA in aging *Drosophila melanogaster*. Genes Genet. Syst. *78*, 245–251.

Yunger, E., Safra, M., Levi-Ferber, M., Haviv-Chesner, A., and Henis-Korenblit, S. (2017). Innate immunity mediated longevity and longevity induced by germ cell removal converge on the C-type lectin domain protein IRG-7. PLOS Genet. *13*, e1006577.

Zhang, B., Xiao, R., Ronan, E.A., He, Y., Hsu, A.L., Liu, J., and Xu, X.Z.S. (2015). Environmental Temperature Differentially Modulates *C. elegans* Longevity through a Thermosensitive TRP Channel. Cell Rep. *11*, 1414–1424.

Zhang, H., Ryu, D., Wu, Y., Gariani, K., Wang, X., Luan, P., DAmico, D., Ropelle, E.R., Lutolf, M.P., Aebersold, R., et al. (2016). NAD^+ repletion improves mitochondrial and stem cell function and enhances life span in mice. Science *352*, 1436–1443.

Zhang, J., Kobert, K., Flouri, T., and Stamatakis, A. (2014). PEAR: A fast and accurate Illumina Paired-End reAd mergeR. Bioinformatics *30*, 614–620.

Zhang, Q., Wu, X., Chen, P., Liu, L., Xin, N., Tian, Y., and Dillin, A. (2018). The Mitochondrial Unfolded Protein Response Is Mediated Cell-Non-autonomously by Retromer-Dependent Wnt Signaling. Cell *174*, 870–883.

Zhang, Y., Chen, D., Smith, M.A., Zhang, B., and Pan, X. (2012). Selection of reliable reference genes in *Caenorhabditis elegans* for analysis of nanotoxicity. PLoS One *7*, e31849.

Zhao, C., and Meng, A. (2005). Sp1-like transcription factors are regulators of embryonic development in vertebrates. Dev. Growth Differ. *47*, 201–211.

Zhou, C., Huang, Y., Shao, Y., May, J., Prou, D., Perier, C., Dauer, W., Schon, E.A., and Przedborski, S. (2008). The kinase domain of mitochondrial PINK1 faces the cytoplasm. Proc. Natl. Acad. Sci. *105*, 12022–12027.

Zid, B.M., Rogers, A.N., Katewa, S.D., Vargas, M.A., Kolipinski, M.C., Lu, T.A., Benzer, S., and Kapahi, P. (2009). 4E-BP Extends Lifespan upon Dietary Restriction by Enhancing Mitochondrial Activity in *Drosophila*. Cell *139*, 149–160.

Zou, J., Guo, Y., Guettouche, T., Smith, D.F., and Voellmy, R. (1998). Repression of Heat Shock Transcription Factor HSF1 Activation by HSP90 (HSP90 Complex) that Forms a Stress-Sensitive Complex with HSF1. Cell *94*, 471–480.